A SHIP OPERATIONAL MODE DETECTION METHODOLOGY USING BINARY CATEGORISATION

Fengshuo Xing

Thesis submitted for the degree of Doctor of Philosophy

Marine, Offshore and Subsea Technology, School of Engineering

Newcastle University

August 2024

Abstract

The shipping industry is rapidly advancing into the industry 4.0 revolution, with the implementation of sensors and the application of digital technologies providing increasingly valuable information to enhance the efficiency, sustainability, and safety of marine shipping. To fully understand the operational performance and efficiency of a vessel, given a specific condition, it is essential to analyse data captured from sensors and identify the operational modes.

A binary categorisation methodology has been developed to detect operational modes across ship types. This methodology acknowledges that operational mode detection typically requires multiple sensing technologies, which can be costly and are not universally installed across all vessels. Furthermore, data harmonisation presents additional complexity. Therefore, this approach is designed to utilise minimum input parameters which are readily available on almost all vessels. These requirements are pivotal for enabling widespread adoption of this methodology within the field.

The input parameters primarily include the running status of the main engine and time series coordinates. The temporal and spatial information derived from these coordinates has been analysed to indicate and evaluate the vessel's trajectory, linking it to the operational modes. The structure of the methodology is flexible, allowing adjustments based on specific vessel types and research objectives.

The effectiveness of the mode detection and the algorithm's generalisability have been tested through three case studies. These studies were selected to evaluate performance across scenarios ranging from simple to complex and spanning common navigational areas. The target vessels include an ocean-going car carrier, a tuna purse seiner, and a tanker operating in inland waterways. The results demonstrated robust and efficient operational mode detection, confirming the algorithm's applicability to various ship types. Understanding the operational modes enables more precise fuel consumption prediction, optimised routing, and enhanced compliance with maritime regulations, thereby supporting more sustainable and efficient shipping operations.

Acknowledgements

I would like to express my deepest appreciation to my supervisors, Dr Kayvan Pazouki, Dr Rose Norman and Professor Alan Murphy, for their support and guidance throughout this study, regularly offering constructive advice and the opportunity to explore my research in different ways.

I owe a huge amount of gratitude to my loving family who have been by my side throughout this wonderful journey. My wife, Dr Yuchan, provides unconditional support outside of my studies, and her strong belief in me encourages me to persevere and complete this thesis. I am also deeply thankful to my parents for their unwavering support to other family members and friends who have supported me along the way.

I would like to thank my fellow PhD candidates and other colleagues at the university who have helped create a comfortable working environment, and fostering creativity, critique and a strong work ethic that enabled me to complete this thesis.

My PhD journey has spanned a period of significant change in my life, during which I have overcome many challenges and enjoyed the magnificent love surrounding me. The arrival of our first baby, Shiqing, has been the most treasured gift of my life to date. On completion of this thesis, I look forward to exploring new ventures, and feel a sense of excitement as to what the future holds.

Table of Contents

List of Tables

List of Figures

Glossary of Terms

AE	Auxiliary Engine
CCNR	Central Commission for the Navigation of the Rhine
DCP	Detected Change Point
EU	European Union
FOC	Fuel Oil Consumption
IMO	International Maritime Organisation
IPCC	Intergovernmental Panel on Climate Change
IQR	Inter Quartile Range
MCR	Maximum Continuous Rating
ME	Main Engine
NaN	Not a Number
NOx	Nitrogen oxides
RIQR	Rolling Inter Quartile Range
RSD	Rolling Standard Deviation
SD	Standard Deviation
SOG	Speed Over Ground
VCP	Visualised Change Point

Chapter 1 Introduction

1.1 Context

Marine shipping is indispensable to the global economy, serving as its backbone by facilitating the efficient movement of goods across international borders. It carries more than 80% of the world's cargo by volume including essential commodities such as food, energy, and other essential materials (UNCTAD, 2023). According to the United Nations Conference on Trade and Development (UNCTAD) Review of Maritime Transport 2023, despite facing numerous challenges such as geopolitical tensions and environmental concerns, the sector is expected to grow by 2.1% annually over the next five years (UNCTAD, 2023). However, this growth is tempered by the complexities of adapting to sustainable practices and navigating a landscape marked by fluctuating freight rates and shifting trade routes. This highlights the need for resilient maritime infrastructure and innovative management strategies to handle the increasing demands of global trade while addressing the urgent issues of environmental impact and trade security (UNCTAD, 2023).

In this context, it is critical for the shipping industry to advance through digitalisation, which aligns with the broader principles of the Fourth Industrial Revolution (Aiello et al., 2020, Razmjooei et al., 2023). This transition is crucial for integrating innovative technologies that enhance efficiency and sustainability within the industry. Central to this shift is the integration of advanced digital technologies such as the Internet of Things (IoT), Big Data Analytics, cloud computing, and artificial intelligence (Bui and Nguyen, 2021). These technologies have the potential to collectively revolutionise traditional maritime operations and, by adopting these innovations, the industry aims to not only achieve greater operational transparency, predictive maintenance of vessels and optimised route planning, but also to introduce levels of automation and smart capabilities that were previously beyond reach (Durlik et al., 2023).

At the heart of marine digitalisation is the adoption and integration of advanced sensor technologies. Sensor data are leveraged across various domains to enhance operational efficiency and safety. These sensors monitor a wide range of parameters, including engine performance, fuel consumption, cargo weight, environmental conditions such as ocean currents and weather patterns, as well as navigational data (Bui and Nguyen, 2021, Tay et al., 2021). Advanced sensors installed on vessels continuously gather data, facilitating critical

applications such as remote sensing for continuous monitoring, intelligent traffic management at ports, and predictive maintenance to prevent equipment failures (Prabowo et al., 2021). These technologies enable precise voyage planning by analysing route and performance data alongside meteorological conditions to optimise travel paths. Furthermore, sensor data supports energy management systems that regulate fuel consumption and emissions, helping ships meet stringent environmental regulations. Real-time performance monitoring and operational predictability are also achieved through these sensors, allowing ship operators to make informed decisions that enhance vessel safety, security, and overall operational effectiveness (Bui and Nguyen, 2021, Tay et al., 2021).

However, the evolution in shipping comes with its own set of challenges, underscored by the '4 Vs' of big data: Volume, Velocity, Variety, and Veracity. Each of these aspects brings complex challenges that must be navigated carefully (Zaman et al., 2017a). The Volume of data produced by modern maritime operations is vast, as ships equipped with advanced sensor technologies generate terabytes of data, presenting significant demands on data storage and processing infrastructure. The Velocity at which this data is generated and needs to be processed in real-time further strains existing capabilities, requiring computational efficient analytical methods and computational processing power. The Variety in data types, ranging from structured formats like logs and sensor readings to unstructured forms such as videos and communications, make it difficult to combine and analyse the information consistently. Lastly, Veracity concerns the accuracy and reliability of data, which are critical when making operational decisions that ensure safety and efficiency at sea.

The financial barriers pose a significant challenge to the implementation of advanced technologies in the marine industry. The adaptation required for these technologies to operate in the hash marine environment represents a considerable cost. Additionally, the hostile conditions of the marine environment and its relative inaccessibility make use of marine sensing technologies far more expensive than similar approach conducted on land (McMeel and Eparkhina, 2018). The age of the fleet compounds these challenges; as of 2023, the average age of commercial ships has risen to 22.2 years, and half of the fleet is over 15 years old (UNCTAD, 2023). Retrofitting such older ships with new technologies is particularly problematic, not only due to the integration complexities but also considering the operational

costs of installing, maintaining, and eventually replacing or recovering sensors (McMeel and Eparkhina, 2018).

Given these constraints, it is vital that the new data-driven methodologies not only adapt to the limited technological upgrades feasible on older vessels but also utilise the minimum parameters that are commonly available across the majority of vessels.

The primary purpose of a vessel is to efficiently and safely fulfil the operational tasks for which it is designed. These tasks can be divided into distinct operational modes, each corresponding to different functions and requirements necessary for the vessel's operation. In this context, an operational mode is defined as a specific state of vessel activity that is utilised to accomplish a designated task (Lützen et al., 2017). For example, manoeuvring, which involves complex navigational techniques often near ports or in confined waters; transiting between ports, where the ship navigates over long distances usually at a consistent speed and course; or conducting offshore drilling, each represent different operational modes. These modes dictate the operational dynamics and energy consumption patterns of the vessel making it challenging to compare or extract useful information from sensor data across different modes.

The identification of operational modes in maritime shipping is of paramount importance for enhancing the efficiency, safety, and sustainability of maritime operations. Accurate mode detection allows for the optimisation of vessel performance across various operational phases, such as manoeuvring, transit, and docking, each associated with distinct requirements and energy consumption patterns. By reliably identifying these modes, operators can implement targeted strategies for energy management, reduce operational costs, and minimise environmental impact. Furthermore, mode identification plays a crucial role in the context of automation and real-time decision-making systems. As vessels become increasingly equipped with advanced automation technologies, the ability to automatically detect and switch between operational modes becomes essential for ensuring seamless operations and enhancing navigational safety. This capability not only supports the operational efficiency of individual vessels but also contributes significantly to the broader goals of maritime traffic management and accident prevention.

Detecting operational modes accurately is a significant challenge due to the diverse and dynamic nature of maritime operations (Basurko et al., 2022). Each mode has distinct characteristics and requirements, and a vessel may switch between these modes multiple

times during a single voyage (Lützen et al., 2017). This variability introduces complexities in data analysis, as the sensor data needs to be contextualised according to the specific operational mode to be meaningful. Despite these challenges, it is essential to identify and classify these operational modes effectively. Doing so not only enhances the interpretability of sensor data but also ensures that performance optimisation and energy management strategies are correctly targeted. Therefore, the development of robust methods for detecting operational modes stands at the forefront of advancing maritime digitalisation and operational intelligence, addressing both immediate operational challenges and long-term strategic goals of the maritime industry.

Building upon the importance of detecting various operational modes, it is equally crucial to acknowledge that different vessel types require tailored algorithmic approaches due to their distinct operational needs and designs (Swider et al., 2018). Vessels can broadly be categorised into two groups: traditional commercial vessels, whose primary function is to transport cargo from port to port, and specialised vessels, which are designed to perform a range of specific tasks beyond mere transportation (Lützen et al., 2017).

Traditional commercial vessels typically operate under well-defined modes such as transit, manoeuvring, at anchor, and port operations. In contrast, specialised vessels, which include research ships, offshore drilling units, fishing vessels, and construction vessels, engage in additional unique modes specific to their operational tasks. For example, a research vessel may have modes dedicated to scientific sampling or data collection, while an offshore drilling unit has modes specific to drilling and dynamic positioning (Lützen et al., 2017).

Given this diversity, developing an algorithm that can adapt to different vessel types is essential. Such an algorithm should be capable of distinguishing between the common operational modes across all vessels but also able to accommodate the unique modes specific to each type of vessel. This adaptability ensures that the algorithm can provide accurate insights and guidance tailored to the specific needs and functions of each vessel.

1.2 Aims and Objectives

The primary aim of this research is to develop a data-driven method capable of detecting operational modes using minimal parameters that are readily available on the majority of vessels, with adaptability across various vessel types.

Overarching criteria:

To guide the development of this method, the research is grounded in three overarching criteria:

- Minimum Input Parameters: The algorithm will utilise the minimum possible number of parameters to ensure simplicity and broader applicability.
- Essential Onboard Measurements: Focus on leveraging data from standard measurements already available on most vessels, avoiding the need for specialised or additional equipment.
- Adaptability Across Vessel Types: The algorithm will be versatile enough to accommodate the operational specifics of different vessel types.

Research objectives:

- Identify Essential Input Parameters:

Determine which parameters are critical and universally available across vessel types that can effectively predict operational modes. This step is fundamental to ensuring the method meets the criterion of minimal input parameters which are available.

- Algorithm Development:

Design and develop an algorithm based on the identified parameters. This involves establishing a clear link between the parameters and specific operational modes, thus enabling the accurate detection of these modes.

- Validation Through Case Studies:

Design a series of case studies that validate the algorithm's effectiveness across different vessel types.

1.3 Novelty and Contribution

This research introduces several contributions to the field of maritime operations, particularly in the detection of operational modes using digital technologies.

Firstly, it pioneers the use of minimal input variables by leveraging temporal and spatial information from coordinates, thus eliminating the need for additional costly onboard measurements. This approach not only simplifies the implementation but also significantly reduces the operational costs associated with data collection.

Secondly, the methodology developed integrates a novel hybrid approach that combines knowledge-based and statistical methods. By employing a visualization technique informed by domain expertise, this method facilitates precise determination of key parameters, effectively addressing the limitations of purely statistical analyses while enhancing computational efficiency.

Additionally, the research employs an innovative geographic representation for result validation, which uses colour-coded trajectory segments to allow for straightforward assessment and validation of the detected operational modes. This visual method ensures that results are easily interpretable and grounded in comprehensive domain knowledge.

Furthermore, the presentation of detected results as continuous time-segmented data, rather than disjointed points, aligns with real-world applications and enhances the practicality of the findings. The detected continuous data sets pave the way for future research into segment-based machine learning models in maritime operations.

1.4 Thesis Outline

This chapter has introduced the context, core aims, and objectives of the research. The remainder of this thesis is structured as follows:

Chapter 2: Literature Review

This chapter reviews existing literature to identify gaps in current research related to the detection of operational modes in maritime operations. It establishes the theoretical foundation for the study and justifies the need for the proposed algorithm.

Chapter 3: Methodology

This chapter discusses in detail the methodology developed for this study, including the identification of key parameters and their linkages to operational modes. It explains the use of

binary categorisation to detect operational modes and describes how the method is customised for different types of vessels, fulfilling the criterion of adaptability.

Chapter 4: Case Study One

The first case study applies the developed algorithm to an ocean-going car carrier. The results are validated through graphical representation, demonstrating the algorithm's performance and applicability to ocean-going vessels.

Chapter 5: Case Study Two

The second case study focuses on a tuna purse seiner to test the algorithm's performance in a complex scenario. This chapter contrasts the operational tasks of typical commercial ships with those of fishing vessels, highlighting the algorithm's effectiveness under varied operational modes.

Chapter 6: Case Study Three

The final case study applies the algorithm to an inland tanker to test its adaptability across different navigational areas, from open seas to inland waterways. It tests the performance of developed methodology under complicated navigation areas. Further expand the adaptability to various types of vessels.

Chapter 7: Conclusion and Future Work

The concluding chapter synthesises the findings from the case studies and discusses the implications of the research. It outlines the contributions of the study to the field and presents recommendations for future work.

Chapter 2 Literature Review

2.1 Shipping 4.0

The concept of the Fourth Industrial Revolution was first introduced in 2011 (Razmjooei et al., 2023). This revolution aims to combine different aspects of information and communication technology (ICT) to improve digitalisation and promote information-driven industrial development (Mohd Salleh et al., 2021). The two terms, Industry 4.0 and digitalisation have a strong relationship since the digitalisation is the cornerstone of the Industry 4.0 (Jahn and Saxe, 2017).

As the backbone of global economy, the shipping industry is now stepping into its own fourth technological revolution, also referred to as Shipping 4.0 or Maritime 4.0 (Bui and Nguyen, 2021, Sullivan et al., 2020). This revolution aims to reshape supply chains in the maritime sector through digitalisation and connectivity (Jahn and Saxe, 2017). This initiative offers substantial benefits, including creating new value, enhancing collaboration among port stakeholders, lowering operational expenses, and boosting overall revenue (Aiello et al., 2020, Di Vaio and Varriale, 2020).

In cyber-physical systems, the physical processes of sensors are seamlessly integrated with software and computational processes, typically involving intelligent sensing technologies for data measurement and monitoring within the system's architecture. These systems require sensors to assist operators, technicians, and engineers in comprehending vital tasks by Prabowo et al. (2021). The characteristics of these sensors are geared towards providing real-time, meaningful information that enhances productivity, efficiency, and flexibility across different sectors, including commercial enterprises and academic research. This integration not only provides onboard machinery with smarter embedded computers but also delivers a wealth of information and data, supported by a range of onshore centres that utilise this data (Yee et al., 2020, Bui and Nguyen, 2021). This wealth of sensor data not only offers an unprecedented level of operational transparency but also provides the necessary information to maritime operators to analyse and optimise performance, safety, compliance and maintain market competitiveness (Razmjooei et al., 2023).

2.2 Sensor Data

The proliferation of data in maritime operations is largely driven by advancements associated with Shipping 4.0, which has introduced a range of technological innovations in navigation and automation systems (Rødseth et al., 2016). These advancements have resulted in a diverse array of data sources, each contributing uniquely to the extensive data landscape in the shipping industry. The variability in how this data is collected and utilised underscores the complexity of integrating these new technologies into existing maritime frameworks. To bring clarity and structure to this vast array of information, marine sensor data can be systematically categorised into four primary groups. These categories not only reflect the type of data but also encapsulate the specific aspects of maritime operations, ranging from navigational metrics to operational efficiencies, environmental conditions, and safety protocols (Prabowo et al., 2021).

2.2.1 Navigational and bridge data network

Bridge data networks include data from diverse navigation sensors and equipment, interconnected using digital interfaces following, for example the IEC 61162 standards, which are a set of IEC standards for 'digital interfaces for navigational equipment with a ship (Wu et al., 2016). This category encompasses standard navigation data along with special-purpose instruments tailored for specific ship operations, such as wave radars, oil spill detectors, and high-accuracy inertial navigation sensors. Additionally, the voyage data recorder (VDR) is sometimes used to record these data, however, it may have limitations regarding the number of data points collected and the frequency of data recording (Rødseth et al., 2016).

External ship monitoring (AIS and VTS) is a significant source of maritime data. Initially, the Automatic Identification System (AIS) was developed to avoid ship collision accidents, and was highly regionalised with most coastal states operating base station networks that monitor ship traffic within the range of very-high-frequency (VHF) radios, only 10-20 nautical miles (Yang et al., 2019a). Since 2008, these systems have been supplemented by Low Earth Orbit satellite AIS receivers to extend coverage beyond coastal ranges to worldwide, capturing vital data like ship position, speed, course, true heading, and rate of turn, with less frequent transmissions covering static data and voyage-specific information (Rødseth et al., 2016). These integrated

monitoring systems provide comprehensive data crucial for maritime operations (Baldauf et al., 2023).

2.2.2 Ship operation and performance monitoring

Conventional automation systems on ships, from older ships to modern complex vessels, collect vast amounts of data through hundreds to tens of thousands of input/output points, but the data quality can vary significantly. Accessing this data often poses a challenge, as it tends to be confined within closed, vendor-specific systems. Additionally, the quality of data is a concern that some sensors may be inaccurate, defective, or even disconnected. Sensors are typically designed with specifications that match their intended uses, aiming to ensure the necessary precision for their tasks. Despite this, these systems frequently lack 'quality attributes' – specific indicators that evaluate whether the sensor outputs are reasonable, consistent and stable. Without these attributes, users must verify if the measurements are reasonable and whether the values are consistent or fluctuate excessively (Rødseth et al., 2016).

Cyber Physical Systems (CPSs) in the maritime industry represent a significant advancement in integrating physical processes with networked computer-based algorithms to enhance efficiency and safety (Bolbot et al., 2020). These systems are pivotal in supporting or even replacing human operations in critical decision-making processes, thereby reducing the potential for human errors that could lead to accidents. In maritime settings, CPSs are exemplified by systems such as Power Management Systems, Propulsion engines, Heat Ventilation Air Conditioning systems, and even autonomous ships, which are supported by advanced automation and control systems (DNV, 2016).

Key components of maritime CPSs include engines, power generation systems, and dynamic positioning systems, which are equipped with sophisticated sensors and computers for continuous condition monitoring and closed-loop control. These systems are designed to handle essential functions such as navigation, torque control in winches, and alarm condition detections, which are crucial for the smooth operation of modern ships. This integration highlights the core principles of Industry 4.0 by merging critical mechanical components with digital monitoring and control technologies, ensuring that operations are both efficient and adaptable to evolving conditions (Rødseth et al., 2016).

In recent years, especially during periods of high oil prices, there was a marked increase in the instrumentation of ships for monitoring and optimising performance. This often involved the installation of shaft torque meters, fuel mass-flow meters, advanced environmental sensors, and trim measurement devices (Rødseth et al., 2016). These instruments were specifically installed to enhance ship performance.

2.3 Application of Data Analytics in Shipping Industry

The report 'Big data - the new data reality and industry impact' indicates that data analytics based on the massive sensor data would be utilised in the six domains of maritime shipping, which are technical operation and maintenance, energy efficiency, safety performance, management and monitoring, commercial operation and automation (DNVGL, 2014).

2.3.1 Technical operation and maintenance

Maintenance activities in marine machinery are typically categorised into three types: reactive maintenance, time-based maintenance, and Condition-Based Maintenance (CBM) (Lu et al., 2018, Emovon et al., 2018). The rise in data utilisation and accessibility has greatly facilitated the adoption of CBM, enabling proactive identification of potential failures and reducing costs by minimising unplanned preventive maintenance and crisis-driven reactive maintenance. Consequently, a large array of sensors is installed on critical ship components and within their operational environments to effectively monitor their condition (Jamshidi et al., 2018, Su et al., 2019).

In the literature, numerous studies have focused on maintenance strategies, employing a range of machine learning models to enhance diagnostic accuracy and efficiency in maritime operations. Liu et al. (2022) provide an approach to evaluate propulsive performance by analysing onboard sensor data. The actual ship condition is represented by the derived engine power-rpm curve. By comparing this with the nominal design engine curve, the deviation can support the predictive condition-based maintenance.

A condition-based maintenance strategy for diagnosing faults in ship engine systems has been proposed by Karatuğ and Arslanoğlu (2022). To achieve this, the authors gathered data from a container ship to carry out condition-based maintenance using an Artificial Neural Network (ANN) detecting faults. The findings showed that the ANN could significantly enhance existing

maintenance approaches in the industry and is versatile enough to be applied to various systems or engines across different types of ships. In another study, the backpropagation neural network was utilised to develop a ship equipment fault detection method, and the results of the case study on a turbocharger indicate the developed approach outperformed the Support Vector Machine (SVMs) (Wu, 2018).

The One-Class Support Vector Machine (OCSVM) is a commonly used SVM technique for fault detection, designed to separate normal operational data from abnormal data indicating possible faults. Makridis et al. (2020) introduced an ensemble model that included OCSVM. Similarly, Michałowska et al. (2021) utilised OCSVM to create an anomaly detection algorithm specifically for marine machinery.

2.3.2 Energy efficiency

Energy efficiency is becoming increasingly critical due to current economic and environmental pressures. In the maritime industry, it involves reducing the amount of energy consumed and greenhouse gas emissions per unit of transportation work (Jia et al., 2017). Strategies for enhancing energy efficiency are typically categorised into technical and operational initiatives. Technical strategies include advancements made during the ship design process, such as optimising the hull form, improving propulsion devices, and implementing waste heat recovery technologies (Brynolf et al., 2016). On the operational side, measures encompass optimal ship operational techniques like trim and ballast management, voyage optimisation through strategies such as weather routing and slow steaming (Ölçer, 2018).

Ship design was historically more an art than a science, relying heavily on the expertise and intuition of experienced naval architects (Papanikolaou et al., 2022). Around 15 years ago, a holistic approach was proposed by Papanikolaou (2010), which redefines the ship design optimisation problem by considering all relevant factors - structural, operational, environmental, and economic, it emphasises the importance of considering the ship's entire lifecycle, from design and construction to operation and decommissioning (Nikolopoulos and Boulougouris, 2020).

With the development of shipping 4.0, the integration of real-time sensor data has become a crucial element in this methodology for assisting on reducing uncertainty. Uncertainty is an unavoidable aspect of ship design, which can be divided into two categories, aleatory and

epistemic (Hang Hou et al., 2019). Aleatory uncertainty, also known as statistical or inherent uncertainty, stems from inherent variability or randomness in system behaviours or environmental conditions. Epistemic uncertainty, or knowledge-based uncertainty, arises from lack of knowledge, information, or understanding about the system or the environment (Li et al., 2023).

To address these two uncertainties, Esmailian et al. (2022) developed a probabilistic-based approach to ship design utilising real operational data and ocean conditions such as shaft power, shaft speed, draught and wave conditions to simulate power profiles and building models that predict how ships will perform in various sea conditions. By incorporating real-world conditions into their designs, the findings indicate that optimising ship designs to match real-world operation and environments might improve ship performance.

Esmailian and Steen (2022) utilise the in-service data of a 13100 TEU container ship operating in real sea conditions to simulate a power profile. This profile has been used to design a ship at the early stage. Tests show that this approach could be incorporated into a holistic ship design process, providing designs with improved performance in real operating conditions. Nikolopoulos and Boulougouris (2020) provide a comprehensive approach to ship design that leverages real sensor data throughout the design process. Real sensor data from two bulk carriers is utilised for operation simulation under different voyage profiles instead of using only one design point. The results highlight the efficacy of using real data.

Even though many methods on design aspect can improve the energy efficiency, which can applied on the early stages on ship construction and design, the already existing ships need a significant cost to employ them (Barreiro et al., 2022). Thus, increasing energy efficiency from operational aspects is necessary as well.

Operational optimisation involves altering the operational strategies of ships, including adjustments to speed (Psaraftis and Kontovas, 2014), routing (Szlapczynska and Szlapczynski, 2019), trim (Tu et al., 2023), and energy management (Zhang et al., 2022). This type of optimisation does not necessitate changes to the ship's equipment and can significantly reduce fuel consumption (Theocharis et al., 2019). For instance, reducing speed by 10% can lead to a 27% reduction in fuel usage (Theocharis et al., 2019, Fan et al., 2022). Although these strategies have different emphases, they both aim to reduce ship fuel consumption (SFC) (Ballou, 2013, Notteboom and Vernimmen, 2009).

SFC models can be categorised into three types: the white box model (WBM), which relies on the first principle analysis; the black box model (BBM), which is based on data analysis; and the grey box model (GBM), which integrates both first principle and data analysis approaches (Fan et al., 2022).

Various factors influence vessels' operations during navigation, making the analysis of the physical laws governing the WBM quite complicated. In extreme navigation conditions, the prediction accuracy of the WBM can be limited (Wei et al., 2021). The WBM can be tailored for a ship's power system. This model can assess ship resistance based on external conditions and then estimate fuel consumption by examining the interaction between the ship and its engine-propeller system. Additionally, by analysing the ship's internal combustion engine within the power system, fuel usage can be calculated using the parameters of each component and relevant formulas (Fan et al., 2022). The performance of the WBM is strongly affected by various assumptions, but its benefit is that the energy efficiency of the vessel can be studied in the early operational phasis (Tillig et al., 2017).

BBMs can be classified into statistical and machine learning methods (Yan et al., 2021). Probability is employed in statistical models to deduce the connections between variables and fuel consumption, whereas machine learning applies approximate functions to forecast fuel consumption. The differences between the BBM and the WBM are distinct: The WBM is transparent in its operations, allowing users to understand its internal processes, whereas BBMs are ambiguous. In the WBM, the relationship between parameters related to fuel consumption are based on its formulas, however, the relationships are explicitly shown through the analysis of data for BBM. The BBM requires substantial amounts of data to function effectively, while the WBM operates efficiently with a considerably smaller dataset (Fan et al., 2022).

Statistical models often use linear regression as a foundational method. In a recent study analysing fuel consumption on a container ship, Uyanık et al. (2020) utilised actual data encompassing 75 distinct parameters of the vessel to evaluate the effectiveness of various predictive models. These included Multiple Linear Regression, Ridge Regression, LASSO Regression, Support Vector Regression, Tree-Based Algorithms, and Boosting Algorithms. The findings indicated that the models providing the most accurate predictions were Bayesian Ridge Regression, Kernel Ridge Regression, Multiple Linear Regression, and Ridge Regression.

Machine learning-based SFC models, which require extensive and specific data, are particularly adept at addressing high-dimensional problems. These models are used in analysing the relationships between fuel consumption and variables that are not easily quantified through traditional principles, such as the impact of wind, waves, ship load, and operational policies (Sigmund and El Moctar, 2018, Hu et al., 2019, Işıklı et al., 2020).

A GBM is a hybrid method, combining mechanical formulae and data driven methods (Chen et al., 2019). The WBM and BBM can be integrated in two distinct approaches to create a GBM. Initially, a BBM can be developed on the foundation of a WBM for relationships that the WBM cannot succinctly formulate into equations. Concurrently, the BBM can employ data to validate the precision of the WBM's outputs. Alternatively, a WBM can be implemented based on the BBM, where the WBM serves to confirm that the outcomes of the BBM are logically sound (Fan et al., 2022). Incorporating the first principal formulas into the BBM can help lessen the burden of data processing. An innovative genetic algorithm-based GBM that models ship fuel consumption using fundamental principles of ship propulsion was proposed by Yang et al. (2019b), where the unknown parameters are estimated through a genetic algorithm-based procedure. To validate the accuracy and reliability of this model, the real ship operational data collected from a crude oil tanker was utilised and it also shows that the amount of data required for accurate predictions can be significantly reduced. In addition, certain data are challenging and costly to acquire, necessitating extended periods of voyage data collection for the ship, the GBM is capable of achieving the same outcomes as the BBM while utilising roughly half the amount of data (Coraddu et al., 2015).

2.3.3 Navigational safety

Numerous studies have explored the use of AIS data to effectively prevent maritime accidents, focusing primarily on two areas: enhancing ship collision avoidance and improving coastal authorities' traffic surveillance capabilities (Yang et al., 2019a).

Ship collision avoidance has been a significant concern for mariners and researchers. The integration of AIS data has revolutionised this field, extending beyond direct ship-to-ship communications to incorporate advanced techniques designed to enhance navigational safety. These state-of-the-art methods include constructing ship domains, assessing collision risks, and planning safer navigation routes. A ship domain is defined as the area around a ship that

the navigator aims to keep clear of other vessels or obstacles (Szlapczynski and Szlapczynska, 2017). Utilising AIS data, Kundakçı et al. (2023) were able to build detailed models of these domains. AIS data plays a crucial role in conducting collision risk assessments, categorising risks into several types such as calculating closest points of approach, quantifying collision probabilities, detecting high-risk collision scenarios, estimating collision frequencies in specific areas, and developing systems to avoid collisions (Liu et al., 2023, Zhang et al., 2021, Goerlandt and Montewka, 2015).

In terms of route planning, the goal is to establish a path that minimises collision risks and detour costs, building on insights gained from ship domain construction and risk assessment. Commonly applied methods in route planning include heuristic algorithms like evolutionary algorithms and ant colony optimisation (Kim et al., 2017).

Additionally, AIS data enhances the surveillance capabilities of coastal authorities. It supports anomaly detection and maritime traffic monitoring, crucial for identifying illegal, suspicious, or unsafe maritime behaviours. Techniques like trajectory clustering help establish normal ship behaviour patterns using historical data, while real-time data monitoring allows for immediate detection of anomalies (Yang et al., 2019a). Furthermore, systems developed for maritime traffic monitoring, such as those by Li et al. (2016) and Wu et al. (2017), focus on vessel detection, tracking, state estimation, trajectory prediction, and traffic situation visualisation, which are essential for pinpointing and mitigating potential navigational risks.

2.3.4 Commercial management

In the dynamic world of global trade, it is crucial for maritime businesses to stay informed about market trends. Data analytics provides a comprehensive overview, helping companies understand market shifts, evaluate trade route profitability, and identify emerging demands. By examining data on trade volumes, route popularity, and types of cargo, companies can predict market demands, adjust their capacities accordingly, and prepare for changes in global trading patterns. This strategic insight allows maritime firms to remain flexible and competitive in a fluctuating market environment (Okumus et al., 2023).

Additionally, applying data analytics to examine customer feedback reveals trends, preferences, and challenges encountered by customers. Insights gained from data on cargo handling efficiency, shipment timeliness, or the quality of onboard services enable businesses

to focus on improving aspects that significantly impact customer satisfaction. Data analytics empowers maritime operators to adjust their offerings based on specific customer needs and market demands. For example, analysing trends in cargo preferences might lead companies to introduce specialised services like temperature-controlled containers for perishable items or enhanced security for valuable goods, thereby meeting niche market requirements more effectively (Durlik et al., 2023).

2.3.5 Smart ship and automation

A smart ship is defined as 'a maritime asset equipped with substantial automation, data communication, system monitoring, and data management capabilities' (Reilly and Jorgensen, 2016). The growing accessibility of sensor data and enhanced data processing capabilities are paving the way for ships to become increasingly automated, potentially leading to the development of fully autonomous ships operated from extensive onshore control centres. This evolution, aimed at increasing satisfaction among maritime stakeholders, poses significant challenges to existing regulatory frameworks, safety performance assessments, and verification processes (DNVGL, 2014). Traditional vessels are being transformed into smart ships or are being replaced by them through the integration of advanced technologies including communication systems, data management, and e-navigation (Aslam et al., 2020).

2.4 Operational Mode

After reviewing the applications of data analytics in marine shipping, it is apparent that a significant aspect involves extracting information from sensor data to determine the operational status or condition of the vessel under actual circumstances. Detecting operational modes of various ship types from onboard measurements is essential to accurately ascertain how the vessel is operating in real conditions.

Operational modes for marine vessels can be defined as the various distinct states or phases through which a vessel operates to accomplish designated tasks and missions (Lützen et al., 2017). These modes are related to the vessel's designed activities, encompassing everything from navigation and docking to periods of waiting at anchorage (Zaman et al., 2017b). Operational modes are informed by and tailored to the specific type of vessel, reflecting the

unique operational demands and environmental interactions each vessel type encounters (Swider et al., 2018).

Additionally, these modes describe how energy flows from sources to consumers onboard, encapsulating the energy dynamics during different operational states. Thus, operational modes serve as a fundamental framework for understanding and optimising the vessel's performance, safety, and energy efficiency through precise and dynamic adjustments based on real-time sensor data.

Lützen et al. (2017) categorised vessels into two groups, one is the traditional commercial vessels, which mainly have a single design purpose, transporting cargo from port to port. Specific types of commercial vessels are designed according to the different types of the transported cargo, such as bulk carriers, container ships, oil tankers or even passenger ships. The other group is the specialised vessels with multiple purposes, such as offshore, fishing and service vessels. It is challenging to detect the operational modes for various vessel types considering the various targets and purposes which would have their own characteristics.

Three common operational modes have been proposed for most vessels: Harbor, Manoeuvring and Passage (Lützen et al., 2017). Within these three common operational modes, the Passage mode has attracted more attention; it is defined as the vessel is on passage between fixed positions. In literature, this mode has many other terms, such as Transit, Cruising or Steady state free running conditions (Zaman et al., 2017b, Trodden et al., 2015, Basurko et al., 2022). Within this mode, the vessel would operate in a relatively steady state condition with constant speed and the same course.

Identifying steady states in the analysis of marine machinery data is essential, as raw data often include non-operational states that can negatively impact the accuracy of data-driven analysis. Marine engines generally operate under steady-state conditions, yet fluctuations can occur due to environmental influences or operational changes, as noted by Theotokatos et al. (2020). If these varying states are not correctly identified and separated from steady-state data, the efficiency of computational processes and the effectiveness of predictive models may be compromised (Velasco-Gallego and Lazakis, 2022).

2.5 Data Preprocessing and Cleaning

Before developing the methodology, it's crucial to preprocess and clean the data for subsequent analytics. In data analytics, the principle of GIGO - garbage in, garbage out - is a well-known rule (Pyle, 1999). It has been found that generally, data preparation would take around 80% of the time of processing the total data analytics (Zhang et al., 2003). Essentially, the quality of data analysis reflects the quality of the input data. Therefore, thorough data preparation is critical for effective modelling in real-world applications (Dalheim and Steen, 2020b). Data collected directly from sensors often contain inaccuracies and distortions. Before this data can be used for deeper analysis, it must undergo preprocessing or filtering. The raw data needs to be removed of noises and cleaned to transform it into actionable information (Tay et al., 2021).

2.5.1 Types of errors

Measurement error arises within the data collection process and can be attributed to imperfections in measuring instruments, leading to discrepancies between the actual values and those recorded. The impact of these measurement errors can be assessed by calculating the mean squared error (MSE). MSE measures the average of the squares of the distances between a regression line and the data points. Data characterised by lower MSE values suggest greater accuracy in the recorded or predicted data. It is important to note that a lower MSE indicates a closer approximation to the ideal fit line (Tay et al., 2021).

Duplicate records can occur due to errors in data management when transferring data between systems. Including such duplicate data in analyses can lead to inaccurate results. Fortunately, these duplicates can typically be eliminated by simply removing these copies, although it is crucial to ensure that the original data remains intact and unduplicated (Tay et al., 2021).

Contradictive data arises when multiple entries are recorded at the same time. Various methods have been suggested for eliminating such contradictory data (Hodge and Austin, 2004), yet removing these entries can lead to gaps in the dataset, diminishing the reliability of any derived insights (Nwagwu et al., 2017).

The term outlier has been defined as 'an outlier is one that appears to deviate markedly from other members of the sample in which it occurs' (Grubbs, 1969). The definition of outliers are typically based on two assumptions: (1) outliers are different from the norm in terms of their features; (2) outliers are rare in a dataset relative to normal instances (Goldstein and Uchida, 2016). Removing these outliers is essential, as they can significantly skew the mean or standard deviation of the data. Consequently, their exclusion is a vital part of data preprocessing (Wedin et al., 2008).

2.5.2 Outlier detection

Outlier detection presents significant challenges, primarily due to the scarcity of labelled data, as outlier instances are rare (Boukerche et al., 2020). Consequently, many detection methods operate on an unsupervised basis. The typical task involves identifying a set number of data instances that significantly deviate from the norm. The responsibility of determining what constitutes an outlier generally falls to the analyst, who must initially define what is considered normal data. This involves analysing the overall shape of the graphed data for key features such as symmetry and deviations from expected patterns. Furthermore, it is crucial to scrutinise the data for standout outlier occurrences. For detecting these outliers, graphical methods like scatter plots and box plots, along with analytical techniques suited for normal distributions, prove to be effective tools (Tay et al., 2021).

The control chart technique (CCT) is a statistical method designed to identify anomalies in time series data. This algorithm functions by sliding a predetermined window over a sequence of data points, which could also be described as Mean ± 3 Standard Deviation (SD). The threshold limit is set at three SD, specifically for data following to a normal distribution. This technique has been applied to detect outliers of fuel oil consumption (FOC) (Kee et al., 2018, Zhou et al., 2023).

Density-Based Spatial Clustering of Applications with Noise (DBSCAN) is a clustering algorithm that relies on density-based spatial techniques (Ester et al., 1996). It has been utilised to detect outliers and remove anomaly coordinates of fishing vessels (Fu et al., 2021).

The median filter technique has been used to detect outliers, it is based on the sliding window technology, with different window size according to specific scenarios. This technique has been utilised to detect outliers (Swider et al., 2018, Abbasi Hoseini and Steen, 2017).

2.6 Methodology of Operational Modes Detection

The methodology for detecting operational modes can be categorised into two groups. The first is knowledge based, where modes are identified using professional domain knowledge, with thresholds for key parameters or location filters established to differentiate between modes. The second group comprises data-driven methods, which can be further subdivided into statistical methods, supervised classification and unsupervised clustering techniques.

2.6.1 Knowledge-based methodology

A typical example of a knowledge-based methodology was used to determine the activity-based fuel consumption of a Spanish tuna purse seiner (Basurko et al., 2022). Four operational modes have been defined: Cruising, Fishing, Inactive at sea, and In port. It is important to note that the Cruising mode encompasses not only the periods when the target vessel is sailing to different fishing locations on a relatively steady course but also includes the periods when it is leaving or returning to port, to or from fishing grounds.

The thresholds for selected key onboard measurements to distinguish these modes have been identified through collaboration between a group of researchers and onboard observers. These key parameters include the running status of the Main Engine (ME), shaft power, propeller pitch, engine speed and ship speed. In addition to these thresholds, time is also considered within the detection framework, for example, the reported arrival and departure times identify the 'In port' mode, and an engine speed of less than 450 rpm during the night-time from 6pm to 4 am characterises the 'Inactive at sea' mode.

This method could be simply understood as an attempt by the authors to differentiate the conditions of each mode by setting various filters on key measurements. These filters are determined based on a deep understanding and observation of the target vessel. Although the authors suggest that this method is the best approach in this scenario, particularly since other clustering and supervised learning methods were neither successful nor useful in distinguishing these modes, it does have its limitations. The method cannot be easily applied to other types of vessels as the deep understanding and domain knowledge required are specific to the target vessel and not readily transferable. Additionally, this method lacks a data pre-processing procedure in advance and the reliance on numerous key parameters may not be feasible for most of vessels.

In the literature, the knowledge-based method is extensively applied in estimating emissions by utilising ship movement information from AIS data. Researchers have been able to determine the operational modes of vessels, and then accurately estimate emissions for specific modes (Chen et al., 2021). This method is often referred to as the activity-based or fuel-based approach for generating ship emission inventories, which is considered more precise than top-down methods (Eyring et al., 2010, Yau et al., 2012). The focus of such emission inventories is typically on estimating emissions for a specific port or for global shipping fleets, rather than individual vessels. The detection of operational modes is relatively straightforward, primarily focusing on distinguishing three common modes: At anchorage, Manoeuvring and Cruising.

Common methods for detecting ship activities, or operational modes in this context, rely on analysing three elements: time, Speed Over Ground (SOG) and geographical delineation. For the time aspect, At anchorage mode is identified based on arrival and departure times provided by port authorities (Maragkogianni and Papaefthimiou, 2015). The detection of Manoeuvring and Cruising modes is based on SOG thresholds or geographical delineation, either separately or in combination.

Olmer et al. (2017) developed a method to distinguish operational modes to estimate GHG emissions for global shipping. Four operational modes - at berth, at anchor, manoeuvring and cruising - are identified by the distance to the port or coast and their SOG for various vessel types. These modes help calculate the ME, auxiliary engine (AE) and boiler power demands of each mode across different types of vessels.

Ng et al. (2013) proposed a methodology to create emission inventories for ocean-going vessels in Hong Kong and the Pearl River Delta. Four operational modes have been detected which are At anchorage, Manoeuvring, Slow cruise and Fairway Cruise/Cruise, based solely on SOG with three distinct thresholds set at 1, 8 and 12 knots respectively. Similar approaches have been used to generate emission inventories for other ports, including port of Dalian (Chen et al., 2021), and Tianjin (Chen et al., 2020).

Geographical delineation is typically used to define a cruising area or generate a cruising ship path for a specific port. Vessels sailing within the area or following the designated ship path are classified as being in cruising mode. Using these methods, emission inventories for the Port of Long Beach (PortofLongBeach, 2010), major ports of Greece (Maragkogianni and

Papaefthimiou, 2015), Port of Yangshan (Song, 2014), Port of Qingdao (Sun et al., 2018) and Turkey's Candarli Gulf region (Deniz et al., 2010) have been developed. Similar approaches have been employed to estimate the operational profile of ships in Norwegian waters to analyse the potential for hybrid and electric propulsion (Jafarzadeh and Schjølberg, 2018).

Chen et al. (2020) introduced a method to analyse the operational modes of tugboats using AIS data. To address the inaccuracies in AIS data, a 10-minute duration has been implemented as a rolling window. The condition of the target data point is determined by the major percentage of data points within this window, either above or below the defined SOG threshold, where the percentage must exceed 80% to detect the corresponding condition. Although this method accounts for errors in AIS data, it does not include a data cleaning process. which is common in most methodologies mentioned.

2.6.2 Statistical methods

Zaman et al. (2017b) developed an automated mode detection system that leverages statistical analysis to identify and validate operational modes from sensor data, effectively reducing the need for human intervention and minimizing errors. Their research utilises 4 key parameters, which are fuel consumption, speed, distance travelled, and position. They employed the Individual – Moving Range (I-MR) control chart from Statistical Process Control (SPC) to establish limits for identifying steady state conditions for key features and conducted correlation analysis to examine the relationships between parameters and various operational modes. Following these analyses, thresholds for each mode were established.

This method was applied to an Offshore Supply Vessel (OSV) using 5 days of data to detect 4 specific modes: Port, Sailing, Stand-By and Dynamic Positioning (DP) modes, as well as transient phases between these modes. Despite the limited number of input variables – which are available for most vessels - and the authors claimed that this algorithm could be applicable to various types of vessels. The methodology assumes that the data follows a normal distribution. The data were sampled on a per-minute basis, with 61 data points within the moving range, and the target data point situated in the middle of this range. This assumption of normal distribution within such intervals is debatable, especially if the vessel changes operational modes one or several times within these periods. Additionally, the study does not address data cleaning processes.

Trodden et al. (2015) introduced a data filtering technique specifically designed to identify the steady-state free running condition (SSFRC) of a harbour tug from its data-stream, providing a benchmark for the baseline operational performance. The harbour tug was selected for this study due to the high variability in operational activities compared to other types of vessels. The technique utilises a checking window that spans 2n+1 data points, centring on the target data with n steps on either side, to analyse the consistency of the data. This window incorporates a tolerance (tol) for mean parameters, with fuel consumption and SOG chosen as the two primary parameters for analysis.

The complexity of setting parameters such as n and tol, which must be tailored to specific ship types and their particular duties, making this method less adaptable to different types of vessels. Although the technique requires only two key parameters, which are generally available across most modern fleets, the intricate settings necessary for its application pose challenges for broader usage.

Dalheim and Steen (2020a) developed a method for detecting steady states in time series data from onboard monitoring systems, using a sliding window technique to analyse the slope of the data points within the window. A t-test was performed on each estimated slope to determine if it significantly differed from zero, indicating a steady state condition. Customisation of the window size and t-test tolerance is required beforehand. However, this method does not account for data cleaning, and extreme values in the raw data could significantly impact the slope estimation. Additionally, this offline method is computationally intensive, as a statistical t-test must be calculated for every data point and is dependent on the window size. The selection of critical variables, such as rpm, engine power, and ship heading, is also tailored to specific research interests, which may vary and not be universally available across vessels.

In the literature, more straightforward methods based on engine manufacturer guidelines are also used to detect steady states. Operating conditions with a load below 10% Maximum Continuous Rating (MCR) (Turbo, 2010) or speed at 15-25% of the engine's nominal maximum continuous speed (A/S, 2004) are considered transient. Typical load changes with a slope of 5% MCR hourly are identified as transit modes as well. These methods have been utilised to predict fuel consumption (Tsitsilonis and Theotokatos, 2018, Gkerekos and Lazakis, 2020).

Beyond these manufacturer-based approaches, Castresana et al. (2023) proposed a method to detect engine steady state conditions, starting with a filter to exclude stop mode, conditions where the rpm is below 400 and the fuel oil pump rack (FORACK) is under 5. A second filter applies a rolling standard deviation (RSD) of 3 minutes to determine steady state, requiring the RSD of RPM and RSD of FORACK to be less than 1% and 5%, respectively.

2.6.3 Unsupervised clustering methods

Abbasi Hoseini and Steen (2017) developed a method to identify ship manoeuvres from multivariate time series onboard measurements using unsupervised clustering techniques. Initially, the self-organizing map (SOM) and k-means algorithms were employed in two sequential steps to cluster datasets representing different ship manoeuvres. Subsequently, the k-nearest neighbours (k-NN) method classifies these clusters into predefined manoeuvres. This approach assumes that the measured variables capture the vessel's full dynamics in calm and level water conditions. To illustrate the planar motion of a ship on calm horizontal water, six measurements are selected as input variables: surge and sway velocities, yaw rate, rudder angle, and incorporating additional variables like yaw acceleration. The principal component analysis (PCA) technique is then applied to these measurements to reduce dimensionality, resulting in three new independent datasets. These datasets, along with the yaw acceleration, serve as input for the SOM algorithm.

Given the uncertainty in the number of clusters, the SOM is constructed with 30x30 neurons, producing 900 clusters with their respective codebook vectors, which represent the centres of gravity of the input vectors. The topological structure of these clusters is then compressed and recorded on a feature map. Upon reviewing the feature map, 13 distinct codebook vectors are identified. These are further clustered using the k-means algorithm to finalise the grouping into 13 distinct clusters.

For data processing, a median filter with a window size of 51 is employed to clean the data by removing spike-like anomalies. Given the data's sampling rate of 2 Hz, this filter size effectively covers a span of approximately 25 seconds, ensuring the removal of transient noise and anomalies from the measurements.

The t-distributed Stochastic Neighbor Embedding (t-SNE) technique, used in conjunction with hierarchical clustering, has been employed to identify operational modes on a platform supply

vessel during a single voyage (Swider et al., 2018). For this analysis, 29 onboard measurements were collected at a sampling rate of 1 Hz, serving as input variables. To clean the data, a median filter of size 7 was applied to eliminate anomalies. The t-SNE method was used to transform the high-dimensional dataset into a 3D map, facilitating the visualisation of potential operational modes. Initially, the results were not satisfactory, so hierarchical clustering was applied to the dimensionally reduced dataset; this method does not require predefining the number of clusters. For validation, the voyage dataset was manually labelled according to operational task definitions, such as Transit, In Port, Station-Keeping, and Manoeuvring.

Observations from the t-SNE 3D map indicated that the operational task definitions aligned well with the operational modes, with data groups from the same operational task not overlapping within individual groups.

Despite these insights, a key limitation identified from these studies is the uncertainty regarding the number of clusters, as both SOM and t-SNE were intended to guide cluster number determination through observational data. However, the results did not align satisfactorily with established domain knowledge. Furthermore, these methods presume that the onboard measurements sufficiently capture the vessel's full dynamics, a complex requirement not typically met by most vessels. This complexity in measurement may limit the applicability of these methods across different shipping contexts.

2.6.4 Supervised classification method

A deep learning model employing a convolutional neural network (CNN) has been developed to differentiate between fishing and non-fishing activities of vessels from AIS data (Arasteh et al., 2020). This model is designed to classify activities without the prerequisite of specifying ship types or fishing gear beforehand, based on the assumption that certain fishing activities, like those of a purse seiner, manifest distinct patterns in their movement, such as circular motions. To capture the trajectory of vessels, five parameters including distance, rectilinear speed, acceleration, jerk, and derivative of course have been extracted. The use of a sliding window technique, with a window size of 11 covering approximately a two-hour period, helped to optimise accuracy while reducing computational load and minimising misleading information through segment-based classification. This model was trained using a dataset manually labelled by experts, achieving nearly 94% accuracy with real-world data.

In another study, Fu et al. (2021) proposed a method using a fusion of machine learning models through a stacking method to predict the operational modes of fishing vessels. This approach integrates Random Forest, Gradient Boosting Machine, and Neural Network classifiers, trained on features derived from spatial-temporal data and then textual data processed via the word2vec model. Operational modes such as trawl, purse seine, and gill net were distinguished using labelled data provided. The raw data from Beidou, which include basic fields like coordinates, speed, and heading, was supplemented with statistical features such as mean, variance, skewness, and kurtosis to enrich the input parameters for the algorithms. DBSCAN was used to filter out anomalies, and the word2vec model was employed to compute embedding features for each position, treating trajectories similarly to textual data to uncover patterns essential for operational mode prediction. This method demonstrated superior accuracy and robustness, validated against a labelled dataset of vessel movements.

Although both studies reported high accuracy in detecting fishing activities, they rely heavily on accurately labelled training datasets - one manually labelled by experts and the other derived from a competitive environment. Acquiring such labelled datasets is challenging for most vessels, limiting the applicability of these supervised classification methods. Insights from these studies include the effective use of secondary features derived from AIS data to represent trajectory patterns and the potential of segment-based algorithms, such as using a sliding window technique or sequence input datasets for training models like word2vec. These methodologies leverage both temporal and spatial information from vessel coordinates to solve practical problems effectively.

2.7 Gaps

To thoroughly assess the previous methods, a comparison is conducted across 4 key aspects, which are number and accessibility of input parameters, computational efficiency, mode detection performance, and limitations.

Given that the primary aim of this research is to detect ship operational modes for individual vessels, applications of knowledge-based approaches used to generate emission inventories, as well as the detection of fishing activities, will be excluded from this analysis. Therefore, the comparison will concentrate specifically on knowledge-based, statistical and clustering approaches.

2.7.1 Number and accessibility of input parameters

The statistical method requires the fewest input parameters and is accessible for most vessels; these parameters typically include distance, SOG, and fuel consumption. In contrast, the knowledge-based approach used to detect operational modes for a tuna purse seiner involves six input parameters, which, while more numerous, are generally easy to obtain for modern vessels. Conversely, the number and accessibility of input parameters for clustering methods pose significant challenges for most vessels. The selection of key parameters for these methods often depends on measurements that capture the six-degrees of motion of the vessel, which are intended to represent the vessel's full dynamics and are difficult to acquire for most commercial vessels.

2.7.2 Mode detection performance

The knowledge-based method generally outperforms clustering methods in detecting operational modes, especially for specific vessel types like tuna purse seiners. Research indicates that the proposed knowledge-based method is the most effective approach for identifying operational modes in such scenarios (Basurko et al., 2022). Swider et al. (2018) also suggest that data clustering is not an optimal strategy for mode detection. Meanwhile, statistical methods have shown promising results; for example, they successfully identified human errors during the verification stage on an OSV (Zaman et al., 2017b). However, validation of these methods can be costly and typically involves comparing detected modes against established domain knowledge.

The operational modes are often predefined based on engineering definitions, and a detailed operational profile for a month is prepared in advance to validate the results, as done in (Swider et al., 2018). Similarly, mode selections made by the crew are used to confirm the accuracy of results in (Zaman et al., 2017b). It should be noted that both the knowledge-based and statistical methods lack a data cleaning procedure, which can result in errors impacting the accuracy of mode detection. This highlights a potential area for improvement in both methodologies, suggesting the need for integrating data cleaning processes to enhance the reliability of detections.

2.7.3 Computational efficiency

Compared to machine learning approaches, knowledge-based and statistical methods generally offer higher computational efficiency. However, an exception is found in the steady-state detection using the rolling window t-test, which involves significantly more calculations compared to state-of-the-art methods (Dalheim and Steen, 2020a).

2.7.4 Limitations

Knowledge-based approaches in operational mode detection require a profound understanding and onboard observations of the target vessel, relying heavily on professional domain knowledge, which can be challenging to acquire in many scenarios. This requirement positions it as less of a data-driven method and more dependent on expert insights, which may not be readily available or applicable across different vessel types or operational contexts.

Statistical methods, while beneficial, come with their own set of assumptions. The process of defining key parameters lacks systematic guidance, such as a sensitivity analysis on these parameters, which can lead to inaccuracies if the chosen parameters do not adequately represent the dynamics being analysed.

Similarly, clustering methods assume that the collected measurements can comprehensively reflect the full dynamics of ship motion in calm waters. A significant limitation of these methods is the uncertainty in the number of clusters to be used, which can complicate the model's ability to accurately segment data into meaningful operational modes.

Despite these challenges, no studies utilising supervised classification methods specifically for operational mode detection were found in the literature reviewed. However, research on detecting fishing activities offers valuable insights that could inform this area of study. A major drawback to adopting supervised classification methods is the absence of a labelled dataset, which is crucial for training accurate models. Nevertheless, the practice of extracting secondary features from latitude and longitude to represent vessel trajectories and the successful implementation of segment-based models, which consider the sequence of coordinates, demonstrate improved performance in detecting patterns. These approaches highlight the effective use of temporal and spatial information from trajectories, suggesting

potential methodologies that could be adapted for operational mode detection in broader maritime research.

After reviewing the literature, it is evident that research on mode detection in maritime operations is still immature, and the specific characteristics and limitations of existing approaches restrict their application, particularly for older vessels. There is a clear need to develop a data-driven method capable of detecting operational modes across various vessel types. High adaptability of the algorithm is a critical challenge in this research.

The external requirements for onboard measurements are relatively straightforward. The basic necessity is for minimal number of input parameters that are already available on most vessels. This ensures the algorithm's adaptability and practicality for widespread use, as reliance on extensive numerical measurements would be impractical for most commercial vessels.

Internally, the characteristics of the methodology are more complex. The developed algorithm must not only offer high computational efficiency and no operation-dependent assumptions but also provide clear guidance on parameter definition to fine-tune the algorithm. Additionally, it should demonstrate robust and reliable detection capabilities with efficient and straightforward validation methods. Only if the algorithm meets these criteria will it be easily applicable to different types of vessels.

To address these challenges, three overarching criteria have been proposed for the algorithm development: minimal input parameters, essential onboard measurements, and adaptability across various vessel types. The detailed methodology to achieve these criteria will be discussed thoroughly in Chapter 3.

Chapter 3 Overall Methodology

As discussed in Chapter 2, the algorithm developed must satisfy three criteria: minimal parameters, essential measurements, and adaptability to various ship types. And the critical point is focusing on the algorithm adaptability which needs to fulfil some requirements from external and internal aspects. In this chapter, the detailed overall methodology will be introduced and describe how the methodology reaches out these requirements.

3.1 Problem Definition

The developed methodology aims to detect operational modes of ships, starting with the intuitive recognition of three basic modes- 'Transit', 'Manoeuvring', and 'Stop'-derived from the author's firsthand experience onboard ships. The characteristics of these modes are as follows:

'Transit' mode involves vessels sailing in a relatively straight-line or rhumb-line pattern with steady state speed, typically in open sea areas.

'Manoeuvring' mode is distinctly different, with both speed and course varying significantly compared to 'Transit' mode. For example, a fishing vessel might navigate in a circular motion to conduct specific fishing activities.

'Stop' mode occurs when vessels are secured at the docks or anchored, characterised by a trajectory that is essentially a single point with duplicated coordinates or minor motions without significant variations.

'Steady state' is defined as the condition in which the variations of key parameters are within a predetermined threshold, reflecting the normal operation of the target vessel. For various types of vessels, these thresholds are determined by the developed objective function and domain knowledge.

It is evident that these intuitive recognitions correlate strongly with the vessels' trajectory patterns: straight-line for 'Transit', circular for 'Manoeuvring', and a single point for 'Stop'. This raises a pertinent question: can operational modes be detected based on vessel trajectory patterns?

3.2 Overarching Criteria

In Chapter 2, three overarching criteria have been identified for this methodology, which pose challenges for the broad utilisation of the developed method within the field. These criteria are minimal input parameters, essential measurements, and adaptability to various vessel types.

Vessel trajectory would be a suitable target to meet these criteria. For the first criterion, the trajectory comprises a time series of coordinates recording the vessel's position through latitude and longitude, along with corresponding time stamps, implying that the primary input variables are latitude and longitude. Secondly, these measurements, typically derived from GPS devices such as the AIS system which records coordinates every 6 minutes, are fundamental and readily available for most vessels.

Lastly, it is complex and impractical to detect and validate mode detection results across all vessel types. This criterion will be further explored in the construction of the algorithm, and the algorithm's adaptability will be tested through case studies. However, it is clear that each specific vessel has its own trajectory, which can, to some extent, reflect its operational activities. Therefore, the strategy of the proposed methodology has been articulated through analysing the vessel's trajectory to detect operational modes. By integrating the temporal and spatial contextual information from the coordinates, further insights can be extracted that are linked to the vessel's operational modes.

3.3 Parameter Selection

Beginning with the intuitive recognition of the 'Transit' mode - where the vessel navigates in a relatively straight-line pattern at a steady state speed - it becomes apparent that the first essential parameter is speed. In this thesis, the first key parameter identified is 'SpeedLL', which denotes the speed derived from latitude and longitude. According to Equation3.1, SpeedLL is calculated for each data point using the corresponding consecutive coordinates. Furthermore, SpeedLL provides valuable insights into the general operational status of the vessel's propulsion system.

$$SpeedLL = \frac{Distance\ between\ consecutive\ coordinates}{Time\ interval} \quad 3.1$$

In the methodology employed in this research, SpeedLL, is chosen over Speed Over Ground (SOG) for several critical reasons. Firstly, notable discrepancies between SpeedLL and SOG were observed in the dataset, as outlined in Section 3.4.1. Additionally, the analysis of this speed difference facilitates the development of a data cleaning strategy that effectively filters out anomalies in coordinates, ensuring higher accuracy in mode detection.

Secondly, integrating SpeedLL with the Curvature parameter, with both derived from the same set of coordinate data, is essential for comprehensively assessing operational modes. This method ensures that the correlation between SpeedLL and Curvature is maintained, thereby enhancing the reliability of the operational mode analysis. By deriving both parameters from the same data points and ensuring that the timestamp of SpeedLL matches with the Curvature, it becomes feasible to define appropriate rolling window combinations that more accurately reflect changes in operational modes. In essence, the algorithm is predicated on the assumption that SpeedLL and Curvature will exhibit variations simultaneously when the operational mode changes. This can be understood as the time-series coordinates influencing or varying in accordance with different operational modes. Consequently, when detecting operational modes, the algorithm utilises two metrics—speed and curvature—providing a dual-faceted approach to mode detection. This contrasts with relying solely on one measurement, such as curvature, for detecting different operational modes, which would be the case if using SOG instead of SpeedLL.

The subsequent challenge involves efficiently linking sets of coordinates to the vessel's trajectory. In geometry, curvature is utilised to describe the degree to which a curve deviates from being straight or a curved surface from a plane. Therefore, calculating the curvature from coordinates presents an efficient method to assess the vessel's trajectory. Consequently, the second key parameter identified is 'Curvature', also derived from coordinates. It is important to note that the concept of geometric curvature is employed here not in comparison to a straight line but to gauge the extent of turning relative to the previous data point.

In this methodology, 'Curvature' is defined as the angle through which the vessel turns per unit distance travelled, expressed in radians per metre (rad/m). Following the calculation of

SpeedLL, it becomes straightforward to determine the bearing and distance between each pair of consecutive coordinates. The ratio of bearing change to distance travelled represents the curvature, effectively quantifying the rate at which the vessel is diverging from its previous course.

For a sequence of three consecutive coordinates, the curvature at the middle point is calculated based on the change in bearing between the two segments formed by these coordinates, divided by the distance covered. Equation3.2, which is used to derive the curvature for the middle point in a trio of coordinates, is outlined as follows:

$$Curvature = \frac{Difference\ (Bearings)}{Average\ (Distance)} \qquad 3.2$$

In this methodology, the bearing is defined as the direction to a target point relative to its predecessor, measured in radians from true north. The difference in bearings between consecutive segments indicates the angle by which the middle point deviates from the preceding one. To minimise calculation errors, the average distance between points 1 to 2 and 2 to 3 is employed.

It is crucial to note that bearings are directional, measured from 0 to 2π radians clockwise from true north. Consequently, the calculated curvature, which reflects this directional nature, also exhibits directionality. However, its absolute value, starting from 0 rad/m, indicates no directional change from the previous point. Thus, a straight-line pattern can be described as a sequence of coordinates where curvatures are close to zero, reflecting minimal directional changes.

This method provides an approximate calculation of curvature, and while numerous other methods for estimating of a horizon's curvature that might offer more precise estimations (Bergbauer and Pollard, 2003), this particular approach has been selected based on considerations from two aspects.

Firstly, this method of calculating curvature is significantly easier to compute compared with other methods. Alternative approaches often require the conversion of raw spherical coordinates into a planar coordinate system for accuracy or necessitate the computation of

the first and second derivatives or the radius of a perfect circle derived from the trio of coordinates (Roberts, 2001). Although these calculations could theoretically yield more precise results, the difference is generally minimal due to the proximity of the trio of coordinates. The distance between consecutive coordinates is determined by the related time interval and the vessel's speed, which, in the case of ships, are typically small.

The second consideration is arguably more crucial. This curvature calculation maintains the integral relationship between SpeedLL and Curvature, as both parameters are derived from the same essential calculations - distance and bearing extracted from the coordinates. This interconnectedness is vital for the developed methodology to ensure consistency across derived data from the same original coordinates. In the first case study detailed in Chapter 4, alternative methods of curvature calculation were tested on an ocean-going car carrier, where the time interval was 6 minutes - substantially longer than the intervales used in subsequent case studies discussed in Chapter 5 and 6, which featured intervals of 1 and 4 seconds, respectively. Consequently, the distance between consecutive coordinates in this case was much greater. Nevertheless, this method demonstrated significant efficacy in mode detection.

Two key parameters, SpeedLL and Curvature, serving as a bridge between coordinates and two distinct operational modes. The third parameter concerns the running status of the main engine (ME), straightforwardly indicating the 'Stop' mode - whether stopped or running. As the purpose of this parameter is solely to reflect ME status, it could involve any available measurements depending on specific cases, such as ME power, %MCR (Maximum Continuous Rating), fuel consumption, or even Speed Over Ground (SOG).

3.4 Overall Mode Detection Methodology

Figure 3.1 presents the flowchart of the developed methodology, which comprises six steps. The first step, data processing, mainly involves leveraging the author's onboard experience and domain knowledge to filter out anomalous coordinates. The second step involves the selection of an exemplary sub-dataset, which requires a deep understanding and observation of the processed datasets.

Subsequent steps, including sensitivity analysis and the definition of thresholds, primarily employ statistical methods to detect 'Steady State' and 'Changing' conditions. The mode detection step utilises binary categorisation, incorporating extensive domain knowledge. This

knowledge, along with associated research interests, guides the selection of key parameters and the reconstruction of the binary detection framework to further classify operational modes.

The final step employs graphic presentation to validate and present the test results in a cost-effective manner, ensuring that the detected operational modes align with the domain knowledge derived from observations of the vessel's trajectory.

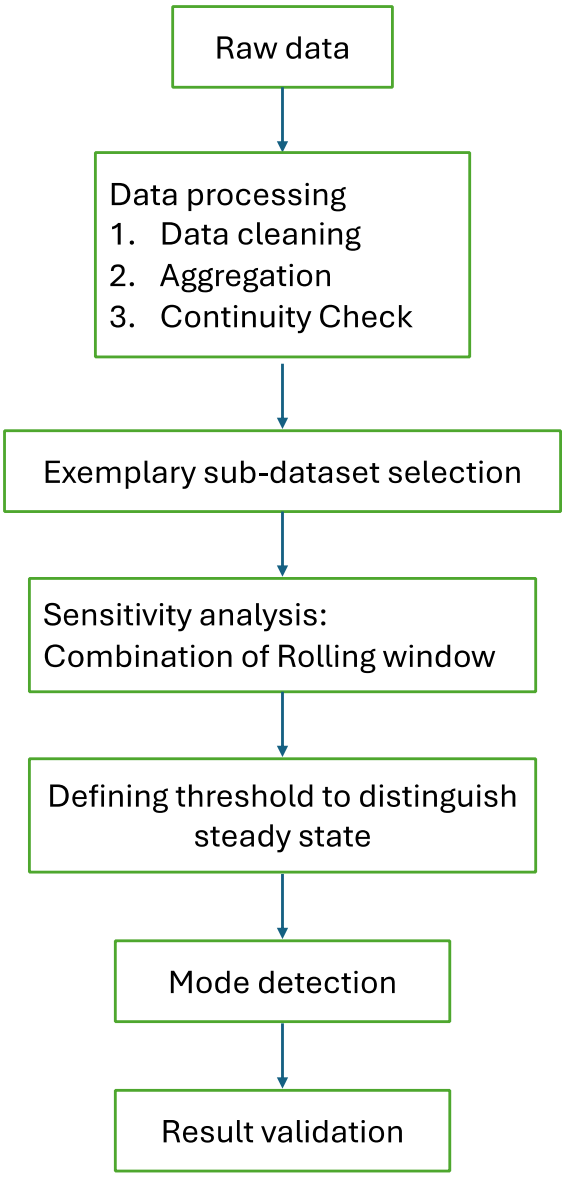

Figure 3.1 The flow chart of the methodology

3.4.1 Data processing

It is crucial to perform data cleaning to ensure the accuracy of subsequent analyses. Initially, duplicated timestamps and missing values, labelled as Not a Number (NaN), must be eliminated. Following the calculations of the two key features using Equations 3.1 and 3.2, instances of SpeedLL with extremely high values were identified.

However, it is essential to recognise that the malfunction of GPS devices does not occur merely at the moment when these extreme values are recorded. Instead, the time series of

coordinates, which tracks the vessel's trajectory, indicates that while the recorded SpeedLL values are unrealistic, the vessel did indeed travel from location A to B, albeit not as recorded by the GPS. Therefore, the data cleaning strategy should not solely focus on the extreme values of SpeedLL but rather on addressing the inaccuracies in the distance anomalies.

Upon detailed examination, extreme data points often result from the accumulation of minor deviations among sets of nearby coordinates. This generally occurs when GPS systems fail to accurately record positions over a period, logging coordinates with only minor differences despite actual movement. When normal GPS functionality resumes and records the accurate position, the sudden apparent distance between previously recorded and actual locations highlights these accumulated inaccuracies.

Consequently, the focus of the data cleaning strategy should be on these minor inaccuracies or instantaneous deviations from the GPS, rather than solely on SpeedLL, since the extreme values are a result of accumulated deviations. To assess these minor inaccuracies, another feature, SOG, measured by GPS, has been introduced. The discrepancy between SOG and SpeedLL, ideally close to zero, indicates the accuracy of GPS recordings. The distribution of the speed difference, as further explored in subsequent chapters through three case studies, support this, being symmetric and highly concentrated around zero knots with high kurtosis and heavy tails.

Given the characteristics of the dataset and the distribution of speed differences, the 1.5 times Inter Quartile Range (IQR) technique (Tukey, 1977) has been employed to identify and exclude outliers. This selection is predicated on the non-parametric nature of the technique, which relies solely on the 25th and 75th percentiles of the data. This method is particularly advantageous as it is not susceptible to extreme values or noise, making it especially suitable for this analysis. The specifics of the 1.5 IQR technique are detailed in Equation 3.3.

$$x_i = \begin{cases} normal, if\ x_i\ within\ the\ band\ [Q_1 - 1.5IQR, Q_3 + 1.5IQR] \\ outlier, otherwise \end{cases} \qquad 3.3$$

$$x_i = \mathrm{SOG} - \mathrm{SpeedLL}$$

$$IQR = Q_3 - Q_1$$

In this equation, x_i represents the difference between SOG and SpeedLL, expressed in knots. Q1 and Q3 correspond to the 25th and 75th percentiles of this speed difference, respectively. Speed differences that fall within the 1.5 IQR band are considered normal, while those outside this range are classified as outliers and subsequently eliminated from the dataset.

3.4.2 Data aggregation

The raw time series coordinates have been segmented through the elimination of detected outliers, resulting in the vessel's overall trajectory being divided into multiple segments or isolated points. Consequently, the data continuity is substantially disrupted, a direct consequence of the outlier detection strategy. However, maintaining continuity is crucial for the developed methodology, as it underpins the accurate extraction of the two key features by ensuring that the coordinates remain continuous and that the time interval remains consistent across all calculations. For instance, the calculation of the two key features relies on consistent time intervals between data points as specified in equations 3.1 and 3.2. If a data gap occurs—for example, a one-hour gap when the typical data interval is six minutes—the calculations become skewed because the time interval used to determine speed or direction would incorrectly assume continuous data collection over that hour. This leads to significant errors in speed calculation and, consequently, in the detection of operational modes. Such discrepancies undermine the accuracy of the analysis, emphasizing the importance of maintaining data continuity throughout the dataset. Continuity is also critical in the subsequent mode detection process, as will be discussed later.

To mitigate the loss of continuity and preserve most of the information in the cleaned dataset, a data aggregation strategy employing averaging techniques was implemented. This approach involves calculating the average value of the cleaned data points within an enlarged time scale, representing the aggregated data point. Thus, despite the original continuity being compromised by outlier removal, the aggregated dataset can remain continuous, provided there are some data points within the aggregated time scale. A break in the original dataset larger than the defined magnified time scale would result in discontinuities in the aggregated

dataset. Moreover, this strategy also serves to smooth the impact of noise and enhance computational efficiency in subsequent analyses.

The applicability of this strategy, however, depends on the frequency of the raw data. The raw information diminishes as the magnified time scale expands. For instance, this technique was not applied in the first case study (presented in Chapter 4), where the time interval was already 6 minutes. Further aggregation would risk diluting the valuable information by potential extending the intervals. However, it was employed in the second and third case studies (Chapters 5 and 6), where the time intervals were 1 and 4 seconds, respectively. The enlarged time scale may be adjusted according to the specific characteristics of the raw dataset. The time scale in these two case studies for aggregation is 15 seconds, which provides a suitable balance between maintaining continuity, preserving raw information, and optimising computational efficiency, as employed in the second and third case studies.

3.4.3 Continuity check

After abovementioned data cleaning procedures, the raw continuous data set was segmented into multiple sub-datasets by the removing of the outliers. As previously mentioned, the primary focus of the data cleaning strategy is on distance anomalies which can be viewed as segment outlier detection. However, the 1.5 IQR technique primarily targets point outliers. In this context, checking the continuity of sub-datasets is an effective method to address this discrepancy.

A threshold size can be defined to further cleanse the sub-datasets; any datasets with a data count below this threshold would be disregarded. This can be understood as follows: after removing outliers using the 1.5 IQR technique, smaller segments lacking sufficient continuity or data length, as defined by the threshold, would be eliminated. This process of segment removal compensates for potential issues arising from these smaller segments, which might be part of the distance anomaly phenomena. For instance, they could be located between locations A and B, with the vessel sailing at a slow speed during this interval, thereby minimising the speed discrepancy within the normal 1.5 IQR band. Moreover, these sub-datasets should also be removed due to the lack of data points for subsequent analysis.

The defined size for the Continuity Check must be synchronised with the sensitivity analysis involving the combination of a rolling window, which will be discussed in Section 3.5.2.2. The

rationale and application of the Continuity Check encompass various aspects, but in this section, it is primarily employed to eliminate small segments. This defined size is considered the minimum requirement for conducting the subsequent mode detection algorithm. After completing the data cleaning process, the raw dataset will be transformed into several continuous sub-datasets, serving as inputs for the developed algorithm.

3.5 Algorithm for Operational Mode Detection Using Binary Categorisation

3.5.1 Concept of the algorithm

The analysis progresses to the next step following the data cleaning process, which can be referred to the Figure 3.1 is to express the operational modes through the key features.

The intuitive recognition of 'Transit' and 'Manoeuvring' serves as the starting point of the methodology. When comparing these two modes, significant contrasts are evident in the conditions for the two key features identified. In 'Transit', SpeedLL is in a relatively steady state; conversely, it exhibits variations during 'Manoeuvring'. Regarding Curvature under 'Transit' mode, the vessel navigates in a relatively straight-line pattern. This 'straight-line pattern' implies that the turning of the vessel is not significant, hence Curvature is close to zero, also maintaining a steady state condition, but it changes significantly during the 'Manoeuvring' mode.

From this initial analysis, the binary condition, 'Steady state' and 'Changing', emerges as the bridge connecting the two key features with the operational modes. Both SpeedLL and Curvature are in 'Steady state' during 'Transit' mode but are 'Changing' during 'Manoeuvring'. Additionally, the status of ME for these two modes is active, which is distinct from the 'Stop' mode.

For the 'Stop' mode, the situation can be summarised as the ME being stopped, with both SpeedLL and Curvature under 'Steady state' conditions. Intuitively, when the vessel is moored, its trajectory reduces to a single point, and SpeedLL and Curvature remain constant at zero, without significant variations. If it is at anchor, then there may be some minor motions.

This analysis reveals a binary relationship among these three key features, which corresponds to the three operational modes. To clearly express the correlations between the binary

conditions and the three key features, each condition has been assigned a binary label ‘0’ and ‘1’. The details can be found in Table 3.1.

Table 3.1 Correlations between binary conditions and three key features

Binary label	ME status	SpeedLL	Curvature
0	Stopped	Steady state	Steady state
1	Running	Changing	Changing

Based on the binary correlations presented in Table 3.1 and maintaining the sequence of three features as ‘ME’ - ‘SpeedLL’ - ‘Curvature’, the operational modes are distinctly categorised. ‘Transit’ mode is encoded as ‘1 - 0 - 0’, indicating that the ME is running, SpeedLL and Curvature is steady. ‘Manoeuvring’ mode is represented by ‘1 - 1 - 1’, where the ME is running, and both SpeedLL and Curvature exhibit significant variations. Conversely, the ‘Stop’ mode is encoded as ‘0 - 0 - 0’, reflecting that the ME is stopped, and both SpeedLL and Curvature remain constant at zero or without significant variations. These binary encodings effectively express the operational modes through the key features. An example of how the ‘Transit’ mode is connected with these key features is illustrated in Figure 3.2.

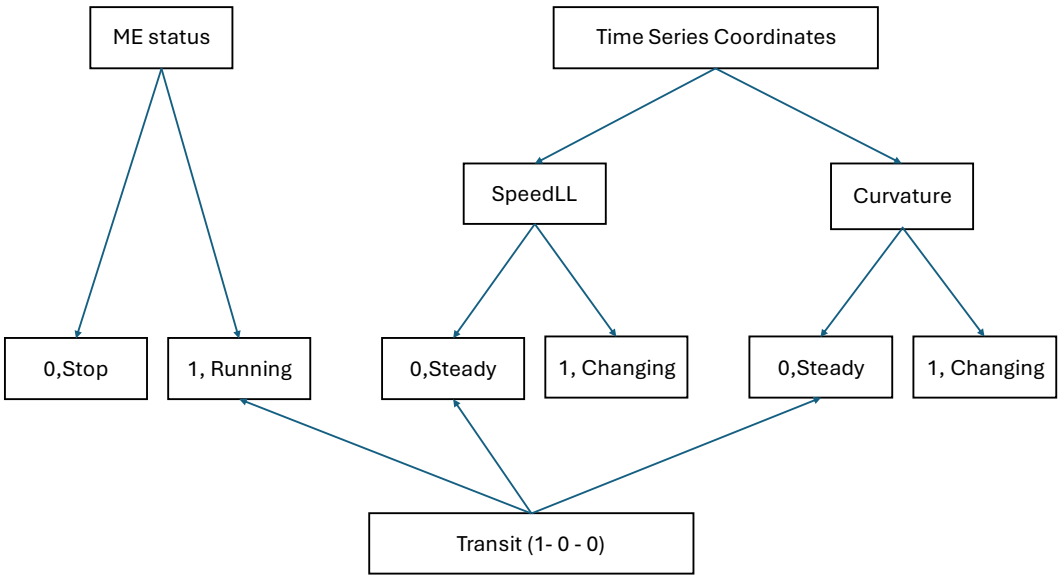

Figure 3.2 An example of linking Transit mode with key features

3.5.2 Steady state detection

The primary challenge of this methodology is the detection of the 'Steady state' for SpeedLL and Curvature. Since the input consists of several continuous sub-datasets, this can be understood as a question of detecting change points within a set of data points. Numerous data-driven methods have been proposed in the literature to address this issue (Blázquez-García et al., 2021, Aminikhanghahi and Cook, 2017). However, a universal threshold strategy has been selected for this methodology (Zaman et al., 2017b, Trodden et al., 2015). This choice is driven by the practical considerations of applying the detection algorithm repeatedly across the number of cleaned segments. A universal threshold simplifies calculations: values below the threshold indicate a 'Steady state', while values above are classified as 'Changing'.

Furthermore, the conditions of the two operational modes - 'Transit' versus 'Manoeuvring'- are quite distinctive, making it relatively intuitive and straightforward to identify visualised change points (VCPs) through observation, an example can be checked in Figure 4.6 and Figure 4.7. However, when examining the results of the tested data-driven methods, for instance, change point detection methodologies such as maximum likelihood techniques, statistical hypothesis testing methods, and machine learning clustering techniques has been tested, the detected change points (DCPs) do not align closely with the VCPs. Although tuning could mitigate these differences, it is complicated and impractical to tune the algorithm repeatedly for all the sub-datasets. Therefore, a universal threshold strategy has been adopted to detect the 'Steady state' condition.

3.5.2.1 Selection of exemplary sub-dataset

Following the universal threshold strategy, the selection of an exemplary sub-dataset is crucial for the subsequent analysis. This requires balancing the inclusion of maximum data and maintaining 'Transit' continuity, while capturing as many operational mode changes as possible. Ideally, the dataset should record extended 'Transit' mode durations along with several operational mode changes necessary for the algorithm to differentiate 'Steady State' from 'Changing' conditions. This is a small sub-dataset of the voyage, and the exemplary data is used to determine the VCPs; subsequently, the thresholds of key parameters are defined by the objective functions. These defined thresholds will be utilised across the dataset to further detect the operational modes.

The threshold defined from the exemplary dataset appears robust and universally applicable across all sub-datasets, as evidenced by the results from three case studies. This may be attributed to the simplicity of the binary categorisation, where the threshold's sole purpose is to determine what is 'Steady state'. Although each specific vessel exhibits unique sailing characteristic influenced by metocean conditions in which it is operating, resulting in numerous changes and variations across operational modes, the 'Steady state' here can be approximately as a comprehensive condition that captures all internal and external influences. Essentially, the algorithm captures a singular comprehensive condition that represents the normal navigation state for a specific vessel, which is unique and can be extracted from the exemplary dataset.

In essence, the algorithm concentrates solely on detecting the steady state of normal operation, rather than attempting to discern variations within each condition. For example, it does not evaluate or define the extent of variation during transit, slow streaming, or manoeuvring. If a vessel remains in a slow streaming condition for an extended period, this data will be classified as 'Steady State'. Slow streaming could be considered an internal influence affecting the target vessel. This 'Steady State' condition is unique to each target vessel, as it reflects the vessel's natural response to both internal and external influences. Regardless of changes in external metocean conditions or internal machinery and operational conditions, the vessel consistently exhibits a normal 'Steady State' condition, which is repeatedly manifested during each voyage. This condition can be identified from the exemplary sub-dataset, allowing the defined key parameters and thresholds to be effectively applied across the entire dataset. Other operational modes are identified through the subsequent binary classification based on the 'Steady state' detection results.

Selecting an exemplary dataset poses a challenge across the three case studies due to the diversity of vessel types. This requires familiarity with each vessel's characteristics and a basic understanding of its operational modes. The method of selection will be detailed in each case study, providing a deeper understanding based of the specific scenarios and offering insights applicable to other types of vessels.

3.5.2.2 Sensitivity analysis on the combination of rolling window

As previously mentioned, the visualisation technique is highly effective for analysing vessel characteristics. The detection and rationale of VCPs will be demonstrated through three case

studies, illustrating the broad applicability and efficiency of the visualisation technique across various vessel types. Most importantly, the VCPs can segment the trajectory, aligning closely with the graphical representations based on intuitive recognition of the operational modes.

The flowchart of the sensitivity analysis is illustrated in the Figure 3.3.

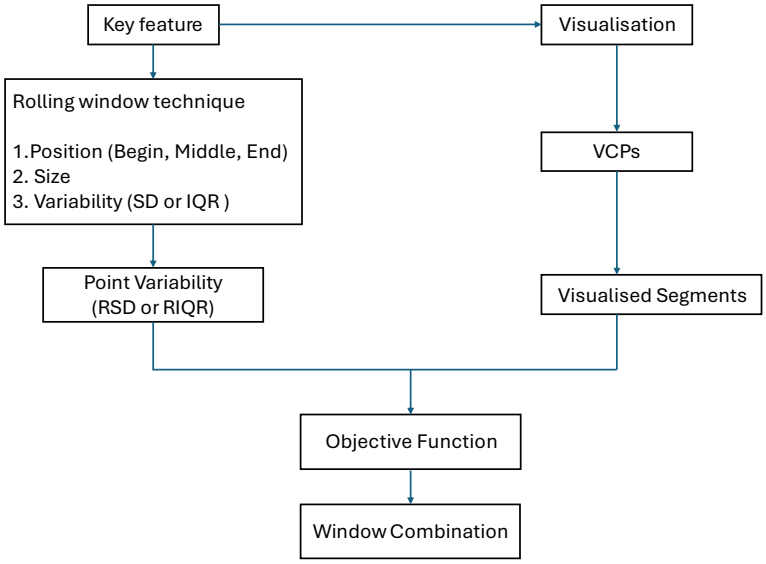

Figure 3.3 Flowchart of the sensitivity analysis on the window combination

The central challenge of the developed algorithm is how to implement this visualisation technique mathematically. Furthermore, VCPs are crucial for tuning the algorithm and defining the threshold, minimising the corresponded discrepancies between DCPs & VCPs.

After selecting the exemplary dataset, VCPs are identified by observing variability across the dataset, segmenting it into several segments under binary conditions: ‘Steady state’ and ‘Changing’. The ‘Steady State’ condition is characterised by relatively consistent and low variability within the segment, whereas the ‘Changing’ condition exhibits higher variability. From an operational perspective, the vessel’s speed and curvature fluctuates between these two conditions, alternating between steady states and periods of change. This fluctuation indicates shifts in the vessel’s operational modes corresponding to the delineated segments. The critical task is to test and ensure the visualised segments align well with the graphical representations.

Recognising that the VCPs originate from an overarching analysis of the entire dataset, this broad observation sets the stage for identifying segments with lower variability. However, to

refine the analysis further, focusing on variability for each data point becomes essential. It logically follows that the variability for each data point within visualised 'Steady state' segments would exhibit relatively low fluctuations. Therefore, applying the threshold to the variability of each data point clearly distinguishes the binary conditions: data points whose variability falls below the threshold confirm their 'Steady state' classification, while those above it are classified as 'Changing'. Consequently, the analysis progresses to evaluating the variability for each data point.

The variability of individual points is not immediately apparent but is instead understood through their comparison with neighbouring points. This comparison is crucial in establishing the local context of each data point. A data point with high variability suggests that it significantly diverges from its neighbours, indicating a potential change. Conversely, low variability implies a degree of similarity or consistency with surrounding data points. To effectively evaluate variability for data points, the rolling window technique is employed, which addresses this need by comparing each data point against a dynamically chosen set of neighbours within the window.

This method is particularly effective for analysing non-stationary time series data, such as SpeedLL, which exemplifies how data can vary with the vessel's operational modes. These modes, largely determined by crew operations tailored to specific tasks, reflect the vessel's purpose and are heavily influenced by human actions, changing over time.

A critical aspect of implementing the rolling window technique is selecting the optimal window, or the local context, for this analysis. This selection necessitates a sensitivity analysis to determine the combination of rolling window settings that best captures the necessary variability. The selection of the window combination should consider two key aspects: not only the window size, but also the location of the target point within the window. The location can be categorised into three positions: 'Begin', 'Middle', and 'End'.

The 'Begin' position places the target point at the start of the rolling window, meaning each new data point is compared with a subsequent set of data points, excluding proceeding data from the window.

The 'Middle' position ensures an equal distribution of preceding and succeeding data points around the target, offering a more balanced and accurate evaluation of its variability. This

setting provides a comprehensive view of the changing patterns, capturing both past and immediate future contexts.

The 'End' position involves comparing the target data point with proceeding points, positioning it at the end of the window.

Furthermore, the sensitivity analysis should also consider the method used to evaluate data variability. In statistical analysis, several methods are commonly employed to assess data variability, each offering unique insights into the dispersion of values within a dataset (Whitley and Ball, 2001). In this study, SD and IQR were chosen for their distinct advantages in assessing variability (Livingston, 2004). The SD, measured in units consistent with the vessel speed (knots), offers a physically meaningful interpretation of how far data points deviate, on average, from the mean speed. The IQR, which uses the same unit as the SD, provides a robust measure of the middle 50% spread of the data, less influenced by outliers compared to the range.

Consequently, the sensitivity analysis of the rolling window combination should incorporate three critical elements: the position of the target point within the window ('Begin', 'Middle' and 'End'), the window size, and the chosen method for evaluating variability (SD and IQR).

To conduct the sensitivity analysis, an objective function has been developed to determine the combination that validates the VCPs and maximises the value of the objective function.

The objective function is defined as:

$$Objective\ Function = B - A - C \tag{3.4}$$

$$B = Sum\ of\ Absolut\ Differences(SD(RSD)\ or\ IQR(RIQR))$$
$$A = Sum(SD(RSD)\ or\ IQR(RIQR))$$
$$C = Average\ of\ Absolut\ Differences\ of\ Variability\ Changes$$

In equation 3.4, SD (RSD) and IQR (RIQR) represent two methods for evaluating the variability of visualised segments, with RSD and RIQR standing for Rolling Standard Deviation & Rolling Inter Quantile Range, respectively.

A. Sum of Variability in Steady State Conditions:

This component aggregates the variability within segments categorised as 'Steady State.' It provides a baseline understanding of intrinsic fluctuations in these segments, where minimal change is anticipated. This measure is crucial for assessing the stability of segments presumed to be in a state of relative constancy.

B. Cumulative Difference in Consecutive Segment Variability:

This metric totals the differences in variability between consecutive segments. It plays a key role in corroborating the change points identified visually. A significant variability gap between adjacent segments suggests a notable shift in segment dynamics, thereby reinforcing the logic behind the visualised change points.

C. Consistency of Variability Changes Across Segments:

The third component evaluates the uniformity of variability shifts throughout the dataset. It measures the extent to which variability changes between successive window size configurations for each segment. This involves comparing the variability metrics derived from two adjacent window size combinations for each segment. The average of these comparative differences is calculated to determine the consistency across the dataset. A lower average difference indicates greater consistency, suggesting that a specific window size configuration provides variability estimates closely aligned with those of its adjacent configurations.

The development of this objective function is based on integrating the visualised technique into programming. Variability is key in this analysis, and the concept of operationalising this technique can be simply expressed as adjusting the variability context, from an overall perspective to a local one and then back to overall.

The VCPs are identified by observing the variability across the dataset, while RSD or RIQR is calculated from a local context for each data point, and subsequently, the objective function is developed from the overall context once again, where its context is the segments divided by VCPs. This approach to developing the objective function, is the method to implement the visualised technique in programming, by defining the appropriate combination to validate the rationale of VCPs, maximising the difference of binary conditions, minimising the variability of 'Steady state', and ensuring the consistency of window size.

It is important to note that the objective function focuses on the stabilisation of point variability (RSD or RIQR) rather than merely achieving smaller values under 'Steady state' condition. A smaller value indicates that the target point is similar within the window, and each point has its own window. Stabilisation investigates this similarity; how similar it is or what the corresponding window looks like. These windows should also be nearly the same when they are in 'Steady state'. Consequently, each rolling window is linked together, the scale of similarity check would increase sequentially with sliding, and the local context of the variability expands from the defined window size across the dataset.

The objective function can provide the optimal combinations with the highest values for two features separately. However, the final selection should be consistent across both features. The rationale for choosing the same combination is to maintain consistency in the rolling window combination, including position and size, for both SpeedLL and Curvature analyses. Since both variables are derived from the raw coordinates, this approach ensures that the point variability derived from the raw coordinates for these two features is synchronised. Maintaining the same local area for analysis is crucial to preserving the potential informational and correlational integrity between them and ensuring that any inherent relationships or patterns present in the dataset are not disrupted by varying analytical parameters.

To synchronise the window combination, some adjustments are necessary based on the results of the objective function. The detailed selection process will be discussed in the three case studies.

Additionally, the manoeuvrability of the target vessel will be considered when defining the window size. From an operational perspective, changes in operational modes do not occur instantaneously; they require a finite time to be fully completed. This manoeuvrability can thus be expressed in terms of how quickly the target vessel can complete a mode change to a normal operation, Transit mode.

Given that the window size is crucial for assessing point variability within a local context, it helps determine if a target point significantly deviates from nearby points. If so, its variability exceeds the threshold, indicating that the operational mode has changed. Moreover, the defined window size should robustly validate the VCPs, which are optimal in capturing the necessary variability. Therefore, linking the window size with the time interval to the brief period required for mode transitions is essential. In practice, the window sizes defined in the

three case studies reflect this principle: approximately 30 minutes for an ocean-going car carrier, 10 minutes for a tuna purse seiner, and 5 minutes for an inland tanker, each aligning with the manoeuvrability characteristics of the respective vessel type.

3.5.2.3 Defining the threshold

The next step involves setting a range of thresholds and systematically comparing DCPs at various threshold levels with the VCPs. The aim is to select a threshold that minimises discrepancies between these two sets of change points.

A Continuity Check is crucial to validate the DCPs, meaning that the condition of a change point must be consistent with the data points in the subsequent window size; otherwise, this change point will be disregarded, and its condition will be adjusted to match the previous one.

As previously mentioned, the vessel cannot complete an operational mode change instantaneously; it requires a brief period to complete this transition. In this methodology, the data points within the subsequent window size are linked to the time needed for the vessel to complete this transition process. Data points within this transitioning period are treated as the end of the previous mode. Therefore, if a change point fails this Continuity Check, its condition must be modified. The check ensures that the mode has indeed changed, disregarding any change points that fall within the transition period or noise on the GPS data.

The universal threshold is established through the Continuity Check and systematic comparisons between DCPs & VCPs.

3.5.3 Binary classification

The rolling window technique based on the defined combination, thresholds and Continuity Check are utilised across all datasets. Three key features are categorised into binary conditions, resulting in a total of eight possible combinations for all data points. Each combination would represent one operational mode, with the combination code ranging from 0 to 7, reflecting the binary-to-decimal conversion system. The details are shown in the Table 3.2.

Table 3.2 Combination of three key features

Combination code	ME status	SpeedLL	Curvature	Operational modes
0	0	0	0	Stop
1	0	0	1	
2	0	1	0	
3	0	1	1	
4	1	0	0	Transit
5	1	0	1	
6	1	1	0	
7	1	1	1	Manoeuvring

In Table 3.2, eight combinations are listed, each group of data points would represent one operational mode. For example, combinations 0, 4 and 7 correspond to the 'Stop', 'Transit' and 'Manoeuvring' modes, respectively, as discussed in Section 3.5.1. However, this categorisation serves merely as an example to illustrate the construction of this methodology and the mathematical categorisation of data points. Depending on the characteristics of the vessel type, some categories may be combined or disregarded; for instance, the combination 5, 6 & 7 are treated as 'Manoeuvring' for the ocean-going car carrier in the first case study presented in Chapter 4.

Moreover, both the selected key features and the binary conditions are flexible and can be adjusted according to different types of vessels and specific research interests. Figure 3.4 illustrates the overall structure of this methodology.

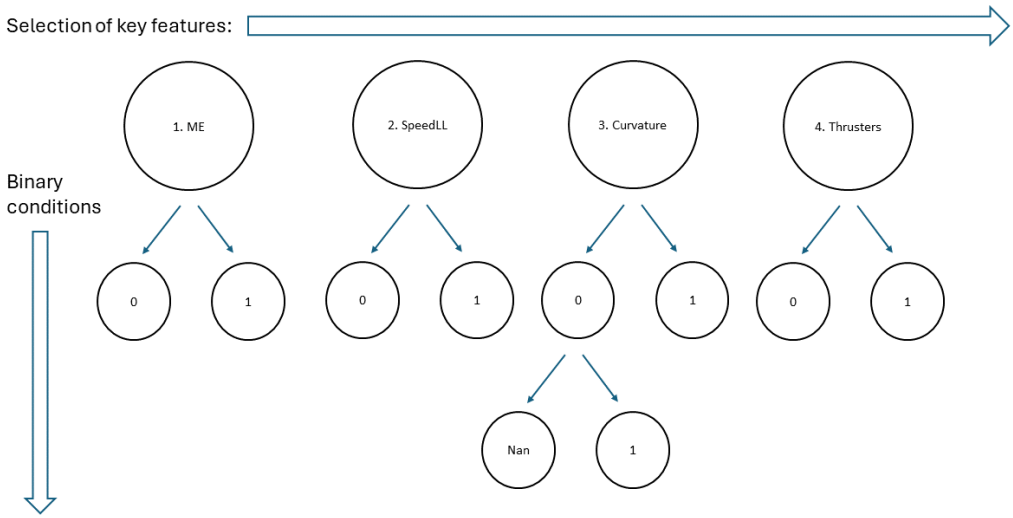

Figure 3.4 Overall structure of the developed methodology

The utilisation of minimum and essential input parameters forms one of the overarching criteria of this methodology, emphasising adaptability and cost-effectiveness. The algorithm's simplicity enhances its adaptability across various vessel types. Notably, older vessels often lack the capability to provide costly measurements, making this approach particularly advantageous for such cases.

Furthermore, the construction of the methodology for binary categorisation is highly flexible, tailored to specific research goals and informed by profound domain knowledge. Key measurements can be adjusted both horizontally and vertically; as shown in Figure 3.4, examples include monitoring the running status of auxiliary thrusters, the running number of auxiliary engines, if the vessel is operating during the day or night, and port call data. The integration of these additional features broadens the applicability and enhances the detection capabilities of the developed methodology.

Two directions of adjustment are illustrated in Figure 3.4. Horizontally, the selection of the key features is adaptable; for example, the running status of thrusters can be added. This is relevant for the target tuna purse seiner in the second case study (Chapter 5), which has two auxiliary thrusters providing propulsion power while the ME is stopped for specific fishing events or overnight drifting. Conversely, for the target inland tanker in the third case study

(Chapter 6), the key features are limited to ME and SpeedLL, omitting the analysis of Curvature due to navigation routes being restricted by the complex shape of the inland waterways.

Vertically, the binary conditions are flexible. Initially, the results of the Curvature calculation included some NaN values because, according to the Equation 3.2, the average distance between a trio of coordinates is zero. Dividing by zero gives NaN, indicating the vessel is stationary with identical coordinates. Since distinguishing between stationary and drifting conditions, with minor movements, is not the key research interest, these NaN values were categorised as ‘0’, aligning with the ‘Steady state’ definition for periods when the vessel is stationary and there is no variation in both SpeedLL and Curvature.

However, for specific purposes, after initial detection, the data points under the 'Steady State' condition can be further categorised, as illustrated in Figure 3.4, as 'NaN' and '1', or '0' and '1'. Here, 'NaN' indicates that the vessel remains stationary, not moving from its position, while '1' represents minor movements, such as drifting, thus exhibiting contrary binary relationships.

Following this concept, the developed methodology can be applied to various types of vessels, fulfilling the third criterion of the algorithm. It is important to note that some key features may not be available, which presents challenges in detecting all operational modes for specific vessels. For instance, for fishing vessels, operational modes such as fishing events often require the main engine to be switched off while the vessel is propelled by auxiliary thrusters. This specific requirement means that detecting all operational modes becomes challenging without access to data on the running status of these auxiliary thrusters. Nonetheless, this approach can still facilitate the detection of data points under one or two particular operational modes. For instance, in the second case study, ‘Transit’ mode is the primary focus, detected solely to predict fuel consumption.

Following the binary classification, the operational modes are detected by the developed algorithm.

3.6 Results Validation

The validation of results is straightforward and intuitive, employing graphical representation to visually confirm the outcomes. Following the detection process, coordinates associated with each operational mode are assigned specific colour. This visual differentiation makes it

distinctly clear and intuitive to observe the detected modes and their corresponding segments along the trajectory.

Furthermore, the graphical representations serve to verify whether the patterns of detected segments align with domain knowledge. For example, segments classified under 'Transit' mode typically exhibit a relatively straight-line pattern in open sea area. Detailed explanations and illustrations of these graphical representation will be provided within the three case studies.

Additionally, the algorithm's adaptability has been rigorously tested through three case studies. The third overarching criterion - adaptability across various ship - is crucial. Although it is impractical to test every type of ship, the focus has been on assessing adaptability across different navigation areas. The first two case studies evaluate performance in open sea area, while the third case involves an inland tanker. The successful application of this methodology across these diverse navigation areas indicates its potential adaptability from open seas to inland waterways.

3.7 Summary

In this chapter, the detailed methodology developed to detect operational modes in maritime shipping was explored, focusing on minimal parameters, essential measurements, and adaptability across various vessel types. The chapter began with a definition of the problem, identifying three basic operational modes—Transit, Manoeuvring, and Stop—based on the author's firsthand onboard experience. The operational characteristics of each mode were outlined, establishing the basis for the tailored algorithm.

The core of the methodology revolves around the innovative use of SpeedLL and Curvature, parameters derived from the time series coordinates. This approach ensures that trajectory data maintains its continuity, which is crucial for accurate mode detection, despite challenges such as data gaps and outliers which could disrupt computational integrity. By maintaining data continuity, the methodology enhances the accuracy of the mode detection process, thereby facilitating effective operational mode analysis across various types of vessels.

Furthermore, the chapter explored the challenges of applying this methodology universally due to the variability in vessel operations and the specific requirements of different ship types.

Lastly, the results can be validated using a straightforward graphical representation method, allowing for intuitive verification of the detected operational modes. This visualisation not only confirmed the algorithm's effectiveness but also provided a clear, visual confirmation of the theoretical constructs proposed in the study.

Chapter 4 Case study – Operational Modes Detection for an Ocean-going Vessel

The detailed methodology for detecting operational modes, explored in depth in Chapter 3, centres on the adaptability of the developed algorithm across various vessel types. This chapter aims to rigorously test its performance and adaptability by applying the algorithm to an ocean-going vessel, specifically, a car carrier engaged in transporting vehicles from port to port. These traditional commercial vessels are designed with a singular purpose based on efficiency and safety in maritime logistics and typically exhibit three common operational modes: 'Transit', 'Manoeuvring', and 'Stop'. The target vessel operates predominantly in open sea areas.

In this chapter, the performance of this detection method, assessing how effectively the algorithm identifies and classifies these three operational modes will be evaluated. The successful application and outcomes of this evaluation will further demonstrate the algorithm's robustness and its utility for commercial vessels operating in open sea areas.

4.1 Vessel Information

The vessel under consideration is an ocean-going car carrier. It is propelled by a main engine, which has a rated power of 15,540 kW. The dimensions of the vessel are a length of 200 metres and a beam of 32 metres with a gross tonnage of 62,380 tonnes.

The dataset utilised for this analysis spans a duration of three months, during which the target vessel undertook a global voyage. The vessel's journey commenced in the Arabian Sea, proceeding to Singapore, then onwards to China and Japan. Subsequently, the vessel navigated to Australia before returning to Japan, and ultimately setting sail for the USA. The recorded trajectory of this vessel is shown in Figure 4.1.

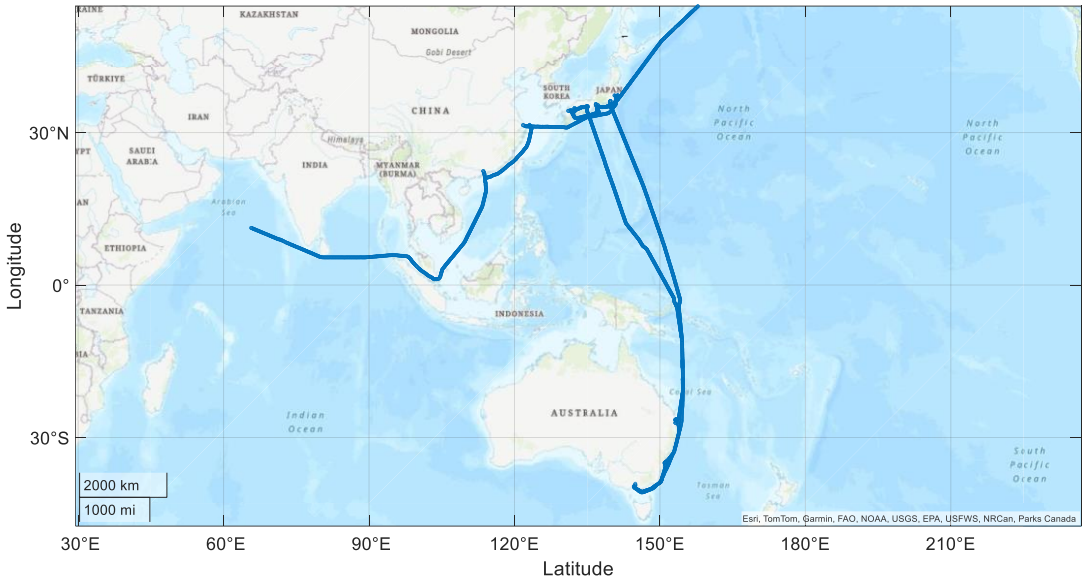

Figure 4.1 Trajectory of the target vessel recorded over three months

4.2 Data Processing

The analysis is conducted using a three-month raw dataset, comprising 140 measurement parameters. With the exception of location information, these measurements predominantly focus on recording the operational status of the vessel. The timestamp for consecutive data points is six minutes. As explained in Section 3.3, the key features selected for this analysis are latitude and longitude coordinates alongside correlated timestamps, and the Main Engine Power. In this context, Main Engine Power is represented as a percentage of MCR. Additionally, two secondary key features, SpeedLL and Curvature, have been derived from the vessel's coordinates and associated timestamps.

4.2.1 Data cleaning

The analysed dataset had been pre-processed by the shipping company, resulting in data quality that is notably superior to that of a typical raw dataset. This pre-processed dataset has no missing values and duplicated timestamps. However, the coordinates are only accurate to two decimal places, which provides an approximately accuracy of 1.1 km in GPS data. Given a timestamp interval of 6 minutes, precision of two decimal places coordinates could result in a speed discrepancy of nearly 6 knots in the limit. This phenomenon is evidenced by the absence of SpeedLL values ranging from 1 to 4 knots.

The coordinates have been further refined using the data cleaning strategy developed and detailed in Section 3.4. Additionally, the 1.5 IQR technique has been applied to identify discrepancies between the SOG and the SpeedLL. Data points where the discrepancy exceeds the range defined by the 1.5 IQR technique have been removed as outliers.

Figure 4.2 illustrates the boxplot of SpeedLL derived from the raw dataset. The figure shows that the maximum SpeedLL exceeds 32 knots, significantly exceeding the target vessel's maximum speed of 19.8 knots. Even when considering environmental influences on the vessel's speed—such as assistance from wind, waves, and currents when operating at maximum rated power—a speed of 32 knots is deemed unrealistic. By contrast, the maximum SOG recorded is approximately 22 knots, indicating a more plausible increase of 2 knots above the vessel's maximum speed. This increment is considered reasonable, accounting for environmental impacts from a physical perspective.

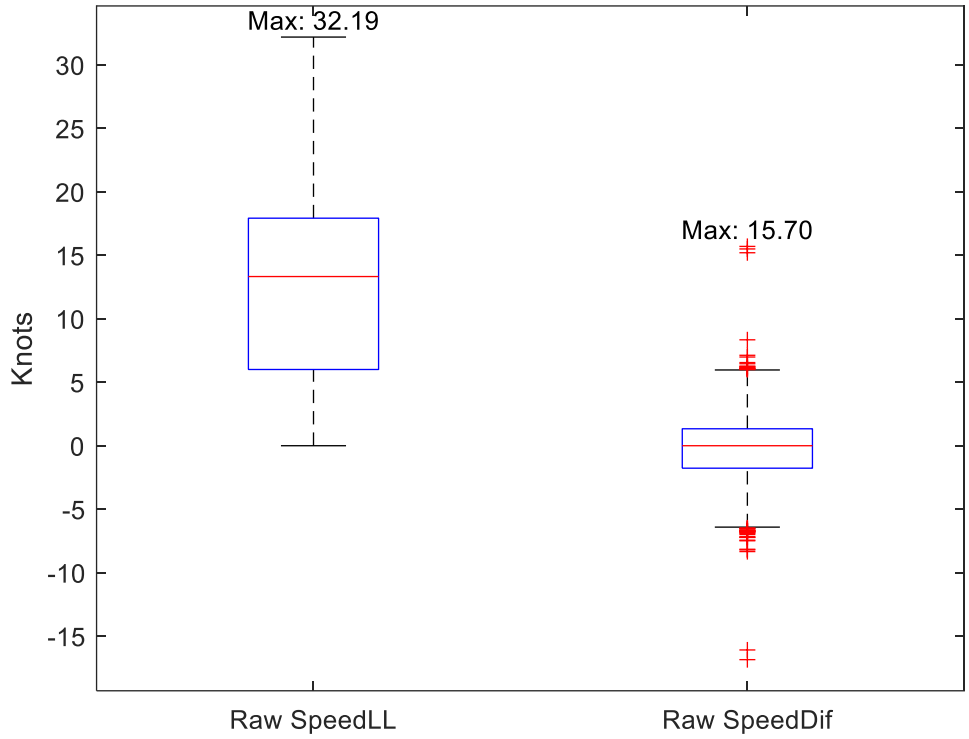

Figure 4.2 The boxplot of raw SpeedLL and corresponding speed discrepancy

As discussed in Section 3.4.1, the primary cause of the anomalously high SpeedLL values can be attributed to inaccuracies in the GPS coordinates, a result from the accumulation of minor deviations among sets of nearby coordinates. Such as the GPS device either failed to record

the vessel's position accurately, recorded the same coordinates, or logged only minor differences from the previous location while the vessel was actually cruising. Although this may result in a slower SpeedLL at the moment, causing a minor speed discrepancy with the actual speed, the long-term accumulation of these discrepancies can lead to significant issues. When the GPS eventually starts recording the correct coordinates, it could display a large distance anomaly compared to previous recordings, thereby generating extreme values.

Furthermore, an extreme SpeedLL value implies a substantial distance travelled between two consecutive data points. For example, a speed of 32 knots suggests that the vessel covered nearly 6 km within a 6-minute timestamp. Such a long-distance anomaly cannot be simply rectified by deleting the corresponding data points. A general overview of the time series coordinates, representing the vessel's trajectory, indicates that the vessel indeed covered a 6 km distance, albeit inaccurately recorded by the GPS devices. Therefore, removing related data points does not address the underlying issue of distance anomalies. These distance anomalies are likely a result of the accumulation of minor inaccuracies in location recording from adjacent points. This hypothesis is further supported by examining the discrepancy between the SOG and the corresponding SpeedLL (SOG - SpeedLL), which is shown in Figure 4.3, being symmetric and highly concentrated around zero knots with high kurtosis and heavy tails.

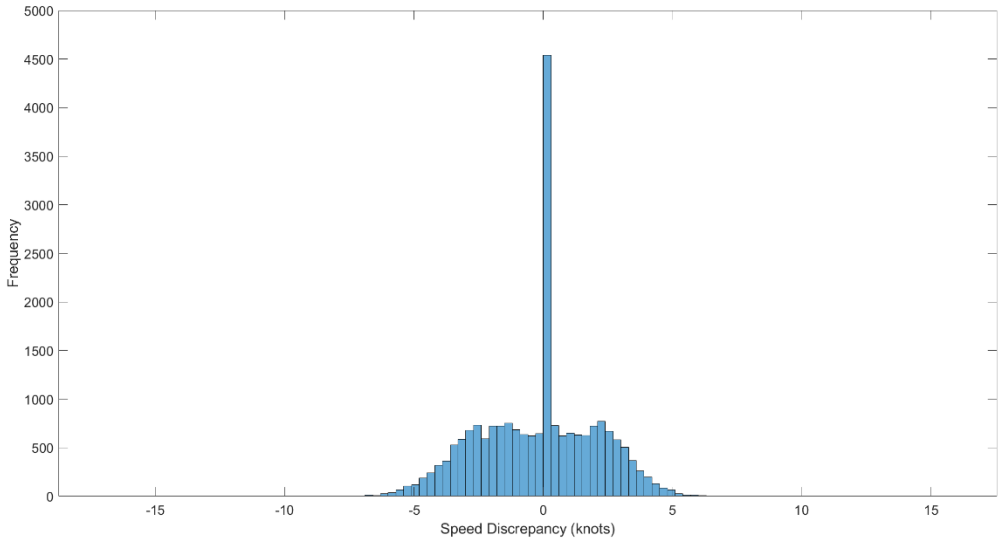

Figure 4.3 Distribution of speed difference between SOG and SpeedLL

Figure 4.2 demonstrates that the maximum speed discrepancy has reached nearly 16 knots in absolute value, a figure which is considered unrealistic. Fundamentally, such a significant

difference would not be expected as the two measurements ostensibly represent the same aspect of vessel movement. This extreme discrepancy in speed underscores the inaccuracies inherent in the GPS coordinates. It supports the earlier hypothesis that an accumulation of minor inaccuracies across a series of data points can lead to anomalous values.

The 1.5 IQR technique has been applied to filter out the outliers according to Equation 3.3. The IQR range has been identified as 3.1026 knots, representing the difference between the 25th and 75th percentiles of the speed difference. Consequently, speed differences within an accepted range of -6.4217 to 5.9887 knots are considered valid, while values outside this range are discarded. Further details of the parameters associated with the 1.5 IQR technique are presented in Table 4.1.

Table 4.1 Key parameters in 1.5 IQR calculation

Speed difference (SOG - SpeedLL)	-16.8499 ~ 15.7003 (knots)
1.5 IQR	-6.4217 ~ 5.9887 (knots)
IQR (25-75 percentile)	3.1026 (knots)
Q1 (25)	-1.7696 (knots)
Q2 (50)	0 (knot)
Q3 (75)	1.3348 (knots)
Q4 (100)	15.7003 (knots)

Despite the 1.5 IQR technique defining a range of speed discrepancy around 6 knots in absolute value, and the maximum cleaned SpeedLL being 26 knots - figures which exceed initial expectations from a domain knowledge perspective—these results are acceptable in light of the low precision, 2 decimal places of the GPS coordinates. After the data cleaning, the distribution of the speed difference and cleaned SpeedLL data are shown in Figure 4.4.

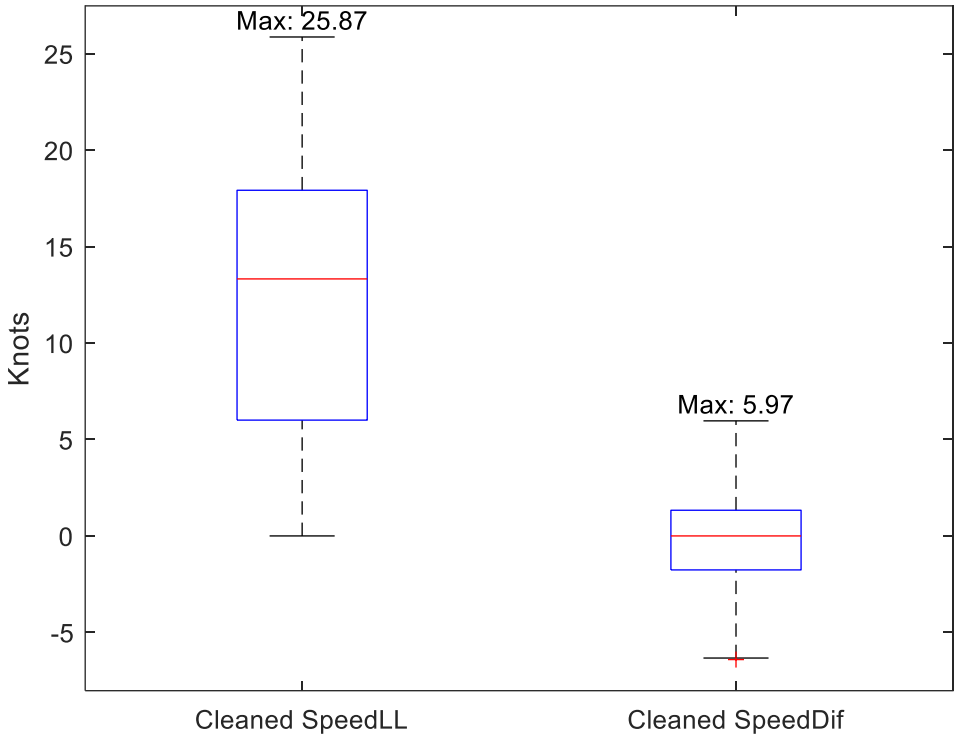

Figure 4.4 Boxplot of cleaned SpeedLL and corresponding speed discrepancy

The data cleaning process has disrupted the continuity of the raw dataset, resulting in its division into several trajectory segments. Segments containing fewer than 6 data points have been disregarded, on the basis that they do not provide a sufficient number of data points for analysis. This threshold of 6 is established based on its significant correlation with the outcomes of sensitivity analysis concerning the combination of rolling window techniques. As detailed in Chapter 3, the RSD and the RIQR are pivotal methods for assessing the variability of each data point. These methods can be further applied to determine the 'Steady State' conditions for the SpeedLL and Curvature. The determination of this threshold is closely linked to the results of the sensitivity analysis, which aims to enhance the accuracy of operational mode detection, a topic that will be elaborated upon in Sections 4.4.1 and 4.4.2.

4.2.2 Selection of exemplary sub-dataset

A specific dataset was chosen to develop the subsequent analysis, aimed at establishing thresholds for the two secondary key features - SpeedLL and Curvature - to identify the 'Steady State' condition. The selection of this dataset is crucial as it requires a balance between maximising data continuity and encompassing a broad spectrum of operational modes. Ideally,

the dataset should include several transitions between operational modes, which are required for the algorithm to accurately delineate the thresholds distinguishing between ‘Steady State’ and ‘Changing’ conditions.

The dataset chosen for analysis comprises 713 data points, spanning a duration of over 71 hours. The trajectory of this dataset is illustrated in Figure 4.5.

Figure 4.5 Trajectory represented by the selected dataset

The dataset records the vessel’s journey from north to south, detailing its trajectory from a channel near Victory to the port at Portland, where it remains for approximately 18 hours before navigating southward. Illustrated in Figure 4.5, this dataset captures the vessel’s entire process of entering and exiting the port. Furthermore, it encompasses the vessel’s navigation through two distinct environments: inland waterways and the open ocean. This diversity in operations, combined with the data continuity, makes the dataset particularly valuable. It encompasses a wide range of operational changes, providing a robust basis for the algorithm to delineate thresholds for identifying the ‘Steady State’ condition.

4.3 Identification of Visualised Change Points

Two key features, SpeedLL and Curvature, have been extracted from the selected dataset. Visualisation techniques have been employed on these features to identify change points, by observing variability across the dataset. VCPs are detected by observing the variations in SpeedLL and Curvature. Figure 4.6 illustrates the VCPs for these two features within the selected continuous dataset.

Regarding SpeedLL, the VCPs segment the dataset into eight distinct intervals. These intervals are demarcated from the beginning of the dataset to VCP1, from VCP1 to VCP2, and so forth, concluding with the interval from VCP7 to the dataset's end. The indices of these VCPs are identified at 21, 61, 76, 194, 293, 457, and 530.

Observational analysis categorises the identified segments into two distinct types, based on the inherent variability observed within them: 'Steady State' and 'Changing'. The 'Steady State' condition is marked by a relatively uniform and low level of variability within a segment, whereas the 'Changing' condition is characterised by a heightened degree of variability. Within this framework, segments 2, 4, 6 and 8 have been classified as 'Steady State', indicative of their stability, whereas segments 1, 3, 5 and 7 are recognised as 'Changing', reflecting their dynamic nature.

The visualised analysis technique was similarly applied to Curvature, identifying VCPs with indices marked at 194, 293, 457, and 530. This analysis segmented the dataset, with segments 1, 3, and 5 being categorised as 'Steady State', indicative of low variability and consistent behaviour. Conversely, segments 2 and 4 were classified as 'Changing', signifying areas of higher variability and transitions in operational conditions.

From an operational standpoint, the vessel's speed and curvature exhibit fluctuations, oscillating between 'Steady State' and 'Changing' conditions, as delineated by the segments identified through VCPs. Notably, with the exception of the first three VCPs for SpeedLL, the indices for the remaining VCPs for both SpeedLL and Curvature coincide, suggesting a strong correlation between changes in operational modes and the conditions of speed and curvature. By synthesising these VCPs, Table 4.2 provides a comprehensive correlation between the segments and their binary classifications of 'Steady State' and 'Changing' for both speed and curvature.

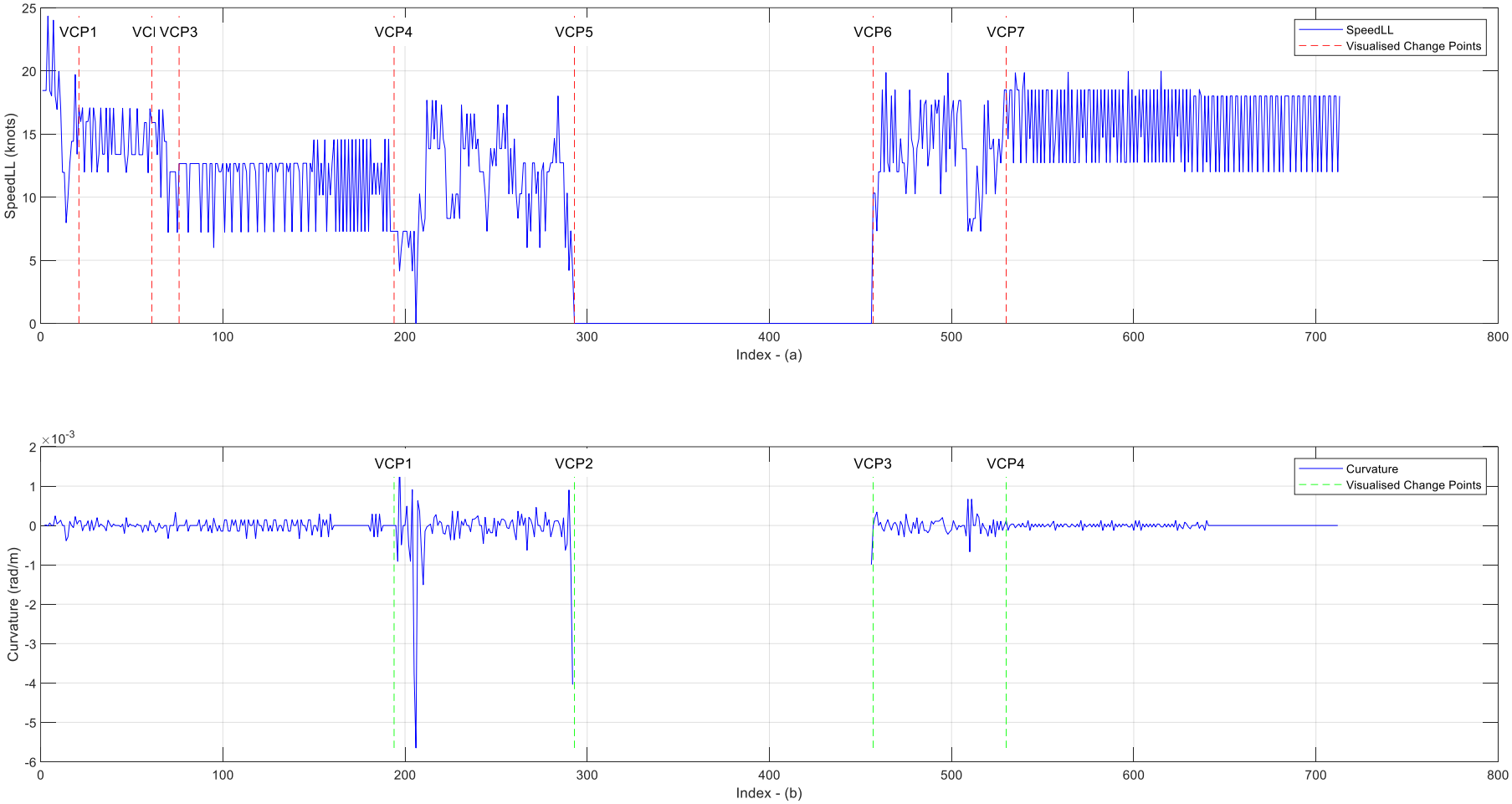

Figure 4.6 VCPs for SpeedLL and Curvature in the exemplary sub-dataset

Table 4.2 Correlation between binary conditions and segments

Segments	1	2	3	4	5	6	7	8
VCPs (Index)	1	21	61	76	194	293	457	530
SpeedLL	1	0	1	0	1	0	1	0
Curvature	0				1	0	1	0

Binary Label (0&1) represents two conditions: 0 – Steady State, 1 – Changing

Given that the VCPs are delineated based on the observed variability across the dataset, Table 4.3 presents the variability characteristics for each segment as identified by the VCPs. This is generated using the IQR and SD as the principal metrics for assessing data variability.

Table 4.3 Variability of visualised segments using IQR and SD

Segments		1	2	3	4	5	6	7	8
SpeedLL	IQR	4.91	3.65	3.90	5.39	5.53	0.00	4.80	5.76
	SD	4.23	1.92	2.87	2.62	3.73	0.33	3.63	2.88
Curvature	IQR(e-05)	7.69				35.22	0.00	23.16	7.06
	SD(e-04)	1.30				7.80	0.00	2.30	0.49

The values in red represent the variabilities under the ‘Steady State’ condition.

In comparing the variability across segments, it becomes apparent that there is no significant difference between the binary conditions for either IQR or SD, particularly for SpeedLL. Moreover, there are instances where the observed variability within segments classified as ‘Steady State’ exceeds that of segments designated as ‘Changing’. For example, the variability (measured in IQR) of segments 4 and 8 is higher than that of segments 3 and 7.

The primary reason for this inconsistency can be attributed to the low precision of the GPS coordinates, which have been pre-processed to include only two decimal places. Such low precision introduces noise into the dataset, thereby increasing the observed variability. This effect is particularly pronounced in segments classified under ‘Steady State’ conditions, especially for those pertaining to SpeedLL.

In Figure 4.6, VCPs 4 and 7 for SpeedLL are identified by examining the pattern of data point changes, indicating that data within segments 4 and 8 undergo changes following a relatively

stable pattern, consistent with ‘Steady State’ conditions. In contrast, the data within segments 5 and 7 exhibit irregular patterns. The stable pattern of data changes can be attributed to a relatively consistent error introduced by the rounding of GPS coordinates to two decimal places. This rounding implies that the second decimal place is adjusted either upwards or downwards based on the value of the third decimal, thereby either decreasing or increasing the actual sailing distance recorded in the rounding process. Consequently, a relatively consistent error is introduced when the vessel sails at a steady speed. This issue of low precision not only affects the SpeedLL but also impacts the Curvature, posing challenges for accurately detecting ‘Steady State’ conditions.

Although the variability data presented in Table 4.3 may not provide robust support for the rationale behind identifying the VCPs, these points are nonetheless validated through an examination of the vessel’s trajectory. Figure 4.7 visually demonstrates the VCPs in relation to the vessel’s trajectory.

Figure 4.7 Illustration of the vessel's trajectory with VCPs indicated by red dots

The red dots illustrated in Figure 4.7 represent the VCPs, showing the vessel's journey from the north (near Victoria) to the port at Portland, before sailing southwards. This illustration reveals that the patterns of segments 2, 4, and 7 are relatively straight, indicative of direct navigation paths. In contrast, segments 1, 3, 5, and 6 exhibit manoeuvring patterns, reflecting more complex navigational manoeuvres. Notably, the red dot in the middle corresponds to the period during which the vessel remains at the port of Portland, resulting in VCPs 5 and 6 being collocated at the same position. These VCPs effectively segment the trajectory into distinct portions, each with unique characteristics that are of considerable importance for further analysis.

4.4 Steady State Detection for SpeedLL and Curvature

The conceptual framework for the subsequent analysis continues to emphasise variability, transitioning from a broad, dataset-wide scale to a more localised perspective. This involves assessing the variability of each data point and establishing a threshold for this metric. Data points exhibiting variability above the threshold are classified as being in a 'Changing' condition, while those with variability below the threshold are considered to be in a 'Steady State'. For a detailed discussion of this methodology, please refer to Section 3.5.

The rolling window technique has been deployed to calculate the variability of data points, proving to be particularly effective for this analysis. This technique calculates the variability of a target point by comparing it with nearby points within a predefined window size. If the calculated variability is relatively low, this indicates that the target data point exhibits similarity to its neighbours, suggesting that the condition within this specific checking scale - the defined window size - is relatively stable. Therefore, identifying an appropriate rolling window size is crucial, as it sets the basis for comparing targeted data points to evaluate their variability.

4.4.1 Sensitivity analysis on the combination of rolling window for SpeedLL

Within this context, the 'local area' is defined by the specific attributes of the rolling window technique employed. This definition encompasses not only the window size - indicating the number of data points within the window - but also the position of the target data point within this window. This necessitates a sensitivity analysis that accounts for the sequence of data

points, given the time-series nature of the dataset, where data points are recorded sequentially.

Three positions within the rolling window have been defined: 'Begin', 'Middle', and 'End'. The 'Begin' position implies that the targeted data point is situated at the start of the window, and its variability is assessed by comparison with subsequent data points. When in the 'Middle' position, the targeted data point is located centrally within the window, and its variability is evaluated by comparing it with an equal number of data points both preceding and following it. The 'End' position indicates that the targeted data point is at the window's conclusion, with variability assessed through comparison with preceding data points. Two methods have been selected to evaluate data variability: the IQR and SD. A detailed discussion on the combinations of rolling window attributes is given in Section 3.5.2.2.

The essence of the sensitivity analysis lies in identifying the most appropriate combination of rolling window attributes that robustly supports the identification of VCPs. This entails each combination yielding a distinct set of variabilities for the data points. Concurrently, the VCPs segment the dataset into discrete intervals, each characterised by either a 'Steady State' or 'Changing' condition. The analysis seeks to identify a particular set of variability measures that most effectively differentiates between these visualised binary conditions. In essence, the optimal combination is determined by referencing the VCPs and evaluating the variability of data points from a local scale, extending this analysis to the broader context of visualised segments throughout the dataset.

An objective function was formulated in the equation 3.4, drawing on the previously discussed concept. This function encompasses three key aspects: Cumulative Difference in Segment Variability, Sum of Variability in 'Steady State' Conditions, and Consistency of Variability Changes Across Segments. The sensitivity analysis proceeds according to this objective function, aiming to identify the combination of rolling window attributes that yields the maximum value - thereby offering robust support to the identification of VCPs.

In this analysis, the rolling window's combination encompasses the three defined positions: 'Begin', 'Middle', and 'End', with the window size varying from 4 to 20 data points. The evaluation of data point variability within these windows utilises two methodologies: IQR & SD.

The chosen minimum window size of 4 is dictated by the requirements for calculating the IQR, specifically for determining the 25th and 75th percentiles of the dataset. Conversely, the maximum window size of 20 is selected to explore the benefits of larger scales in identifying the most suitable combination for analysis. A window size of 20, corresponding to a period of 2 hours given the 6-minute interval between data points, may appear excessively long and potentially unrealistic for reflecting operational mode changes, however this broader range facilitates easier observation of the trend in the objective function's value. Figure 4.8 illustrates the results of the objective function for SpeedLL.

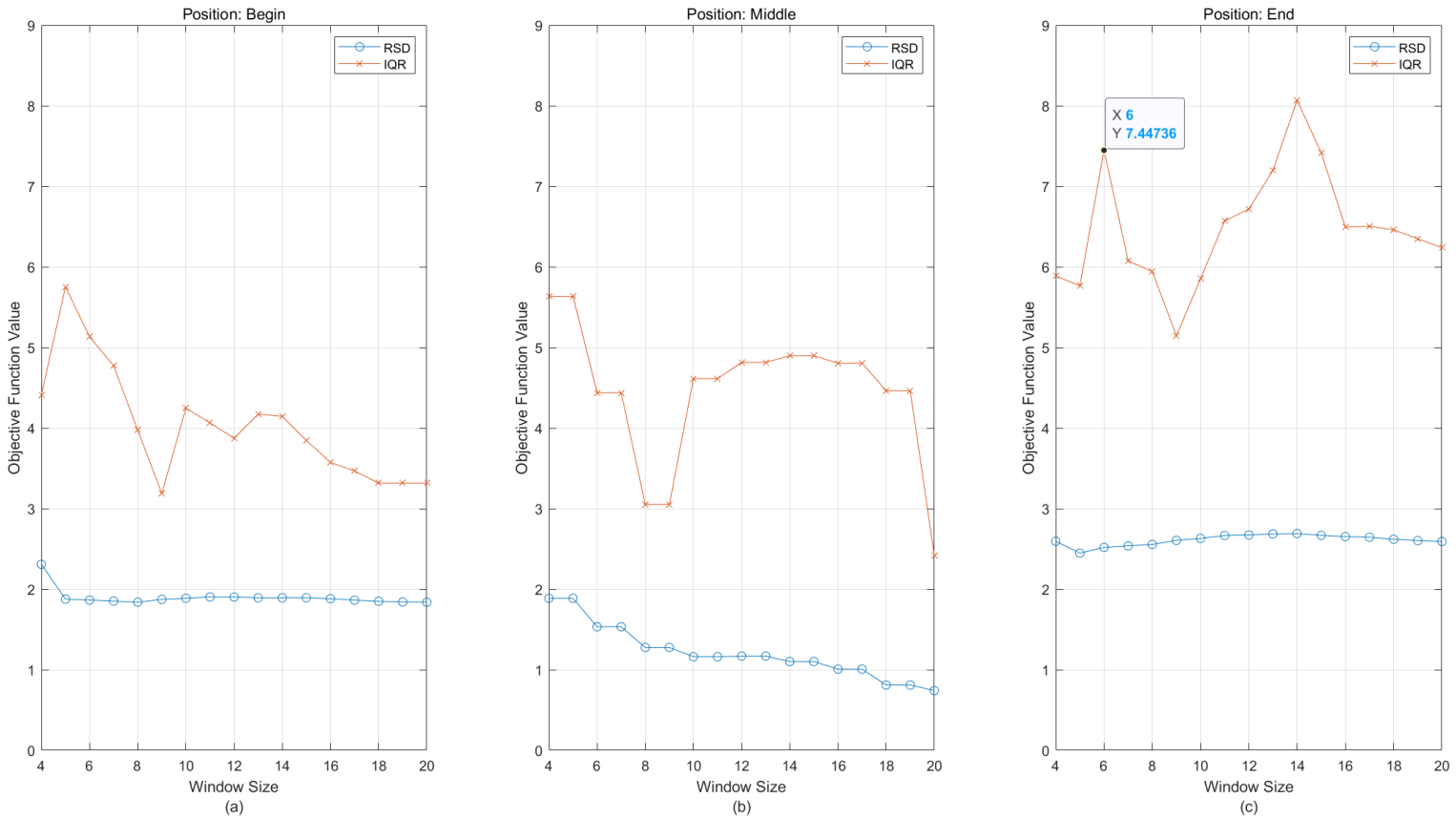

Figure 4.8 Results of the objective function for SpeedLL analysis

As illustrated in Figure 4.8, the IQR outperforms SD in evaluating data variability, as evidenced by higher objective function values across the three positions. In comparison, SD not only yields lower values than IQR but also fails to identify a significant trend that could indicate the optimal combination of rolling window attributes; it does not reveal a distinct peak value across all combinations. The trend patterns associated with SD exhibit a slight decrease followed by stabilisation at the 'Begin' position, a gradual decrease at the 'Middle', and relative steadiness at the 'End' position.

In contrast, the IQR demonstrates superior performance within the objective function. Specifically, in Figure 4.8 (a), the objective function value peaks at a window size of 5 before experiencing a sharp decline up to the size of 9. At the 'Middle' position, illustrated in Figure 4.8 (b), the maximum value is observed at window sizes of 4 and 5, thereafter declining until sizes 8 and 9, before rebounding slightly. Figure 4.8 (c) reveals two peak values at window sizes of 6 and 14, respectively. Although the window size of 14 exhibits a higher objective function value than size 6, it may not be the preferable choice. A shorter window size retains more information from the raw dataset, whereas, given a 6-minute interval, a window size of 14 corresponds to an 84-minute period, nearly one and a half hours. Such an extended period could potentially exclude essential information, rendering it impractical for accurately reflecting the vessel's operational mode changes over such a duration.

In comparing the influence of the rolling window's positions, the 'End' position emerges as the most effective, yielding higher objective function values than the 'Begin' and 'Middle' positions. Consequently, the optimal combination for the rolling window has been determined as: a window size of 6, positioned at the 'End', i.e. with the target data point positioned at the end of the rolling window, and with the IQR selected as the method for evaluating data variability for SpeedLL. The rolling window size is 6, and the time interval is 6 minutes, therefore, the duration of the rolling window is 36 minutes. That means, it would take around half an hour for an ocean-going vessel to complete an operational mode change, which comply with the domain knowledge.

4.4.2 Sensitivity analysis on the combination of rolling window for curvature

Following the methodology discussed previously, a sensitivity analysis has also been applied to Curvature. This analysis similarly evaluates three key aspects: the position of the targeted data point within the rolling window, the window size, and the methods used to assess data variability. Figure 4.9 presents the outcomes of the objective function when applied to the curvature analysis.

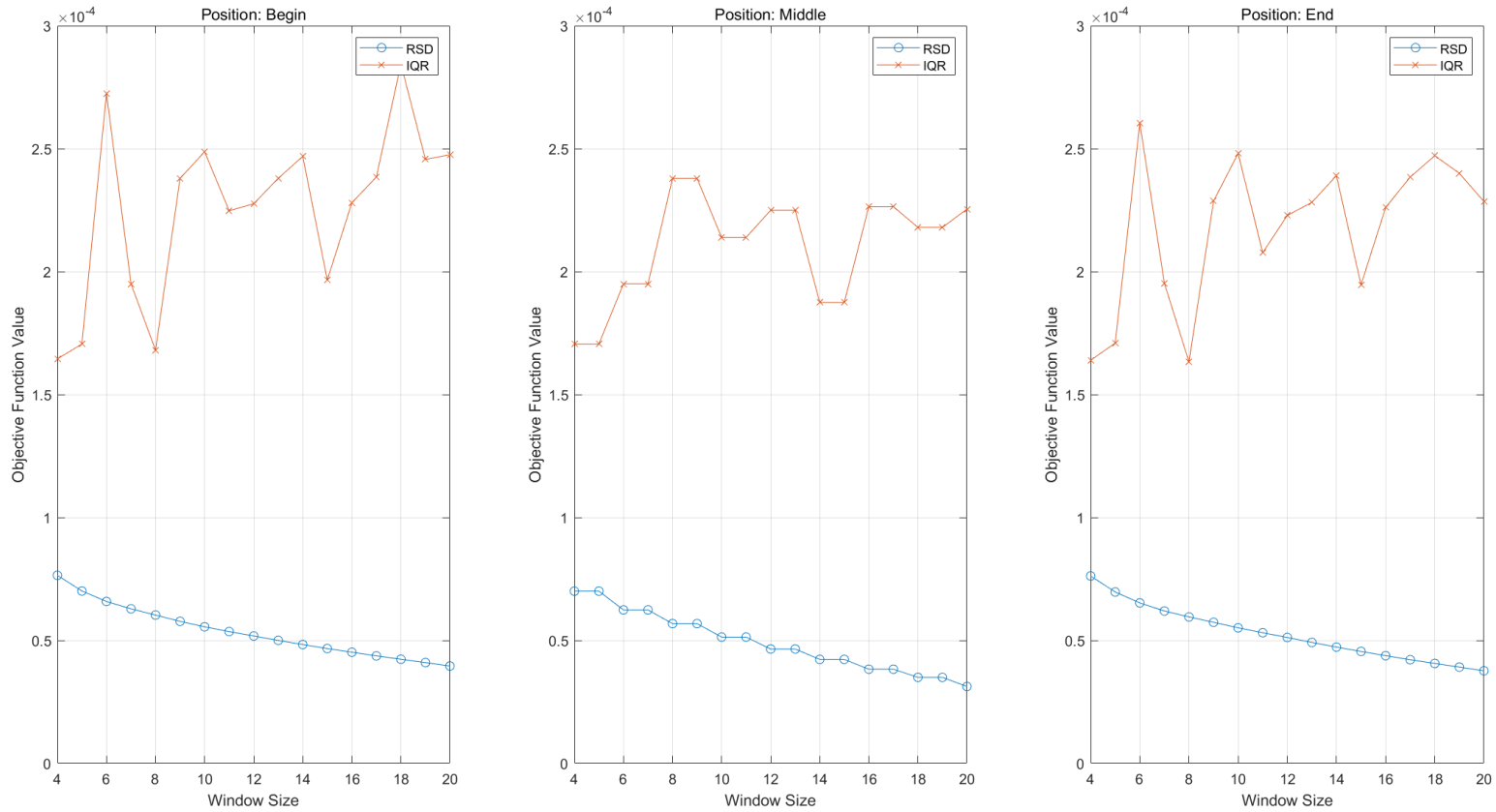

Figure 4.9 Results of the objective function for Curvature analysis

The IQR outperforms the SD in evaluating curvature, as evidenced by higher objective function values across all three positions shown in Figure 4.9. Unlike IQR, the trend patterns of objective function values for SD fail to identify an optimal combination for the rolling window, with values gradually decreasing until the end of the predefined window size range. This indicates that the peak value for SD is reached at the outset, at a window size of 4, across all positions.

In Figure 4.9 (a), two significant peaks are observed at window sizes of 6 and 18. The objective function value initially rises sharply to its first peak at size 6, then after a period of fluctuation, reaches the maximum value at size 18. Despite the higher objective function value at size 18 for the 'Begin' position, a window size of 6 is deemed more suitable. The larger window size of 18 risks omitting pertinent information from the raw dataset and extends almost to 2 hours, a duration considered excessively long for realistically capturing changes in the vessel's operational modes.

As illustrated in Figure 4.9 (b) and (c), the objective function values exhibit similar trends across both positions, characterised by a sharp increase at the outset, peaking early, followed by a decrease and subsequent fluctuations until the end of the predefined window size range. Notably, the peak values are observed at sizes 8 and 9 for the 'Middle' position and at size 6 for the 'End' position. Furthermore, the peak value at the 'End' position is higher than that observed in the 'Middle'. Consequently, a window size of 6 has been selected based on these observations.

The 'End' position has been chosen for the rolling window configuration. When comparing the objective function values of window size 6 at the 'Begin' position (6B) with those at the 'End' position (6E), as illustrated in Figure 4.9 (a) and (c), the difference is marginal, with 6B being slightly higher than 6E. The primary rationale for opting for the 'End' position, despite this slight variance, is to maintain consistency in the rolling window configuration across SpeedLL and curvature analyses. This approach ensures that the variability derived from the raw coordinates for these two features is synchronised, promoting a coherent analytical framework.

Since both variables are derived from the raw coordinates, maintaining the same local area for analysis is crucial to preserving the potential informational and correlational integrity between them. This approach ensures that any inherent relationships or patterns present in the dataset are not disrupted by varying analytical parameters. Furthermore, the selected combination of

rolling window attributes will be employed to verify the consistency of detected change points. Specifically, detected change points should align with the condition of subsequent data points within the local area defined by the parameters of the rolling window. This methodological consistency is essential for ensuring the reliability of the change point detection process.

4.4.3 Setting the thresholds to detect steady state for SpeedLL

The variability of data points has been calculated utilising the parameters defined by the sensitivity analysis of the rolling window combination. Figure 4.10 presents SpeedLL alongside its pointed variability with VCPs indicated by red vertical dots.

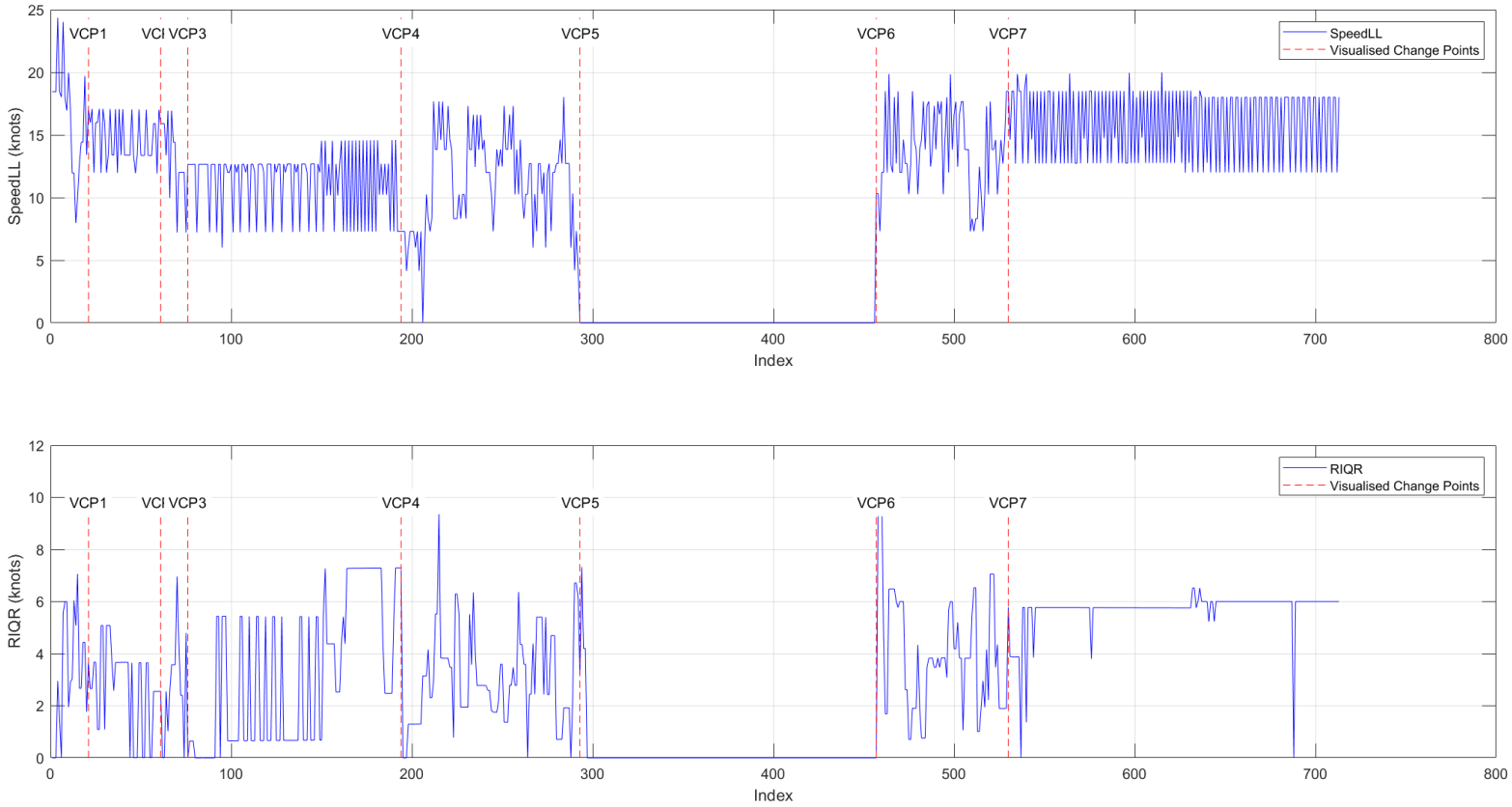

Figure 4.10 SpeedLL and its pointed variability with VCPs in red vertical dots

A notable observation from Figure 4.10 is that the RIQR does not effectively differentiate between the binary conditions of ‘Steady State’ and ‘Changing’. This is evidenced by the elevated RIQR values observed in both conditions. For instance, the segments between VCP3 and VCP4, as well as from VCP7 to the end of the dataset, exhibit significant data variability under both ‘Steady State’ and ‘Changing’ conditions.

The issue identified, pertaining to the limitations of the RIQR in effectively differentiating between ‘Steady State’ and ‘Changing’ conditions, can largely be attributed to the low precision of GPS coordinates. As previously discussed, the resolution of two decimal places in GPS data, introduces a relatively consistent error, especially when the vessel navigates under ‘Steady State’ conditions. This is further corroborated by Table 4.3, which illustrates that segmented variability fails to provide robust support for the identification of VCPs for SpeedLL.

Given the substantial noise associated with SpeedLL, particularly in ‘Steady State’ conditions, directly applying a threshold on the RIQR to distinguish between the binary conditions is impractical. To address the noise resulting from low GPS precision, the moving average technique has been employed on SpeedLL. The parameters of the rolling window have been aligned with the outcomes of the sensitivity analysis to ensure consistency in the local analysis area for each targeted data point. This means that both the local variability and the moving average for each data point are calculated using the same adjacent points. Such an approach aims to preserve the integrity of the information and the correlation between them. Figure 4.11 illustrates the SpeedLL after applying the moving average, alongside the variability for each data point, with VCPs indicated.

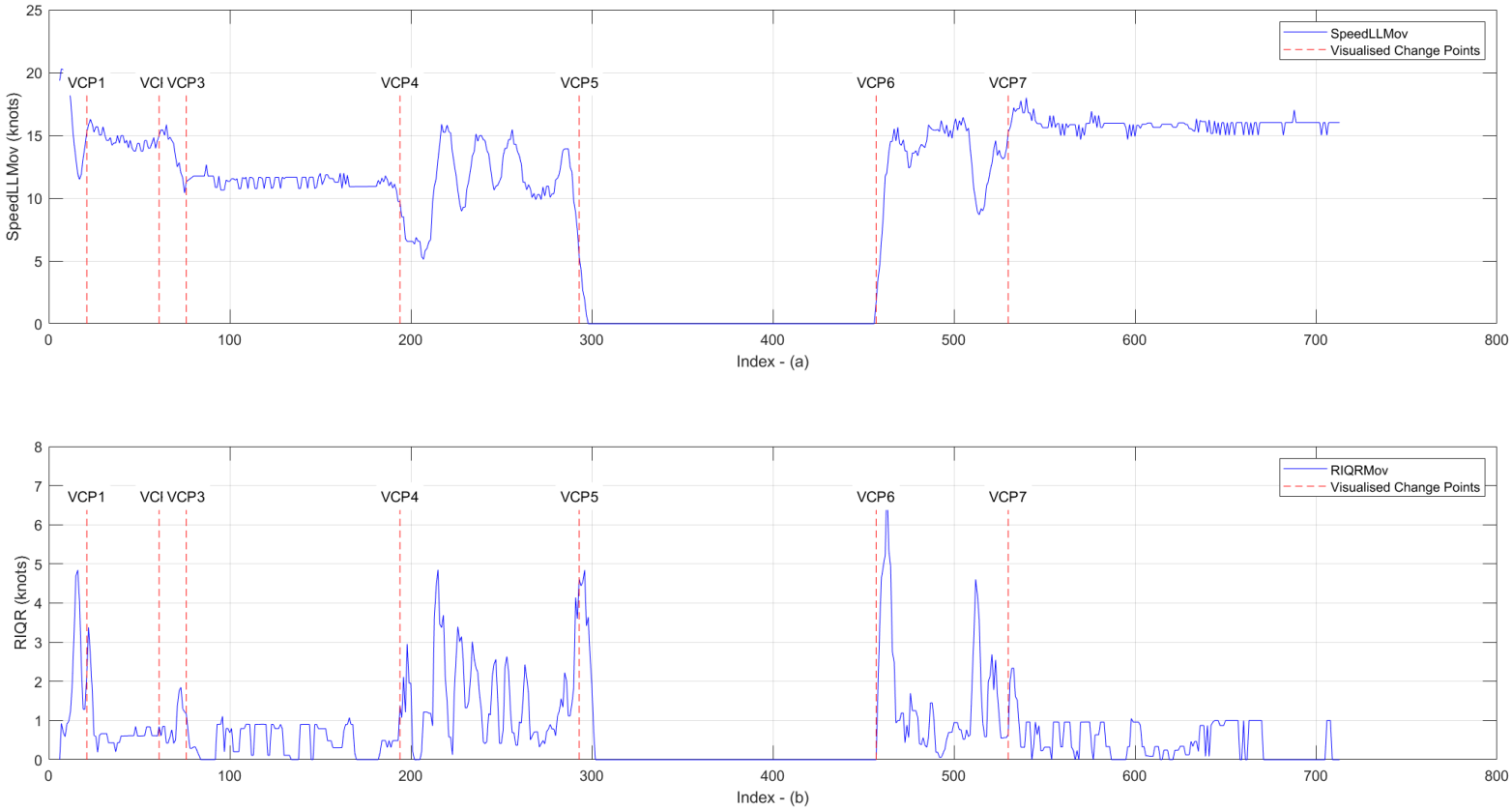

Figure 4.11 Moving averaged SpeedLL and variability for each data point

Figure 4.11 demonstrates that the application of the moving average technique has markedly reduced the noise in the data. The fluctuations observed in the segments between VCP3 and VCP4, as well as from VCP7 to the end of the dataset, have been effectively smoothed out, offering a clear improvement over the representations seen in Figure 4.10 (a). Moreover, the variability within each visualised segment now aligns more closely with the expected binary conditions; 'Steady State' conditions exhibit relatively low variability. This enhancement is particularly evident in Figure 4.11 (b).

The next step involves establishing a threshold for the RIQR to effectively delineate 'Steady State' conditions. The validation of this threshold is carried out as follows: a range for potential thresholds is defined, and the aim is to identify the threshold that yields change points most closely aligned with the VCPs. It is crucial to note that detected change points must undergo a consistency check to ensure their validity; any that do not meet the consistency criteria are disregarded.

The rationale behind the consistency check is founded on the assumption that changes in the operational modes of the target vessel cannot occur within an excessively brief timeframe. For the purposes of this analysis, a 'short time' is defined as a period of 36 minutes, corresponding to a window size of 6. This duration is in line with the findings from the sensitivity analysis concerning the optimal rolling window configuration. If the identified condition continues for less than 36 minutes, it is disregarded.

Observations from Figure 4.11 (b) highlight two segments distinctly classified as 'Steady State' conditions, positioned between VCP3 & VCP4 and from VCP7 to the dataset's end. The upper limit of the RIQR for these segments approaches approximately 1 knot. Consequently, the threshold range has been established from 0.5 to 1.5 knots, with increments of 0.1 knots. Table 4.4 Indices of DCPs for SpeedLL details the indices of DCPs corresponding to each threshold value.

Table 4.4 Indices of DCPs for SpeedLL

Threshold	Indices of DCPs
0.5	32;39;77;105;129;138;153;162;168;193;200;206;301;457;489;495;547;569;583;597;603;641;670
0.6	32;39;77;105;129;138;153;162;168;193;200;206;301;457;480;496;547;569;583;597;603;641;670
0.7	24;70;76;105;129;138;153;162;168;193;200;206;300;457;480;498;547;569;583;597;603;641;670
0.8	24;70;76;113;128;138;148;193;200;206;265;280;300;457;480;509;547;569;583;597;603;641;670
0.9	24;70;76;113;128;138;148;193;200;212;265;280;300;457;480;509;545;569;583;649;670
1.0	11;24;70;76;193;200;212;255;280;300;457;480;509;535;649;670
1.1	11;24;70;76;212;255;280;300;457;479;509;524
1.2	11;24;212;255;288;300;457;467;509;524
1.3	12;24;212;238;288;300;457;467;509;524
1.4	12;24;212;238;288;300;457;467;509;524
1.5	12;24;212;238;289;300;457;467;509;524

Analysis of Table 4.4 reveals that the DCPs exhibit similarities within specific threshold bands, notably from 0.5 to 0.6 knots, 0.7 to 0.9 knots, and 1.2 to 1.5 knots. Thresholds below 1 knot prove to be less effective in change point detection, evidenced by an excessive number of DCPs identified within these ranges. This suggests that a higher precision in threshold setting may inadvertently lead to increased fluctuations in detection outcomes. When contrasted with the total of 7 VCPs identified, the detection process yields more than 20 DCPs, indicating a potential over-detection issue at lower thresholds.

In comparing the indices of the VCPs, a threshold of 1.1 knots has been chosen. Although the DCPs show stability within the range of 1.2 to 1.5 knots, a threshold of 1.1 knots identifies an additional segment between indices 70 to 76, aligning more closely with the VCPs. Figure 4.12 shows the comparison between the VCPs and DCPs. Here, the VCPs are marked on the moving-averaged SpeedLL, and the DCPs are indicated alongside the corresponding RIQR values.

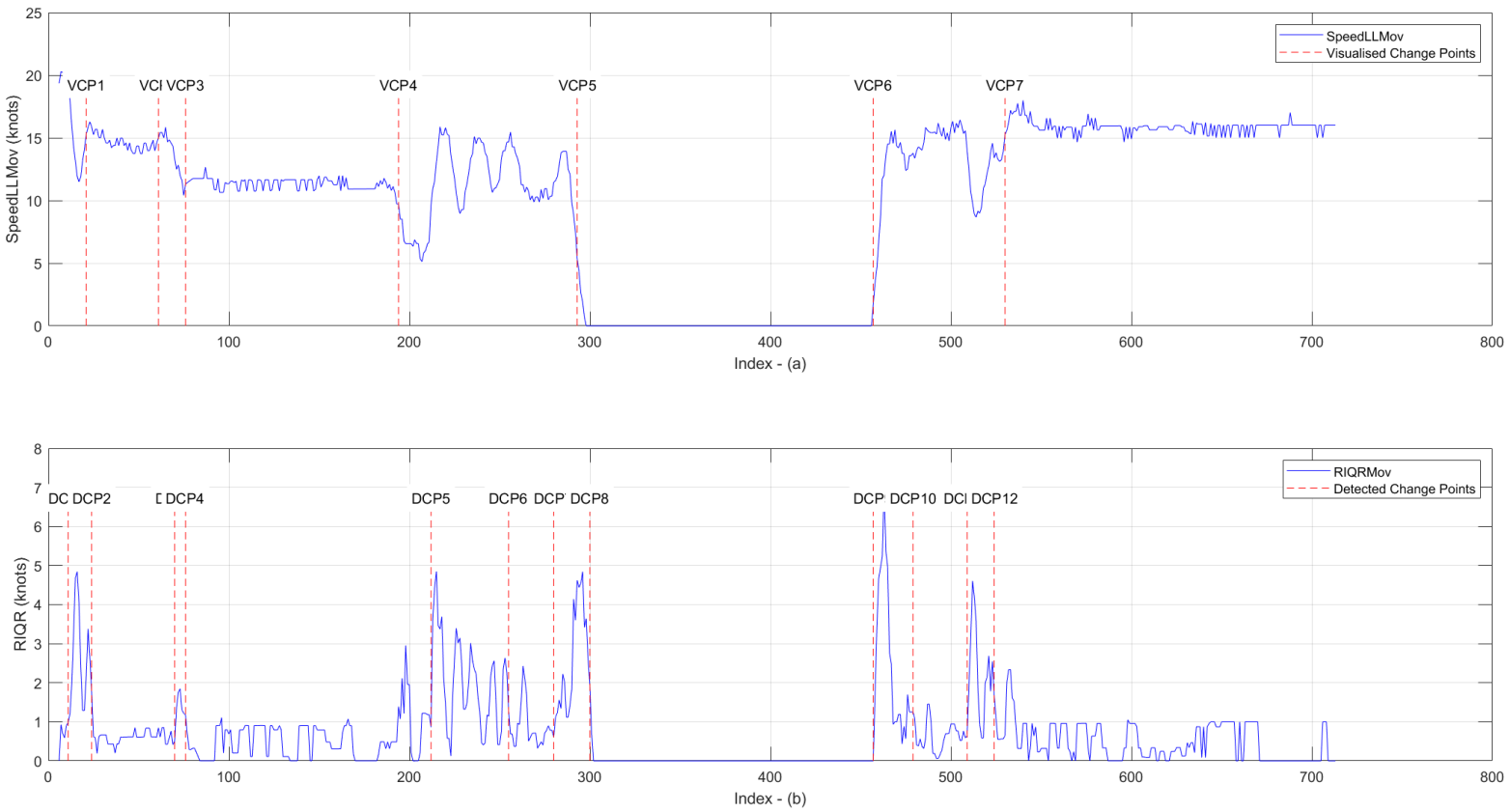

Figure 4.12 Comparison between VCPs and DCPs

In Figure 4.12, the comparison reveals that DCPs successfully identify all changes proximal to those detected by the VCPs, affirming the efficacy of DCPs in differentiating the binary conditions. However, three additional segments were detected and classified as 'Steady State', which did not correspond to changes indicated by VCPs. These extra segments are delineated by the indices from the starting point to DCP1, from DCP6 to DCP7, and from DCP10 to DCP11. They are located at the dataset's outset and within the segments visually marked as 'Changing' between VCP4 & VCP5 and VCP6 & VCP7.

The identification of extra segments as 'Steady State' primarily stems from the low precision inherent in the GPS coordinates. Despite the expectation that these segments, identified between specific DCPs, would be classified under 'Changing' conditions as indicated by VCPs, their variabilities fall below the threshold or are smaller than those observed in typical 'Steady State' segments (specifically between DCP4 to DCP5 and from DCP12 to the end).

For 'Steady State' segments, the application of the moving average technique has significantly mitigated the fluctuations attributed to the low precision of GPS data. Nonetheless, a minor variation persists, with data points oscillating regularly within a narrower band compared to the raw dataset. This residual fluctuation contributes to an increase in the pointed variability, as measured by the RIQR, for segments identified as 'Steady State'.

For 'Changing' segments, the application of the moving average technique has effectively reduced fluctuations, subsequently decreasing their variabilities. The variabilities of the three additional segments, which were anticipated to be classified as 'Changing', have been diminished below the threshold due to the moving average technique. This suggests that the primary cause of this phenomenon is the data noise stemming from the low precision of the GPS coordinates. While the moving average technique serves to mitigate the fluctuations caused by this noise, it cannot wholly eliminate the impact of the low precision issue.

This limitation is further elucidated through an analysis of the Speed Over Ground (SOG), which benefits from greater precision than that offered by coordinates with two decimal places. Employing the same analytical methodology as previously discussed, Figure 4.13 illustrates the SOG alongside its RIQR, with VCPs indicated by red vertical dots.

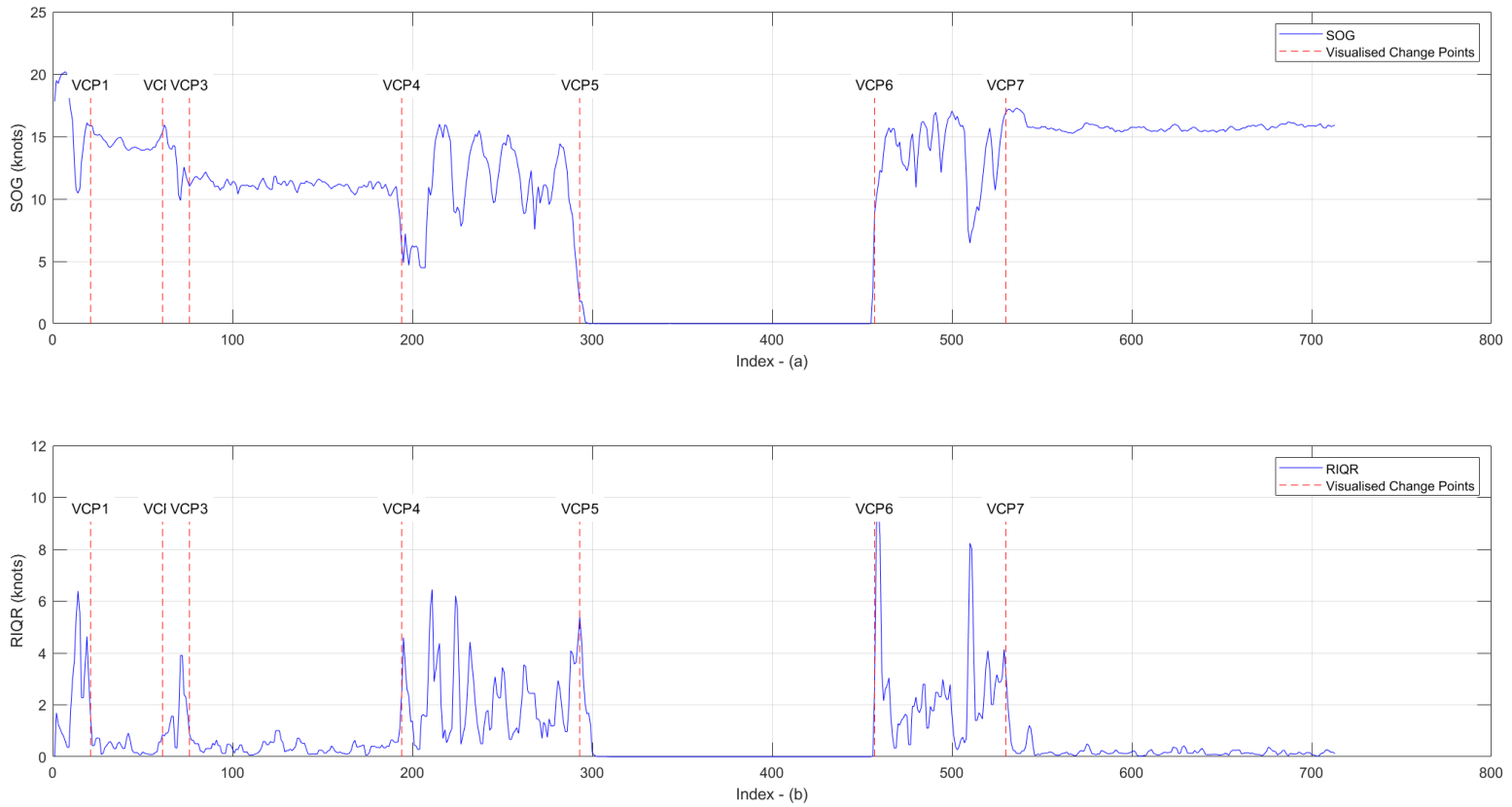

Figure 4.13 SOG and pointed variability with VCPs in red vertical dots

Figure 4.13 demonstrates a distinct difference between the binary conditions, attributed to the high precision of the SOG. Notably, when the vessel operates at a steady speed, the periods exhibit an absence of the regular fluctuations observed with less precise data. To further assess this, a validation of thresholds has been applied to the RIQR of the SOG. The range for these thresholds has been set from 0.1 to 1 knot, incremented by 0.1 knots. The indices of the DCPs resulting from this analysis are detailed in Table 4.5.

Table 4.5 Indices of DCPs of SOG

Threshold (knots)	Indices of DCPs
0.1	300;456;602;616;640;654
0.2	44;58;105;114;141;165;299;456;545;674;685
0.3	43;58;105;115;140;166;299;456;533
0.4	43;58;81;116;128;187;299;456;533
0.5	43;58;81;120;128;187;299;456;533
0.6	9;26;60;78;192;299;456;532
0.7	9;25;60;76;192;299;456;532
0.8	9;21;60;76;192;299;456;501;508;532
0.9	9;21;69;75;192;299;456;500;508;532
1.0	9;21;69;75;192;299;456;500;508;532

In comparison with the VCPs, a threshold of 0.7 knots has been identified as providing the most accurate DCPs for the SOG data. Figure 4.14 illustrates the comparison between the VCPs and DCPs within the context of SOG analysis.

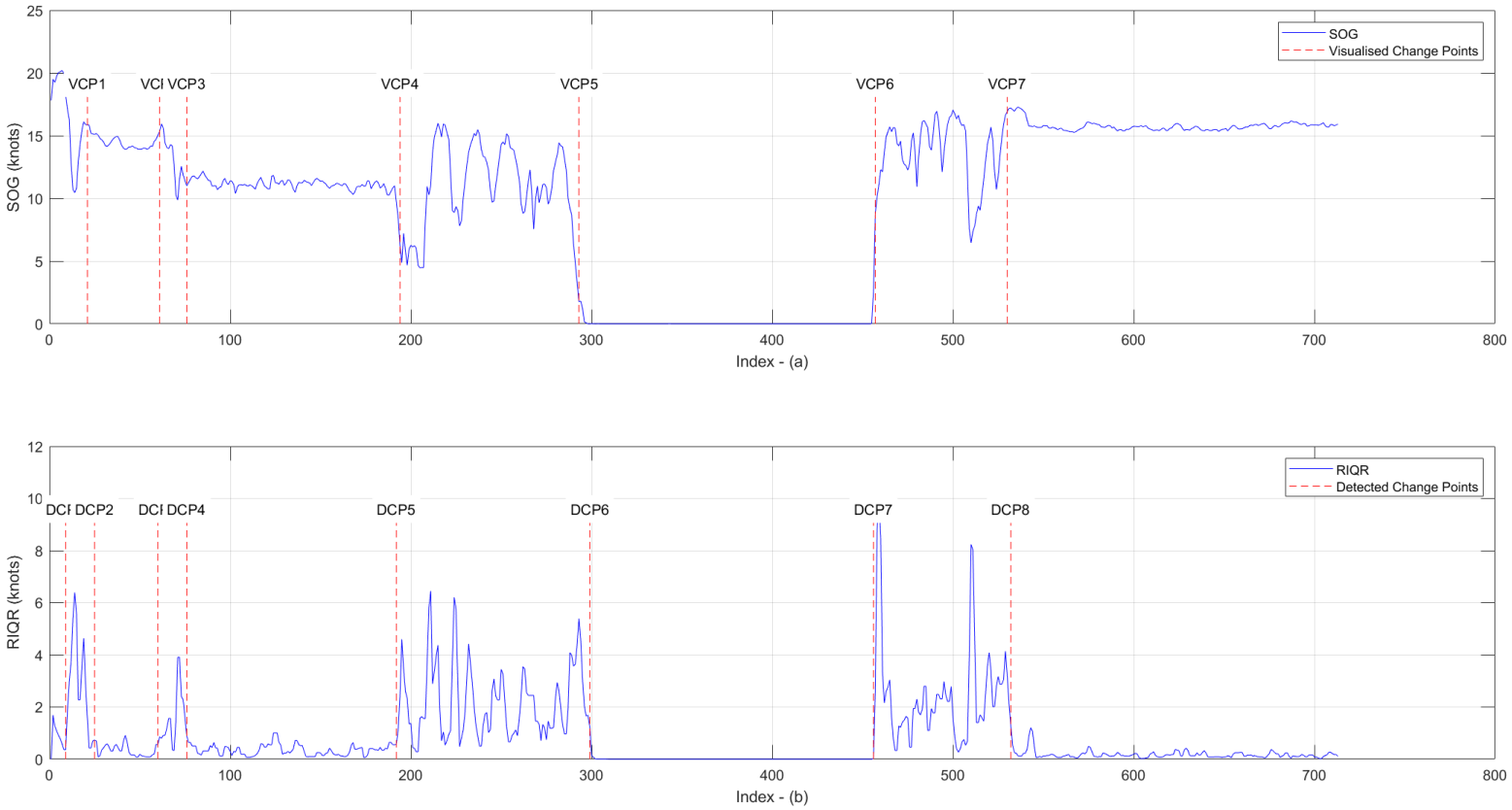

Figure 4.14 Comparisons between VCPs and DCPs for SOG data

Figure 4.14 demonstrates that the DCPs for SOG closely align with the VCPs, effectively distinguishing between the binary conditions. This alignment further substantiates the notion that inaccuracies in SpeedLL detection predominantly stem from the low precision of the GPS coordinates.

A comparison between the 'Steady State' detection results for SpeedLL and SOG reveals a similarity rate of 86.25%, with 615 data points sharing the same detected condition. This underscores that the developed algorithm maintains high performance and robustness even when applied to datasets characterised by significant fluctuations due to the low precision of coordinates. It is important to note that the available data from this particular vessel was pre-processed and rounded to two decimal points. Nevertheless, the methodology demonstrated an accuracy of 86.25% similarity despite the availability of only pre-processed data.

The decision to use SpeedLL rather than SOG is twofold. Firstly, SOG is calculated by evaluating the time differences between the GPS signals received from at least four satellites, a method that differs significantly from the SpeedLL calculation. Secondly, the developed data cleaning strategy based on the speed difference effectively filters out anomalies in the coordinates, enhancing the accuracy of both SpeedLL and Curvature calculations. Moreover, maintaining the intercorrelation between these two features is crucial, as both are derived from the distance and angle between consecutive coordinates, according to the equations. This correlation aids in defining key parameters and the rolling window combination. Upon deeper analysis, mode changes affect both parameters simultaneously, allowing the methodology to reference two parameters when detecting the operational mode. Particularly for the continuity check in binary categorisation, the status of the change points must align with the subsequent data points within the rolling window size. The continuity check is developed based on the premise that both parameters have a strong interrelationship, and that operational mode changes will simultaneously influence their statuses. Opting to use SOG instead of SpeedLL would disregard the interrelationship between these two parameters.

4.4.4 Setting the thresholds to detect steady state for Curvature

As previously discussed, the low precision of GPS coordinates affects the extracted curvature data, complicating the direct application of a threshold on its RIQR for ‘Steady State’ detection. To address this, the moving average technique has been employed on the curvature data to

smooth out fluctuations. Figure 4.15 illustrates the Curvature after applying the moving average, alongside its RIQR, with VCPs indicated.

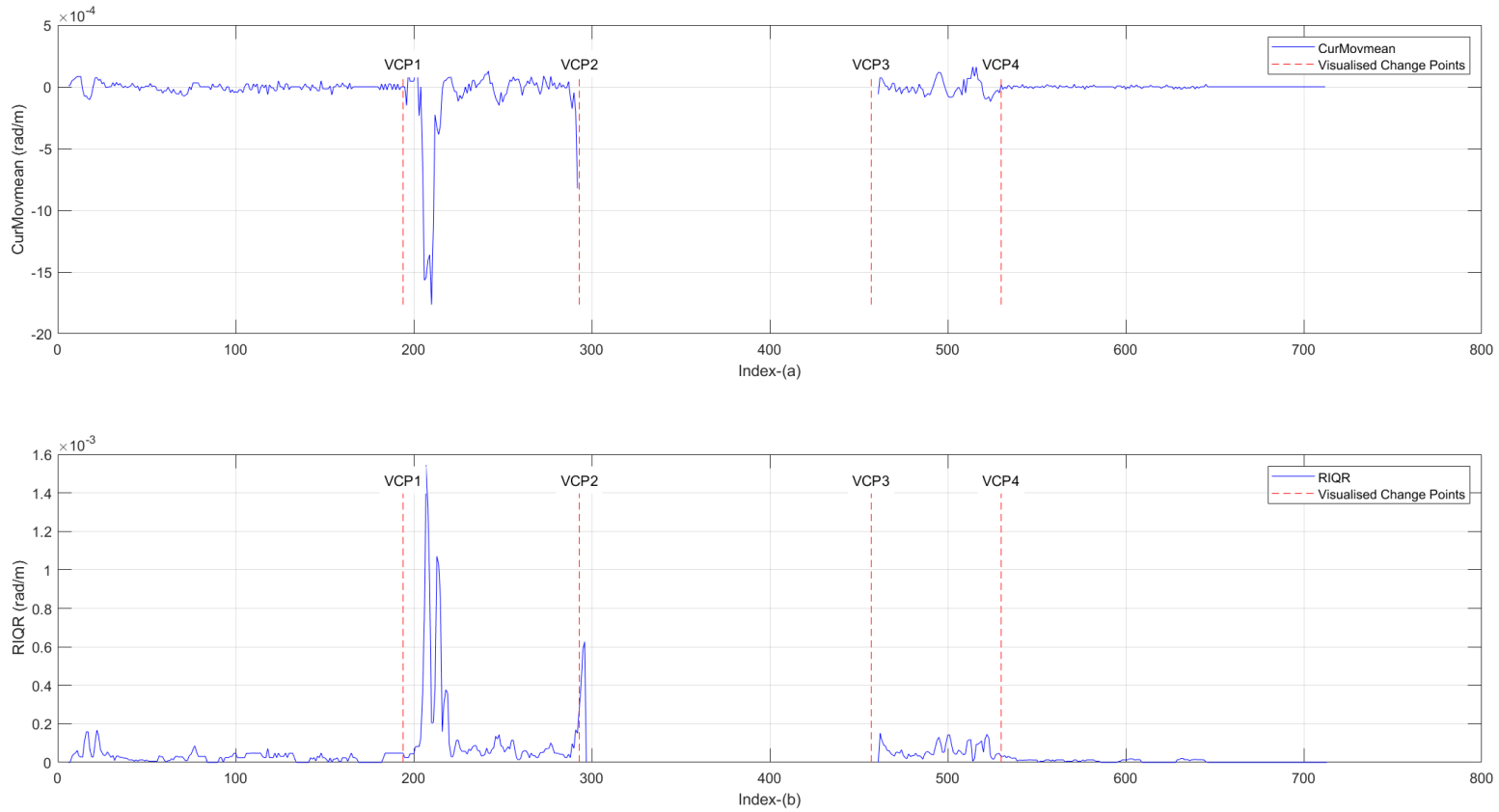

Figure 4.15 Moving averaged Curvature and its RIQR with VCPs in red vertical dots

Figure 4.15 (a) presents the curvature data subjected to the moving average technique, while Figure 4.15 (b) details the associated RIQR. VCPs are identified by red vertical dots. The application of the moving average has led to RIQR values that are consistent with the visualised 'Steady State' conditions, exhibiting relatively low values in segments from the starting point to VCP1, and from VCP4 to the dataset's end. Notably, the interval between VCP2 and VCP3 corresponds to the period during which the vessel was docked at port.

Following the observation of the RIQR for Curvature, a validation process for determining appropriate thresholds was undertaken. The range for these thresholds has been established from 3e-5 to 7e-5 rad/m, with increments of 1e-6 rad/m. Selected results from this analysis, including some of the DCPs, are presented in Table 4.6.

Table 4.6 Indices of DCPs for Curvature

Thresholds	Indices of DCPs
5e-5	200;263;271;278;288;296;461;474;492;523
5.1e-5	200;263;271;278;288;296;461;474;492;523
5.2e-5	200;263;288;296;461;474;492;523
5.3e-5	200;263;288;296;461;467
5.4e-5	200;263;288;296;461;467
5.5e-5	200;263;288;296;461;467
5.6e-5	200;263;288;296;461;467
5.7e-5	200;263;288;296;461;467
5.8e-5	200;263;288;296;461;467
5.9e-5	200;263;288;296;461;467

Table 4.6 presents a selection of indices for DCPs. It is observed that thresholds below 5e-5 rad/m do not yield effective DCPs in comparison with the indices of VCPs. For thresholds above 5.9e-5 rad/m, the indices of DCPs tend to stabilise and align closely with those detected at thresholds beyond 5.3e-5 rad/m. However, these higher thresholds fail to identify a critical change point, specifically VCP4, which has an index of 530. This omission highlights a limitation in the ability of these thresholds to capture all key operational mode transitions as indicated by the VCPs.

Detailed examination indicates that thresholds above 5.3e-5 rad/m omit VCP4, whereas thresholds below 5.2e-5 rad/m identify more segments than those indicated by the VCPs. Consequently, the threshold has been set at 5.2e-5 rad/m. Figure 4.16 presents the Curvature alongside the VCPs and shows the RIQR of the moving averaged Curvature with the DCPs indicated.

The relatively low threshold value is attributed to the application of the moving average technique to the Curvature, which is employed to mitigate inaccuracies arising from the low precision of the coordinates. On one hand, the moving average technique serves to minimize the value of the RIQR; on the other hand, considering that the target vessel is an ocean-going vessel, it is more likely to maintain a relatively straight-line pattern compared to fishing and inland waterway vessels. This operational characteristic means that the variation in Curvature for the target vessel is comparatively small. Additionally, the geographic presentation of the detected results demonstrates the effectiveness of the developed algorithm in distinguishing operational modes. This indicates that the relatively small defined threshold for curvature still performs well even in scenarios of low precision. However, the defined threshold may not hold significant meaning or be directly applicable to other ocean-going vessels, nor can it be directly inferred from domain knowledge alone.

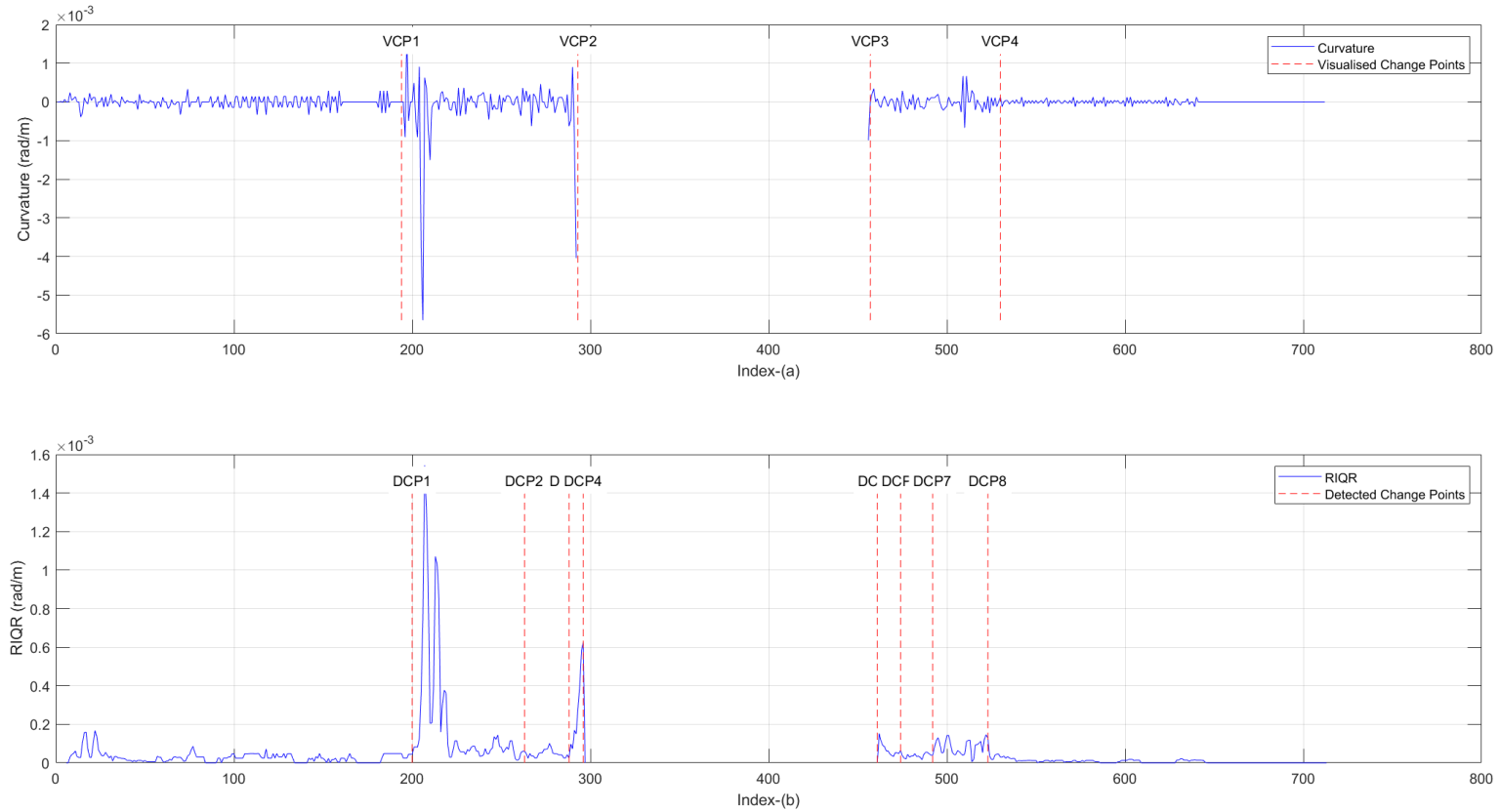

Figure 4.16 Comparison between VCPs and DCPs for moving averaged Curvature

The comparison of DCPs with VCPs in Figure 4.16 demonstrates that DCPs effectively identify 'Steady State' conditions for Curvature, with the exception of two additional segments detected within these conditions. These segments, identified between DCP2 & DCP3 and DCP6 & DCP7, fall within the segments visually delineated between VCP1 & VCP2 and VCP3 & VCP4, respectively. In Figure 4.16 (b), it is noted that the RIQR values for these segments are low, suggesting they fall beneath the defined threshold, despite being visually classified under 'Changing' conditions. This discrepancy is likely due to the moving average technique reducing their variability to below the threshold level. As previously discussed, the primary contributor to detection inaccuracies is the low precision of GPS coordinates, which affects the variability of curvature. This, in turn, complicates the detection of binary conditions by increasing the variability within 'Steady State' segments.

4.5 Operational Modes Detection

The operational modes of the target vessel have been determined through an analysis of binary conditions across three key features: SpeedLL, Curvature, and ME Load (expressed as a percentage of MCR, in this case). In this binary system, the symbol '0' denotes a 'Steady State' condition, whereas '1' indicates a 'Changing' condition for SpeedLL and Curvature. For the ME Load, a value less than 0.1% MCR is classified as 'Stop' and represented by the binary symbol '0', while values above 0.1% MCR signify 'Running' and are denoted by '1'. The correlations between these binary conditions and the three key features are detailed in Table 4.6.

Table 4.7 Correlations between binary conditions and three key features

Key features	0	1
ME Load	Stop	Running
SpeedLL	Steady State	Changing
Curvature	Steady State	Changing

Table 4.7 shows the correlation between binary conditions and the three key features, resulting in a total of eight possible combinations. Importantly, these combinations must also undergo a consistency check to ensure the accuracy of detected operational modes. Specifically, if the combination associated with a targeted data point differs from its predecessor, it must remain consistent with the data points within the subsequent window, whose size is set at 6, as determined by the sensitivity analysis of the rolling window. This

requirement stems from the understanding that operational modes cannot feasibly change within such a brief timeframe. Therefore, any change in combination that fails to meet this criterion of consistency is disregarded.

For the target vessel, distinct operational modes are represented by specific combinations of the binary conditions associated with the three key features. These combinations, and their corresponding operational modes, are systematically outlined in Table 4.8.

Table 4.8 Combination of three key features

Combination	ME load	SpeedLL	Curvature	Modes	Colour
0	0	0	0	Stop	Black
1	0	0	1		White
2	0	1	0		Purple
3	0	1	1		Orange
4	1	0	0	Transit	Green
5	1	0	1	Manoeuvring	Blue
6	1	1	0	Manoeuvring	Yellow
7	1	1	1	Manoeuvring	Red

Table 4.8 details the combinations of the three key features, with the combination codes ranging from 0 to 7, reflecting the binary-to-decimal conversion system. Each code is associated with a specific operational mode, providing a clear explanation for each unique combination.

Combination ‘0’, indicated by the binary sequence 0 - 0 - 0, signifies that the ME is stopped, and both speed and curvature are in ‘Steady State’ conditions. Given that the vessel’s propulsion is solely dependent on the ME, this combination logically suggests that the vessel has no forward motion, exhibiting a speed of nearly zero knots and no change in curvature. Accordingly, this specific combination of conditions has been designated as ‘Stop’ for the target vessel, indicating a state of complete inactivity with respect to both movement and navigational adjustments.

Combinations ‘1 to 3’ are characterised by the ME being in a stopped state, accompanied by detectable variations in either speed or curvature. Such scenarios are highly unlikely for the target vessel, given its reliance on the ME for propulsion, and would signify a potentially

hazardous emergency situation if an ocean-going vessel were to lose propulsion at sea. It is important to note, however, that the interpretation of these combinations may vary across different types of vessels. For instance, a purse seiner might still exhibit movement through the use of auxiliary thrusters during some specific fishing operations, even when the main propulsion system is inactive. This highlights the necessity of contextualising these combinations within the specific operational capabilities and practices of each vessel type.

Combination ‘4’, characterised by the binary sequence 1 - 0 - 0, indicates that the ME is operational while both speed and curvature are in ‘Steady State’ conditions. This suggests that the vessel is navigating with a consistent speed and maintaining a steady course, resulting in a trajectory that approximates a straight line. Such conditions are indicative of the vessel engaging in a ‘Transit’ mode of operation, wherein it is actively moving between two points without significant navigational adjustments or variations in speed.

Combination ‘7’, denoted by the binary sequence 1 - 1 - 1, signifies that the ME is operational, accompanied by variations in both speed and curvature. This condition suggests that the vessel is actively adjusting its speed and altering its course, behaviours characteristic of a ‘Manoeuvring’ operational mode. Such a mode is typically engaged when the vessel is navigating through complex navigational scenarios, requiring dynamic adjustments to maintain or change its trajectory and speed in response to immediate environmental or operational demands.

Combinations ‘5’ and ‘6’ signify that either speed or curvature, respectively, remains in a ‘Steady State’ condition while the ME is operational. For the target vessel, these combinations are also classified under the ‘Manoeuvring’ operational mode. Based on the author’s domain knowledge, there is common recognition to distinguish 'Manoeuvring' from 'Transit', typically marked by the number of auxiliary engines running exceeding two, particularly for ocean-going vessels. In this case, an additional test has been conducted to verify whether the detected combinations '5', '6', and '7' align with this domain knowledge. During conditions represented by combinations ‘5’ and ‘6’, 89% and 78% of data points, respectively, indicate the operation of two auxiliary engines, with the remainder involving just one auxiliary engine. In contrast, combination ‘7’ shows a slightly different pattern, with 66% of data points reflecting the use of two auxiliary engines, and 34% indicating the operation of three auxiliary engines.

Given the frequency of auxiliary engine usage under these conditions, combinations ‘5’, ‘6’, and ‘7’ collectively characterise the ‘Manoeuvring’ mode for the target vessel. This amalgamation complies with the domain knowledge, signifying active navigational adjustments. For other vessel types, combinations ‘5’ and ‘6’ might denote specific operational modes, highlighting the importance of contextual and vessel-specific considerations in operational mode classification.

To facilitate a clear visual differentiation of the detected operational modes, each mode has been assigned a unique colour, as detailed in Table 4.7. This approach allows for an intuitive understanding of the operational state of the vessel at any given point in the dataset. The application of this colour coding to represent the various operational modes identified within the example dataset is illustrated in Figure 4.17.

Figure 4.17 Detected operational modes for the exemplary sub-dataset

In Figure 4.17, segments shown in green indicate that the vessel is operating in ‘Transit’ mode, characterised by a trajectory that approximates a relatively straight line. Conversely, the 'Stop' mode is depicted by black dots, which are primarily clustered at a single coordinate, indicating the vessel's stationary position at the port near Portland. However, when the vessel begins to

manoeuvre at the same coordinates, this activity is represented by a red dot that overlays the original black one. As a result, in Figure 4.17, the initial black dot representing the stationary state is obscured by the red dot indicating movement, effectively hiding the visual representation of the 'Stop' mode at that coordinate.

The segments coloured blue, yellow, and red are collectively classified under ‘Manoeuvring’, corresponding to combinations ‘5’, ‘6’, and ‘7’. The colour red is used to indicate segments where both speed and curvature are in ‘Changing’ conditions, typically found in the winding and complex inland waterways leading to the port at Portland. Blue segments denote instances where only the curvature is changing, a detection that aligns with the vessel navigating through certain parts of the winding inland waterways. Yellow segments, on the other hand, signify conditions where speed is changing while curvature remains in a ‘Steady State’. An interesting case is a yellow segment near Victoria, where the vessel is navigating a turn, yet the curvature is classified as ‘Steady State’. This discrepancy arises because the detected change points failed the consistency check; although four consecutive data points indicated ‘Changing’ conditions, this state did not persist for the required 36-minute checking period, leading to the curvature variation being disregarded as a spike rather than a mode change.

This anomaly, as well as the general challenge in accurately detecting changes in operational modes, is exacerbated by the low precision of the GPS coordinates. This limitation can notably increase data variability when in a ‘Steady State’, contributing to potential inaccuracies in mode detection.

The outcomes presented in Figure 4.17 demonstrate the efficacy of the developed algorithm in accurately identifying the operational modes of the target vessel from the selected dataset, even in the context of low GPS precision. The analysed thresholds for the two key features—SpeedLL and Curvature—along with the systematic approach of the algorithm, have been applied across the entire dataset. This comprehensive application further validates the algorithm’s capability to discern the operational modes under low precision context.

4.6 Results and Discussion

The developed algorithm, alongside the thresholds analysed for key features, has been applied to a three-month dataset for the target vessel to assess its operational modes over an

extended period. The distribution of the detected combinations, representing various operational modes as identified by the algorithm, is illustrated in Figure 4.18.

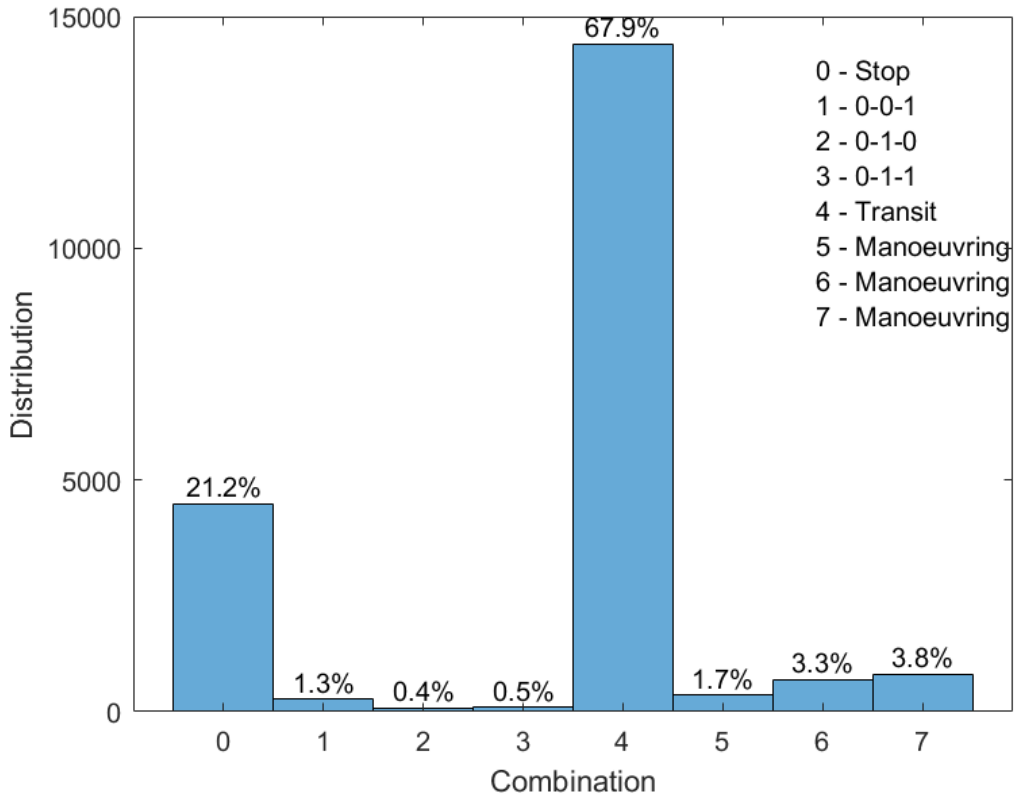

Figure 4.18 Distribution of the detected combinations of the target vessel

Figure 4.18 reveals the operational mode distribution for the target vessel, indicating that the majority of the time, 67.9%, the vessel operates in 'Transit' mode. It is stationary, or in 'Stop' mode, 21.2% of the time, while 'Manoeuvring' accounts for 8.8% of the operational period. Notably, combinations '1 to 3' have been detected, comprising 2.2% of the data points. These combinations present a challenge for interpretation within the context of domain knowledge concerning the target vessel. Given their unexpected presence in the dataset, a thorough examination of these categories was conducted, beginning with an analysis of combinations '1 to 3'.

The integrity of continuous data points is crucial for the performance of the developed algorithm, with the most direct method of evaluating detection accuracy involving the visualisation of operational mode categories along the vessel's trajectory. This approach offers a comprehensive view of the vessel's operational patterns, incorporating multiple modes, as opposed to isolated analysis of data points within individual categories. It's important to note

that the ‘Stop’ mode may not be distinctly visible in such visual representations, primarily because ocean-going vessels often remain stationary at ports, leading to the aggregation of ‘Stop’ mode data points at a single coordinate or at anchor outside of ports with no significant motions. Figure 4.19 includes illustrations of the continuous dataset segments that encompass combinations ‘1 to 3’.

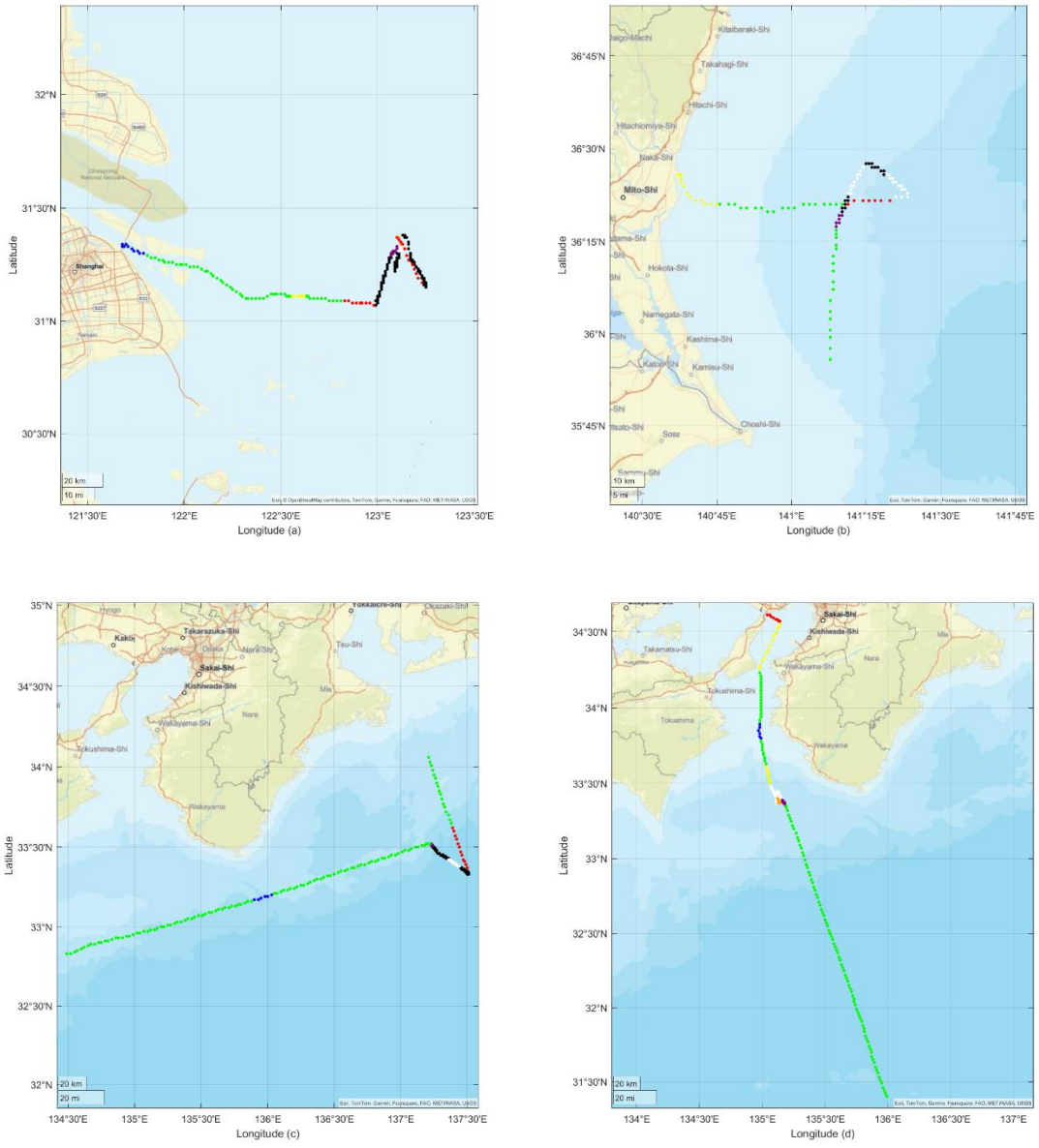

Figure 4.19 Trajectories of the dataset with detected combinations of ‘1 to 3’

Figure 4.19 displays the trajectories of the dataset, highlighting detected combinations ‘1 to 3’ through the use of distinct colours for each specific combination, as detailed in Table 4.7. In this graphical representation, black is used to denote combination ‘0’, signifying a ‘Stop’ mode. White indicates the combination ‘0 - 0 - 1’, purple represents ‘0 - 1 - 0’, and orange signifies ‘0

- 1 - 1'. These colour-coded trajectories across Figures 4.19 (a) to (d) uniformly show the vessel's journey as it approaches the port from a distance.

The intervals characterised by combinations '1 to 3' in the dataset can be understood as periods during which the vessel remains stationed at the outer anchorage, pending clearance from port authorities or preparing for docking due to other reasons. Upon receiving the necessary authorisation, the vessel then proceeds to dock at the port. This interpretation suggests that these combinations signify a transitional phase in the vessel's operations, bridging the gap between active navigation and stationary periods at the port.

Given that the ME is inactive during these intervals, which are relatively brief, and considering the complex and unpredictable environmental influences on the vessel's trajectory, it is practical to aggregate combinations '1 to 3' as a specific phase denoting the vessel's preparatory actions for port entry. While some data points categorised under 'Stop' mode, represented by the colour black, also occur during this period, distinguishing these from the preparatory phase in the figure does not present significant challenges. Moreover, the frequency of such 'Stop' mode data points within this particular context is relatively low, further supporting the decision not to segregate them explicitly for this analysis. This approach simplifies the interpretation of operational modes by recognising a specialised period of port approach, distinct from standard 'Stop at port' instances.

To assess the effectiveness of the developed algorithm in detecting 'Manoeuvring' operational modes, specifically through the lens of combinations '5 to 7', a representative trajectory is presented in Figure 4.20.

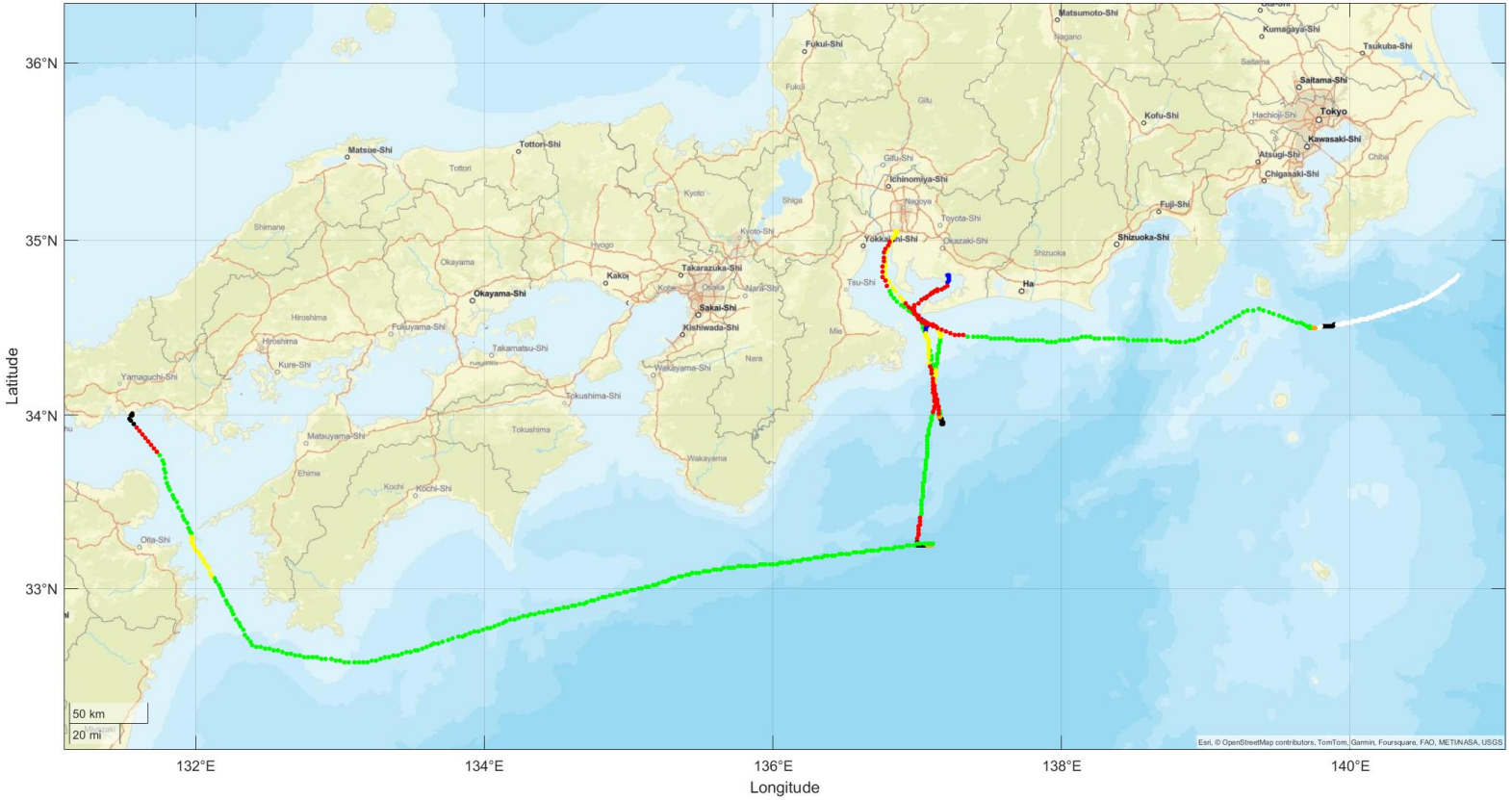

Figure 4.20 Trajectory of one continuous dataset to evaluate ‘Manoeuvring’ detection

Figure 4.20 illustrates the trajectory of a continuous dataset, employing colour coding to differentiate between specific detected combinations indicative of ‘Manoeuvring’ actions.

The trajectory, commencing from the west and progressing eastward, encompasses the vessel’s journey to three different ports. For analytical clarity, this journey will be divided into three distinct sections, each demarcated by outer anchorage areas. The outer anchorage areas are defined by visual inspection of the trajectory. These intervals serve as transitional phases in the vessel’s operational behaviour, facilitating a segmented analysis of its navigational patterns as it approaches and departs from each port.

1. Trajectory from port of Hofu-Shi to the first outer anchorage area

Initially, the vessel is docked at the port of Hofu-Shi, located on the left-hand side of the overall trajectory. It then begins to manoeuvre out of the port and enters ‘Transit’ mode, navigating towards the outer anchorage area positioned in the middle of the figure, where it awaits clearance while preparing to proceed to the port of Chita-Shi. Notably, within the ‘Green - Transit’ mode segments on the left-hand side, a segment-coloured yellow is observed. Upon closer examination, this segment can be interpreted as a navigational adjustment made by the vessel to reduce speed while safely navigating through closely situated islands. This operational detail is further illustrated in Figure 4.21.

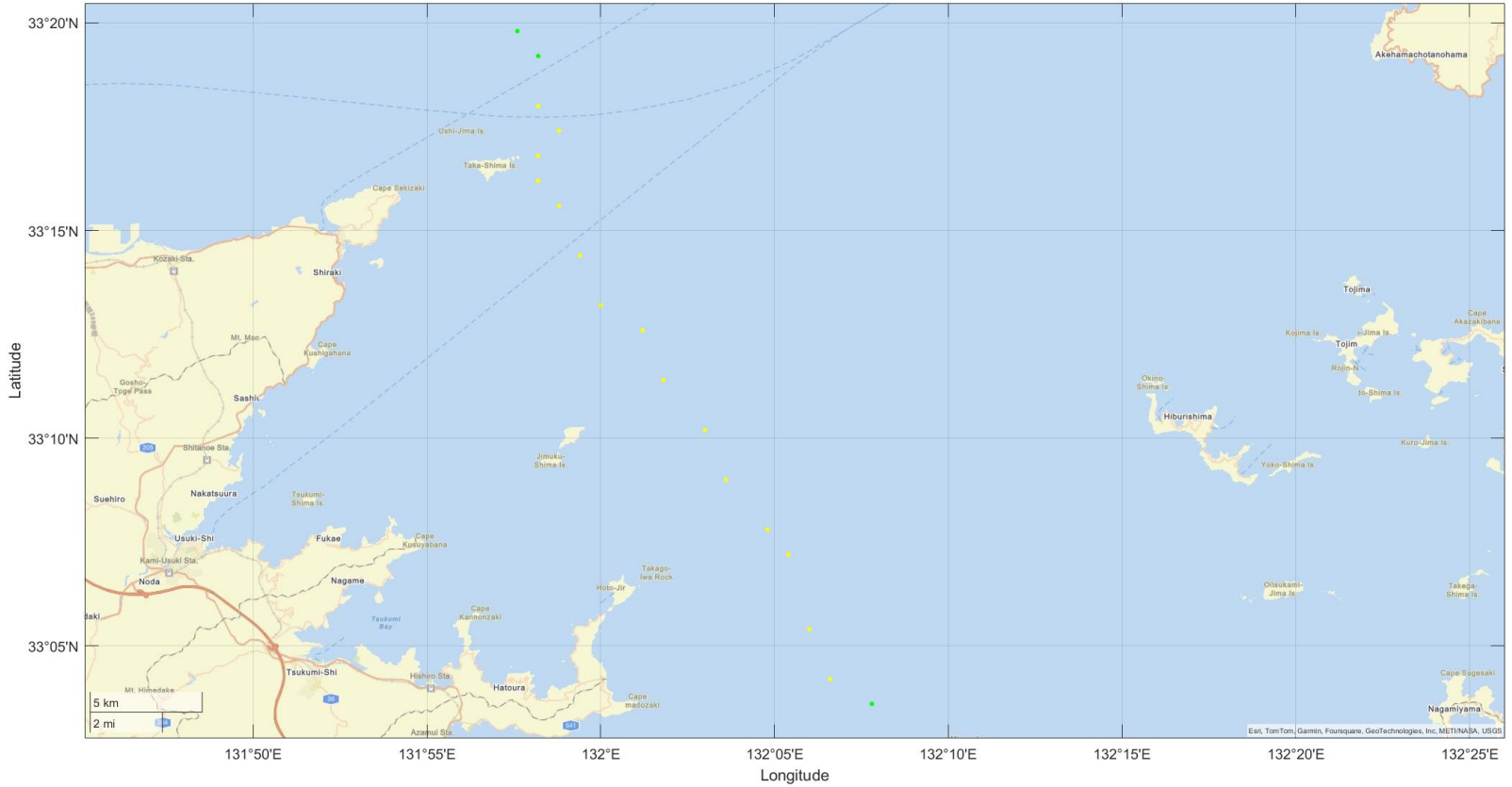

Figure 4.21 Trajectory that the vessel passes through islands

At the outset of the trajectory, near the port of Hofu-Shi, several data points are black, suggesting an operational mode of ‘Stop’. However, these points do not align with the anticipated operational category of ‘Stop’, they are the transient mode between the ‘Stop’ and ‘Manoeuvring’ modes. Figure 4.22 provides a detailed visualisation of these black data points.

Figure 4.22 Details of the black data points

Figure 4.22 identifies six black data points, indicative of a ‘Stop’ operational mode. Among these, one point accurately represents the vessel’s position when stopped at the port, while the remaining five points are under transient mode. These detections arise from the algorithm’s consistency check requirement, wherein change points must sustain their status for a minimum duration (36 minutes in this case) and match the operational mode of subsequent data points within the window size. The original detected combinations for these points were classified as ‘4-4-6-6-6’. Given that the preceding data point is marked as ‘0’ (Stop) and the following as ‘7’ (Manoeuvring), these five points were initially identified as change points. However, they failed the consistency check because their ‘Changing’ status did not persist for the requisite duration nor did they align with the subsequent five data points’ combinations. Consequently, these points’ statuses were disregarded, and they were retroactively adjusted to reflect the previous combination.

As discussed in Section 3.5.2.3, vessels require a brief period to complete a mode change, and data points during this transient mode are detected as the end of previous mode by this algorithm. The originally detected combinations, ‘4-4-6-6-6’, indicated that the ME of the target vessel was running initially but showed no significant variations in both SpeedLL and

Curvature. After 12 minutes, the SpeedLL was detected as ‘Changing’ only, and transition of the operational mode operational mode from ‘Stop’ to ‘Manoeuvring’ had been completed from the 7th data point. This brief period for mode transitioning has a strong relationship with the vessel’s manoeuvrability, indicating the time required to complete the mode change. In this case, a half-hour with five data points closely aligns with the expectation for the target vessel, an ocean-going car carrier.

2. Trajectory from 1st to 2nd outer anchorage area

Figure 4.23 presents the detailed trajectory of the vessel in section 2. Upon receiving clearance, the vessel manoeuvres away from the first anchorage area and adopts ‘Transit’ mode as it heads north, passing a second outer anchorage area. As the vessel navigates around Cape Largo towards the port of Chita-Shi, it transitions into ‘Manoeuvring’ mode, reflective of the navigational adjustments required to safely approach the port. Following its departure from Chita-Shi, the vessel moves back to the second outer anchorage area, primarily in ‘Manoeuvring’ mode. Notably, a segment within this trajectory is detected as operating in ‘Transit’ mode; however, given the vessel’s operational context and the engagement of three auxiliary engines while reducing speed for safety near Cape Largo, this segment more accurately represents ‘Manoeuvring’. The SOG and SpeedLL for this segment are further detailed in Figure 4.24.

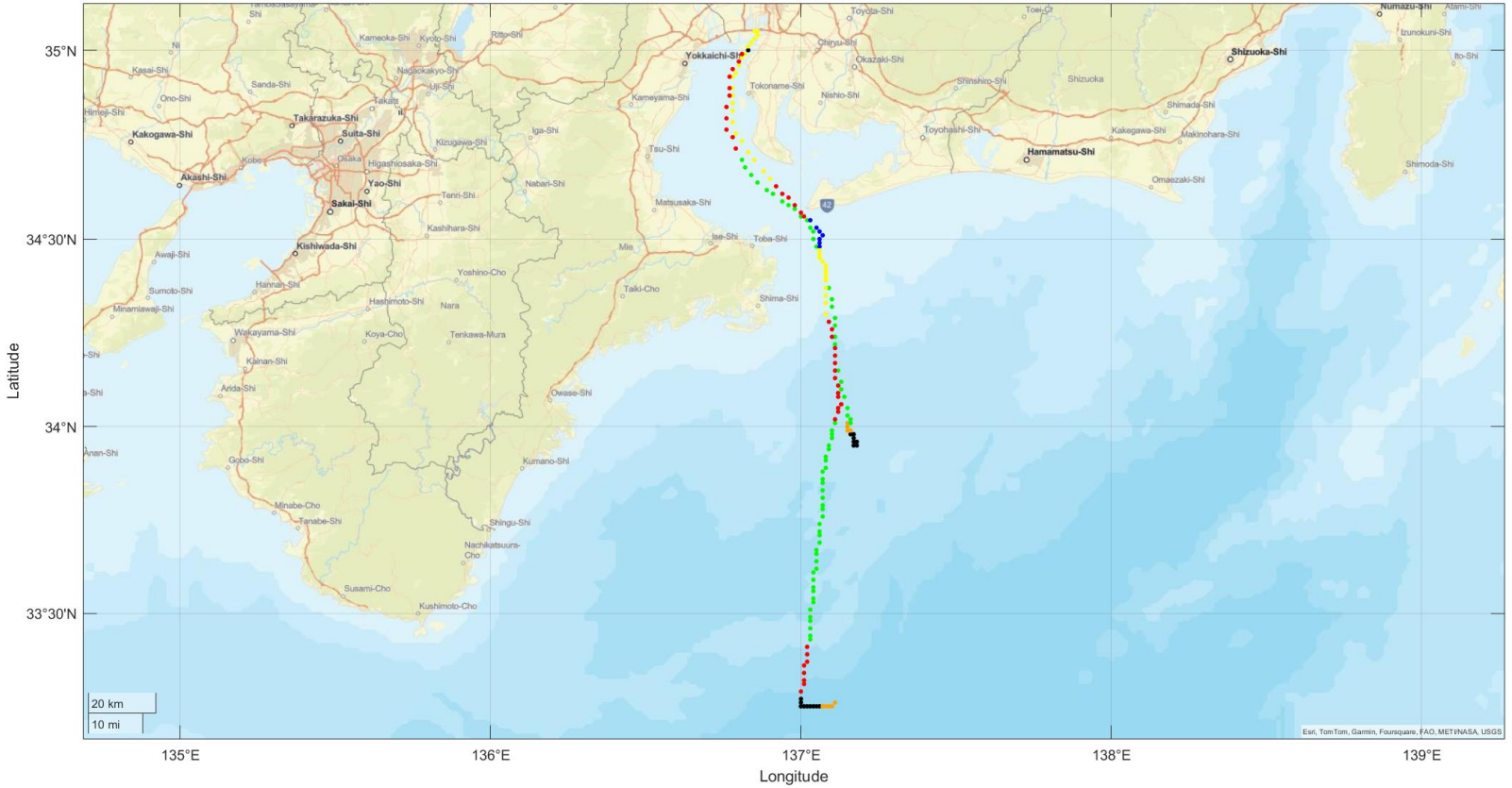

Figure 4.23 Trajectory of section 2

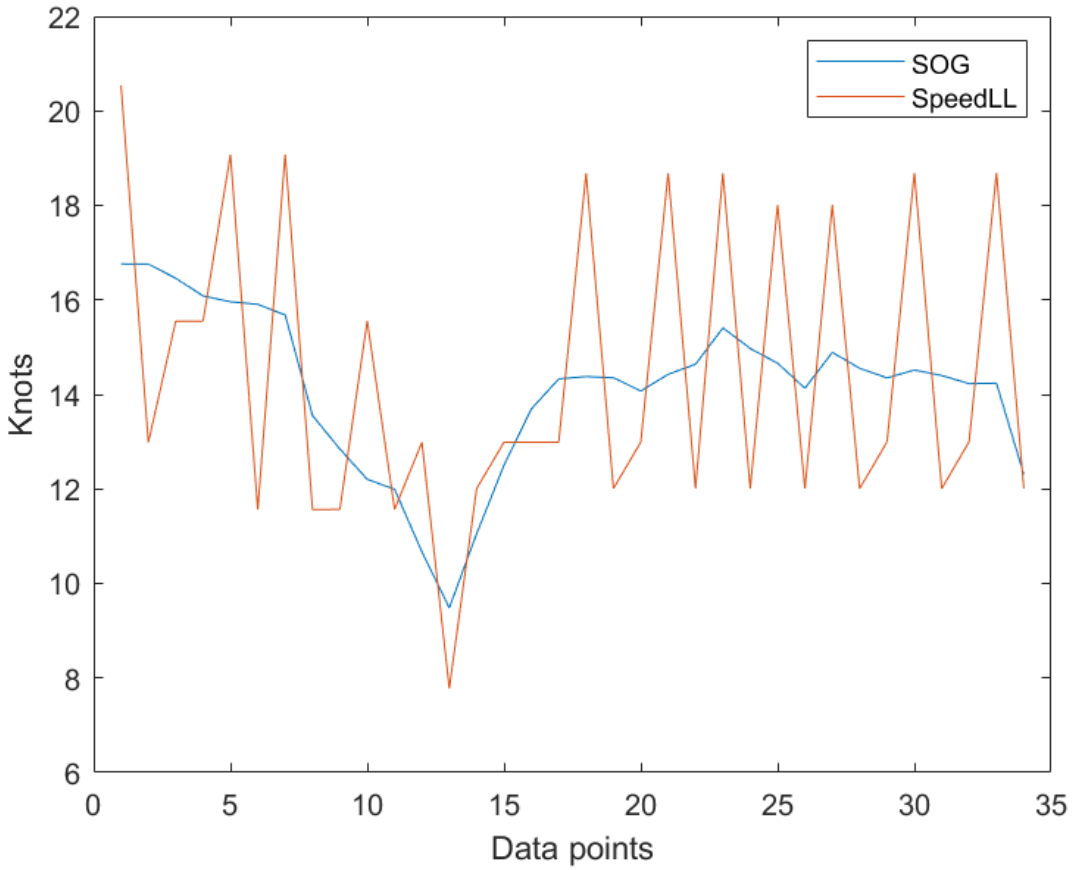

Figure 4.24 Detailed SOG and SpeedLL for particular segment

Figure 4.24 illustrates a significant reduction in SOG, with speed decreasing sharply from above 16 knots to around 9 knots to safely navigate past Cape Largo, before recovering to approximately 15 knots. The SpeedLL data exhibits similar trends, albeit with regular fluctuations before and after the speed reduction. This phenomenon suggests that the conditions preceding and following the speed decrease are relatively similar, or, that the speed recovers so swiftly that the algorithm fails to register this as a significant change. A closer examination reveals that 4 to 5 data points are encompassed within this speed variation phase. Furthermore, as previously mentioned, the low precision of GPS coordinates likely contributes to a reduction in the detection accuracy, affecting the algorithm's ability to accurately discern such rapid operational changes.

3. Trajectory from 2nd out anchorage to the end point

Figure 4.25 presents the vessel's trajectory as it departs from the second anchorage area and manoeuvres towards the port of Gamagori-Shi before proceeding to the third anchorage area.

‘Manoeuvring’ modes are detected as the vessel navigates in and out of the Cape Largo area, indicative of the intricate navigational adjustments required. In contrast, the vessel operates in ‘Transit’ mode while traversing open water areas, signifying a period of straightforward navigation with a steady course and speed. This distinction between ‘Manoeuvring’ and ‘Transit’ modes highlights the vessel’s adaptive operational responses to varying navigational challenges encountered along its route.

Figure 4.25 Trajectory of section 3

A segment detected as combination ‘1’ occurs from the third anchorage area to the endpoint, suggesting the vessel might be drifting for an extended distance without active propulsion. This period is characterised by the operation of only a single set of auxiliary engines. Further examination of the dataset, which follows a one-time stamp gap, reveals that the vessel is in preparation to dock before proceeding to the next port. This continuation of activity suggests a brief transitional phase rather than a prolonged stop. Figure 4.26 provides a visualisation of the vessel’s trajectory in the following dataset, offering insights into its operational status and navigational adjustments as it prepares for further port calls.

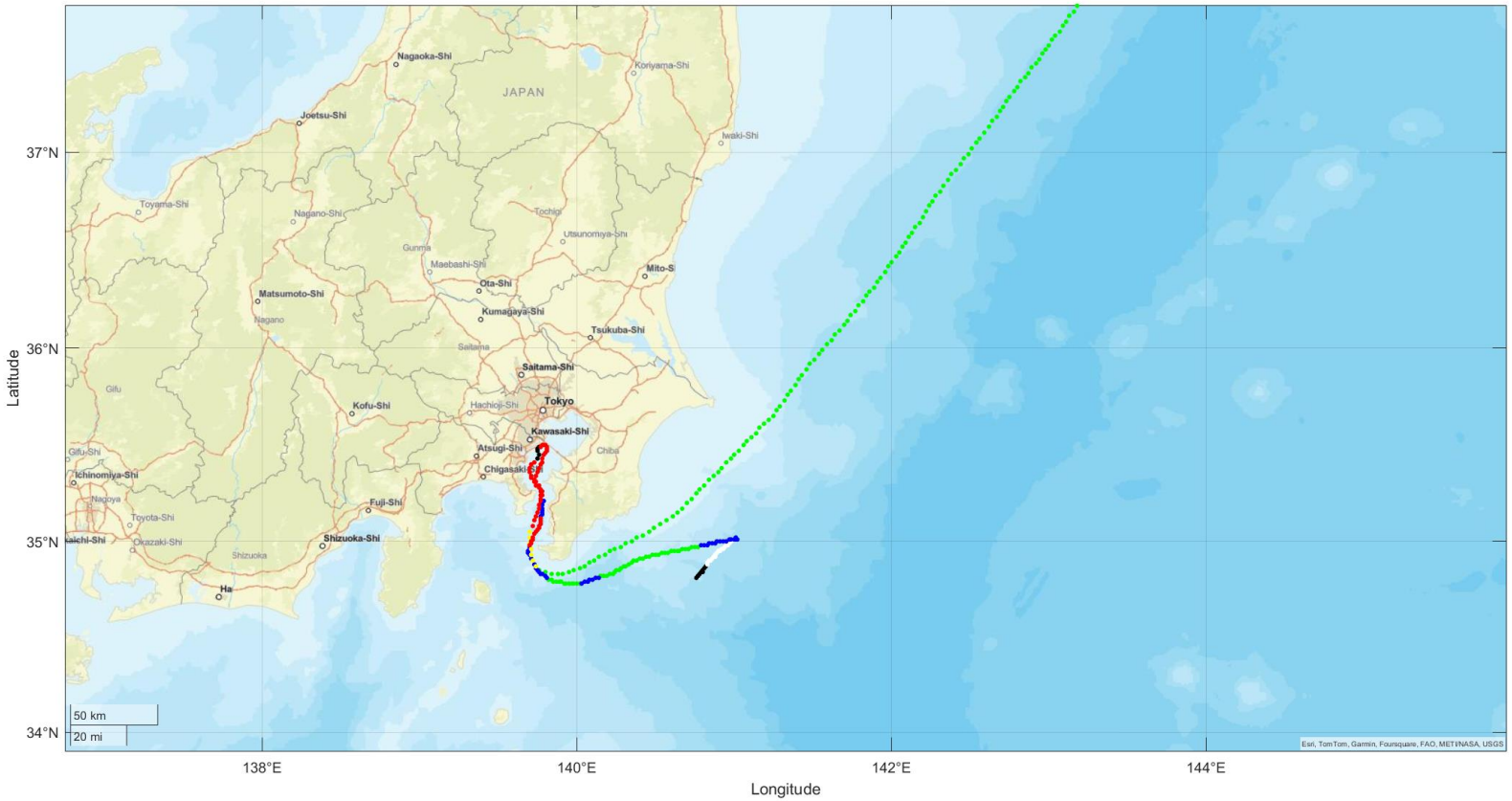

Figure 4.26 Trajectory of the proceeding dataset

Following the thorough examination detailed above, the operational modes for the target vessel have been classified as follows: ‘Stop’; ‘Preparing for port’, which aggregates combinations ‘1 to 3’; ‘Manoeuvring’, encompassing combinations ‘5 to 7’; and ‘Transit’ mode. By overlooking the single data point gap between the two datasets, and assigning black, red, and green colours to represent ‘Preparing for port’, ‘Manoeuvring’, and ‘Transit’ operational modes respectively, a coherent visualisation of the vessel’s operational dynamics across the combined dataset is achieved. Figure 4.27 illustrates the operational modes detected across this comprehensive dataset.

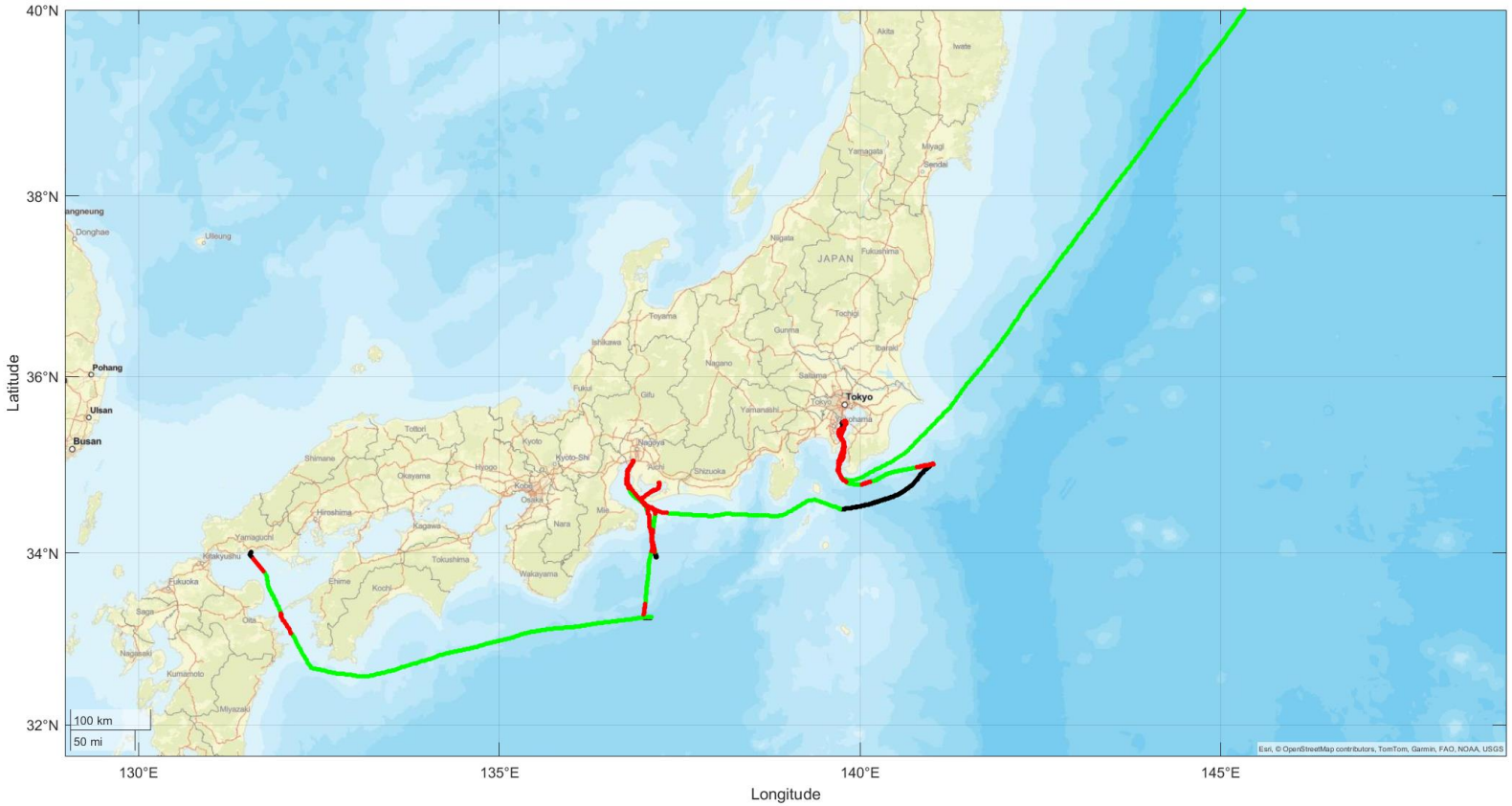

Figure 4.27 Operational modes detection for the combined dataset

Disregarding a single data point gap, the algorithm has been applied to a combined dataset encompassing 1564 data points over a duration of 156.4 hours—equivalent to approximately one week. During this period, the vessel visited four ports, navigating through the complex and diverse topography of the maritime area around Japan, characterised by a coastline with numerous twists and turns that complicate navigation routes and pose significant challenges to operational mode detection.

Despite these challenges and the extended timeframe of analysis, the operational modes detected by the algorithm closely align with graphical representation based on domain knowledge. This alignment is maintained with the exception of two brief segments, discussed in the context of Figure 4.22 and Figure 4.24, involving a total of 40 data points.

All navigational activities associated with entering and exiting ports have been accurately classified as 'Manoeuvring'. Furthermore, three distinct periods of outer anchorage have been identified, each linked to the approach towards subsequent ports, effectively characterising these intervals as preparatory phases for port clearance. These anchorage periods could also be conceptualised as 'at anchor', with the vessel's navigation into and out of these areas similarly classified under 'Manoeuvring'.

The examination of the algorithm's performance in identifying 'Transit' mode, as evidenced in Figures 4.20 to 4.27, demonstrates its adeptness at detecting segments correctly marked in green as representing 'Transit'. These segments, noted for their relatively straight-line trajectories, accurately reflect operational characteristics consistent with domain knowledge, particularly in shallow water areas.

The algorithm's efficacy extends to open ocean conditions, an environment where ocean-going vessels predominantly operate. This is substantiated by the distribution of the 'Transit' mode, which accounts for 67.9% of the operational time, indicating that the vessel spends a significant portion of its journey traversing the ocean**.** Figure 4.28 illustrates a representative continuous dataset identified by the algorithm as an instance when the vessel is operating in 'Transit' mode. This dataset contains 1286 datapoints, spanning 128.6 hours, more than 5 days. It records the trajectory form Japan to the USA, with all data points consistently classified as 'Transit', in accordance with the geographic representation.

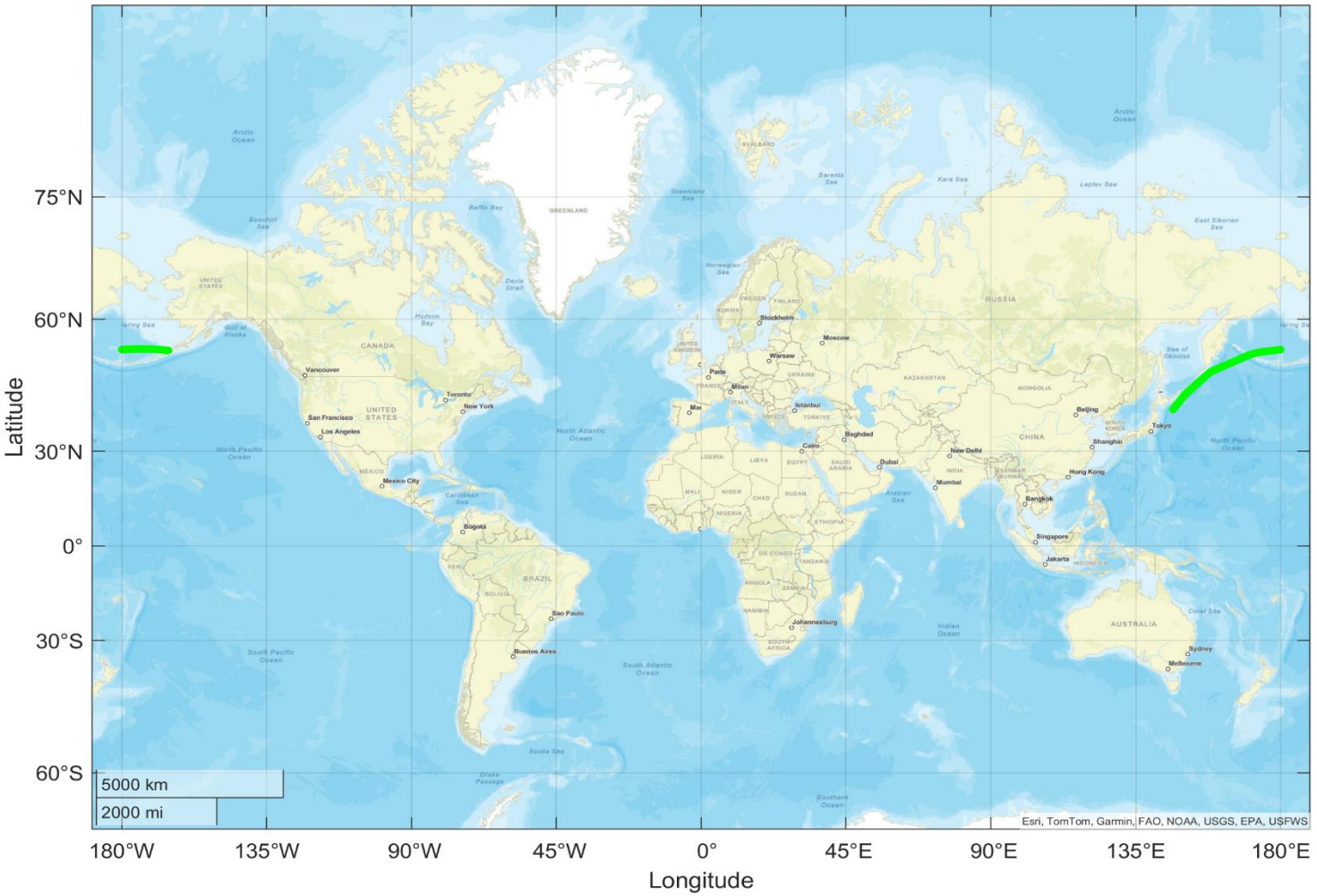

Figure 4.28 Trajectory of target vessel from Japan to the USA under ‘Transit’

Another eight continuous datasets classified under ‘Transit’ mode in open sea navigation areas are detailed in the Appendix A. Each dataset spans extensive periods, with durations of at least 20 hours, during which the vessel covers significant distances.

4.7 Summary

In this chapter, the application of the developed algorithm to a three-month dataset for an ocean-going vessel has demonstrated excellent performance in detecting operational modes. Four specific modes—’Stop’, ‘Manoeuvring’, ‘Preparing to the port’, and ‘Transit’—were identified for the target vessel. To address the issue of data noise resulting from low precision GPS coordinates, the moving average technique was employed, significantly enhancing the detection accuracy. The successful detection outcomes not only underscore the algorithm’s robustness but also its ability to perform effectively amidst substantial data noise.

The algorithm’s performance may also be attributed to the inherently straightforward and limited range of operational modes characteristic of ocean-going vessels. Chapter 5 will investigate the algorithm’s performance in more complex scenarios, aiming to further assess its efficacy and generalisability. To this end, a case study involving a tuna purse seiner—a vessel type known for its complicated operational modes and higher precision GPS coordinates—will be conducted. This exploration will provide deeper insights into the algorithm’s adaptability and utility across different maritime operational contexts.

Chapter 5 Case study – Transit Mode Detection for a Fishing Vessel

In Chapter 4, the developed methodology was applied to an ocean-going vessel, where its navigation area is predominantly at open seas. The successfully application and high performance of mode detection indicate the robust and efficiency of the developed algorithm and its adaptability to the ocean-going vessels. To further evaluate the algorithm's adaptability, the methodology will be conducted on a tuna purse seiner where predominantly operates at open seas as well.

As discussed in Chapter 4, the single design purpose of the traditional commercial vessels makes the operational modes detection relatively straight-forward, with three common operational modes to be detected. In this chapter, the tuna purse seiner would be an example of specific vessels with multiple design purposes.

Not similar with the commercial vessels, various types of specialised vessels are designed for specific tasks. Therefore, in addition to the three common operational modes, the specifically designed operational modes will vary for different types of specialised vessels. Thus, the particular focus in this chapter is to identify the 'Transit' mode amidst intricate operational patterns typical to fishing activities, as this mode's data is crucial for developing a fuel consumption prediction model in later analysis. This approach demonstrates how the methodology serves as a preliminary step, laying the groundwork for more targeted and purpose-driven research.

5.1 Introduction of the Target Vessel

5.1.1 General parameters of the tuna purse seiner

The vessel selected for this case study is a Spanish tuna purse seiner, operational in the tropical Indian Ocean. The key parameters of the purse seiner are presented in Table 5.1. Its propulsion system features a 4,500 kW main engine powering a single line shaft and with a controllable pitch propeller (CPP). Additionally, the vessel is equipped with five auxiliary engines. These engines provide power for various fishing operations and two thrusters.

Table 5.1 General parameters for the target tuna purse seiner

Overall Length	89.28 m
Length between PP	75.20 m
Maximum Beam	14.35 m
Crew	42
Propulsion Power	4500 kW
Propulsion Type	Single line shaft, CPP
Power Plant	4*968 kW; 1*768 kW

5.1.2 Operational modes of the tuna purse seiner

The operational modes of this fishing vessel are notably complex, posing additional challenges in accurately detecting the 'Transit' mode. Basurko et al. (2022) identified three operational modes for the target vessel during its voyages: 'Cruising', 'Fishing events' and 'Inactive at Sea'. There are six distinct phases during 'Fishing events'.

Fishing events are typically initiated when the vessel approaches a Fishing Aggregating Device (FAD) or identifies a Free-Swimming School (FSC). Then, the skippers need to make a critical decision within the following approximately 10 to 40 minutes, assessing whether to proceed with a fishing attempt ('set'). This decision is based on factors such as the likelihood of a successful catch and the estimated quantity of fish available. If the potential for a successful set is high, the operation is commenced.

A 'set', in the context of purse seiner operations, encompasses the entire process of fishing – starting from the deployment of the net to the completion of the seine haul. As outlined by (Basurko et al., 2022, Ben-Yami, 1994, Poisson et al., 2014), a set is divided into six distinct phases: Setting, Pursing, Net Hauling, Preparation of the Bunt, Brailing, and Ending.

The 'Setting' phase is a critical period in purse seine fishing, encompassing the moments before and during the deployment of the net. During this phase, the purse seine net is deployed around a school of tuna. The process involves encircling the fish with the net, forming a complete loop, to ensure that the entire school is enclosed. This encirclement is crucial for the success of the fishing operation. The vessel speed is maintained at around 14-15 knots, with no significant variations in engine speed.

Pursing: This phase follows the deployment of the net. During this process, the bottom of the net is cinched closed, akin to a drawstring bag. This action prevents the fish from escaping downwards. Termed 'Pursing', this technique effectively entraps the school of tuna within the net, ensuring that they are securely contained and unable to escape. Once the setting phase has concluded, the shaft power reduces sharply and is then maintained constant for 15-25 minutes. This phase ends when the main engine is stopped.

Net Hauling: This phase involves the gradual retrieval of the net onto the fishing vessel. As the net is methodically hauled in, the fish within it are increasingly concentrated. This process not only serves to secure the catch but also progressively reduces the area available to the fish, effectively intensifying the concentration of the catch as the net is drawn closer to the vessel.

Preparation of the Bunt: The 'bunt' is the term used to describe the deepest part of the net, which serves as the primary collection point for the fish during harvesting. After the fish are completely encircled and the purse line is securely closed, attention shifts to the bunt. This phase involves preparing the bunt for the crucial task of hauling the catch onboard. It becomes the focal point of the operation, as it holds the concentrated mass of fish that have been trapped by the net.

Brailing: In this crucial phase, the captured tuna are transferred from the seine net into the vessel's hold. This transfer is typically accomplished using a specialised smaller net known as a 'brail'. The brail is used to scoop the fish out of the larger seine net and onto the vessel. This process is essential for the efficient and effective retrieval of the catch, ensuring that the tuna are securely and safely moved from the net to the storage area of the ship.

During the Net hauling, Preparation of the Bunt, and Brailing phases, the main engine remains off, and the vessel is usually adrift. Auxiliary thrusters are used to control the vessel.

Ending: This final phase of a set encompasses several crucial activities. It begins with the re-boarding of the skiff, which is a high-powered support boat instrumental in the encirclement process during the net setting phase. Following this, there is preparation of the fishing gear and the deck. This preparation is to ensure that the vessel is ready to depart from the current fishing site and is fully equipped for the subsequent fishing operation. These concluding steps are essential for maintaining the efficiency and readiness of the vessel for continuous fishing

activities. During this period, the vessel speed increased from 1-2 knots, propelled by auxiliary thrusters, to its normal cruising speed.

In addition to the six distinct phases during fishing events, Basurko et al. (2022) identified two extra operational profiles for the target vessel during its voyages: Cruising and Inactive at Sea. However, their definition of 'Cruising' does not completely align with the definition used in this case study. It includes not only periods when the vessel navigates at a relatively constant course to various fishing grounds or FADs but also times when the vessel is entering or leaving a port. However, during port entry and exit, manoeuvring is necessary, often involving variable speeds and courses.

In contrast, for the purposes of this case study, 'Transit' is specifically defined as periods when the vessel is operating at a fairly constant speed and maintaining a stable course. This distinction is crucial for the accurate detection and analysis of the cruising mode in the context of the developed algorithm.

The activity profile termed 'Inactive at Sea' is defined as a state wherein the main engine of the vessel is inactive or shut down for a duration exceeding three hours at night. This definition implies that the vessel is neither engaged in 'Cruising' nor 'Fishing'.

5.1.3 Challenges of detecting 'Transit' for tuna purse seiner

There are similarities in machinery status between the 'Inactive at Sea' mode and certain fishing phases, specifically 'Net Hauling', 'Preparation of the Bunt', and 'Brailing'. For instance, during these activities, the vessel primarily relies on auxiliary thrusters, and the shaft power is negligible. This similarity in machinery operation during different phases adds a layer of complexity to the task of accurately identifying and differentiating between these modes, especially in the context of algorithmic detection.

The inherent complexities in the operational modes of the fishing vessel pose significant challenges for accurate detection. Basurko et al. (2022) have proposed a methodology to define these modes for the target vessel, relying on the analysis of machinery status. This approach involves setting thresholds on key features and time intervals to represent the engine and vessel behaviours for each activity. However, this methodology requires extensive prior

knowledge. As noted by the authors, the determination of threshold values was a collaborative effort, involving a team of researchers and onboard observers.

Moreover, Basurko et al. (2022) also explored data-driven technologies, including clustering approaches based on supervised learning, however, they indicated these technologies cannot entirely be successful in detecting the activities accurately. This situation underscores the need for developing a data-driven method that requires limited input resources with broad algorithm adaptability.

Despite the aforementioned complexities in identifying various operational modes of fishing vessels, the central aim of this case study is the detection of the 'Transit' mode. As detailed in (Basurko et al., 2022), 'Cruising Mode' accounts for approximately 68.5% of the total trip duration and a significant 90.4% of the fuel consumption. These statistics underscore the importance of effectively identifying 'Cruising mode', which has substantial implications for both operational efficiency and environmental impact, aligning with the objective of developing an effective FOC prediction model in the later analysis.

5.2 Data Processing

The raw data for this case study is one month in-situ measured data from onboard sensors of a Spanish tuna purse seiner operating at the India Ocean. The onboard measured data is synchronised to the onshore servers periodically. It contains 172 measurement parameters, including various operational data and some weather data, all of which are measured at a frequency of 1 Hz.

During the pre-processing stage, timestamps for which there was missing data, and the duplicated time stamps have been removed. The raw coordinates, latitude & longitude have been truncated to the fifth decimal place, giving a precision of 1.1 metre. The precision of 1.1 m is appropriate for the vessel and truncating the redundant decimals can reduce the computational effort for the following analysis. Two key features, 'SpeedLL' and 'Curvature' have been extracted from the coordinates according to the equation 3.1 and 3.2, and the 1.5 IQR technique based on equation 3.3, has been utilised to the discrepancies between the SOG and SpeedLL to filter out the outliers.

In this case, the extreme values of the SpeedLL go up to hundreds or even more than 1,500 knots which are unrealistic, considering the maximum speed of the target vessel is 20 knots. As discussed in Section 3.4.1 and 4.2.1, these extreme values likely result from the accumulation of minor deviations among nearby data points.

For instance, the maximum SpeedLL is over 1500 knots in this case, considering the timestamp is 1 second, the distance of the related consecutive coordinates is over 770 m. Considering the timeseries coordinates recorded the vessel's trajectory over a long-time range, it means even though some of the coordinates are not recorded correctly by the GPS, the vessel truly sailed through this anomaly distance. Upon closely examining on these extreme data points, it could be found this generally occurs when GPS systems fail to accurately record positions over a period, logging coordinates with only minor differences despite actual movement. When normal GPS functionality resumes and records the accurate position, the sudden apparent distance between previously recorded and actual locations highlights these accumulated inaccuracies. The discrepancy between the SOG and SpeedLL for each time stamp is the way to evaluate this minor deviation, theoretically, the difference should be close to zero since they reflect the same thing and the SOG are measured by GPS as well. Figure 5.1 shows the raw SpeedLL and the discrepancy (SOG - SpeedLL).

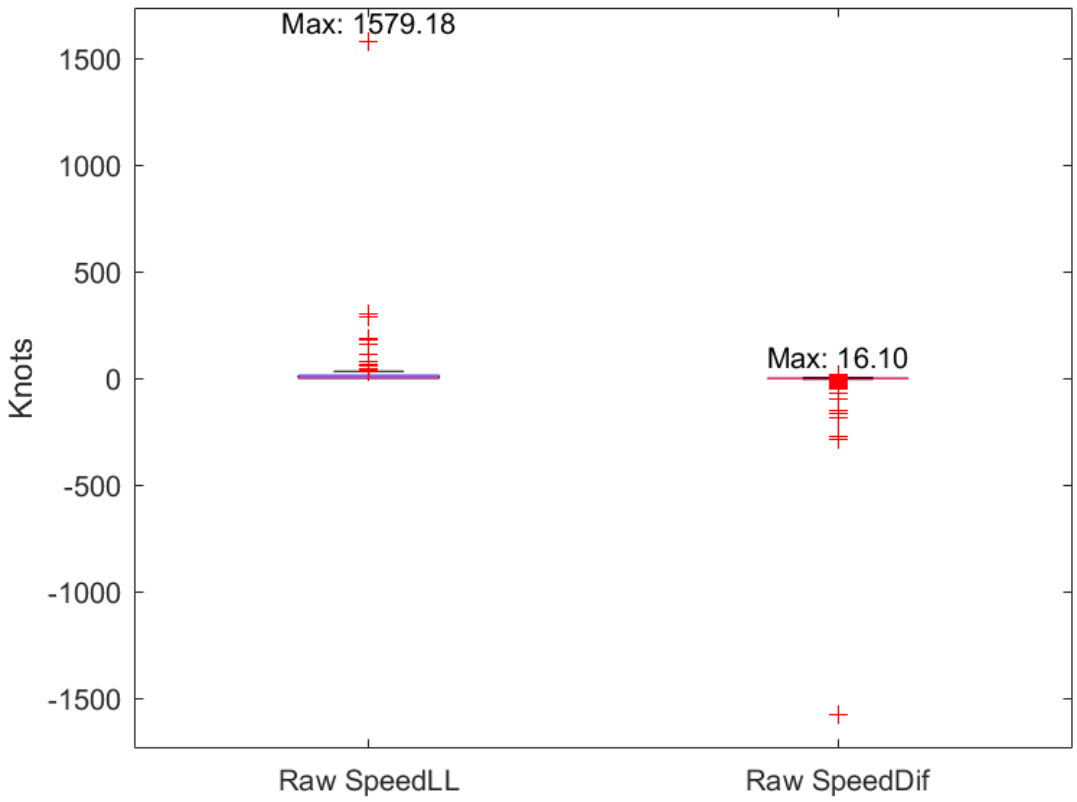

Figure 5.1 Boxplots of raw SpeedLL and corresponding speed discrepancy

The 1.5 IQR technique has been applied on the speed difference, such that if the difference is within the defined range, the data is treated as normal, otherwise, it will be deleted as an outlier. The detailed discussion on the 1.5 IQR technique and data cleaning strategies are presented in Section 3.4.1. In this analysis, the IQR range has been identified as 2.0597 knots, representing the difference between the 25th and 75th percentiles of the speed discrepancy. Consequently, speed difference with an accepted range of -4.4493 to 3.7896 knots are considered valid, while values outside this range are discarded. Further details of the parameters associated with the 1.5 IQR technique are presented in the Table 5.2.

Table 5.2 Key parameters in 1.5 IQR calculation

Speed difference (SOG - SpeedLL)	-1578.2 ~ 16.1 (knots)
1.5 IQR	-4.4493 ~ 3.7896 (knots)
IQR (25-75 percentile)	2.0597 (knots)
Q1 (25)	-1.3597 (knots)
Q2 (50)	0 (knot)
Q3 (75)	0.7 (knot)
Q4 (100)	16.1 (knots)

After filtering out the outliers, the range of the SpeedLL is from 0 to 19.44 knots, which is reasonable for the target tuna purse seiner, considering its physical maximum speed is 20 knots. The average speed for cruising is around 15 knots, during the setting phase, the speed would increase to higher than the normal cruising speed to facilitate circling the net around the fish school, it normally lasts around 10 minutes. Thus, the cleaned speed range is reasonable for the target vessel. The cleaned SpeedLL and corresponding discrepancy are illustrated in the Figure 5.2.

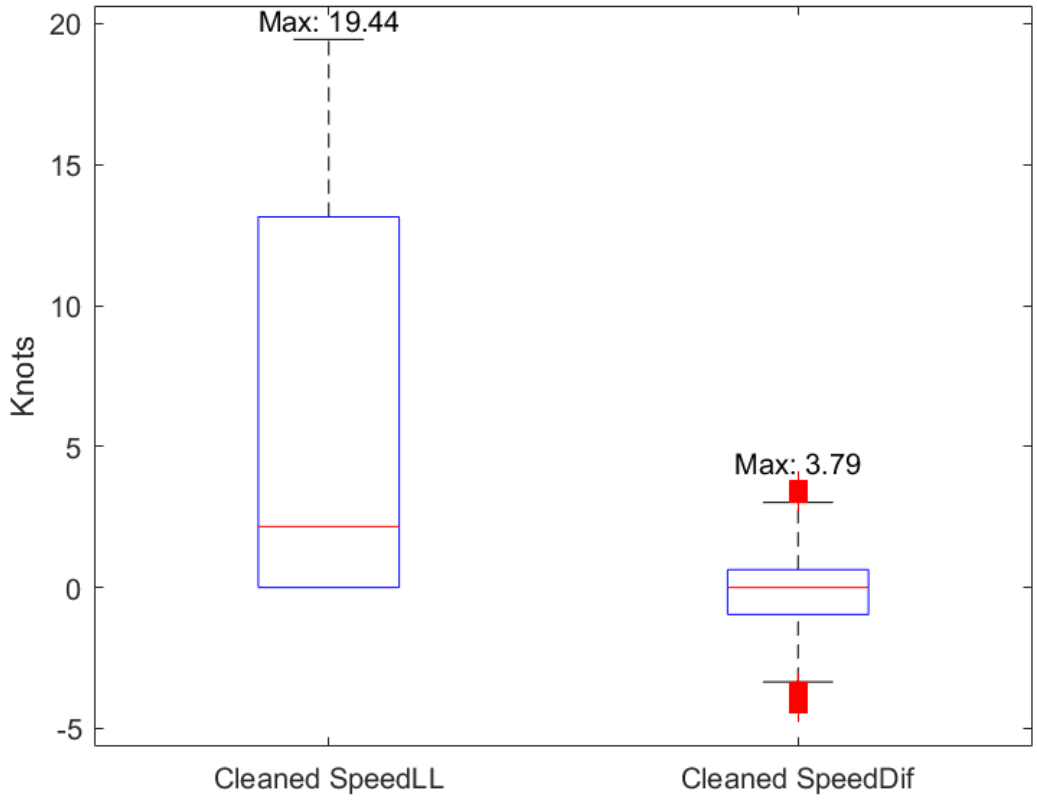

Figure 5.2 Boxplot of cleaned SpeedLL and corresponding discrepancy

The raw continues time series coordinates have been divided into several segments through the elimination of the detected outliers. This means that the overall trajectory of the vessel is separated into several segments or even single point. As discussed in Section 3.4.3, data continuity is essential for the effectiveness of the developed methodology. To mitigate this issue, data aggregation technique has been employed by averaging the data points with the frequency of every 1 seconds to a 15-second interval. This ensures that continuity is maintained if there is at least one data point within each defined 15-second period, using the average value to represent the aggregated data point. Meanwhile, this averaging strategy utilised in the data aggregation process can smooth the impact of the noise and keep the necessary information of the raw data.

The aggregated dataset will be divided into several continuous sub-datasets based on the time gaps. Furthermore, any sub-datasets containing fewer than 37 data points, equivalent to 9.25 minutes, will be disregarded. On the one hand, they are considered not to have enough data points to be analysed. On the other hand, they are potentially some parts of the anomaly distances need to be discarded. The detailed discussion of Continuity Check can be checked in the Section 3.4.3. In addition, from the physical perspective, there would not be an operational mode change in less than 10 minutes for the target vessel. The threshold of 37 data points aligns with the sensitivity analysis on the combination of the rolling window, which will be discussed in detail in Section 5.3.3.3.

An exemplary sub-dataset has been selected as a key element for analysis, with the primary purpose of defining thresholds for SpeedLL and Curvature to distinguish the ‘Steady State’ condition. The selection of the dataset is crucial for the research, it needs to balance the maximum data continuity whilst recording as many operational modes as possible. In other words, it would be better to record several operational mode changes, which are necessary for the algorithm to define the threshold to separate ‘Steady State’ and ‘Changing’ conditions. Additionally, in this case study, the aim is to detect ‘Transit’ for the target vessel, therefore, the selection also considers the continuity for the ‘Transit’ mode.

The selected dataset has nearly 1,900 data points, lasting almost 8 hours as the time interval between consecutive points is 15 seconds. The trajectory is shown in Figure 5.3.

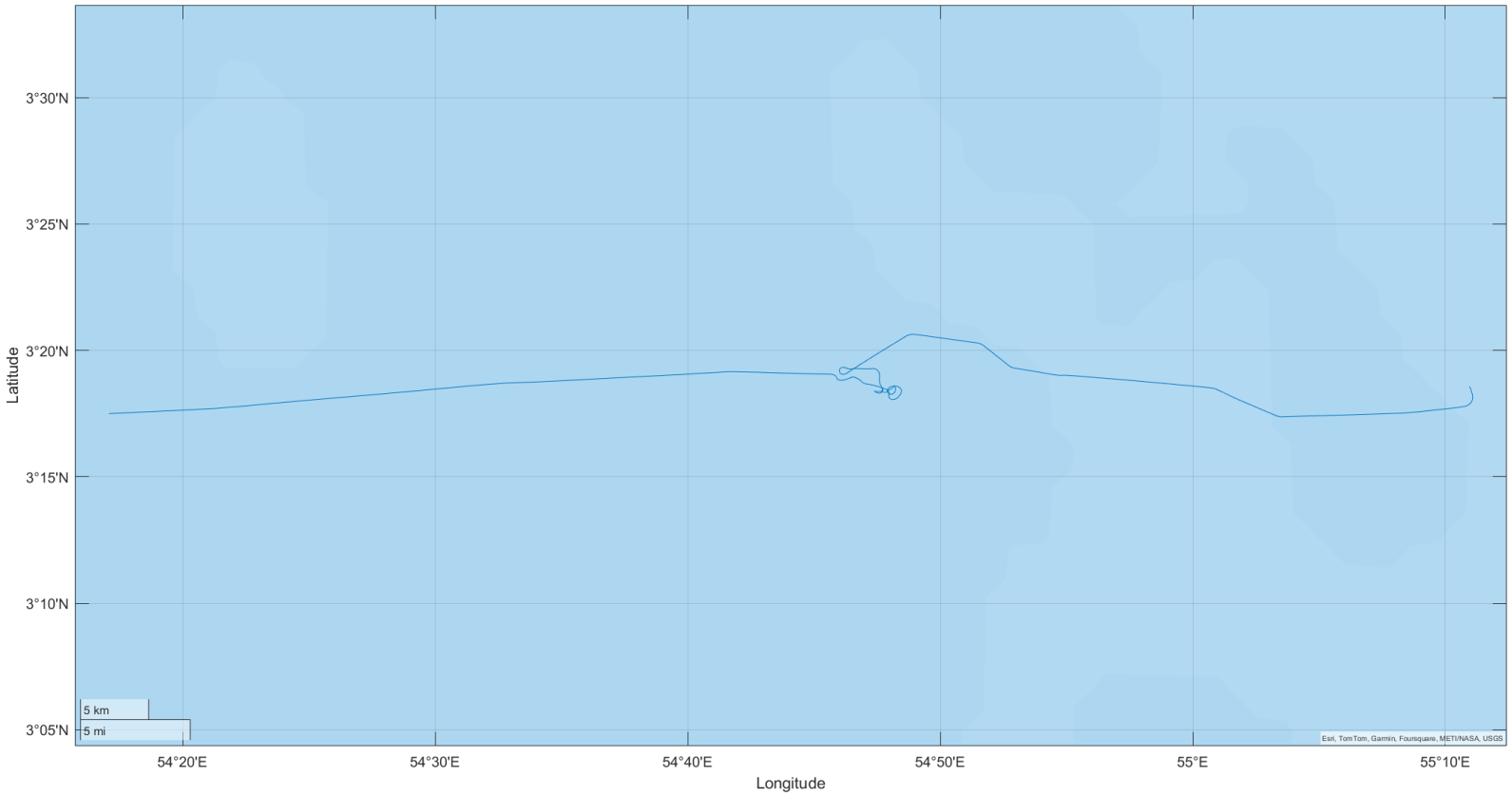

Figure 5.3 Trajectory of the exemplary sub-dataset

In Figure 5.3 the vessel sails from right to left. It can be seen that the vessel travels in a relatively straight-line at the beginning and the end of its trajectory, but the middle part of the figure shows several circular motions. This dataset has balanced the data continuity of the 'Transit' mode and also records the trajectory of fishing events.

5.3 Steady State Detection for SpeedLL

5.3.1 Identification of visualised change points

Five VCPs for the exemplary sub-dataset have been identified through the visualisation technique. These VCPs were identified by observing variability across the dataset. The VCPs divide the dataset into six distinct segments, beginning from the start of the dataset to VCP1, then from VCP1 to VCP2, and so forth, culminating with the segment from VCP5 to the end of the dataset. Figure 5.4 illustrates the SpeedLL, with the indices of the visualised change points marked at 697, 914, 1321, 1425, and 1833.

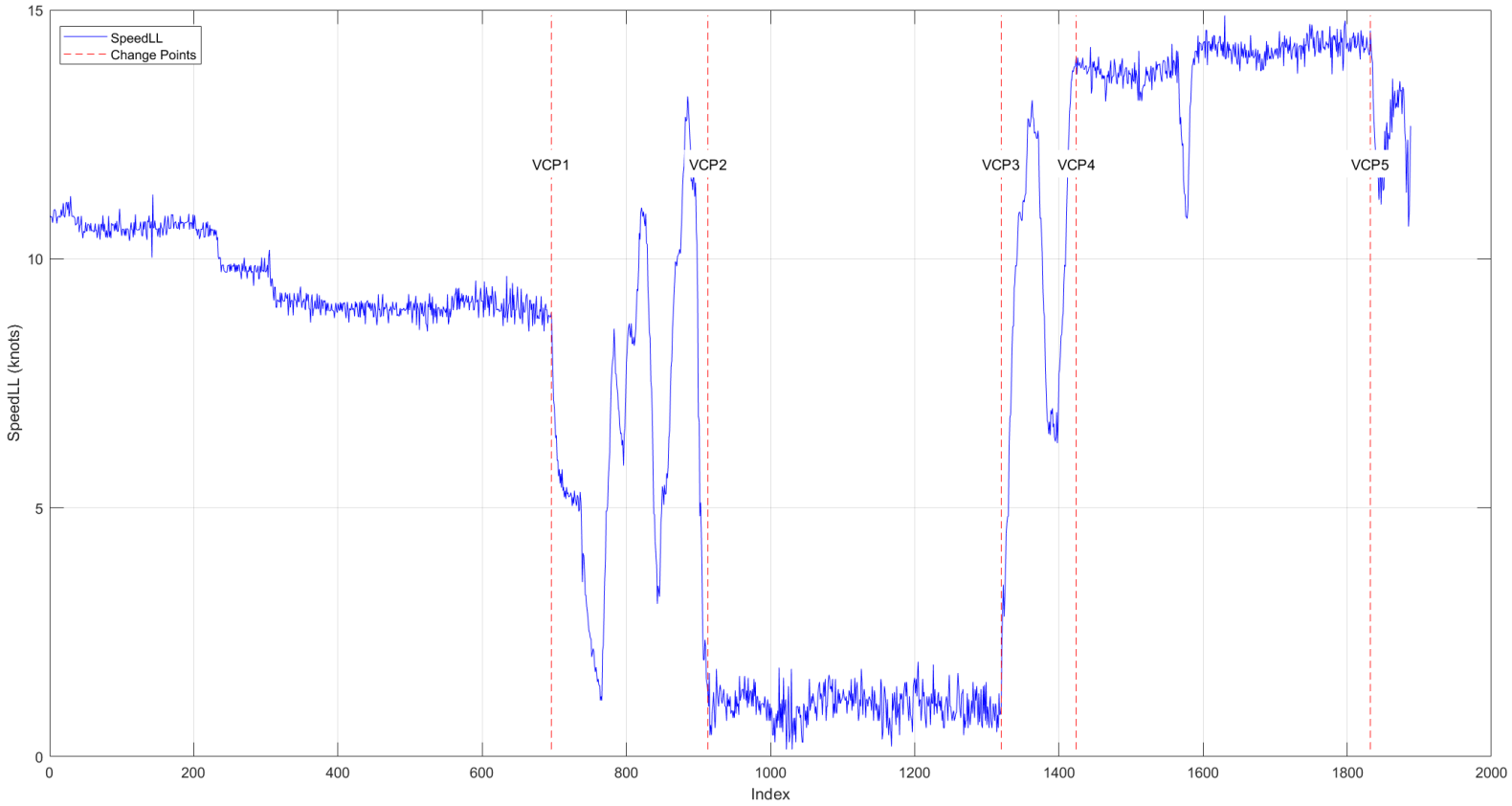

Figure 5.4 SpeedLL for the exemplary sub-dataset with VCPs in red vertical dotted lines

Observational analysis categorises these segments into two types based on inherent variability: 'Steady State' and 'Changing'. The 'Steady State' condition is characterised by relatively consistent and low variability within the segment, in contrast to the 'Changing' condition, which exhibits higher variability. In this context, segments 1, 3, and 5 are identified as 'Steady State', while segments 2, 4, and 6 are designated as 'Changing'.

From an operational perspective, the vessel's speed fluctuates between these two conditions, alternating between steady states and periods of change. This pattern indicates shifts in the vessel's operational modes corresponding to the delineated segments. The variabilities of the visualised segments in terms of IQR and SD are shown in Table 5.3.

Table 5.3 Variability of visualised segments using IQR and SD

Segments	1	2	3	4	5	6
VCPs (Index)	1	697	914	1321	1425	1833
Binary Label	0	1	0	1	0	1
IQR	1.5773	3.8430	0.4068	5.5016	0.4929	1.4436
SD	0.7674	3.0987	0.3181	3.0172	0.5443	0.8502

Binary Label (0&1) represents two conditions: 0 – Steady State, 1 – Changing

The variabilities of the visualised segments documented in Table 5.3 indicate that the VCPs can distinguish between binary conditions: the variabilities under the 'Steady state' conditions are smaller than those under 'Changing' conditions. However, the difference between binary conditions vary significantly, from more than double in segments 1 to 2, to more than tenfold in segments 3 to 4. For segments 5 and 6, the variabilities of the SD are quite similar. This similarity arises from the SD'S sensitivity to extreme values, illustrated by a rapid speed drop from around 14 to 11 knots, followed by a quick rebound to 14 knots within 6 minutes.

From the perspective of trajectory analysis, the VCPs effectively segment the trajectory, closely aligns with domain knowledge expectations and graphical representation. The trajectory of the sub-dataset, marked with VCPs in red, is illustrated in Figure 5.5, and the Figure 5.6 illustrates the details of magnified area for the first four VCPs.

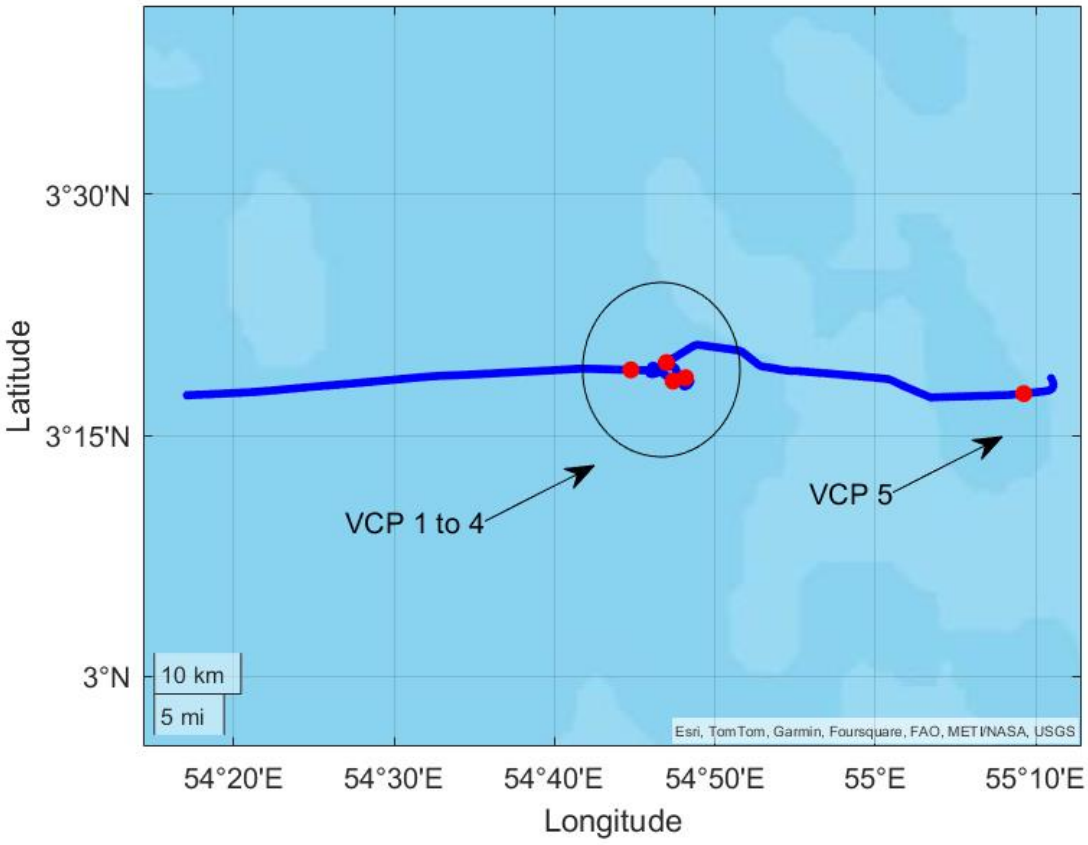

Figure 5.5 Illustration of the vessel's trajectory with VCPs marked by red dots

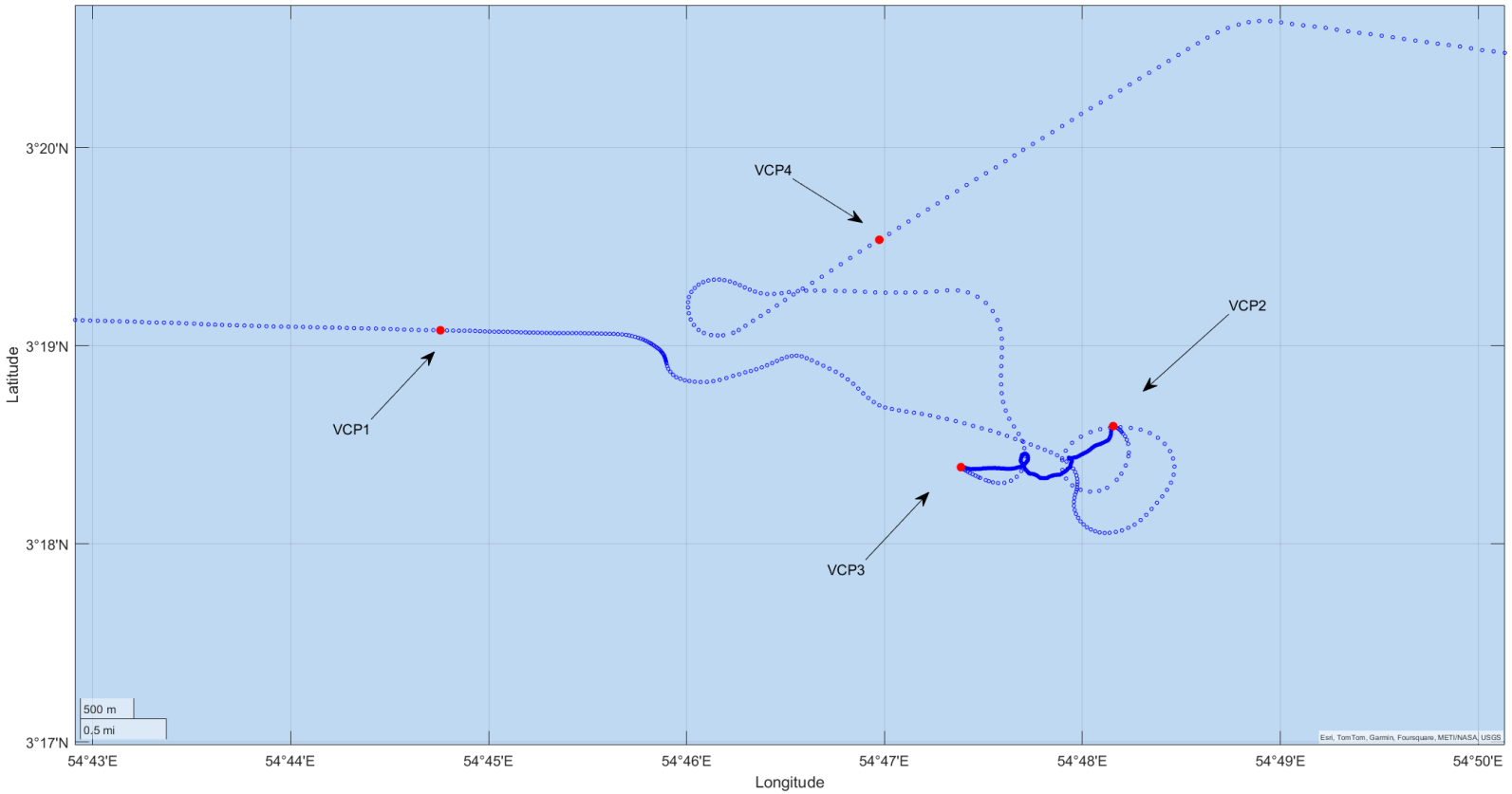

Figure 5.6 Illustration of the vessel's trajectory in details of VCP1 to VCP4

5.3.2 Sensitivity analysis on the combination of rolling window

As detailed in Chapter 3, the subsequent step involves conducting a sensitivity analysis to determine the appropriate combination of the rolling window parameters for evaluating the variability of each data point.

A critical aspect of implementing the rolling window technique is selecting the optimal window size. This selection requires a sensitivity analysis to determine the window size that best captures the necessary variability. The selection of the window size should consider two key aspects: the location of the target point within the window, and the size of the window itself. The location of the target point within the rolling window is categorised into three distinct positions: 'Begin', 'Middle', and 'End'.

Understanding the dynamics of time series data, where each data point emerges sequentially over time, is pivotal in this analysis. Typically, data points are compared with preceding points, positioning the target data at the end of the window. This means that each new data point is compared with a preceding set of data points, without subsequent data included in the window.

The 'Middle' position implies an equal distribution of preceding and succeeding data points around the target, offering a more balanced and accurate evaluation of its variability. This position provides a comprehensive view of the changing patterns, capturing both past and immediate future contexts.

On the other hand, the 'Begin' position is crucial for assessing the consistency of local data patterns. In the main algorithm for detecting operational modes, the final step involves verifying the consistency of these modes. Here, a change point's mode is validated against the subsequent dataset within a predetermined window size, which represents a fixed time period. If the subsequent data points within this window align with the mode of the change point, the change is considered valid; otherwise, it is treated as a transient fluctuation and disregarded. This approach stems from the understanding that vessel operational modes do not shift instantaneously but require a transitional period. Therefore, the 'Begin' position ensures a consistent comparison framework, both for assessing variability and for validating detected operational modes.

Moreover, different methods for calculating data variability, SD and IQR, should also be considered in this sensitivity analysis. The appropriate combination of the rolling window will be determined by the developed objective function, where the highest objective function values indicates that the corresponded combination provides the strongest support for identifying VCPs, the details on the objective function can be checked in Section 3.5.2.2.

The range of the rolling window size has been set from 10 to 200. Sizes of 10 and 200 represent the time periods are 2.5 and 50 minutes, which allow for the observation of a relatively complete pattern in the objective function values, aiding in the identification of the optimal parameter combination. Figure 5.7 illustrates the results of the objective function under three positions: ‘Begin’, ‘Middle’, and ‘End’.

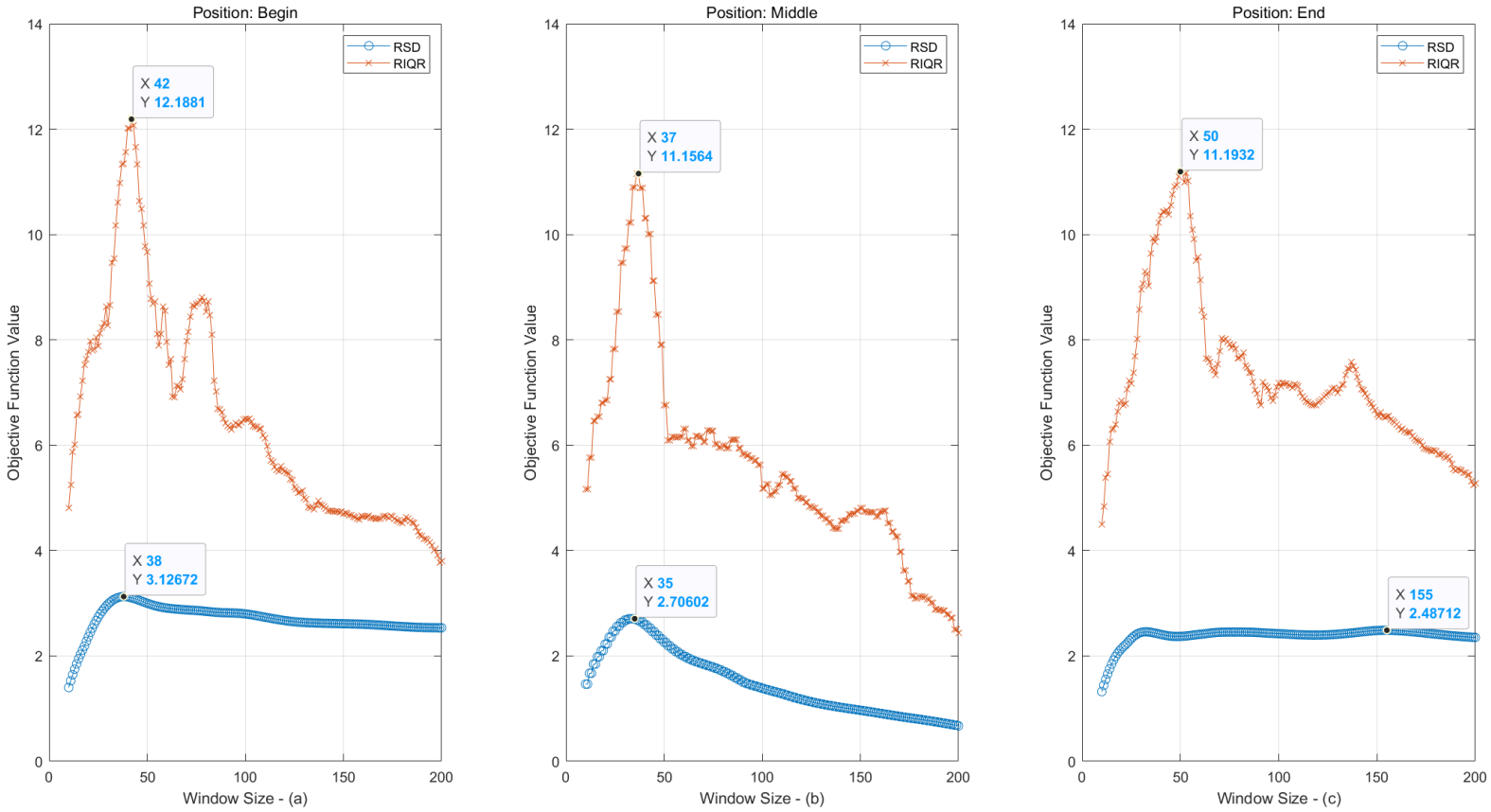

Figure 5.7 Results of the objective function for SpeedLL analysis

Table 5.4 summarises the peak values of the objective function and their corresponding window sizes for each position.

Table 5.4 Peak values of the objective function and related combinations

Positions	Begin	Middle	End
RIQR	42	37	50
RSD	38	35	155

For the RIQR Approach: The positions (Begin, Middle, End) show minimal impact on sensitivity analysis. The maximum objective function values for these positions are closely aligned (Begin: 12.19, Middle: 11.16, End: 11.19), indicating a negligible difference, particularly between Middle and End. Additionally, the objective function values across all positions display a similar pattern: an initial increase followed by a peak and a gradual decrease. The peak window sizes are 42, 37, and 50, corresponding to time intervals of approximately 10.5, 9.25, and 12 minutes, respectively.

For the RSD Approach: Position significantly influences the objective function values, with notable discrepancies (Begin: 3.127, Middle: 2.706, End: 2.487). The difference between Begin and End positions is particularly pronounced (~26%). The trend patterns differ across positions, with only the Middle position clearly indicating the peak value. The peak window sizes are 38, 35, and 155, respectively.

The RIQR approach yields higher objective function values than RSD, possibly due to IQR's focus on the central 50% of the dataset, offering computational efficiency and a clear peak value trend. In contrast, RSD calculates variability over the entire dataset, demanding more computational resources. The preference for IQR in evaluating local variability will be further examined in subsequent analyses.

The Middle position consistently shows smaller peak window sizes (37 for RIQR and 35 for RSD), however, the corresponded window size is the smallest compared to the other two positions. Based on the analysis above, the defined combination of the rolling window for the SpeedLL is M37 (window size of 37 at Middle position) in IQR, on one hand, a smaller rolling window size preserves more information from the raw data, on the other hand, the optimal window size 37, equivalent to 9.25 minutes, correlates closely with the high manoeuvrability

of the target vessel. This chosen size aligns with the Continuity Check of the change points, where the basic premise is that operational mode changes do not occur within the defined brief period, approximately 9.25 minutes in this case.

5.3.3 Define threshold on SpeedLL to distinguish steady state condition

The process of establishing a threshold for SpeedLL involves a systematic comparison of change points identified at various threshold levels with the initial VCPs. The aim is to select the threshold that minimises discrepancies between these two sets of change points, thereby ensuring accuracy and consistency in the identification of operational mode changes.

Based on the optimal window combination, M37 in IQR, the SpeedLL and associated point variability with the VCPs in vertical red dotted lines are illustrated in the Figure 5.8.

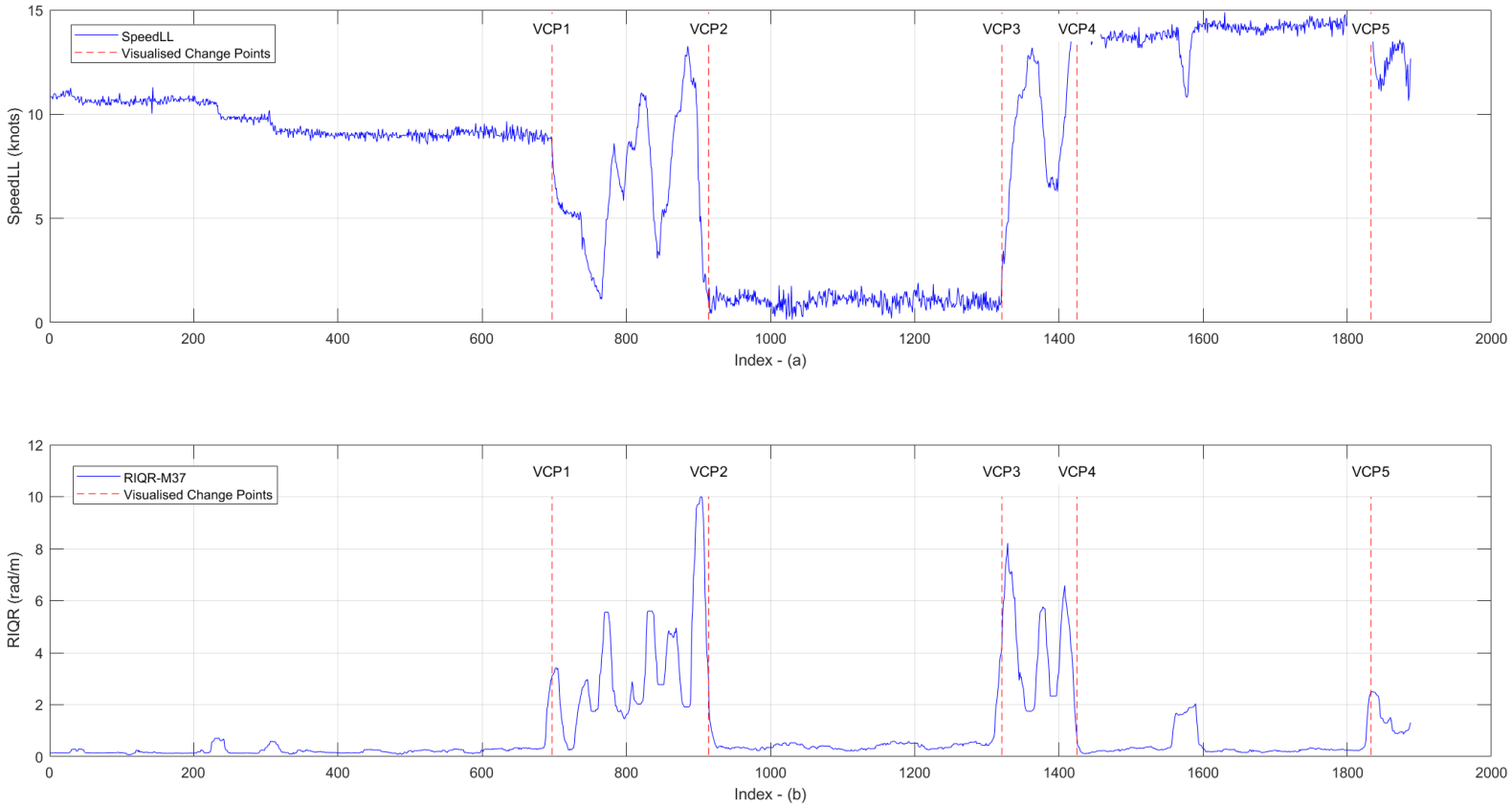

Figure 5.8 Illustration of SpeedLL and its pointed variability with VCPs in vertical red dotted lines

Figure 5.8 illustrates the relationship between SpeedLL and its pointed variability. The variability, calculated using the sensitivity analysis-based rolling combination (M37), effectively captures the variations in SpeedLL. There is a small peak near index 1600, which corresponds to a quick variation in SpeedLL, however, since the duration of this variation is approximately 5 minutes, it is still be treated as the 'Steady state' condition.

After careful observation of Figure 5.8 (b), the threshold range is defined from 0.1 to 1 knot, in increments of 0.01 knots. For each threshold within this range, change points are detected and then validated for Continuity Check, where a change point is recognised only if its status matches the proceeding points within the length of the predefined window size. Table 5.5 presents the detected change points for each threshold:

Table 5.5 Thresholds and related indices of DCPs

Thresholds (knots)	Indices of DCP
0.44~0.47	727;924;1150;1210;1303;1425;1556;1596;1824
0.48~0.53	727;923;1303;1425;1556;1594;1825
0.54~1.0	728;922;1305;1425;1825

Threshold in bold represent the minor differences of DCPs has been neglected.

In Table 5.5, thresholds and the related DCPs marked in bold indicate that minor differences in the indices of DCPs have been neglected. This highlights a key finding: the DCPs tend to be consistent within certain threshold ranges. For instance, within the range of 0.54 to 1 rad/m, the indices of DCPs are generally identical, with only 2 to 3 variations. After comparing with VCPs, the thresholds for Curvature have been defined as 0.6 rad/m. The comparison between VCPs and DCPs is illustrated in the Figure 5.9, which indicates that the DCPs effectively segment the dataset into binary conditions, closely mirroring the VCPs. There is a minor difference between the VCP1 and DCP1, involving 32 data points over approximately 8 minutes. This difference is attributed to a sharp decrease in SpeedLL from around 9 to 5 knots, after which the SpeedLL remained at 5 knots for a period. The algorithm treated this as a temporary fluctuation and classified it as steady state; in other words, this variation did not past the Continuity Check.

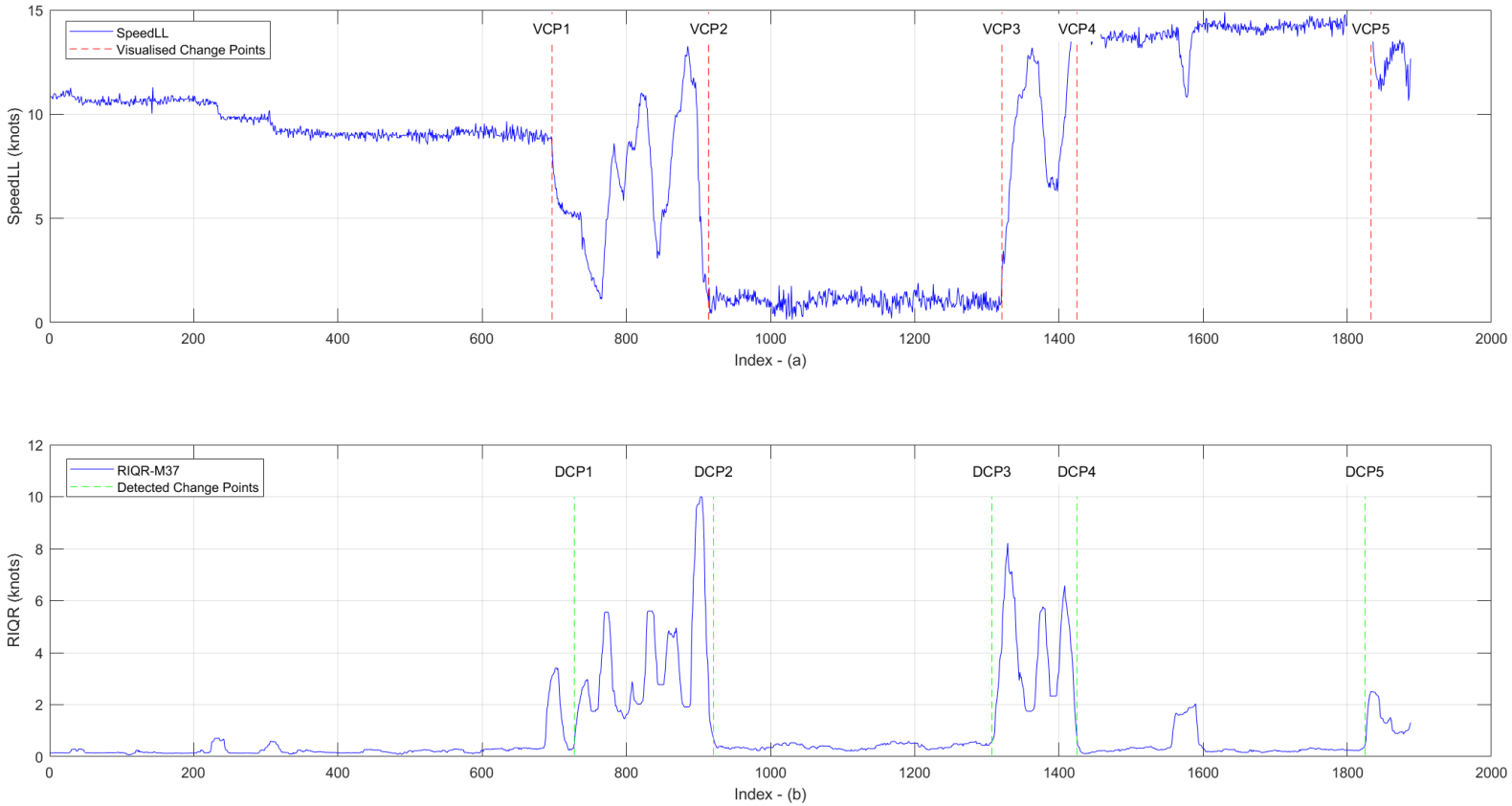

Figure 5.9 Comparison between VCPs and DCPs for SpeedLL

5.4 Steady State Detection for Curvature

The Curvature of the exemplary sub-dataset has been illustrated in the Figure 5.10, with VCPs in vertical red dotted lines.

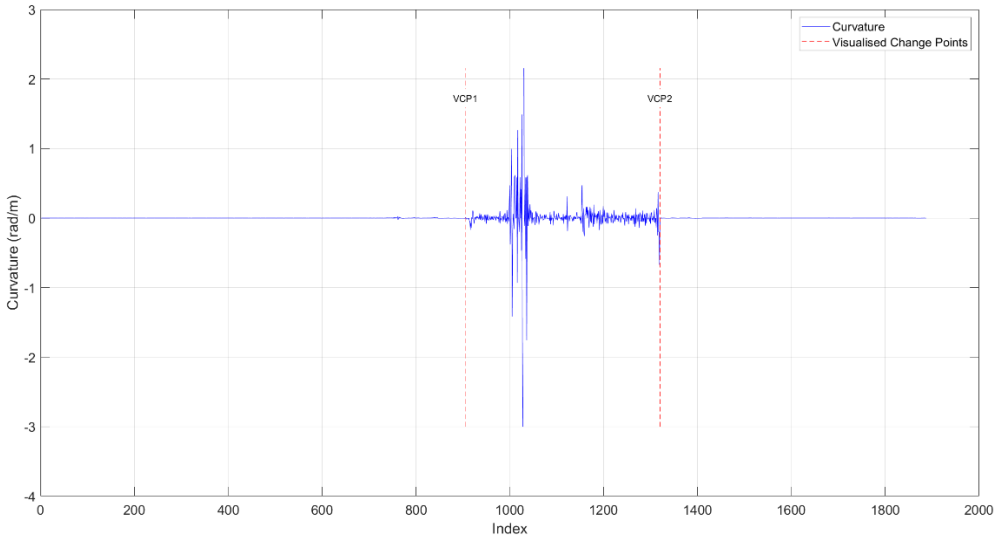

Figure 5.10 Illustration of Curvature and VCPs in vertical red dotted lines

In the Figure 5.10, the VCPs occur at indices 905 and 1320. These VCPs divide the dataset into three distinct segments. According to visual analysis, segments 1 and 3 are categorised as being in the 'Steady State' condition, while segment 2, between VCP1 and VCP2, is classified as 'Changing'.

To refine the threshold setting for curvature, a sensitivity analysis is conducted. The initial range for window size is set between 10 and 200, syntonising the settings used SpeedLL, and the positions considered for the target point within the window are 'Begin', 'Middle', and 'End'. By referencing these VCPs and the corresponding segments, the analysis seeks to identify the optimal window combination which can mostly validate the VCPs. The objective function values at three positions are illustrated in the Figure 5.11.

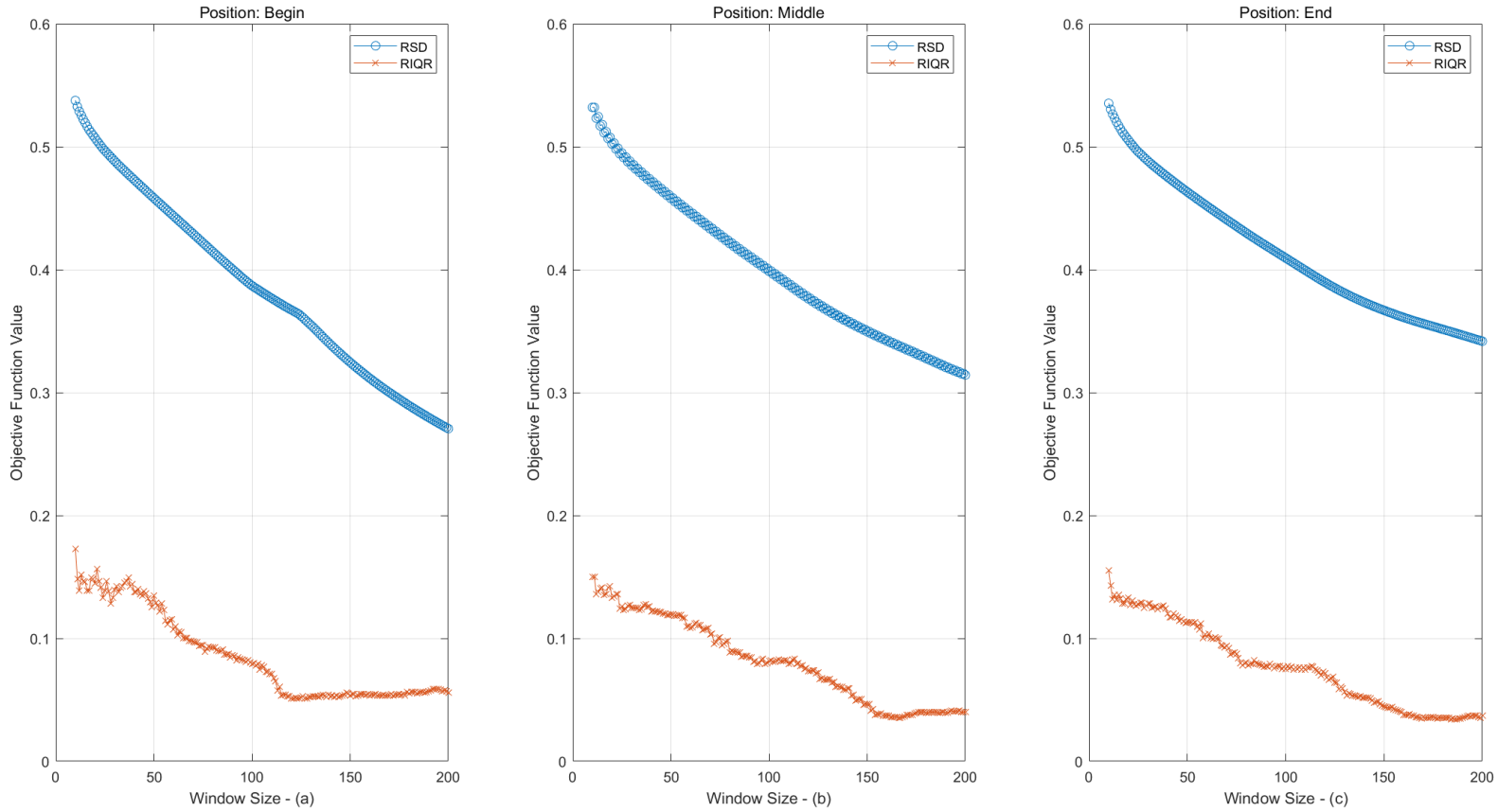

Figure 5.11 Objective function values at three positions based on VCPs

Figure 5.11 indicates that the objective function cannot adequately identify the optimal window combination, with the peak values occurring initially and then decreasing as the window size increases for all positions. This is probably because the influence of the extreme Curvature values, unlike the vessel's speed. From a physical standpoint, the vessel's speed has a natural range—from zero to the maximum operational capacity, approximately 15 knots during transit. This finite range means that speed variability does not exhibit as much extreme fluctuation as the curvature might. In contrast, the curvature's range is subject to substantial variation, especially when the vessel is not in a 'Steady State'. Extreme Curvature values, indicative of sharp turns, occur with considerable variability during 'Changing' conditions such as fishing events. Given these variations, the range of Curvature values is inherently large and unpredictable.

Additionally, the objective function values are higher when using RSD as opposed to RIQR for assessing pointed variability. A possible explanation lies in the inherent characteristics of the IQR, which focuses on the middle 50% of data within the window, essentially considering the 25th to 75th percentiles. This method tends to ignore extreme values.

Another reason might be the inability of the developed algorithm to accept the VCPs, despite their distinct appearance in Figure 5.10. These two VCPs cannot be adequately explained by the graphical representation, partly due to the influence of extreme curvature values. In comparison with the range of Curvature between VCP1 and VCP2 shown in Figure 5.10, the variations in the adjacent segments are so minor that they are classified as 'Steady State'. However, when focusing on the segments from the beginning to VCP1, and from VCP2 to the end, three additional VCPs, VCP 1', VCP 2', and VCP3' are evident. These variations are overshadowed by the larger variability in the middle segment, making segments 1 and 3 appear almost linear. If isolate and examine segments 1 and 3, disregarding the extreme values in segment 2, it can clearly identify three additional VCPs, as illustrated in Figure 5.12.

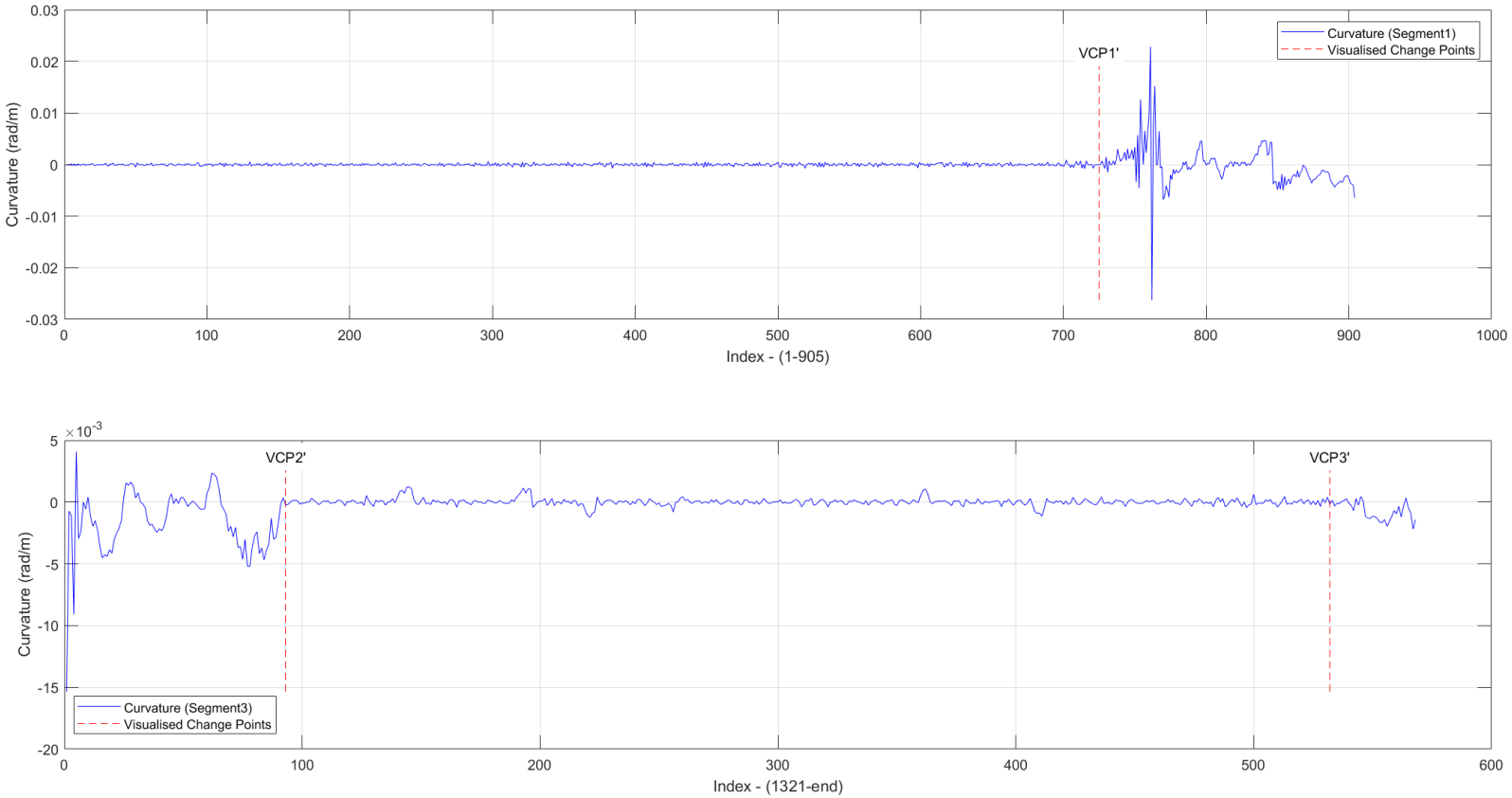

Figure 5.12 Additional VCPs in segment 1 and 3

Two sets of VCPs have been identified as shown in Figure 5.10 and Figure 5.12. Indices of two sets of VCPs for Curvature and SpeedLL are shown in the Table 5.6.

Table 5.6 Indices of VCPs for SpeedLL and Curvature

Features	VCP1	VCP2	VCP3	VCP4	VCP5
SpeedLL	697	914	1321	1425	1833
Curvature (Set1)		905	1320		
Curvature (Set2)	725			1412	1858

In Table 5.6, it can be observed that the VCPs for Curvature are highly correlated with the VCPs for SpeedLL, albeit with minor differences. Figure 5.13 illustrates the two sets of VCPs on the trajectory.

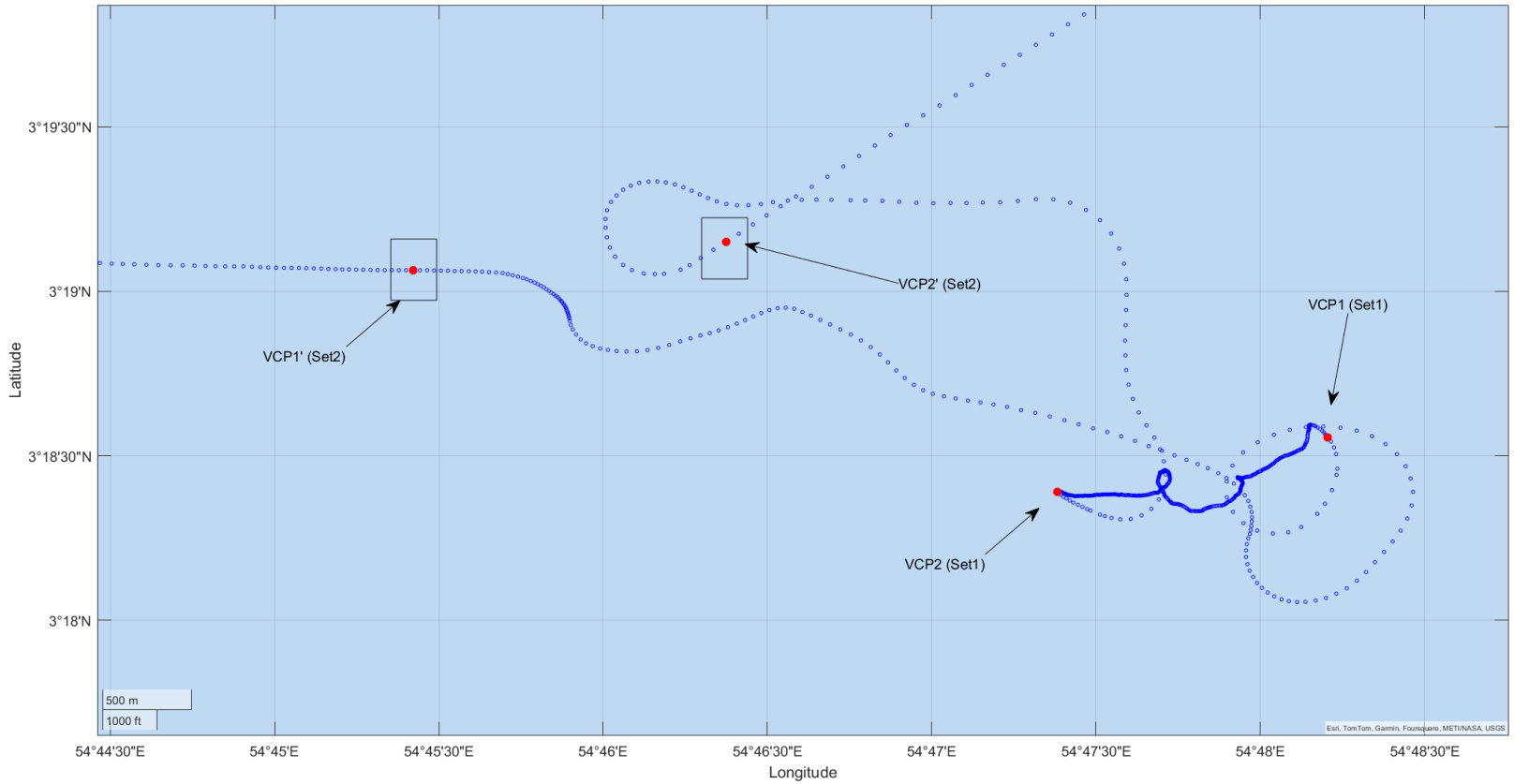

Figure 5.13 Comparison between two sets of Curvature VCPs on the trajectory

The segment between VCP1 and VCP2 records the period during which the target vessel was engaged in various phases of fishing events. During this period, the ME was stopped, and the vessel was propelled by two thrusters while executing sharp turnings. For set 2, which includes VCP1', VCP2' and VCP3', the change points more adhere to the definition of the developed algorithm, which categorises the Curvature into binary conditions and segments the trajectory into relatively straight-line and turning patterns. Consequently, the VCPs for Curvature have been determined to be VCP1', VCP2' and VCP3', dividing the trajectory into 4 segments, as shown in Figure 5.14.

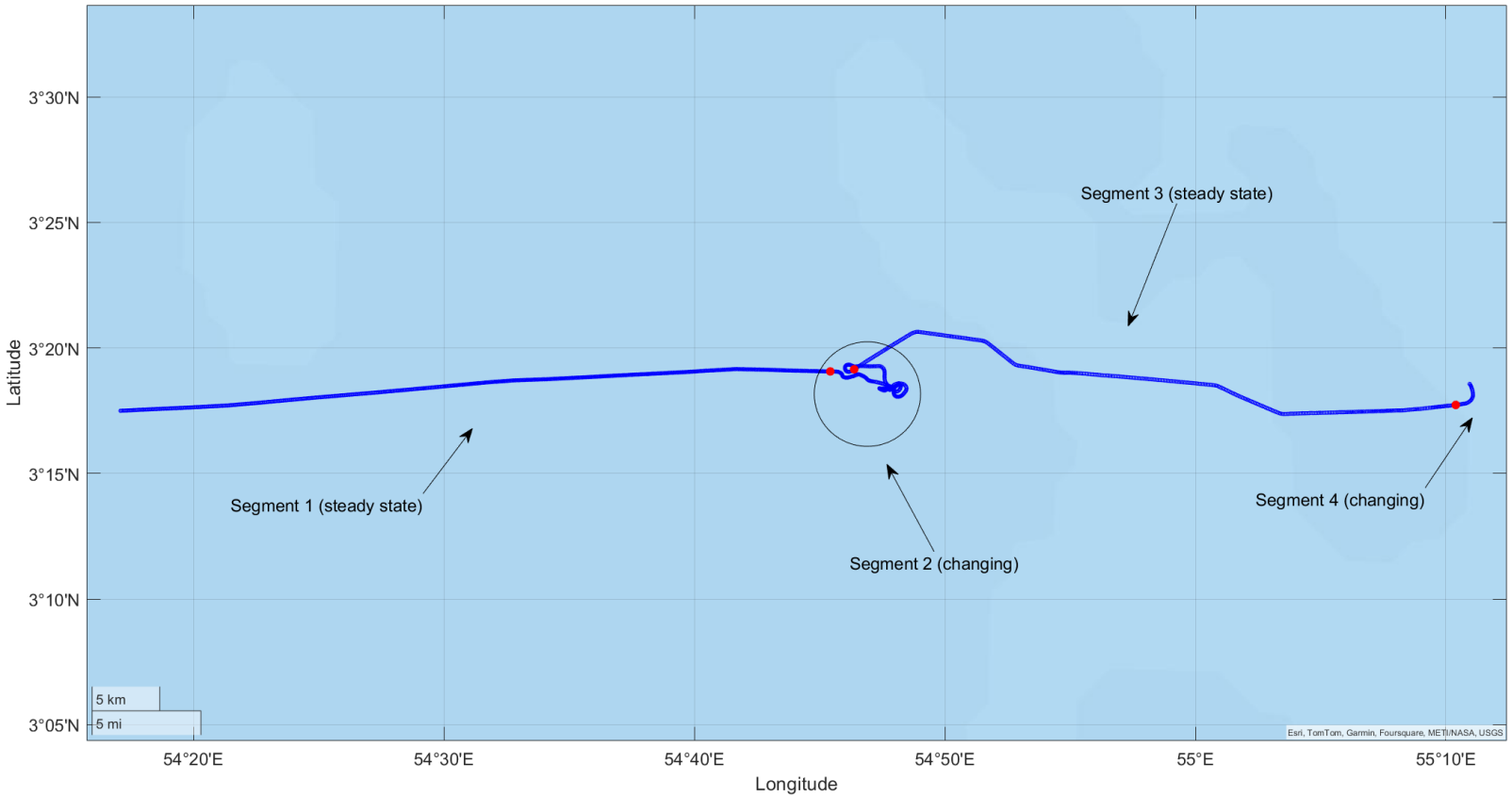

Figure 5.14 Trajectory of exemplary sub-dataset with VCPs of Curvature in red dots.

However, even after utilising the redefined VCPs in set 2, the objective function still cannot adequately identify the optimal window combination. The objective function values at three positions are illustrated in Figure 5.15. The patterns of these values are similar to those in Figure 5.11, peaking initially and then decreasing as the window size increases across all positions.

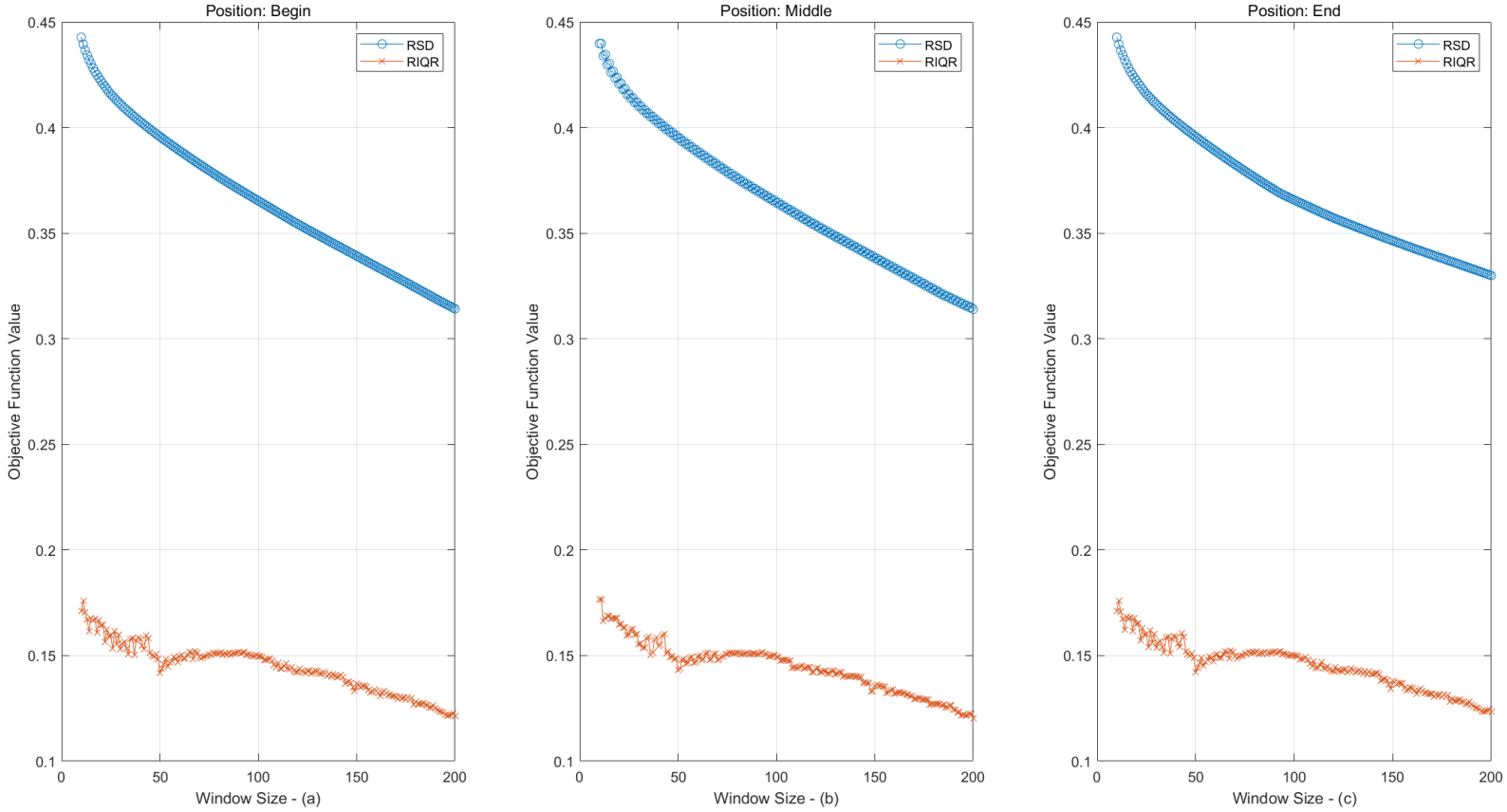

Figure 5.15 Illustration of objective function values at three positions for redefined VCPs

In this scenario, the rolling window combination for Curvature has been synchronised to SpeedLL, M37, with the variability calculated using SD. This decision is based on the high correlation between the VCPs for SpeedLL and Curvature, as shown in Table 5.6. Furthermore, both SpeedLL and Curvature are derived from the same raw coordinate data; therefore, using the same local data points for their calculation is logically sound. Maintaining the same local area for the analysis of both variables not only stems from their shared origin but also helps preserve the potential informational and correlational integrity between them.

The relationship between Curvature and its pointed variability is segmented into three parts and illustrated in Figure 5.16, 5.17 and 5.18, with two sets of VCPs marked by vertical red dotted lines. To efficiently evaluate the performance of the synchronised window combination, M37 in SD, without the influence of extreme Curvature values, Figure 5.16 focuses on the first segment, from beginning to VCP1. Conversely, Figure 5.17 shows the relationship for the last segment, starting from the index of VCP2 at 1320 to the end of the dataset. This segmentation is necessary because, when viewed together, the middle segment's large value makes the first and last segments appear almost as straight lines. While VCPs in set 2 align well with the definition of change points in the developed algorithm, the VCPs in set 1 still useful as they capture the fishing event. Consequently, Figure 5.18 focuses on the middle segment reveal clear insights into the VCPs in set 1.

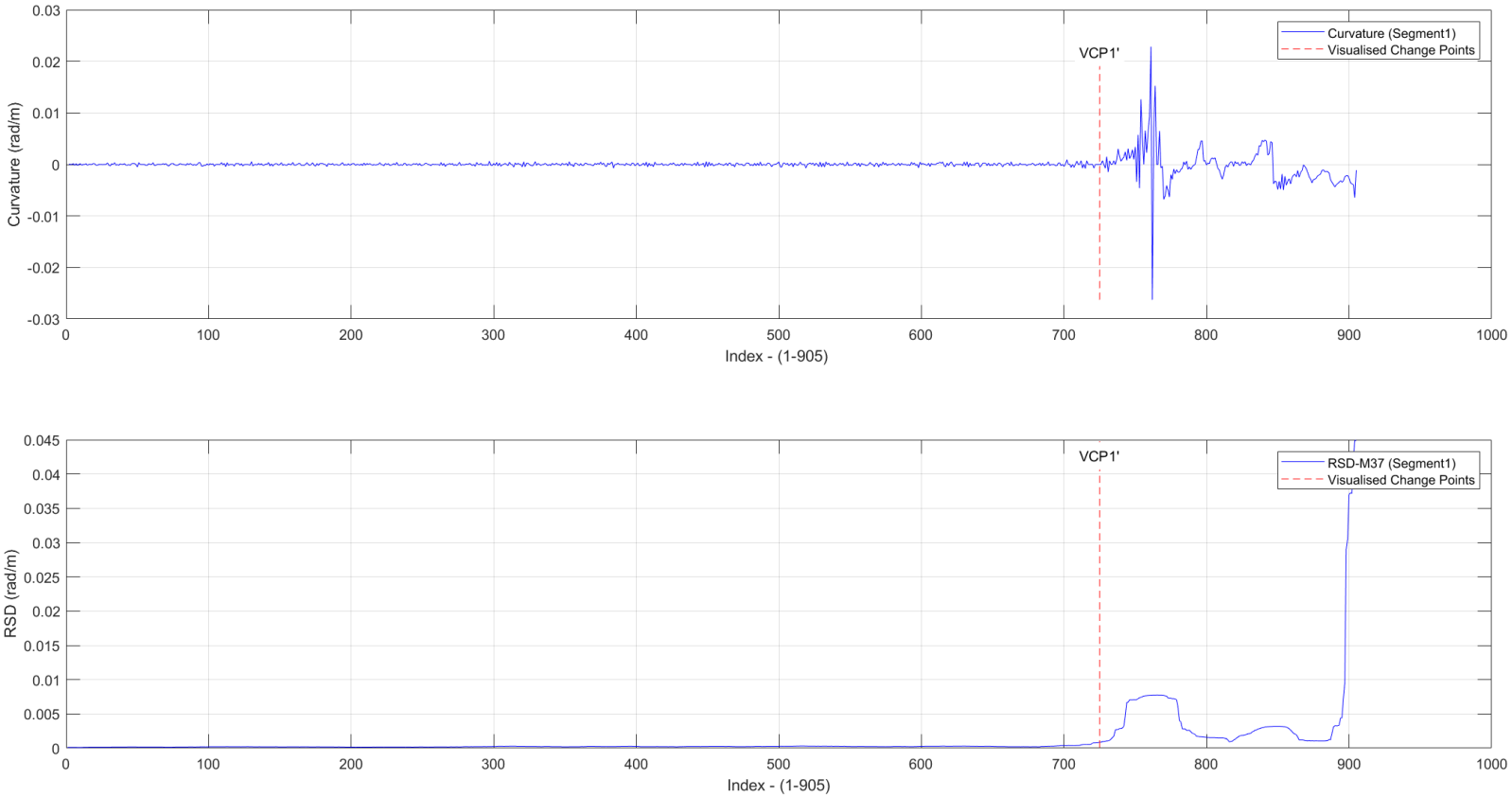

Figure 5.16 Illustration of Curvature and its pointed variability for the first segment focusing on VCPs of set 2

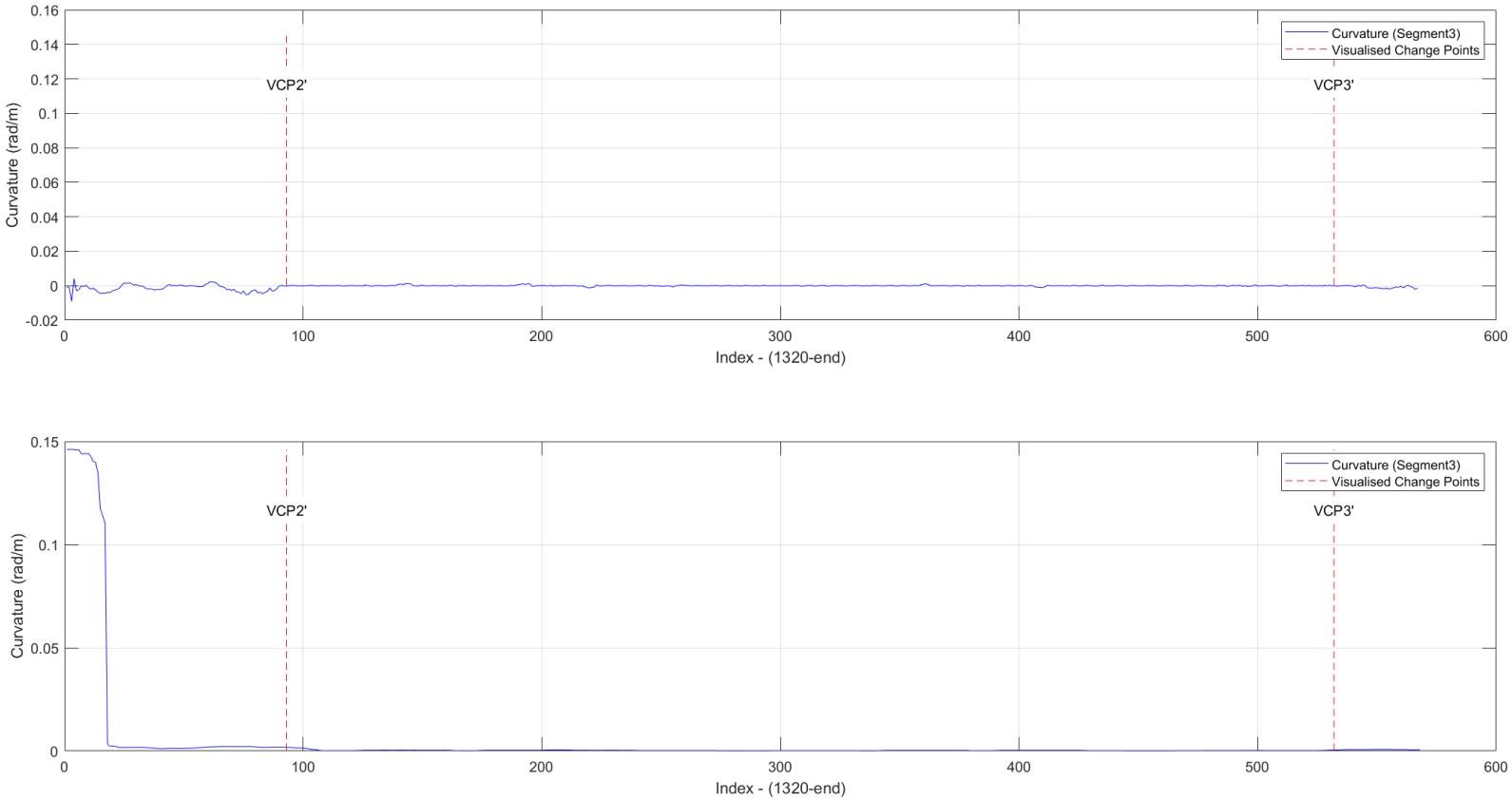

Figure 5.17 Illustration of Curvature and its pointed variability for the last segment focusing on VCPs of set 2

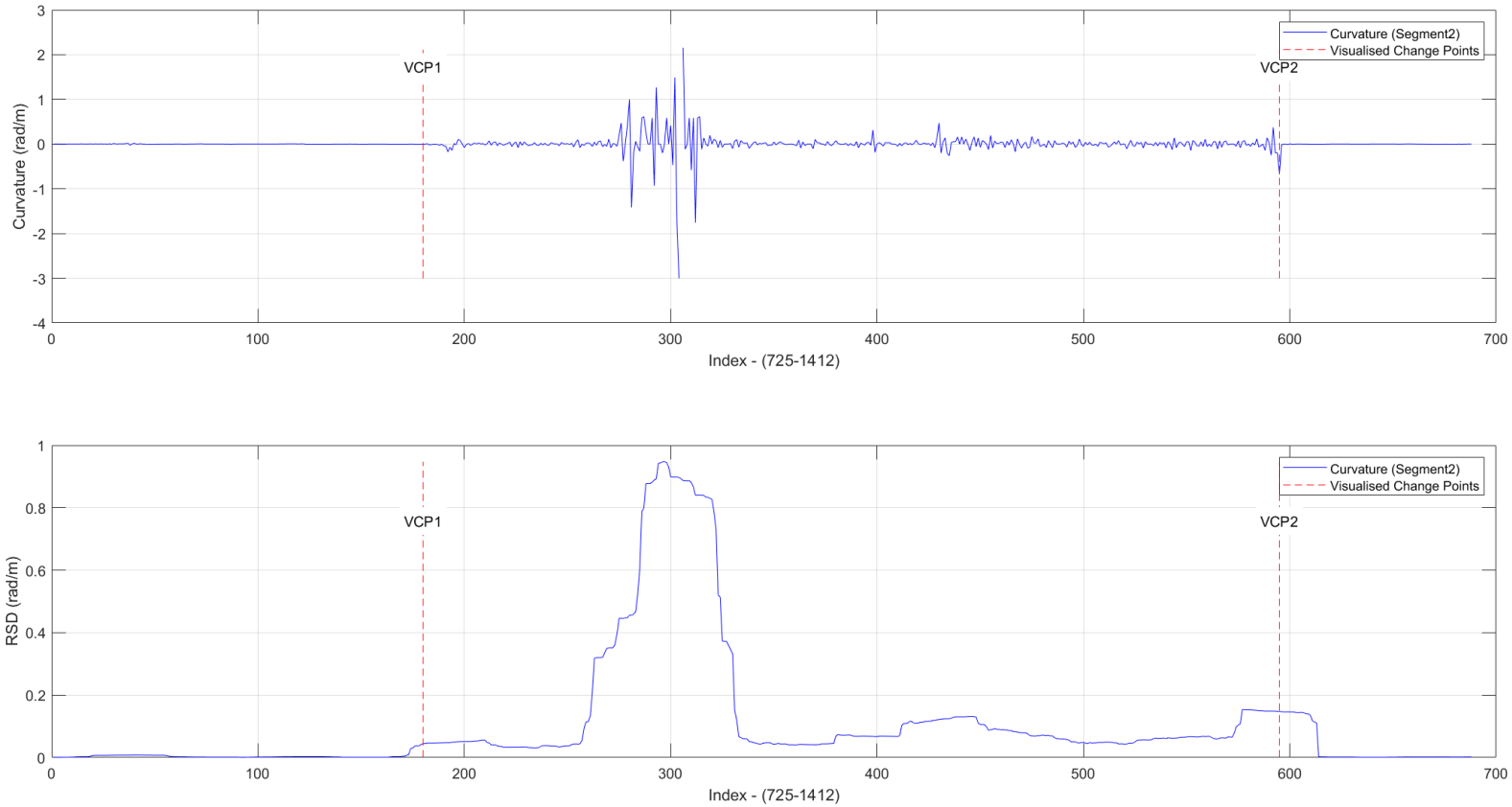

Figure 5.18 Illustration of Curvature and its pointed variability for the middle segment focusing on VCPs of set 1

In Figure 5.16 to 5.18, the synchronised window combination effectively captures the variation in Curvature, with its patterns closely aligning with the VCPs.

After closely observing Figure 5.16 to 5.18, the threshold range for VCPs in set 2 has been set from 0.4e-3 to 1.0e-3 rad/m, with increments of 0.01e-3 rad/m. For VCPs in set 1, the range has been set from 0.4e-2 to 1.0e-2 rad/m, with increments of 0.01e-2 rad/m. The duration of the Continuity Check has been synchronised to a period of 37. Details regarding some of the DCPs and associated thresholds are presented separately in Table 5.7 and 5.9 for the two sets of VCPs.

Table 5.7 Thresholds and related indices of DCPs focusing on VCPs in set 2

Thresholds (e-3) (rad/m)	Indices of DCP
0.27~0.28	**690;1559;1710;1747;1847**
0.29~0.37	**694;1558;1847**
0.38~0.42	**708;1480;1849**
0.43~0.54	**711;1426;1850**
0.55~0.56	**716;1426;1853**
0.57	719;1425;1854
0.58~0.63	**719;1425;1886**
0.64~1.0	**719;1423**

Threshold in bold represent the minor differences of DCPs has been neglected.

Table 5.8 Threshold and related indices of DCPs focusing on VCPs in set 1

Thresholds (e-2) (rad/m)	Indices of DCP
0.4~0.59	**742;781;893;1337**
0.6~0.71	**895;1337**
0.72~1.0	**896;1337**

Threshold in bold represent the minor differences of DCPs has been neglected.

In Table 5.7 and 5.8, thresholds and the related DCPs marked in bold indicate that minor differences in the indices of DCPs have been neglected. This highlights a key finding: the DCPs tend to be consistent within certain threshold ranges. For instance, within the range of 0.58 to

0.63e-3 rad/m in Table 5.7, and range of 0.6e-2 to 1.0e-2 rad/m in Table 5.8, the indices of DCPs are generally identical, with only 2 to 3 variations. After comparing with VCPs, the thresholds for Curvature have been defined as 0.57e-3 rad/m for set 2, and 0.006 rad/m for set 1. The detailed comparison between VCPs and DCPs are shown in the Table 5.9.

Table 5.9 Comparisons between VCPs and DCPs for two sets

VCPs	Thresholds (rad/m)	Indices of VCPs	Indices of DCPs
Set 1 (Fishing events)	0.006	905;1320	895;1337
Set 2 (Turning)	0.57e-3	725;1412;1858	719;1425;1854

In Table 5.9, the proximity between VCPs and DCPs highlights the high performance of the developed algorithm in detecting change points, underscoring the importance of maintaining the consistency of the original coordinates. This consistency preserves the interrelationship between these two parameters. Moreover, synchronising the combination of the rolling window has demonstrated effective performance in detecting change points under the situation when the objective function cannot identify combinations.

5.5 Transit Mode Detection for Target Vessel

Since the purpose of this case study is to detect 'Transit' mode for the target vessel, the threshold for Curvature goes for 0.57e-3 rad/m, which can effectively distinguish the straight-line and turning patterns.

Data points categorised under 'Transit' must satisfy three criteria simultaneously: the Main Engine (ME) must be in a 'Running' condition, while the SpeedLL and Curvature must be in a 'Steady State'. This combination is represented by the binary code '1 - 0 - 0'.

The ME power serves as in indicator of the operational status of the main engine, whether running or stopped. Although the extracted speed is strongly correlated with the ME power, fluctuations in speed can partially indicate changes in the ME power status. It is important to note, as discussed in section 5.1.3, the vessel's propulsion is not solely dependent on the main engine. During periods of inactive at sea and specific fishing events, the vessel is also driven by two auxiliary thrusters. This fact is crucial for the detection of 'Transit', especially for distinguishing scenarios where the vessel maintains a speed of approximately 4 knots while

the main engine is stopped. An ME power output of less than 0.1 kW is classified as the ‘Stop’ condition, and anything above that threshold is considered to be a ‘Running’ condition.

The Continuity Check is a critical component of this algorithm. Detected change points must pass this check by comparing their status with a predefined number of preceding data points, or else they will be disregarded. This procedure is integral to establishing the thresholds for ‘Steady State’, ‘Running’, and the ultimate detection of ‘Cruising Mode’. The Continuity Check serves a dual purpose: it not only filters out fluctuations or noise in the identified change points but also ensures that the duration of the detected operational modes is at least as long as the defined check length, which in this context is 9.25 minutes. This is also complied with the domain knowledge that a fishing vessel is unlikely to alter its operational modes in a span shorter than 10 minutes.

Even though the operational mode of a fishing vessel may change multiple times within a ten-minute interval, the algorithm is primarily designed to identify the 'Transit' mode, which is regarded as the normal operation of the target vessel. Thus, although several operational mode changes may be detected within this brief period, these modes are not deemed normal operations for a fishing vessel and would not pass the Continuity Check.

Figure 5.19 illustrates the ‘Transit’ mode for the exemplary sub-dataset, with the trajectory marked in green indicating the detected ‘Transit’ mode.

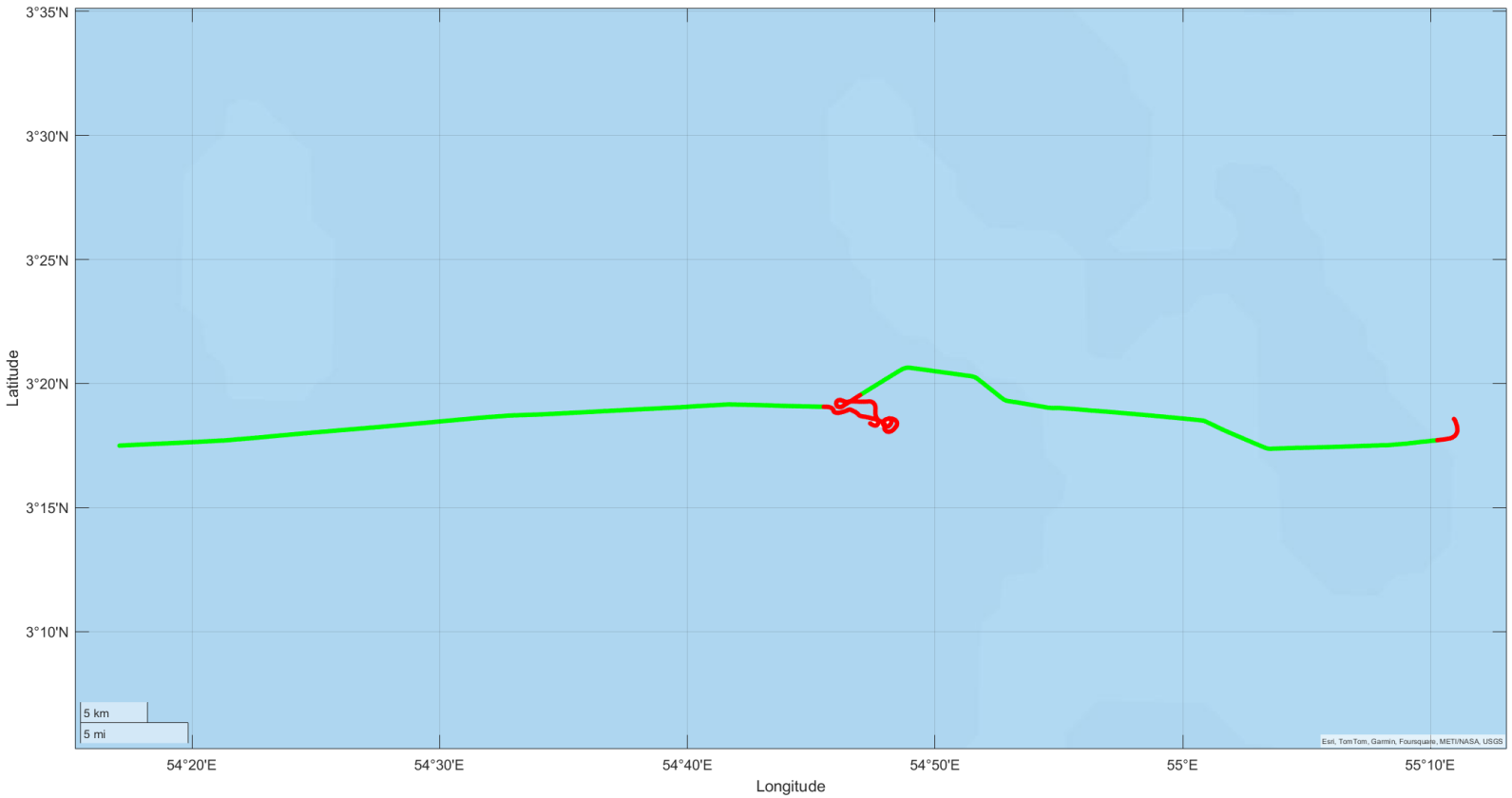

Figure 5.19 Transit mode detection for the exemplary sub-dataset with segments in green

The fishing event has also been detected by the algorithm, as illustrated in Figure 5.20 by white segment. During this period, the detected combination was ‘0 - 0 - 1’: the ME was stopped, the SpeedLL was classified as ‘Steday state’ with a relatively constant speed of around 1 knot propelled by two thrusters, and the Curvature was in a ‘Changing’ condition.

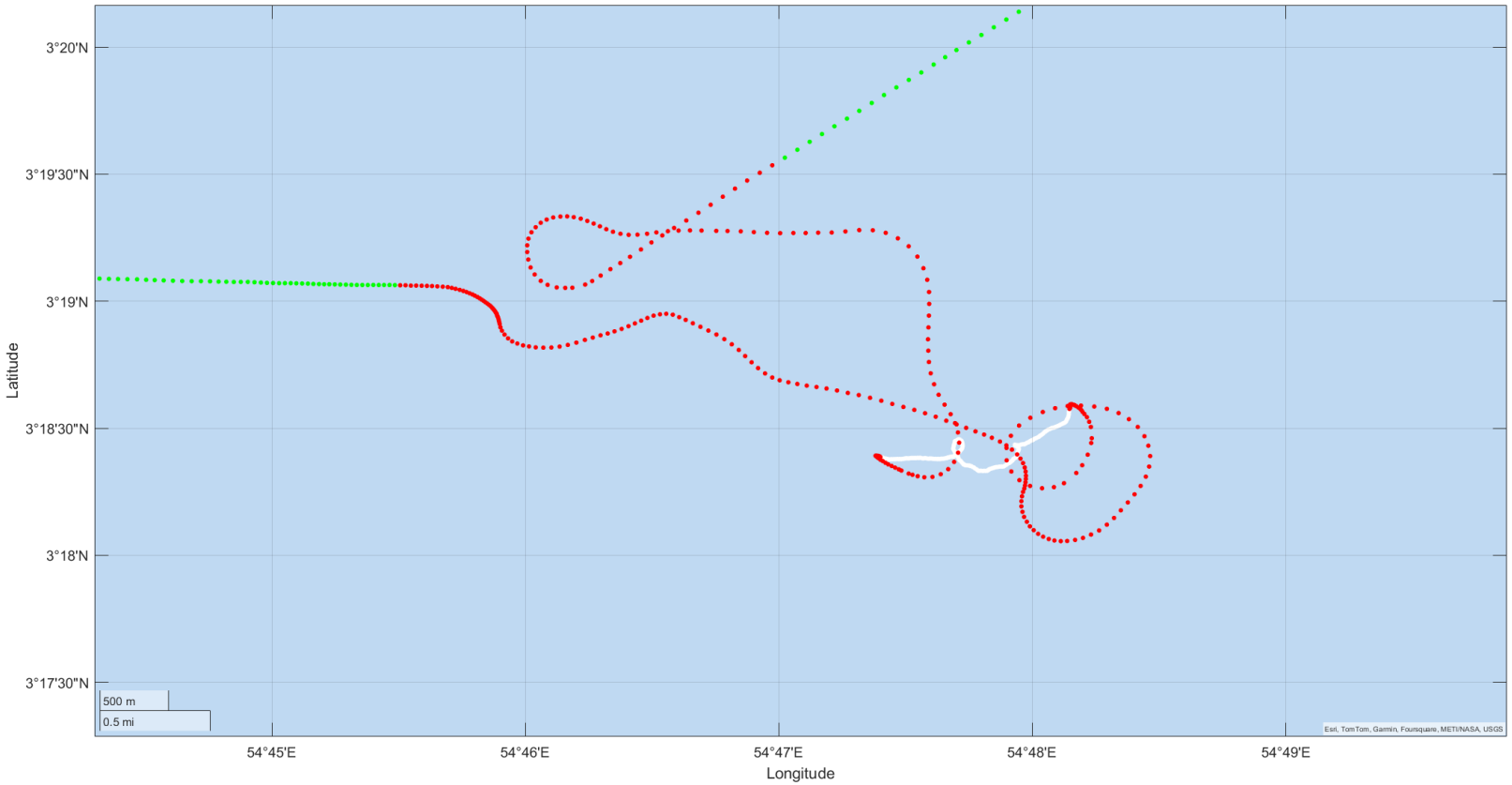

Figure 5.20 Fishing event detection for the exemplary sub-dataset

The tuna purse seiner commences its journey from the left side of Figure 5.19, navigating in a relatively straight-line pattern. Following the fishing activities illustrated in the central part of Figure 5.20, the vessel shifts to 'Transit' mode as it moves to another location. The continuity of data is interrupted towards the end due to the data cleaning process, which precludes a precise interpretation of the vessel's operational mode shift in the final phase. Nonetheless, the results confirm the efficacy of the developed algorithm in detecting 'Transit' mode, particularly in the phase following fishing activities. Despite the trajectory featuring several turns, the algorithm consistently identifies these segments as part of the 'Transit' mode.

The established thresholds for SpeedLL and Curvature, along with the window combination, have been applied to the entire dataset. A detailed discussion of the results pertaining to the detection of 'Transit' mode is provided in the subsequent section.

5.6 Results and Discussion

The graphical representation technique has been applied to the outcomes to examine if the detected results align well with the professional domain knowledge. Four sub-datasets have been selected as the typical examples to illustrate the performance of 'Transit' detection which are illustrated in Figures 5.21 to 5.24.

Figure 5.21 records the trajectory of selected sub-dataset 1, which contains 1260 continuous data points, spanning more than 5 hours. The algorithm has successfully detected 'Transit' mode among various operational modes, including fishing events, night adrift and manoeuvring, aligning closely with domain knowledge. Even though, the binary combination code for 'Night adrift' is '0 - 0 - 1', same as fishing events in Figure 5.20, the number of running auxiliary engine is 1, in contrast to 3 of the white segment.

It is important to clarify that the primary purpose of the mode detection is to distinguish the 'Transit' mode, rather than to classify all operational modes of the target vessel. Given the limitations of using only three input parameters, it is challenging for the algorithm to detect all modes comprehensively. As previously mentioned, the number of operational auxiliary engines serves as a reference to interpret the detection results. Domain knowledge suggests that three sets of auxiliary engines under the '0-0-1' configuration typically indicate 'Fishing events', while a running number of one usually represents 'Night Adrift'. It is important to note that the running number of generators is not used to distinguish operational modes; it merely

aids in explaining the detection outcomes. This approach allows for an interpretation of the vessel's behaviour based on domain knowledge; however, it cannot distinguish these two modes based solely on the number of operational auxiliary engines. In this context, the main objective is to detect the 'Transit' mode, which is crucial for predicting the FOC of the target vessel. Should there be a specific interest in detecting all operational modes of the fishing vessel, a deeper understanding of domain knowledge is essential, requiring further verification and insights through direct interactions or consultations with onboard operators to incorporate additional input measurements.

Figure 5.22 and Figure 5.23 are another two example datasets, which contain 1783 and 1502 continuous data points, spanning more than 7 and 6 hours, respectively. The algorithm has successfully detected 'Transit' mode under complicated operational conditions. Fishing events and manoeuvrings detected align highly with the explanations from domain knowledge.

Figure 5.24 illustrates the last example dataset, with 2459 continuous data points, spanning more than 10 hours. All the data points are detected as 'Transit', which is the largest continuous sub-dataset. The target vessel was sailing under a constant speed and with a relatively straight-line trajectory. All graphical representations indicate that the developed algorithm has performed effectively in detecting 'Transit' mode for the target tuna purse seiner. Another eight continuous datasets classified under 'Transit' mode in open sea navigation areas are detailed in the Appendix B. Each dataset spans extensive periods, with durations of at least 4 hours, during which the vessel covers significant distances.

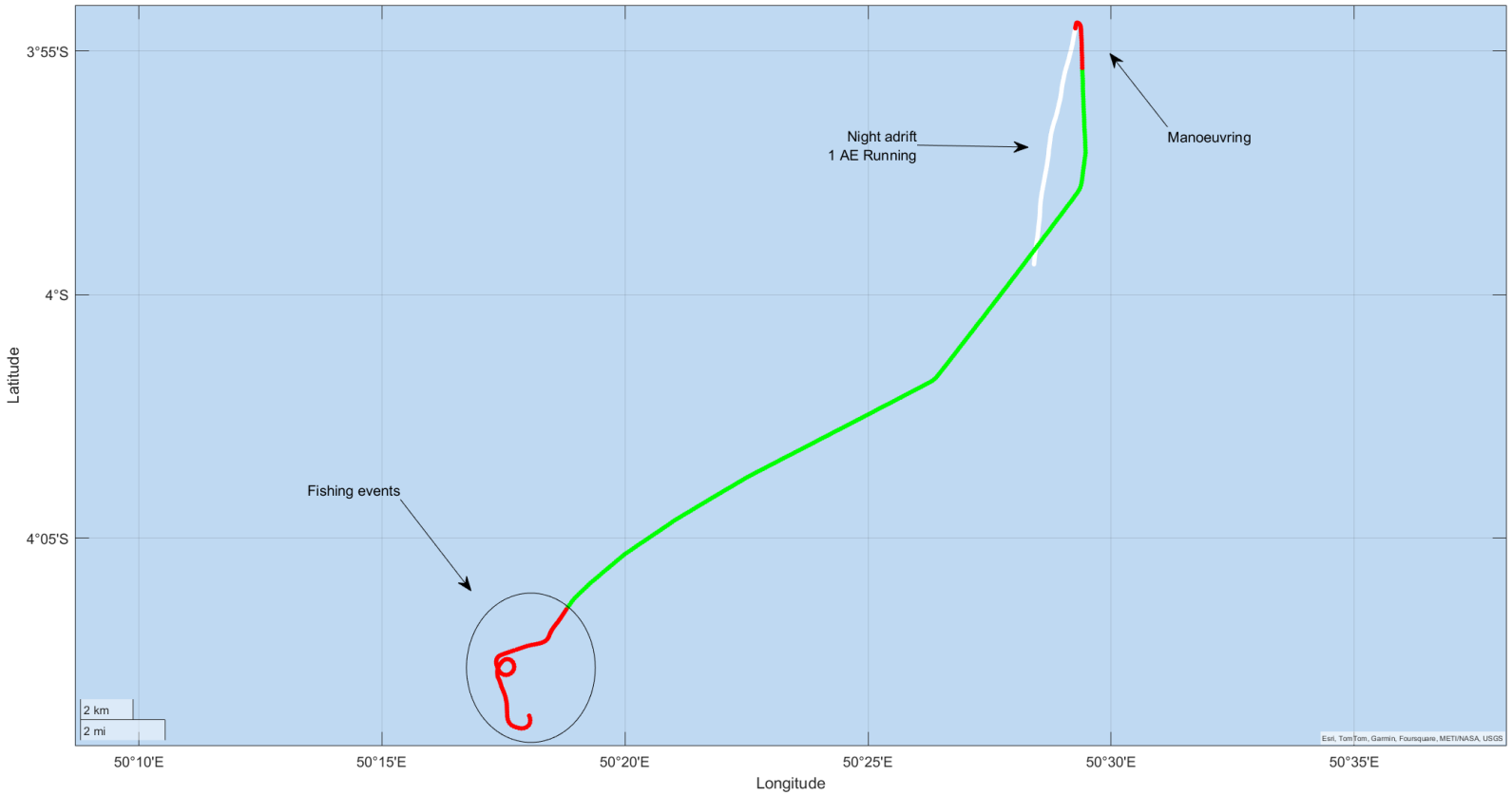

Figure 5.21 Graphical representation of the selected sub-dataset 1

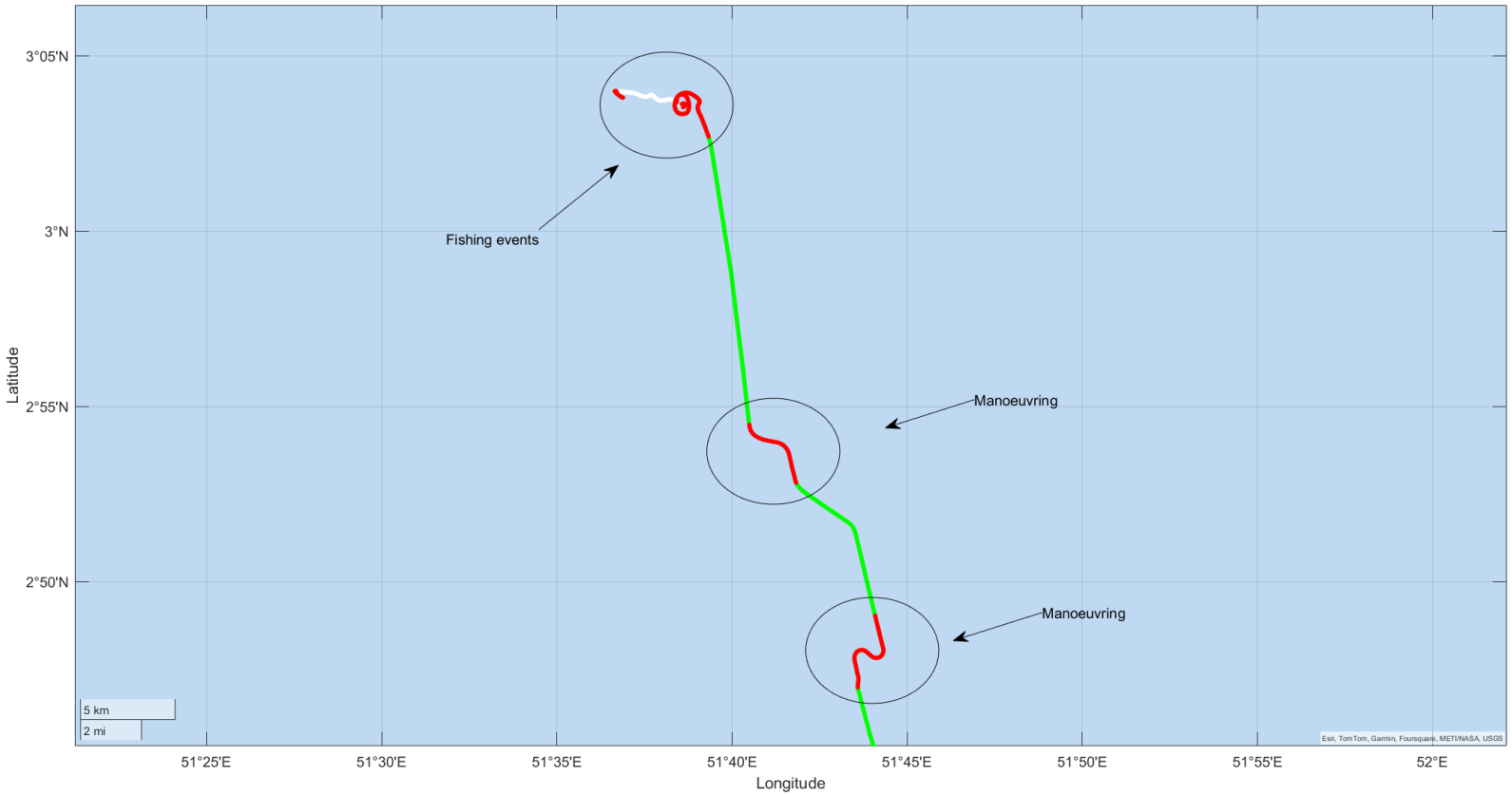

Figure 5.22 Graphical representation of the selected sub-dataset 2

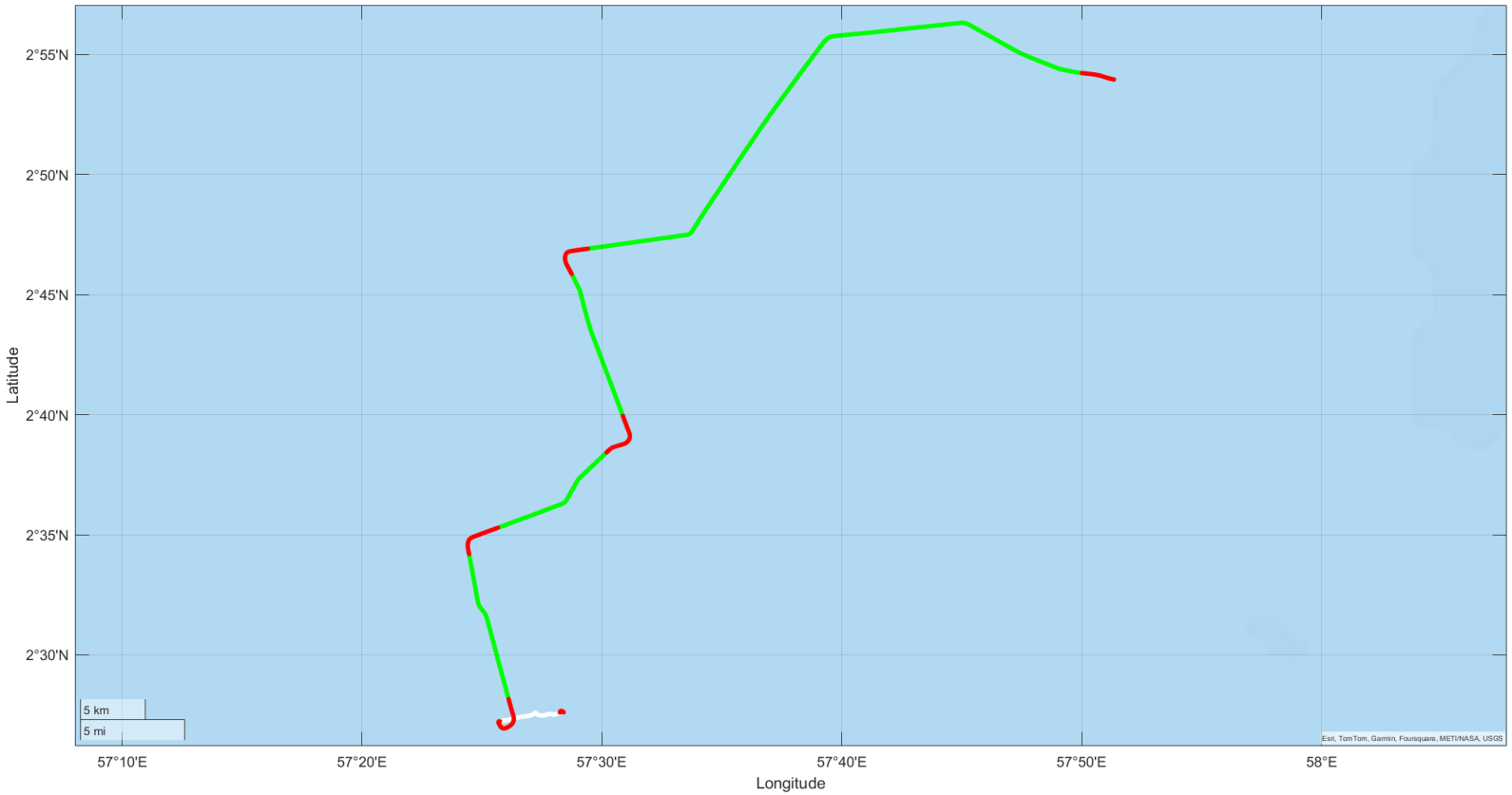

Figure 5.23 Graphical representation of the selected sub-dataset 3

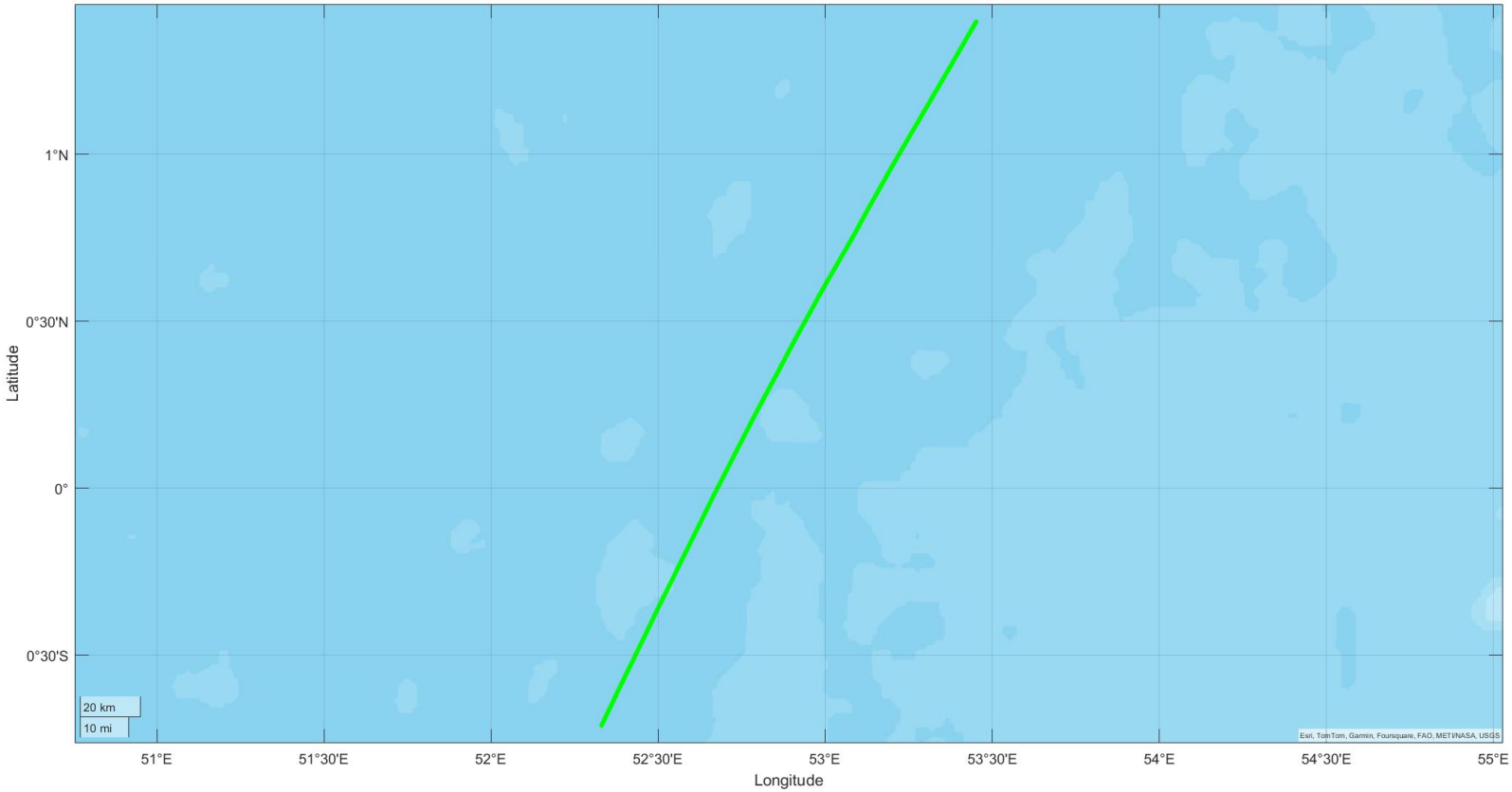

Figure 5.24 Graphical representation of the selected sub-dataset 4

5.7 Summary

In this chapter, the developed algorithm has been successfully applied to a tuna purse seiner and has effectively detected the 'Transit' mode. This task tested not only the robustness of the algorithm but also its applicability in complex scenarios. Successfully detecting this mode demonstrates the algorithm's robustness and provides insights into its adaptability across diverse vessel types, from traditional commercial to specialised vessels. Moreover, this case study has broadened the algorithm's generalisability, ensuring its effectiveness across various scenarios and datasets. This is pivotal as it underscores the method's versatility in addressing specific research needs and its efficacy in handling the nuanced operational patterns of different vessel types. Consequently, the adaptability of the algorithm has been validated for commercial and specialised vessels in open sea navigation areas. The next chapter will focus on testing the performance of the algorithm in inland waterway navigation areas, to encompass most navigation environments.

Chapter 6 Case study – Operational Modes Detection for an Inland Waterway Vessel

Chapters 4 and 5 have reported on the development of the algorithm for two different target vessels, the focus of the previous case studies was to test the performance of the algorithm in open-water or high-sea areas, environments in which the target vessels—ocean-going and tuna purse seiner—typically operate. The case study involving the tuna purse seiner specifically demonstrated the algorithm's capability to accurately detect the 'Transit' mode, even under circumstances where distinguishing 'Transit' from various complex operational modes presents significant challenges.

In this chapter, the developed algorithm will be applied to an inland waterway tanker to evaluate its performance in a distinct navigation area: inland waterways. Unlike open sea areas, the conditions within inland waterways are considerably more complex due to factors such as limited water depth, currents, and navigation routes which are restricted to the complex shapes of rivers. Furthermore, the target vessel is required to navigate through locks, movable bridges, dangerous curves, busy junctions, and other challenging scenarios. Consequently, the operational behaviours of inland vessels differ significantly from those operating in open sea areas, presenting unique challenges for the algorithm in detecting their operational modes.

One key difference is the method of defining the 'Transit' mode. For vessels navigating in open water areas, the defining characteristic of 'Transit' mode is a relatively straight-line trajectory pattern while the vessel sails at a 'Steady State' speed. However, in the context of inland waterways, environmental conditions restrict the navigation route, meaning that inland vessels are less likely to maintain straight-line patterns. Consequently, this feature may not be suitable for defining 'Transit' mode under such circumstances.

According to the EU research project 'Modernisation of Vessels for Inland Waterway Freight Transportation' (MoVe IT!) (MoVeIT!, 2014), operational modes for inland vessels are defined as 'Manoeuvring', 'Sailing Upstream', and 'Sailing Downstream'. However, these categorisations are determined solely by the mission profile (Godjevac and Drijver, 2015). In the present case study, the developed algorithm is designed to detect 'Transit', 'Manoeuvring', and 'Stop' modes for the target inland tanker. Here, the 'Transit' mode encompasses both 'Sailing Upstream' and 'Sailing Downstream', signifying normal operations when the vessel is

navigating between ports. The successful application of the algorithm to inland waterways would broaden its utility across a wider range of navigation areas.

6.1 Data Processing

The target vessel is an inland waterway tanker with dimensions of 135 metres in length and 14.15 metres in beam, with a tonnage of 6,752 tonnes. It is powered by four engines, each producing 294.2 kW, and is equipped with two sets of rudder propellers and one bow thruster.

The raw data was obtained from an EU LIFE-funded project entitled 'CLean INland SHipping' (CLINSH) (CLINSH, 2021). This project measured and recorded NOx and CO2 emissions, along with other key operational parameters, over a period of 10 months for the target vessel. The data points were collected at 4-second intervals, and the GPS coordinates were originally recorded with a precision of six decimal places. This precision has been truncated to five decimal places, providing an accuracy of approximately 1.1 metres for the target vessel. Reducing the precision to five decimal places, as opposed to six—which offers an accuracy of 0.11 metres—enhances computational efficiency for subsequent analyses. Considering the full length of the target vessel, which measures 135 metres, a 1.1 metre difference in position may not impact the accuracy of mode detection.

The initial data processing steps involve eliminating timestamps for which there was missing data and duplicated timestamps. Subsequently, the 1.5 IQR technique is applied to the discrepancies between the SOG and the extracted speed from coordinates, termed SpeedLL, to identify and remove outliers.

In this case, the maximum SpeedLL, which was derived from the coordinates, was recorded as 42.73 knots—an unrealistic figure given that the maximum speed of the target vessel is 12.7 knots. As discussed in sections 4.2.1 and 5.2, this significant discrepancy likely results from the accumulation of minor deviations among nearby data points. Therefore, a critical aspect of data cleaning in this context involves focusing on these minor deviations, specifically the speed discrepancies between the SOG and SpeedLL for each data point. The deviation is calculated by subtracting SpeedLL from SOG, and the 1.5 IQR technique is then applied to these calculated discrepancies to filter out outliers. The raw SpeedLL and the discrepancy between SOG and SpeedLL have been illustrated in the Figure 6.1.

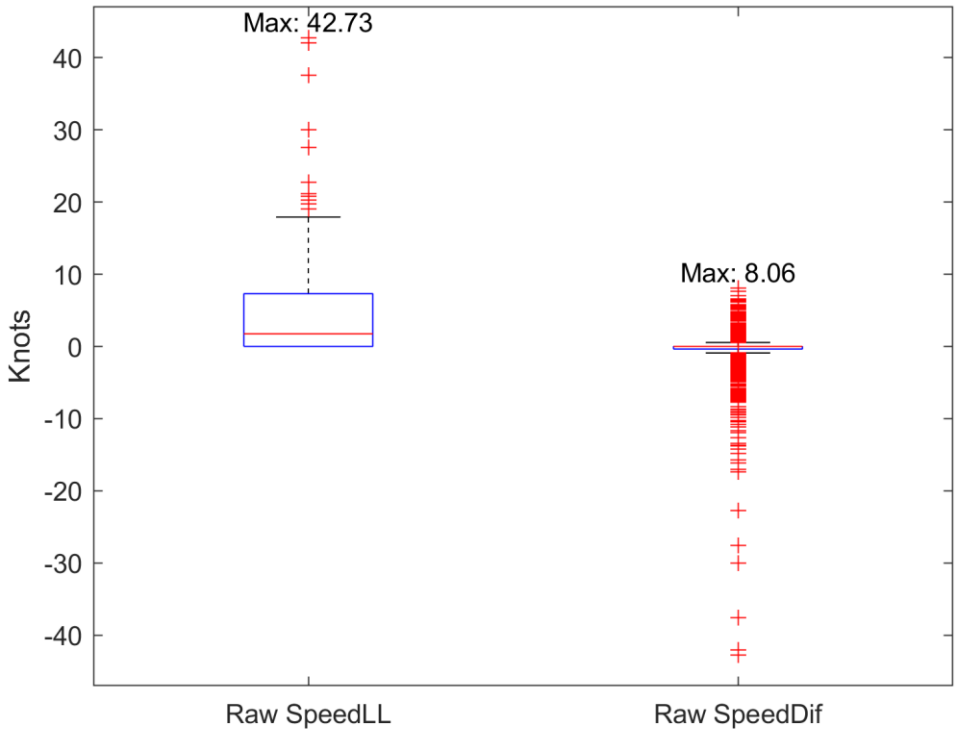

Figure 6.1 Boxplots of raw SpeedLL and corresponding speed discrepancy

The detailed discussion on the 1.5 IQR technique and data cleaning strategies are presented in Section 3.4.1. In this analysis, the IQR range has been identified as 0.3631 knots, representing the difference between the 25th and 75th percentiles of the speed differences. Consequently, speed differences within an accepted range of -0.9077 to 0.5446 knots are considered valid, while values outside this range are discarded. This range is deemed reasonable as the maximum difference between these two speeds, which theoretically measure the same parameter, is less than 1 knot. Further details of the parameters associated with the 1.5 IQR technique are presented in Table 6.1.

Table 6.1 Key parameters in 1.5 IQR calculation

Speed difference (SOG - SpeedLL)	-42.7253 ~ 8.0641 (knots)
1.5 IQR	-0.9077 ~ 0.5446 (knots)
IQR (25-75 percentile)	0.3631 (knots)
Q1 (25)	-0.3631 (knots)
Q2 (50)	0 (knot)
Q3 (75)	0 (knot)
Q4 (100)	8.0641 (knots)

After the data cleaning, the cleaned speed difference and cleaned SpeedLL are illustrated in the Figure 6.2.

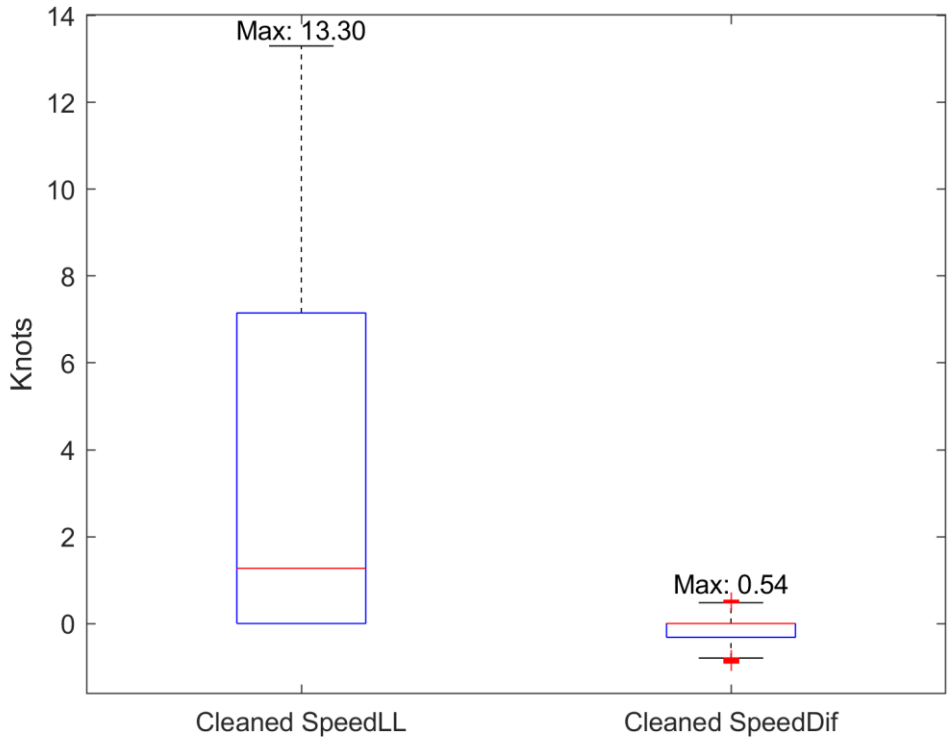

Figure 6.2 Boxplot of cleaned SpeedLL and corresponding speed discrepancy

Figure 6.2 illustrates that the 1.5 IQR technique has effectively removed the outliers from the dataset. After the cleaning process, the maximum speed of the cleaned SpeedLL is 13.3 knots, which is reasonable and acceptable with respect to the vessel speed. Additionally, the range of the speed difference is from -0.9 to 0.5 knots, demonstrating a satisfactory result with the speed discrepancy being less than 1 knot.

As discussed in Section 3.4.3, data continuity is essential for the effectiveness of the developed algorithm. The previous data cleaning process may significantly disrupt this continuity. To mitigate this issue, the following aggregation technique has been employed: data points are aggregated by averaging the frequency of every 4 seconds into a 15-second interval. This ensures that continuity is maintained if there is at least one data point within each defined 15-second period, using the average value to represent the aggregated data point.

The aggregated dataset will be divided into several continuous sub-datasets based on the time gaps. Furthermore, any sub-datasets containing fewer than 20 data points, equivalent to 5

minutes, will be disregarded, as they lack sufficient data for analysis. The threshold of 20 data points aligns with the sensitivity analysis on the combination of the rolling window, which will be discussed in detail in Section 6.2.2.

An exemplary sub-dataset has been selected as a key element for analysis, aimed at defining thresholds to distinguish the 'Steady State' for extracted speed and curvature. The selection of this dataset must balance data continuity with the presence of various operational mode changes. However, selecting a suitable dataset for the target vessel is challenging due to the presence of extreme curvature values, which are more than one thousand times greater than those observed under normal navigating conditions for this vessel, and the occurrence of extreme values stops the algorithm from detecting the 'Steady State' conditions successfully.

These extreme values indicate significant course changes at specific times. Closer examination reveals that these extreme curvature values are primarily concentrated during periods when the vessel either stops or begins to manoeuvre, such as when approaching a dock, or when slowing down or stopping to navigate through a bridge or lock. Therefore, it is preferable to select an example dataset in which the vessel is continuously sailing in the inland waterway, and which demonstrates prolonged data continuity. The trajectory of the selected example dataset is shown in Figure 6.3.

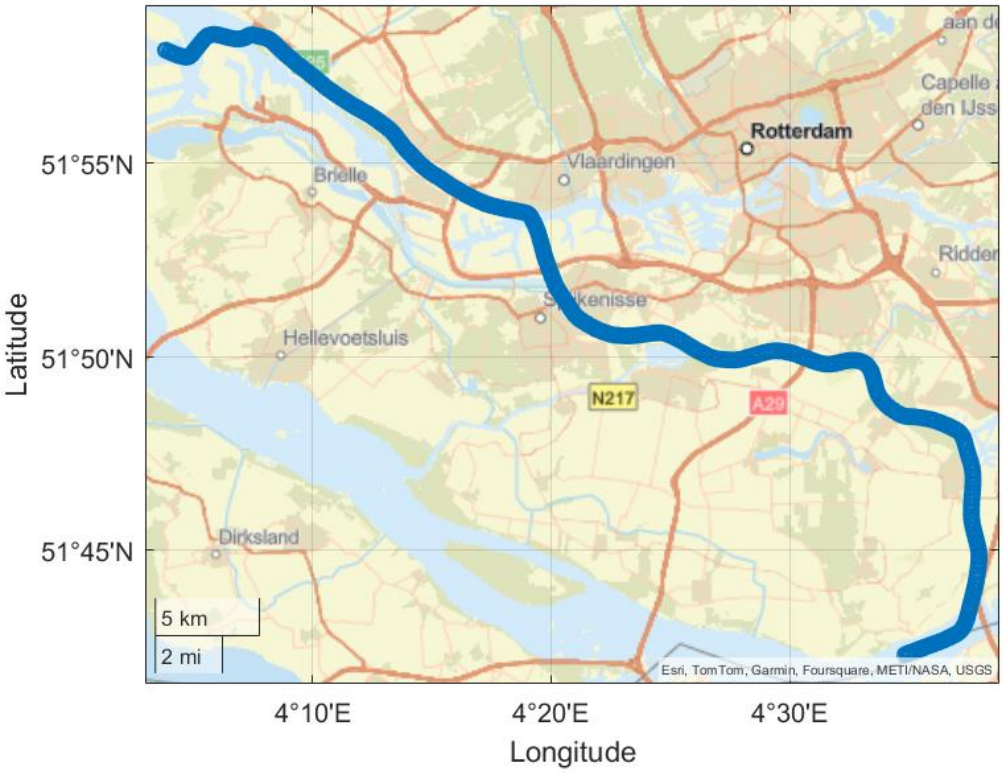

Figure 6.3 Trajectory of the selected example dataset

The selected sub-dataset contains 990 data points, recorded at 15-second intervals, capturing the vessel's trajectory over a period of 247.5 minutes, or just over 4 hours. During this time, the vessel sails predominantly north-west the inland waterway, as illustrated in Figure 6.3. Notably, this sub-dataset does not contain any extreme curvature values, making it ideal for the subsequent 'Steady State' analysis.

6.2 Steady State Detection for SpeedLL

6.2.1 Identification of visualised change points

Now that the example sub-dataset has been selected, the next step involves defining thresholds to distinguish the 'Steady State' for the extracted key features, SpeedLL and Curvature. The SpeedLL values for the selected sub-dataset, along with VCPs marked with red vertical dotted lines are illustrated in Figure 6.4.

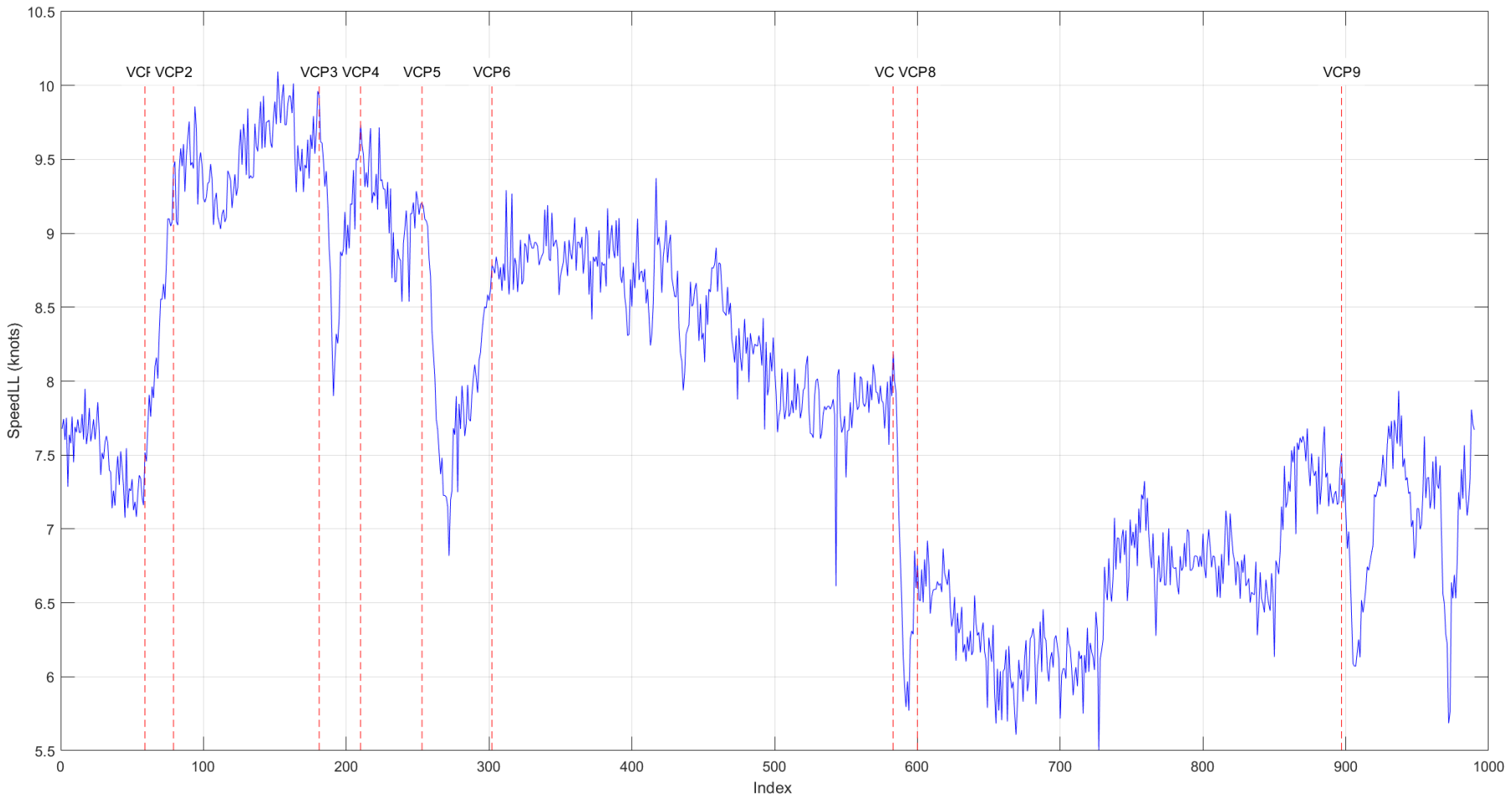

Figure 6.4 SpeedLL for the exemplary sub-dataset with VCPs in vertical red dotted lines

In Figure 6.4, nine VCPs have been identified, dividing the dataset into ten segments. These segments represent binary conditions of 'Steady State' and 'Changing.' The sequence begins with a 'Steady State' from the start to VCP1, followed by a 'Changing' condition from VCP1 to VCP2, and continues in this pattern until the segment from VCP9 to the end of the data points, which remains under a 'Changing' condition. These VCPs are determined by observing the general variability in the data, which serves to distinguish segments with distinctly different data variabilities. This approach results in consecutive segments exhibiting contrasting levels of high and low variability, thereby representing the binary conditions.

However, it can be observed that the segments defined as 'Steady State' still exhibit significant fluctuations. For example, there is a notable speed drop in the segment between VCP6 and VCP7, and two sharp speed increases within the segment between VCP8 and VCP9. This observation suggests that the differences in variability between the binary conditions are not as distinct as expected, indicating substantial data fluctuations within the points categorised under the 'Steady State' conditions. As previously discussed, two methods for evaluating data variability - IQR and SD - have been employed in the developed algorithm. The variabilities of the visualised segments in terms of IQR and SD are documented in

Table 6.2, which reinforces this observation.

Table 6.2 Variability of visualised segments using IQR and SD

Segments	1	2	3	4	5	6	7	8	9	10
VCPs (Index)	1	59	79	181	210	253	302	583	600	897
Binary Label	0	1	0	1	0	1	0	1	0	1
IQR	0.36	0.83	0.38	0.63	0.34	0.81	0.81	1.10	0.66	0.66
SD	0.22	0.54	0.26	0.51	0.30	0.60	0.47	0.79	0.46	0.49

Binary Label (0&1) represents two conditions: 0 – Steady State, 1 – Changing

The values in bold represent the unusual variabilities under the 'Steady State' condition.

The variabilities of visualised segments documented in Table 6.2 suggest that the VCPs do not effectively distinguish the binary conditions, especially in cases where the variabilities, highlighted in red, are comparable to those in the consecutive 'Changing' segments. Nonetheless, the pattern of variabilities in SD aligns with the expected binary conditions, exhibiting low variability under 'Steady State' and higher variability under 'Changing'

conditions. However, the differences between these binary conditions are not markedly distinct, particularly when comparing segments 9 and 10.

Both Figure 6.4 and Table 6.2 reveal significant fluctuations within the visualised segments. These fluctuations are likely due to the complexity of the inland waterway environment, where winding navigation routes and shallow waters necessitate high manoeuvrability. The target vessel is equipped with two sets of rudder propellers, enhancing its manoeuvrability. This feature, while advantageous for navigation, may contribute to the observed speed variations even under 'Steady State' conditions.

In this case, the VCPs have been identified primarily by comparing the speed status before and after significant variations. For instance, the identification of Segment 2, between VCP1 and VCP2, features a sharp increase in speed from approximately 7.5 knots to 9.5 knots. Furthermore, the speed status in Segments 1 and 3 fluctuates around these two speeds, respectively.

In contrast, significant speed variations between Segments 4 and 6 have been identified, despite the speeds before and after being approximately constant. These variations are recognised as mode changes due to the lengthy duration of the variation periods, which contain 29 and 49 data points, spanning more than 7 and 12 minutes, respectively. Considering the high manoeuvrability of the target vessel, this is to be expected. Furthermore, the fact that the number of data points in Segments 2 and 8 is around 20 suggests that the vessel does indeed have high manoeuvrability, enabling it to rapidly accelerate or decelerate within approximately 5 minutes.

From the perspective of trajectory analysis, the VCPs effectively segment the trajectory and accurately indicate all periods when the vessel navigates through junctions and sharp corners. This segmentation closely aligns with domain knowledge expectations and graphical representation. The trajectory of the sub dataset, marked with VCPs in red, is illustrated in Figure 6.5.

Figure 6.5 Illustration of the vessel's trajectory with VCPs marked by red dots

6.2.2 Sensitivity analysis on the combination of rolling window

As detailed in Chapter 3, after identifying the VCPs, the subsequent step involves conducting a sensitivity analysis to determine the appropriate combination of the rolling window for evaluating the variability of each data point.

The parameters of the combination of rolling window encompasses two key aspects: the positions - 'Begin', 'Middle', and 'End' - which indicate where the target data point is located within the rolling window, and the length of the window itself. Moreover, the developed objective function considers different methods for calculating data variability, SD and IQR. The optimal combination of these parameters will be determined based on the value of the objective function, where the highest value indicates that the combination provides the strongest support for identifying the VCPs. Further details on the objective function are available in Section 3.5.2.2.

The range of the rolling window size has been set from 4 to 100. A size of 4 represents the minimum requirement for utilising the IQR, ensuring sufficient data points for reliable calculations. Conversely, a window size of 100 allows for the observation of a relatively complete pattern in the objective function values, aiding in the identification of the optimal parameter combination. Figure 6.6 illustrates the results of the objective function under the three positions: 'Begin', 'Middle', and 'End'.

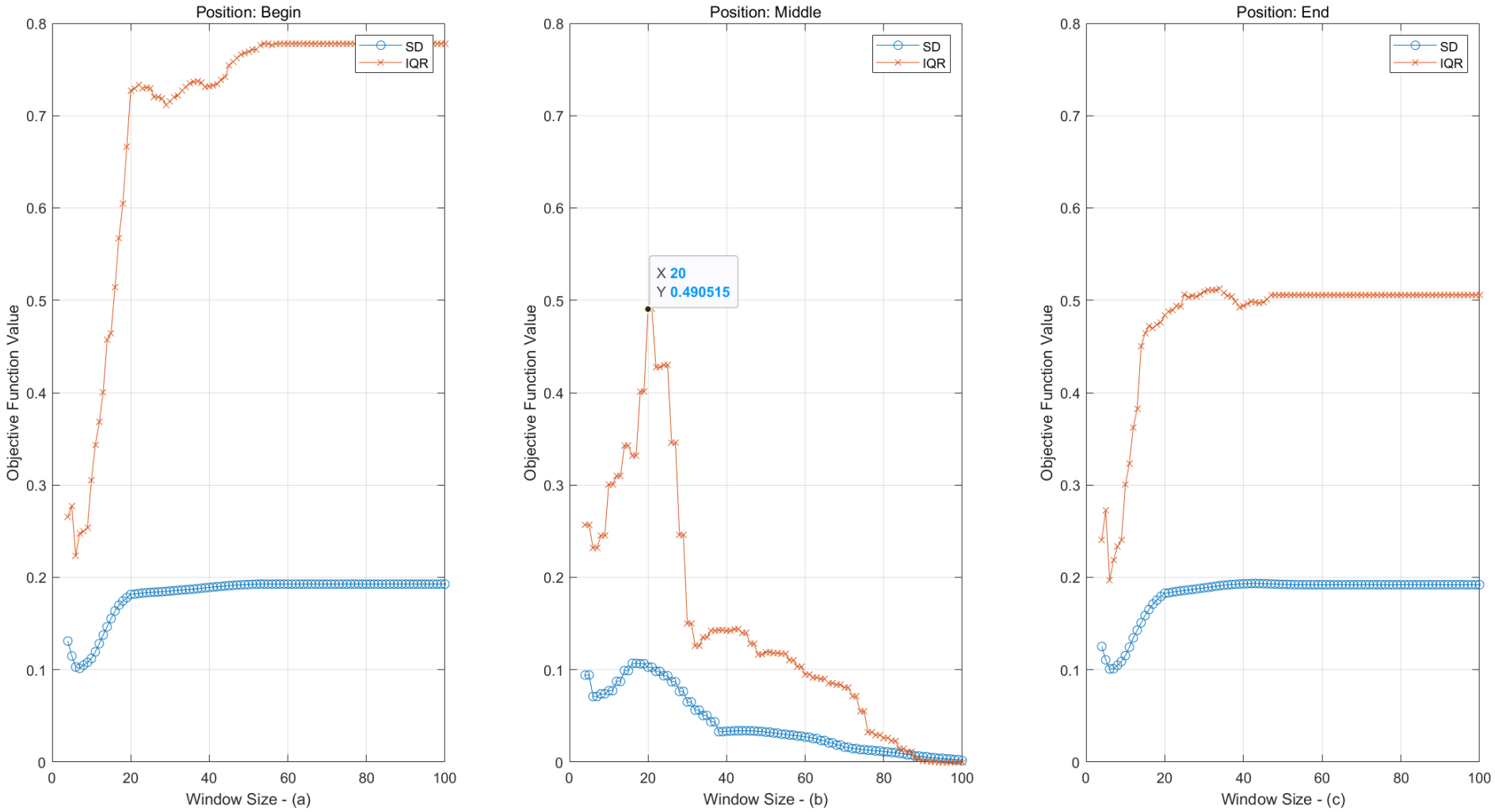

Figure 6.6 Results of the objective function for SpeedLL analysis

Figure 6.6 illustrate that the IQR consistently yields higher objective function values than the SD across all three positions. Additionally, the pattern of the SD values is similar to the pattern of the IQR values. Consequently, the method for evaluating variability for each data point of SpeedLL has been defined using the IQR.

In the analysis of rolling window positions, only the 'Middle' position demonstrates a clear peak in the objective function value, as illustrated in Figure 6.6 (b). The objective function value increases sharply to reach a peak, followed by a significant decrease with a minor rebound, and then tapers off gradually to its minimum as the window size increases. In contrast, the 'Begin' and 'End' positions show a similar pattern, characterised by a slight initial decrease, a sharp subsequent increase, and a gradual ascent to their maximum values, where they tend to stabilise towards the end of the size range.

Table 6.3 displays the window sizes for the three positions that provide the maximum objective function values. It is observed that the window size at the 'Middle' position is the smallest compared to the other two positions, with sizes of 20 for the IQR and 16 for the SD, respectively.

Table 6.3 The maximum related window sizes of three positions

Position	Begin	Middle	End
IQR	54	20	34
SD	59	16	43

On one hand, a smaller rolling window size preserves more information from the raw data. On the other hand, the optimal window size of approximately 20 at the 'Middle' position correlates closely with the high manoeuvrability of the target vessel. This chosen size aligns with the Continuity Check of the change points, where the basic premise is that operational mode changes do not occur within the defined period, approximately 5 minutes in this case. This is consistent with the duration of the visualised segments 2 and 8, which also span around 5 minutes. Consequently, a window size of 20 at the 'Middle' position is more appropriate compared to the other two options and has been established as the preferred rolling window combination.

6.2.3 Define threshold on SpeedLL to distinguish steady state condition

Having defined the optimal rolling window combination in the sensitivity analysis as M20, which represents the 'Middle' position with a window size of 20, the next step is to establish the threshold for the variability of each point to distinguish 'Steady State'. Figure 6.7 illustrates the SpeedLL and its associated point variability, with the VCPs indicated by vertical red dotted lines.

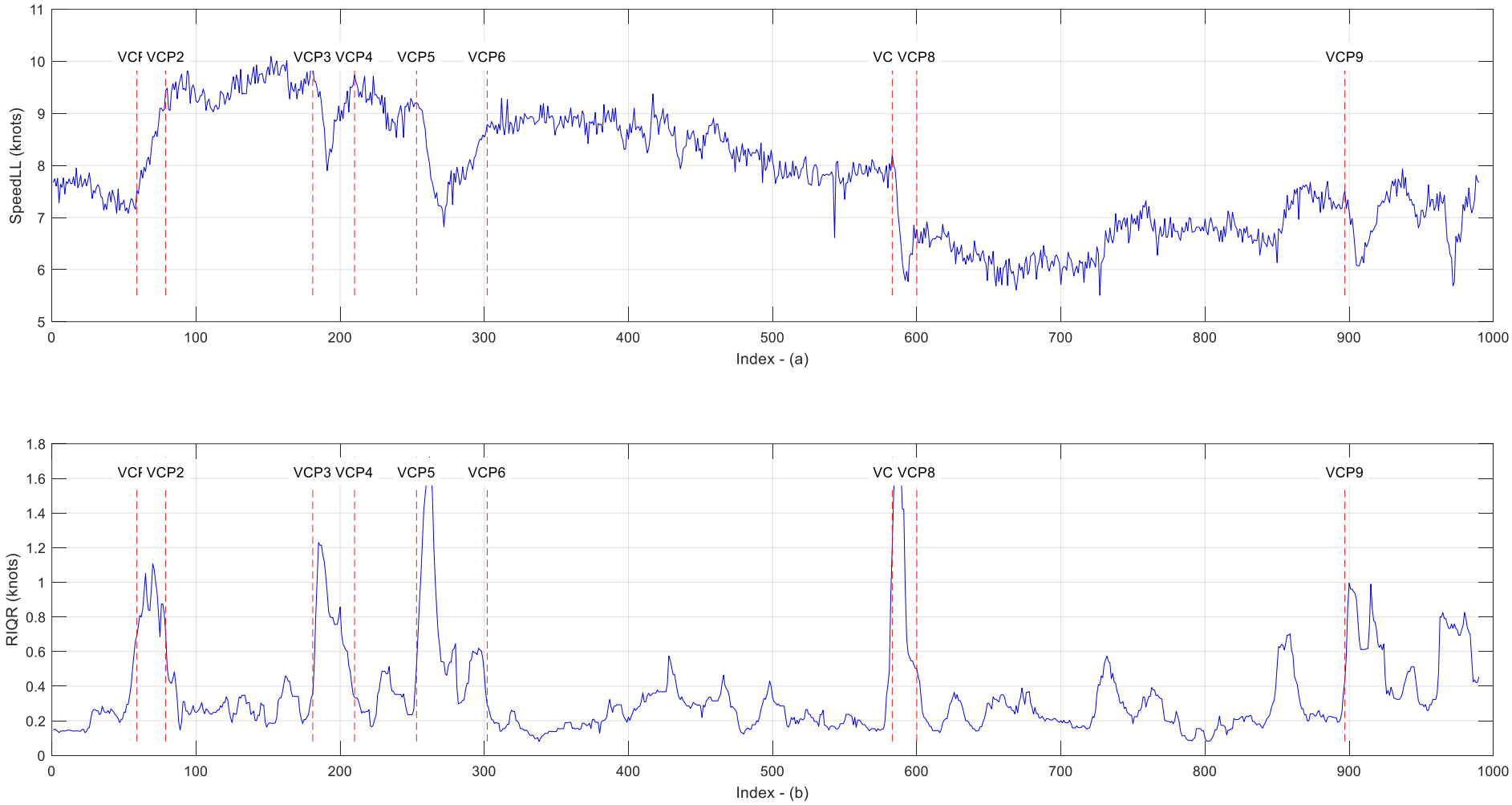

Figure 6.7 Illustration of SpeedLL and its pointed variability with VCPs in vertical red dotted lines

Figure 6.7 reveals the relationship between SpeedLL and its pointed variability. The variability calculated using the sensitivity analysis based rolling combination (M20) effectively captures the variations in SpeedLL. Notably, there are four peak values that correspond to significant speed variations. Additionally, the variabilities in the last visualised segments display relatively higher values compared to others, which are illustrated under the 'Steady State' condition.

After careful observation of Figure 6.7 (b), the threshold range has been established from 0.4 to 0.6 knots, with increments of 0.01 knots. Each threshold within this range is applied to the pointed variability, if the variability is below the threshold, it is labelled as '0' ('Steady State'), otherwise, it is labelled as '1' ('Changing'). The identified change points then undergo a Continuity Check, where a change point is recognised only if its status matches the preceding points within the defined rolling window size. The optimal threshold is determined by comparing the related DCPs and VCPs, selecting the threshold where the DCPs are closest to the VCPs. Table 6.4 presents the detected DCPs for each threshold.

Table 6.4 Indices of DCPs and related thresholds

Threshold(knots)	Indices of DCPs
0.4	54;86;181;300;579;602;896
0.41	55;86;181;300;580;602;896
0.42	55;85;181;207;252;300;580;602;896
0.43	55;85;181;207;252;300;580;601;896
0.44~0.45	55;85;181;207;252;300;580;601;897
0.46~0.47	55;85;181;207;252;300;580;600;897;985
0.48	55;85;181;207;252;299;580;600;897;985
0.49	55;80;181;206;252;299;580;600;897;985
0.50	56;80;181;206;252;299;897;985
0.51	56;79;181;206;252;299;897;985
0.52~0.55	56;79;182;205;897;924;962;985
0.56~0.60	56;79;182;205;897;924;962;984

Table 6.4 displays the indices of DCPs for each threshold. Despite minor differences in the indices of DCPs, such as those at 54, 55, and 56, the DCPs tend to be consistent within specific threshold bands. These bands are 0.4 to 0.41, 0.42 to 0.45, 0.46 to 0.49, 0.5 to 0.51, and 0.52 to 0.6 knots, within which the DCPs are generally uniform. Furthermore, certain DCPs repeatedly appear across the entire range; for example, the first three DCPs, located around indices 55, 80, and 181, are detected by all thresholds. This consistency indicates that the

developed algorithm can successfully recognise specific speed variations by adjusting the thresholds, enhancing the precision of mode detection.

After comparing the DCPs with the VCPs, it has been observed that thresholds within the bandwidth of 0.42 to 0.45 knots can detect DCPs that are highly similar to the VCPs. Given that a smaller threshold tends to provide higher precision, the threshold for SpeedLL has been set at 0.42 knots. This comparison is illustrated in Figure 6.8, which illustrates that the DCPs effectively segment the dataset into binary conditions, closely mirroring the VCPs.

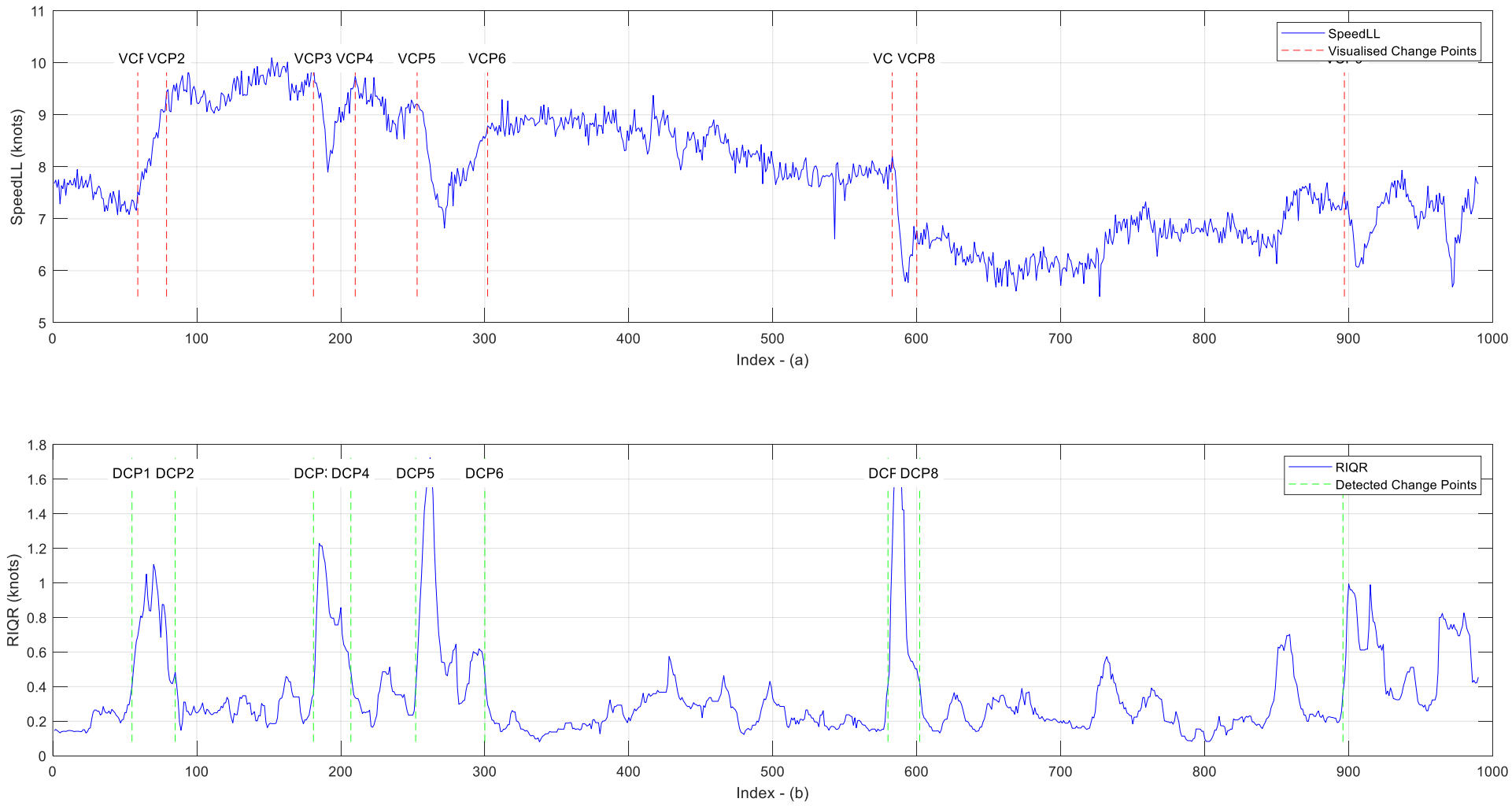

Figure 6.8 Comparison between VCPs and DCPs

6.3 Steady State Detection for Curvature

The detection of Steady State in curvature in this case is complicated due to the absence of distinctive clues for defining the VCPs. This complexity likely comes from the complicated navigation routes of the inland waterway, which demand superior manoeuvrability. Despite these challenges, the developed algorithm has still been applied to assess its performance under these conditions. The Curvature of the selected dataset has been illustrated in the Figure 6.9.

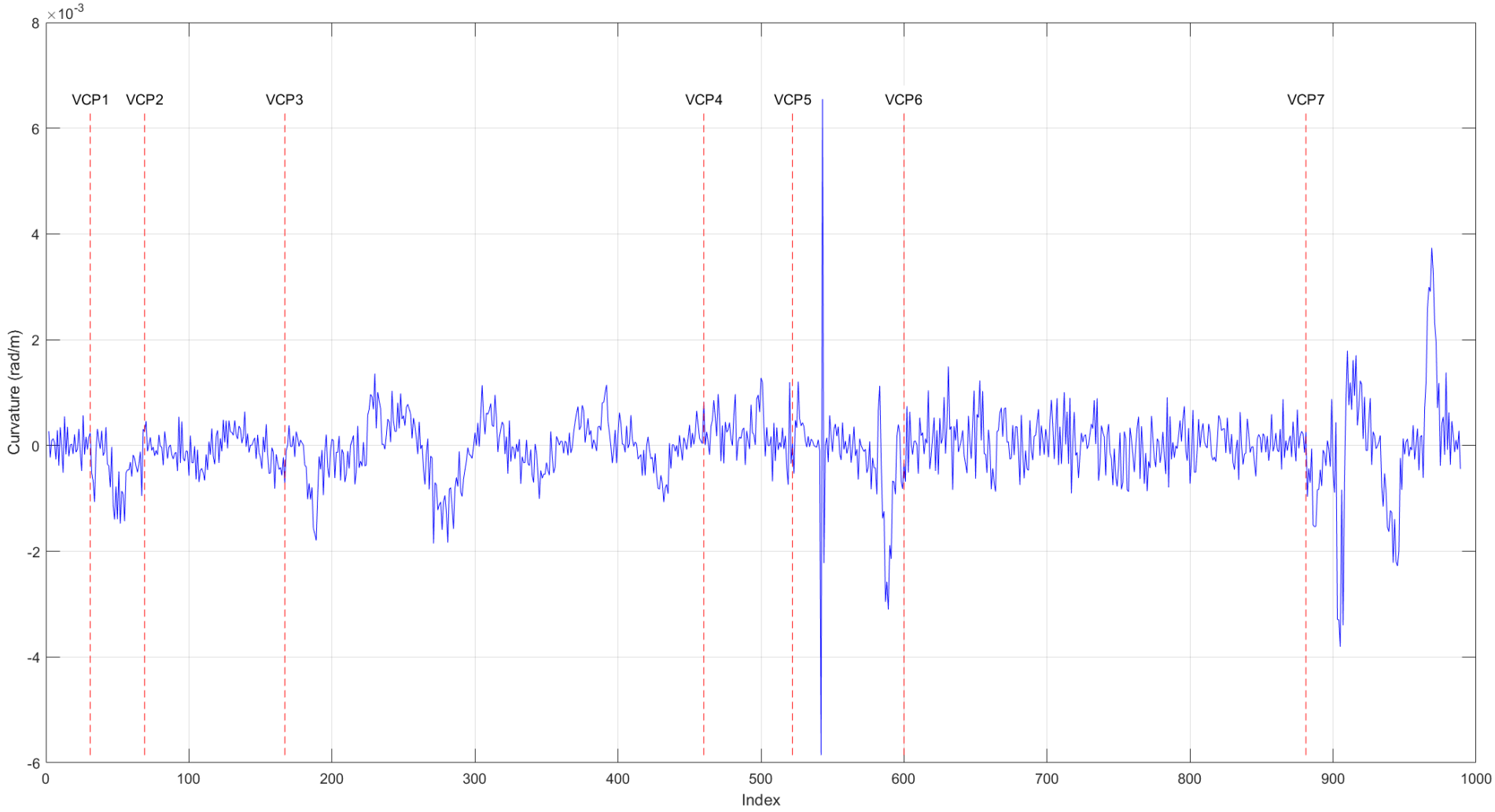

Figure 6.9 Illustration of Curvature and VCPs in vertical red dotted lines

In Figure 6.9, it is evident that there are many fluctuations in the curvature data, which is challenging to define VCPs based solely on the observation of general variability. For testing the performance of the developed algorithm, seven VCPs have been identified based on an intuitive observation of the curvature pattern. Segments exhibiting regular patterns - such as from the beginning to VCP1, from VCP2 to VCP3, from VCP4 to VCP5, and from VCP6 to VCP7- are categorised as 'Steady State'. The curvatures within these segments consistently fluctuate within a relatively defined range, with similar upper and lower limits. Conversely, the remaining segments, which display irregular patterns, are classified as being under 'Changing' conditions.

However, these VCPs do not effectively distinguish the binary conditions within the selected dataset. The variabilities for the visualised segments, as measured by IQR and SD, do not provide strong support for this distinction, as detailed in Table 6.5.

Table 6.5 Variabilities in IQR & SD for visualised segments

Segments	1	2	3	4	5	6	7	8
VCPs (Index)	1	31	69	167	460	522	600	881
Binary	0	1	0	1	0	1	0	1
IQR (e-4)	3.923	6.715	4.243	6.711	4.477	6.016	5.477	12.122
SD (e-4)	2.782	5.091	3.120	5.540	4.419	12.842	4.368	12.897

In Table 6.5, except for the last segment, which shows higher variability in both IQR and SD, there is no significant difference in variability among the other segments that could be used to distinguish binary conditions. The elevated variability in SD for segment 6 can be attributed to the occurrence of extreme values, as illustrated in Figure 6.9. Furthermore, when compared with previous case studies involving an ocean-going vessel and a tuna purse seiner, the differences in variability between segment 8 and the other segments are much smaller, still proving insufficient to distinctly identify binary conditions for curvature.

Additionally, these VCPs cannot be explained as effectively by examining the vessel's trajectory, unlike the SpeedLL. The subsequent sensitivity analysis using the selected rolling window combinations has not performed well. The objective function values derived from these VCPs are illustrated in Figure 6.10, with the range of the window size set from 4 to 100, synchronising the settings used for SpeedLL.

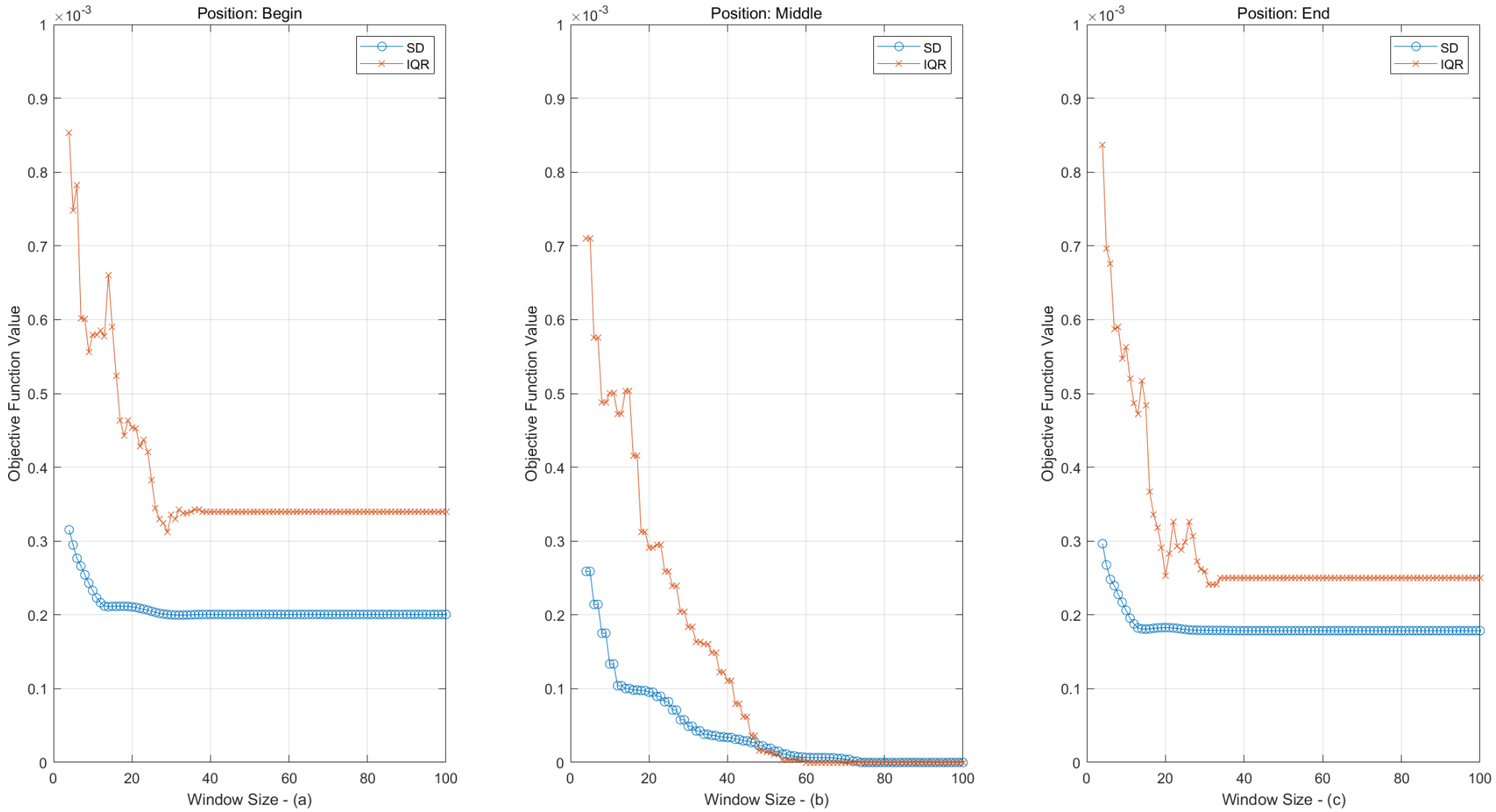

Figure 6.10 Objective function values at three positions based on VCPs

From Figure 6.10, it is evident that the results of the objective function do not indicate an appropriate rolling combination, as no distinctive peak values occur within the specified size range. Additionally, the patterns of these values tend to decrease sharply from the onset and then stabilise at lower values as the window size increases. The smallest window size of 4 consistently provides the highest objective function values across all three positions. Moreover, the IQR generally provides higher values than the SD.

In this circumstance, the selected rolling combination has been designated as ‘B4’ in IQR, representing a window size of 4 at the ‘Begin’ position. However, this selection does not account for the interrelationship between SpeedLL and Curvature. The extracted curvature and the variability for each data point, alongside the VCPs, are illustrated in Figure 6.11.

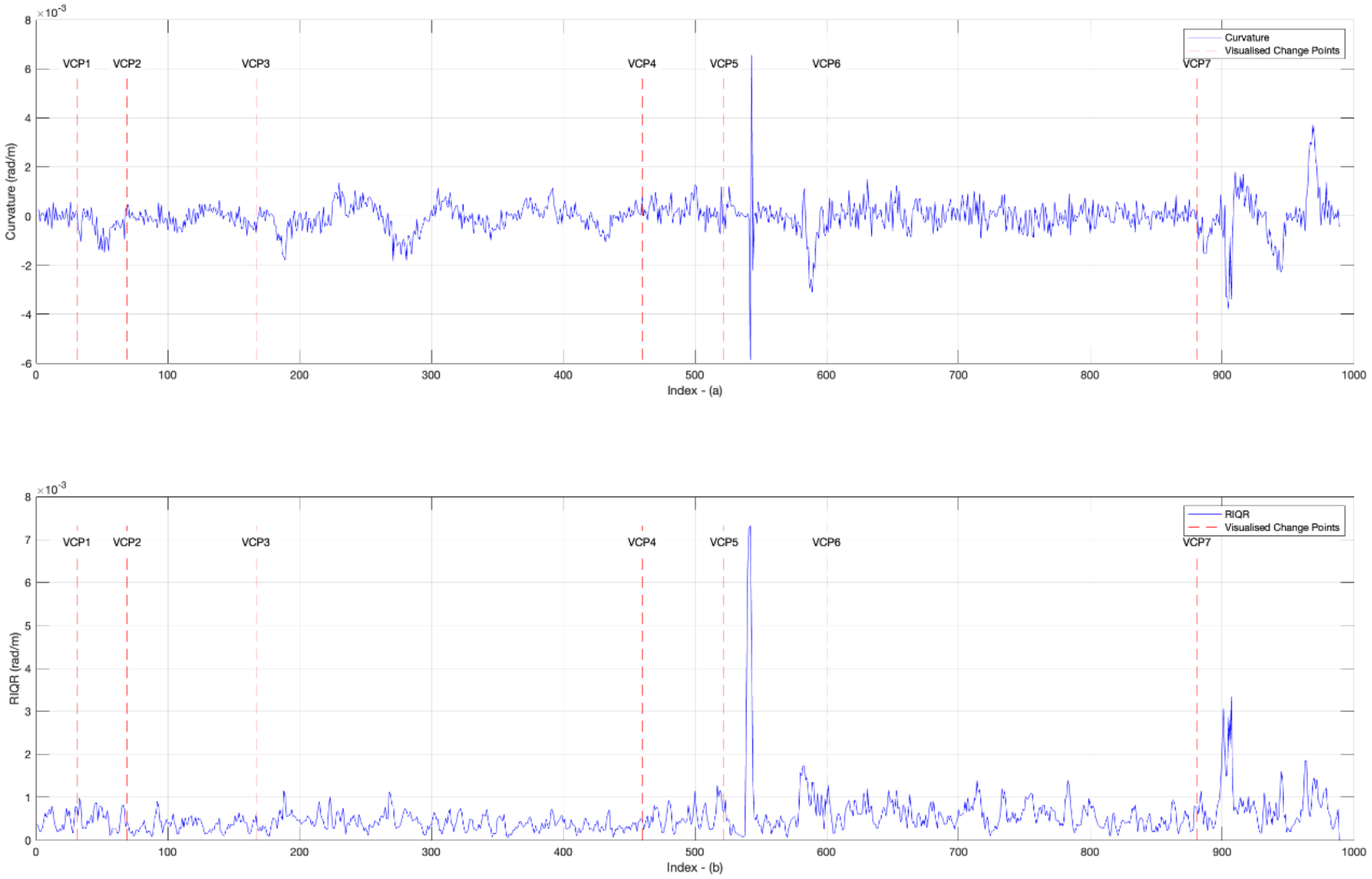

Figure 6.11 Illustration of Curvature and pointed variability with VCPs in vertical red dotted lines

In Figure 6.11, it is evident that the RIQR, calculated using the 'B4' rolling combination, fails to effectively capture the variations in curvature. This inefficacy is further reflected in the subsequent analysis of DCPs. The threshold range was set from 0.1e-3 to 1.5e-3 rad/m, with increments of 0.01e-3 rad/m, and the Continuity Check was synchronised to a size of 4. Within the middle range of these thresholds, an excessive number of DCPs were detected, peaking at 69 at the threshold of 0.46e-3 rad/m. This high detection rate is primarily due to the minimal variability in RIQR values, and the brief period required for the Continuity Check, which allows many points to easily pass this check. Conversely, the number of DCPs drops dramatically to 2 or 3 when thresholds approach the upper and lower limits. This reduction occurs because the thresholds set near extreme values only allow a few points to be detected as 'Changing' or 'Steady State.' Nevertheless, across the entire threshold range, the DCPs fail to provide meaningful insights or utility in defining operational modes, indicating that this approach does not successfully detect 'Steady State' conditions for curvature.

The primary challenge is that the VCPs have not been effectively accepted by the developed algorithm, indicating an inability to distinguish binary conditions for curvature accurately. Detecting VCPs is a crucial initial step in the algorithm's process, forming the foundation for subsequent 'Steady State' analysis. Despite testing several sets of VCPs, the results have consistently been unsatisfactory. The VCPs illustrated in Figure 6.9, which align most closely with personal intuitive judgment, exemplify this issue.

Furthermore, as noted in the section discussing the selection of exemplary sub-dataset, other sub-datasets with extremely high curvature values were also tested. Despite the significant differences these extreme values introduce, often exceeding a thousandfold, they do not provide a reliable standard or reference for distinguishing 'Changing' status from 'Steady State'. The algorithm's purpose is to detect binary conditions under normal sailing circumstances, not extreme scenarios.

The difficulty in accurately detecting VCPs is aligned with the characteristics of the target vessel. The substantial fluctuation in Curvature not only complicates VCP detection but also reflects the vessel's superior manoeuvrability. This suggests that the vessel is typically navigating with frequent minor course adjustments, a scenario that inherently challenges the algorithm's capacity to define clear binary states.

Under these challenging circumstances, it was observed that the VCPs for curvature were not effectively recognised by the algorithm, thereby failing to provide a suitable rolling window combination. To address this issue, a method has been introduced to mitigate the difficulties associated with VCP detection. As previously discussed, the two key features, SpeedLL and Curvature, are extracted from the same coordinates, underscoring their interrelationship. This connection is a primary justification for synchronising the analysed rolling combinations, ensuring that the evaluation of variability is consistent and based on the same original coordinates. Essentially, this approach is predicated on the premise that these extracted features would change simultaneously with changes in the operational mode; that is, any alteration in the operational mode of the vessel will concurrently affect both the speed and curvature, or in other words, the trajectory, composed of time-series coordinates, will exhibit variations corresponding to different operational modes. Since the objective function was unable to provide appropriate key features for the rolling combinations, the interrelationship between these two features became a critical reference point. Consequently, the best-performing option for SpeedLL, which is the ‘M20’ in IQR, has been applied to Curvature. The comparison between the RIQR of the ‘M20’ and ‘B4’ combinations for curvature are illustrated in Figure 6.12.

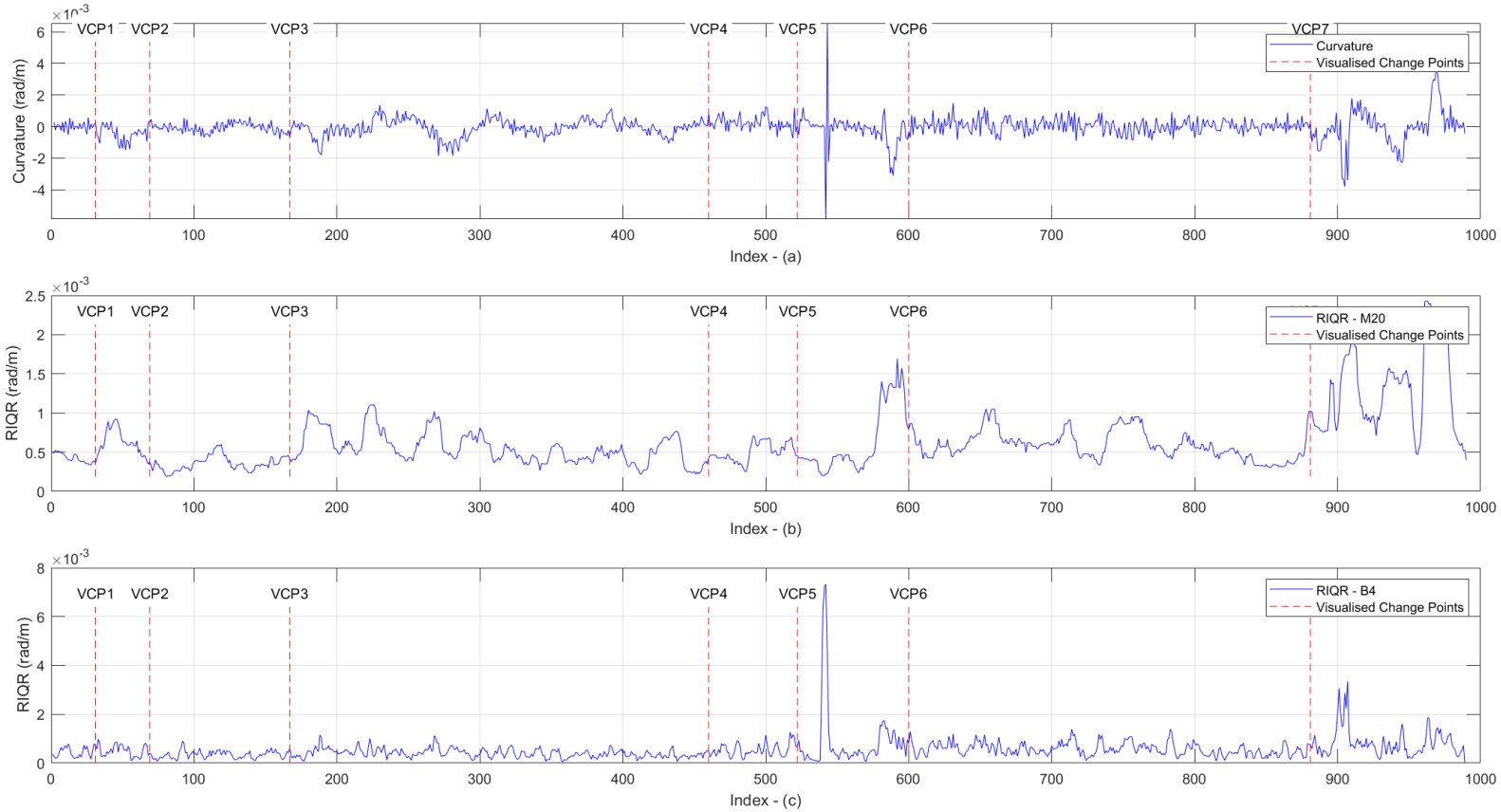

Figure 6.12 Comparison between two combinations of the rolling window

In Figure 6.12, the RIQR values for the 'M20' combination are significantly more distinctive than those for the 'B4' combination, aligning well with expectations derived from the VCPs. Notably, except for the segments between VCP6 and VCP7, which exhibit slightly elevated RIQR, the trends in other visualised segments comply with the anticipated behaviours from the VCPs. The threshold range has been set from 0.3e-3 to 1.0e-3 rad/m, with increments of 0.01e-3 rad/m, and the duration of the Continuity Check has been synchronised to a period of 20. Details regarding some of the DCPs and associated thresholds are presented in Table 6.6.

Table 6.6 Thresholds and related indices of DCPs

Thresholds (e-3) (rad/m)	Indices of DCP
0.42	66;171;526;571;840;871
0.43-0.44	66;171;522;571;840;872
0.45	65;172;522;574;839;876
0.46	62;172;358;418;520;574;839;876
0.47	62;172;324;418;441;575;839;876
0.48	8;33;62;174;324;575;839;876
0.49	7;33;62;174;324;575;830;876
0.50	33;62;174;324;575;830;876
0.51~0.58	33;62;175;324;576;717;737;830;876
0.59~0.66	176;318;576;717;737;768;877
0.67~0.68	176;196;577;621;642;677;738;766;877
0.67~0.74	176;196;577;604;738;766;877
0.75~0.85	577;603;739;764;878

Thresholds in bold represent the minor differences of DCPs has been neglected.

In Table 6.6, thresholds and the related DCPs marked in bold indicate that minor differences in the indices of DCPs have been neglected. This highlights a key finding: the DCPs tend to be consistent within certain threshold ranges. For instance, within the range of 0.51 to 0.58e-3 rad/m, the indices of DCPs are generally identical, with only 2 to 3 variations. Despite the VCPs not being well accepted by the algorithm, they still serve as valuable references for defining the optimal threshold. After comparing the DCPs with the VCPs, a threshold of 0.5e-3 rad/m has been identified as providing the fewest yet most accurate DCPs. The comparison between DCPs and VCPs is illustrated in Figure 6.13.

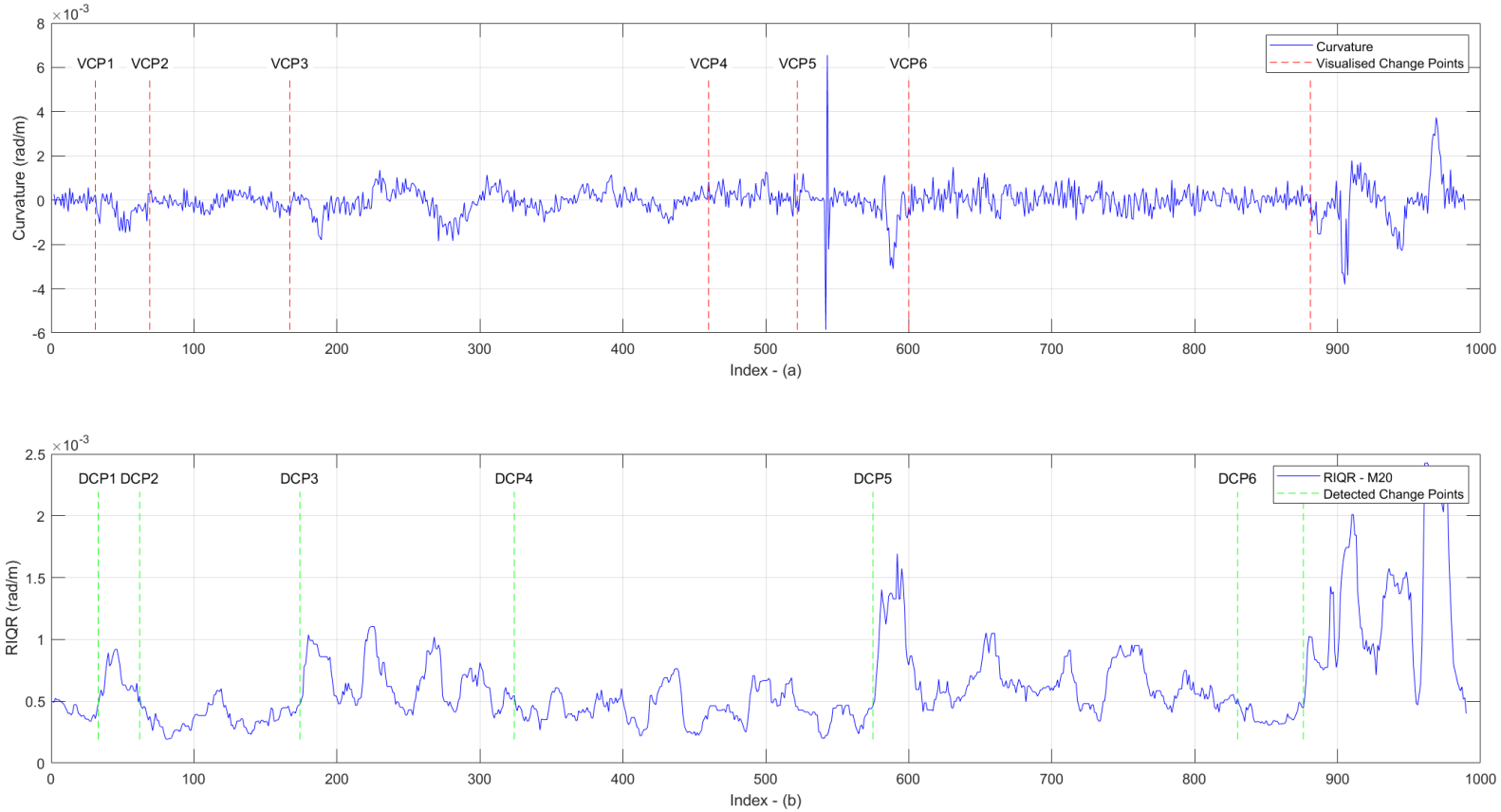

Figure 6.13 Comparison between VCPs & DCPs for Curvature

In Figure 6.13, it is observed that the DCPs effectively segment the dataset at the first three and the last positions similarly to the VCPs. However, there is a notable discrepancy for the data points between VCP3 and VCP7. The VCPs in this segment are primarily concentrated around the peak curvature values, particularly near VCP5. In contrast, the DCPs distribute the segmentation more evenly across this segment. This difference arises because the RIQR, which considers only the 25th and 75th percentiles within the rolling window, tends to neglect these peak curvature values. As previously discussed, the discrepancies between DCPs and VCPs are understandable given the challenges in defining VCPs that are not well recognised by the algorithm.

Although the DCPs are more acceptable and align with the majority binary conditions, as illustrated in Figure 6.13 (b), they remain challenging to interpret from a domain knowledge perspective. The trajectory of the sub-dataset is illustrated in Figure 6.14, where segments defined as ‘Steady State’ are marked in green, and those identified as ‘Changing’ are marked in red.

Figure 6.14 Curvature Steady State detection for the exemplary sub-dataset

The detection of steady state for Curvature is visualised in Figure 6.14. The trajectory begins at the bottom right with a short green segment indicating ‘Steady State’, before transitioning to a ‘Changing’ status as the vessel navigates northward along the waterway towards the upper left corner. However, this segmentation is challenging to justify, especially considering one lengthy red segment starting near Vlaardingen. It is understandable that the status changes to ‘Changing’ at the outset, as the vessel makes a sharp turn at a junction. Following this turn, the vessel continues for a considerable distance through the waterway with a relatively straight-line pattern yet remains classified as ‘Changing’. Subsequently, the status switches back to ‘Steady State’ within the same waterway. This indicates that the typical pattern may not serve as a reliable reference for evaluating curvature detection, as binary conditions are both detected under consistent straight-line conditions within an inland waterway.

As discussed in Section 3.3, curvature extraction evaluates the variations in a vessel’s course. The primary aim of curvature analysis is to identify segments of the trajectory that follow relatively straight-line patterns through ‘Steady State’ detection, which is closely associated with the ‘Transit’ mode in open sea areas. However, in the current case study, the course of the target vessel is confined to the winding and complex paths typical of riverine routes. Consequently, it is not suitable to rely on curvature analysis to define operational modes in this scenario. Given the performance of the SpeedLL detection, it is more effective to base the operational mode detection for the target inland tanker solely on speed analysis. The operational modes detection for the selected sub-dataset, have been illustrated in the Figure 6.15.

Figure 6.15 Operational modes detection for the exemplary sub-dataset based on SpeedLL analysis

Figure 6.15 illustrates the detected operational modes of the target vessel, with segments in green representing the 'Transit' mode, the SpeedLL are under 'Steady State' conditions, and segments in red indicating 'Manoeuvring' under 'Changing' conditions. The effectiveness of the SpeedLL analysis in segmenting the trajectory is notably high, and the results align well with domain knowledge expectations. Notably, the lengths of the red segments, which denote 'Changing' conditions, are short and precisely defined. This indicates that the algorithm can accurately identify all periods when the vessel navigates through junctions, sharp corners, and experiences significant speed variations. The remainder of the trajectory, defined as 'Steady State', suggests a consistent 'Transit' mode, affirming that, despite navigation constraints imposed by the river's shape, the vessel primarily manoeuvres only when encountering junctions, sharp turns, or other complex navigational challenges. The detailed mode detection for the target vessel will be discussed in the following section.

Although curvature analysis may not be suitable for detecting operational modes in this specific scenario, inland waterway, due to the vessel's constrained navigation paths, it still effectively highlights segments with significant curvature variations. Given that the developed algorithm is purpose-driven, it remains a valuable compensatory tool for addressing challenges associated with defining VCPs in other contexts or for different types of vessels.

6.4 Operational Mode Detection for Target Vessel

As discussed previously, the operational mode detection for the target vessel will primarily rely on SpeedLL analysis. Through 'Steady State' detection, SpeedLL will be categorised into binary groups labelled '0' for 'Steady State' and '1' for 'Changing.' Another feature considered is the ME power, intended to indicate the running status of the ME, also labelled binary as '0' for 'Stop' and '1' for 'Running.' However, in this scenario, direct onboard measurements of ME power are unavailable. Instead, the recorded power is inferred from fuel consumption, calculated using the specific engine consumption rate. Consequently, ME power cannot reliably indicate the ME's running status, as ME power is recorded regardless of whether the SOG speed is zero due to ongoing fuel consumption. Therefore, this feature has been replaced by SOG, where an SOG above 0 knots indicates the ME is running, while an SOG of 0 knots indicates a 'Stop' condition. This threshold for SOG was chosen due to the low precision of the SOG measurements, which are recorded as integers only. The correlations between these binary conditions and the two key features are detailed in Table 6.7.

Table 6.7 Correlations between binary conditions and key features

Key features	0	1
SOG	Stop	Running
SpeedLL	Steady State	Changing

Table 6.7 displays the correlations between binary conditions and two key features, resulting in a total of four possible combinations. Each combination corresponds to a specific operational mode for the target vessel. These combinations are coded from 0 to 3, following the binary-to-decimal conversion system. The specific operational modes associated with each combination code are detailed in Table 6.8. For ease of interpretation and to facilitate intuitive result checking, each mode is assigned a distinct colour.

Table 6.8 Combinations of two key features with specific colour

Combination Code	SOG	SpeedLL	Mode	Colour
0	0	0	Stop	Black
1	0	1		Blue
2	1	0	Transit	Green
3	1	1	Manoeuvring	Red

The combination code ‘0’ represents the ‘Stop’ mode of the target vessel. Under this condition, the SOG speed is 0 knots, indicating that the ME is stopped, and the SpeedLL is categorised as ‘Steady State.’ Theoretically, since the vessel is solely propelled by the ME, the SpeedLL should consistently register as zero when the ME is not operating.

Combination code ‘1’ would typically not exist because the SOG and SpeedLL both measure similar aspects of the vessel’s movement, and significant discrepancies between these measures are unlikely. Data points categorised under this combination will be further checked in the next section.

Combination code ‘2’ represents the ‘Transit’ mode, where data points indicate that the ME is operational, and the vessel is maintaining a ‘Steady State’ speed. This scenario typically signifies that the vessel is navigating smoothly and steadily within the inland waterway, reflecting stable operational conditions.

Combination code ‘3’ characterises periods when the vessel is manoeuvring within the waterway. During these instances, the ME is active, but there are significant speed variations. This indicates that the vessel is engaging in operations such as turning, docking, or navigating through tight or complex sections of the waterway.

It's important to note that all change points, including those for SOG, SpeedLL, and the final combination codes, must undergo a Continuity Check. This check ensures that the status of a change point remains consistent with the preceding data points over a length of 20, which corresponds to the parameters set in the sensitivity analysis of the rolling combination. Only change points that meet this consistency criterion are accepted; others are disregarded. The defined thresholds for SpeedLL and the protocols established by the developed algorithm are applied uniformly across all datasets. Detailed results and further discussions of the algorithm will be presented in the subsequent section.

6.5 Results and Discussion

The developed algorithm has been applied across all datasets, and the distribution of the operational modes identified by this analysis is illustrated in Figure 6.16.

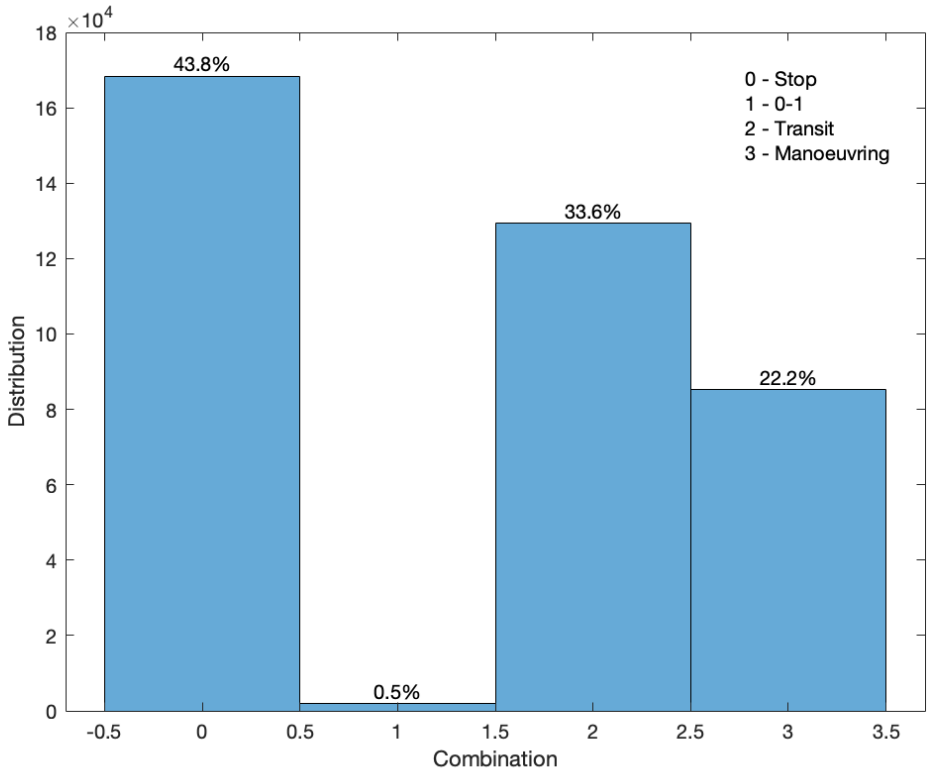

Figure 6.16 Distribution of operational modes across all the dataset

In Figure 6.16, the distribution of operational modes over a 10-month period shows that the vessel spends most of its time in 'Stop' mode, accounting for 43.8% of the data points. 'Transit' mode represents 33.6% of the data, while 22.2% of the points are defined as 'Manoeuvring'. Notably, when considering the periods when the vessel is sailing, the proportion of data points

classified as ‘Manoeuvring’ is relatively high. In comparison, as analysed in Chapter 4, the target ocean-going vessel has less than 10% of its data points defined as ‘Manoeuvring’. This difference is expected and aligns with the operational characteristics of the target inland tanker, which frequently manoeuvres through complex inland waterways.

Additionally, combination ‘1’, which corresponds to the binary status ‘0-1’, indicating that the SOG is 0 knots (the ME is stopped) while SpeedLL shows significant variations, was detected, comprising 0.5% of the data points. Although this percentage is relatively small and might seem negligible, it still suggests an anomaly since it is unlikely for the SpeedLL to vary significantly when the ME is stopped and the SOG is zero. The results for each combination will be thoroughly checked and analysed, starting specifically with combination ‘1’ to address and understand this apparent discrepancy.

6.5.1 Checking the detection of combination ‘1’

To further investigate Combination ‘1’, Figure 6.19 (a), (b), and (c) present illustrations of three continuous dataset segments where this combination occurs. These visuals are critical for understanding the specific conditions under which the anomaly of ‘0-1’ is recorded. Analysing these segments will help determine if these instances are due to data errors, sensor inaccuracies, or if they reveal a plausible scenario not initially considered in the model.

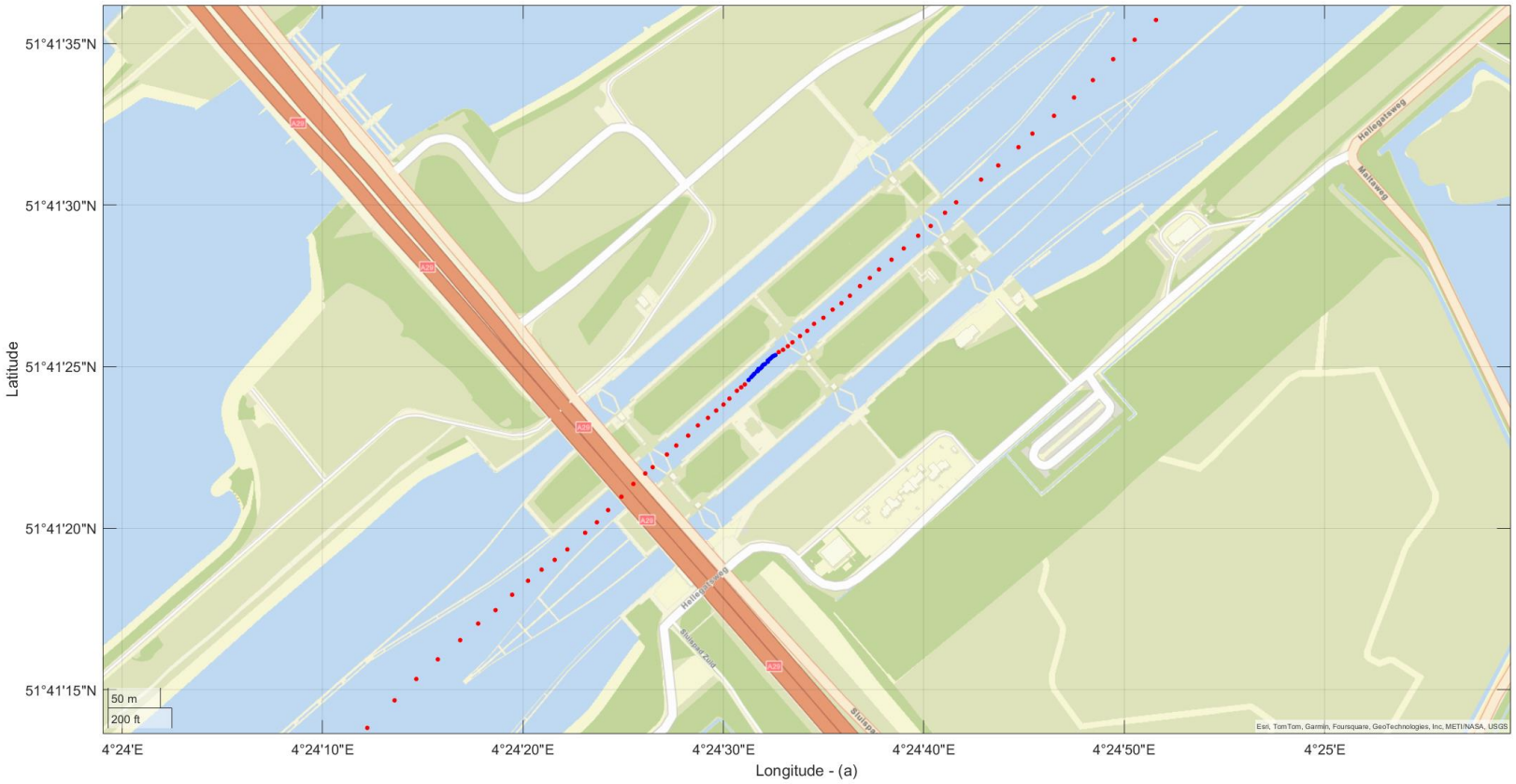

Figure 6.17 (a) Trajectories of continuous datasets encompassing combination '1'

Figure 6.18 (b) Trajectories of continuous datasets encompassing combination '1'

Figure 6.19 (c) Trajectories of continuous datasets encompassing combination '1'

As illustrated in Figure 6.17 (a), the data points in blue, representing combination ‘1’, occur while the target vessel is passing through a lock. Upon closer inspection, during this period, the SpeedLL varies, bouncing from 0.4 to 0 and then back to 0.6 knots over 24 data points. This indicates that the vessel might be adrift slightly within the lock chamber for a duration of 6 minutes. Although the SOG is used to indicate the running status of the ME, and is recorded as integers only, potentially leading to inaccuracies in reflecting the ME’s actual status. It is important to note that according to boating safety guidelines, such as those outlined in ‘EN Passing through Bridges and Locks Safely and Quickly’ (SAFEBOATING.EU), mandate that vessels must be moored and have their engines switched off during lock passage. Considering the brief duration of this segment, the behaviour observed does not necessitate a detailed correction, and thus, this detection has been accepted.

Upon reviewing the detailed data points in blue, as illustrated in Figures 6.15 (b) & (c), these segments can be identified as transition periods between the ‘Stop’ and ‘Manoeuvring’ modes. During these periods, most of the SOG readings are not at 0 knots, yet the ME status is defined as ‘Stop’. This categorisation occurs because the status of the preceding data point is ‘0’ under the ‘Stop’ mode, and although the initial point of the blue segment indicates a status change to ‘1’ (reflecting ‘Manoeuvring’), this change point fails the Continuity Check. It is disrupted by intermittent readings of zero knots within these segments, leading to their exclusion and subsequent classification according to the prior status as ‘0’.

The algorithm, adhering to the principles of the Continuity Check, assumes continuity of the previous mode unless a change can be sustained for 5 minutes, represented by 20 consecutive data points. Meanwhile, the status of SpeedLL is identified as ‘Changing’, indicating that the transition in SpeedLL occurs earlier than the change in ME status but not simultaneously. This asynchronous change is the reason why the combination ‘1’ is detected in these instances.

Given that the durations of these blue segments are 9.5 and 10minutes respectively, they are short enough to validate this detection approach, treating them as transition periods between the two operational modes.

The detailed analysis of the data points under Combination ‘1’ reveals that these instances do not represent meaningful operational changes. Considering that such data points constitute only 0.5% of the total dataset, this percentage is relatively small, making it reasonable to accept this anomaly within the broader context of the data analysis.

6.5.2 Performance of 'Transit' detection

To effectively assess the performance of the 'Transit' mode detection, combination '2', it is advantageous to analyse it in conjunction with the 'Manoeuvring' mode rather than examining each mode separately. On one hand, maintaining the continuity of the dataset is crucial for the algorithm's effectiveness, and analysing these modes together allows for a more efficient observation of the distinctions between these two combinations. On the other hand, given that the target vessel is an inland tanker operating in a complex environment, its operational modes are likely to switch more frequently compared to other types of vessels sailing in open sea area. It is challenging to identify extended continuous datasets defined solely as 'Transit.' Therefore, the focus for assessing performance will be on long-duration continuous datasets where the vessel is actively sailing. These segments will be distinctly illustrated in specific colours representing different modes, facilitating a clearer evaluation of how effectively the algorithm distinguishes between 'Transit' and 'Manoeuvring' modes.

Figure 6.20 illustrates the trajectory of a dataset consisting of 2,013 data points, which covers a duration of 503.25 minutes, or just over 8 hours, with each data point recorded at 15 second intervals. The trajectory initiates from the middle bottom of the figure, with the vessel primarily navigating from south to north. Notably, five red segments have been identified and labelled starting from the beginning of the trajectory.

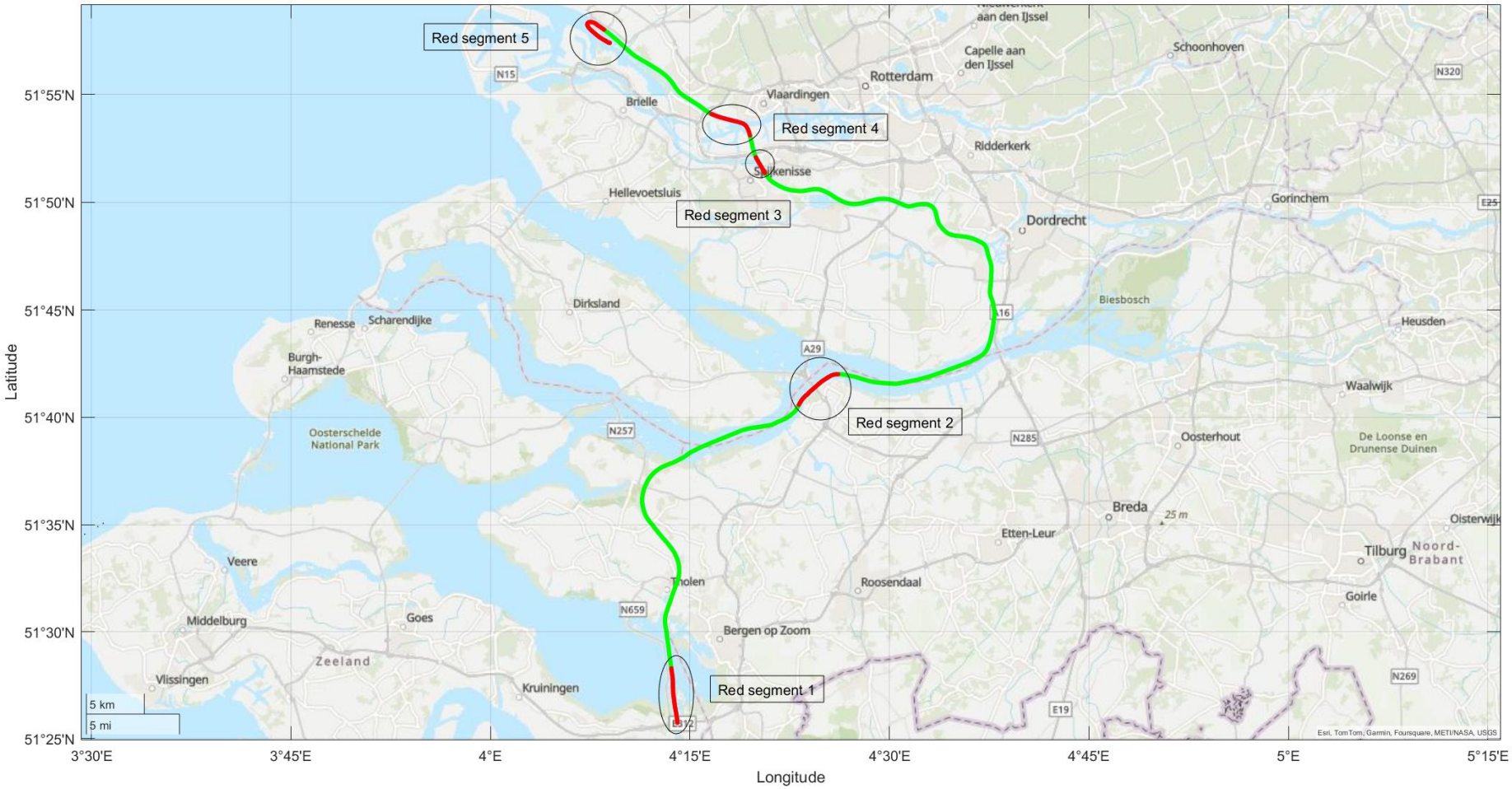

Figure 6.20 Trajectory of selected dataset for ‘Transit’ performance checking analysis

Although curvature analysis is not used to define operational modes, it is interesting to note that the first and second red segments, identified as ‘Manoeuvring’, follow straight-line trajectories. Upon closer inspection, these segments correspond to the vessel passing through two locks, which justifiably categorises them as ‘Manoeuvring.’ Additionally, within these two segments, two ‘Stop’ modes have been detected, lasting approximately 14 and 13 minutes respectively. These ‘Stop’ modes are not visible in the figure, due to the duplication of coordinates. This can be interpreted as the black dots (representing ‘Stop’ mode) being obscured by overlapping red dots (representing ‘Manoeuvring’ mode), since the vessel was stationary, secured by ropes in the lock chambers.

Observations confirm that the detections of the last three red segments are reasonable, particularly notable is the final segment where the vessel executes a 180-degree turn, clearly justifying its categorisation as ‘Manoeuvring.’ The third and fourth segments correspond to periods when the vessel passes through two separate junctions. However, it’s important to note that not all sharp corners or junctions are detected as ‘Manoeuvring’, exemplified by the long green segment between the second and third red segments. Additionally, the short green segment between the third and fourth red ones needs closer examination to determine why these were not categorised as ‘Manoeuvring.’ Figure 6.21 illustrates the SpeedLL and its RIQR with DCPs marked by green vertical dots, providing further detail on these segments.

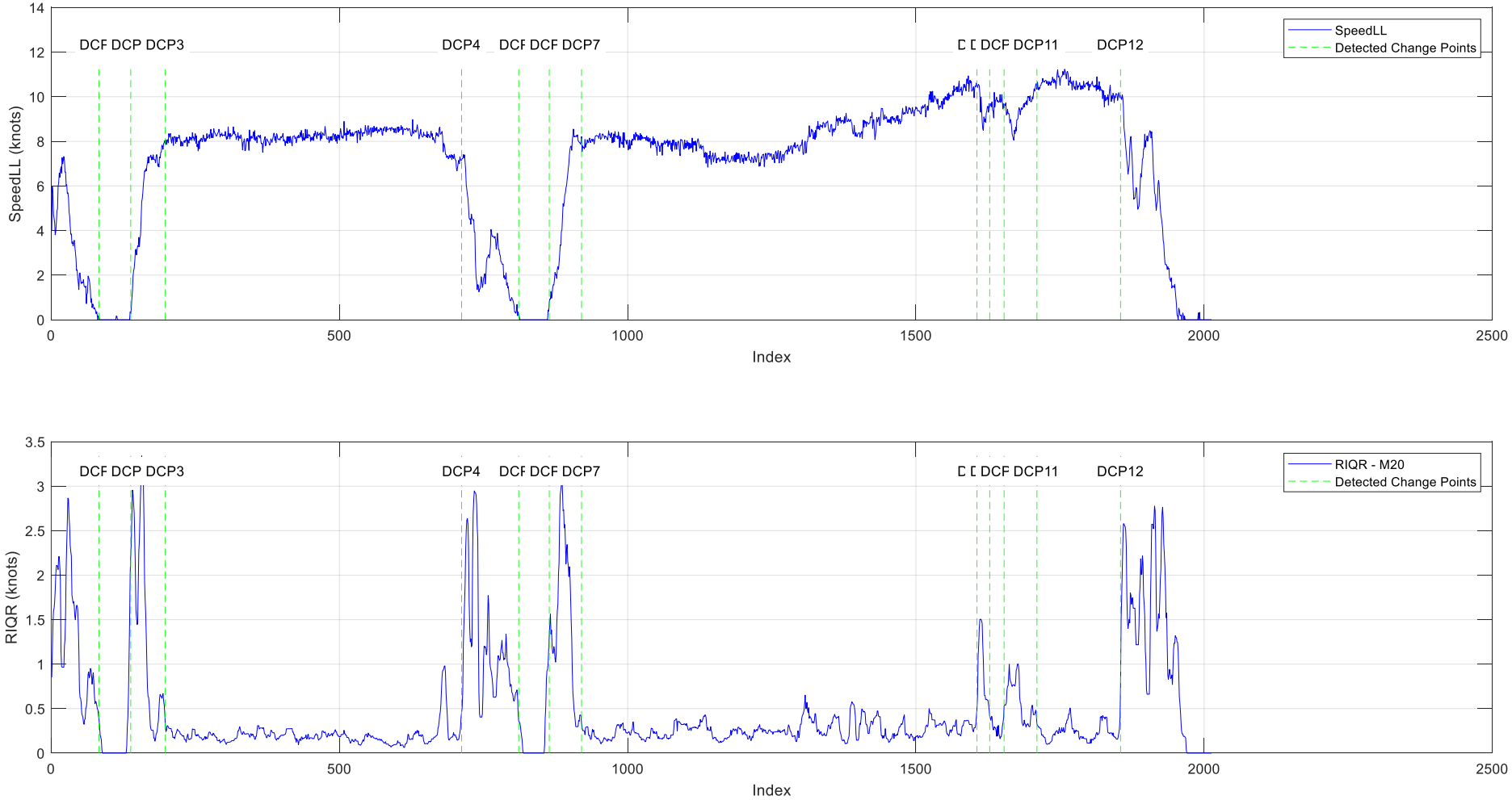

Figure 6.21 SpeedLL and RIQR with DCPs in vertical green dotted lines

In Figure 6.19, it is evident that the developed algorithm effectively distinguishes the 'Steady State' conditions for SpeedLL. From the beginning of the dataset up to DCP3, and between DCP4 and DCP7, lie the first and second red segments. Notably, the segments between DCP1 & DCP2, and DCP5 & DCP6 represent detected 'Stop' modes. These are covered by red dots, indicating that during these periods, the vessel was moored in the lock chambers.

The focused long green segment between DCP7 and DCP8, located near Dordrecht, shows a slight increase in SpeedLL from approximately 8 to 10 knots. Additionally, the RIQR in the latter half of this segment is higher than in the first half, indicating increased speed variation. Reference to the related trajectory in Figure 6.20 reveals that the vessel was navigating through complex winding waterways during this segment. Furthermore, as illustrated in Figure 6.19 (b), it is evident that some RIQR values in the latter part of the segment exceed the defined threshold of 0.42 knots. However, these change points do not persist long enough to be recognised as a mode change. While it is not certain that the complex shape of the river directly correlates with speed variation, this observation suggests that the detection based on SpeedLL is robust and aligns well with the strategy of omitting curvature analysis.

Another noteworthy green segment, located between DCP9 and DCP10 and situated among the third and fourth red segments, is highlighted. Observations from Figure 6.19 (a) place this segment amidst significant speed variations, which might typically suggest a 'Manoeuvring' classification during the selection of VCPs. However, a closer examination of Figure 6.19 (b) shows that the RIQR for this segment remains below the predefined threshold and successfully passes the Continuity Check, lasting for a duration of 6 minutes. Despite the substantial speed variations, the data underpinning this segment do not support a 'Manoeuvring' status, indicating the robustness and accuracy of the threshold settings in distinguishing between operational modes.

The detailed discussion of the selected dataset demonstrates that the developed algorithm effectively distinguishes between the 'Transit' and 'Manoeuvring' modes, even in complex navigation areas. This analysis of performance has also been applied to other long continuous datasets, consistently providing reasonable detections. To further substantiate these findings, eight additional examples are selected from the top continuous datasets when the vessel is actively sailing. The trajectories of these datasets are provided in Appendix C. These examples

indicate the algorithm's robustness across a variety of operational scenarios, further validating its effectiveness.

A discovery emerges from reviewing the example datasets is that six of the eight trajectories, specifically shown in Appendices C1, C2, C3, C6, C7 and C8, follow similar navigation routes. This pattern suggests that, although these represent different voyages, the navigation routes traversed by the vessel are comparable.

Comparative analysis of the six datasets where trajectories follow similar navigation routes reveals consistent detection patterns. Specifically, all periods during which the vessel passes through locks are correctly identified as 'Manoeuvring'. Additionally, the 'Stop' mode is consistently detected during the lock process.

However, an unusual segment has been identified and is notably marked as 'Manoeuvring', a distinction that sets it apart from other voyage trajectories through the same area, which are typically classified as 'Transit'. This anomaly is particularly striking because, unlike other instances where the vessel navigates through this region under 'Transit' conditions, this specific segment involves 'Manoeuvring' detection even though the vessel maintains a relatively straight-line pattern. This segment's distinct characteristics have been highlighted as an 'Unusual segment' in Figure 6.22.

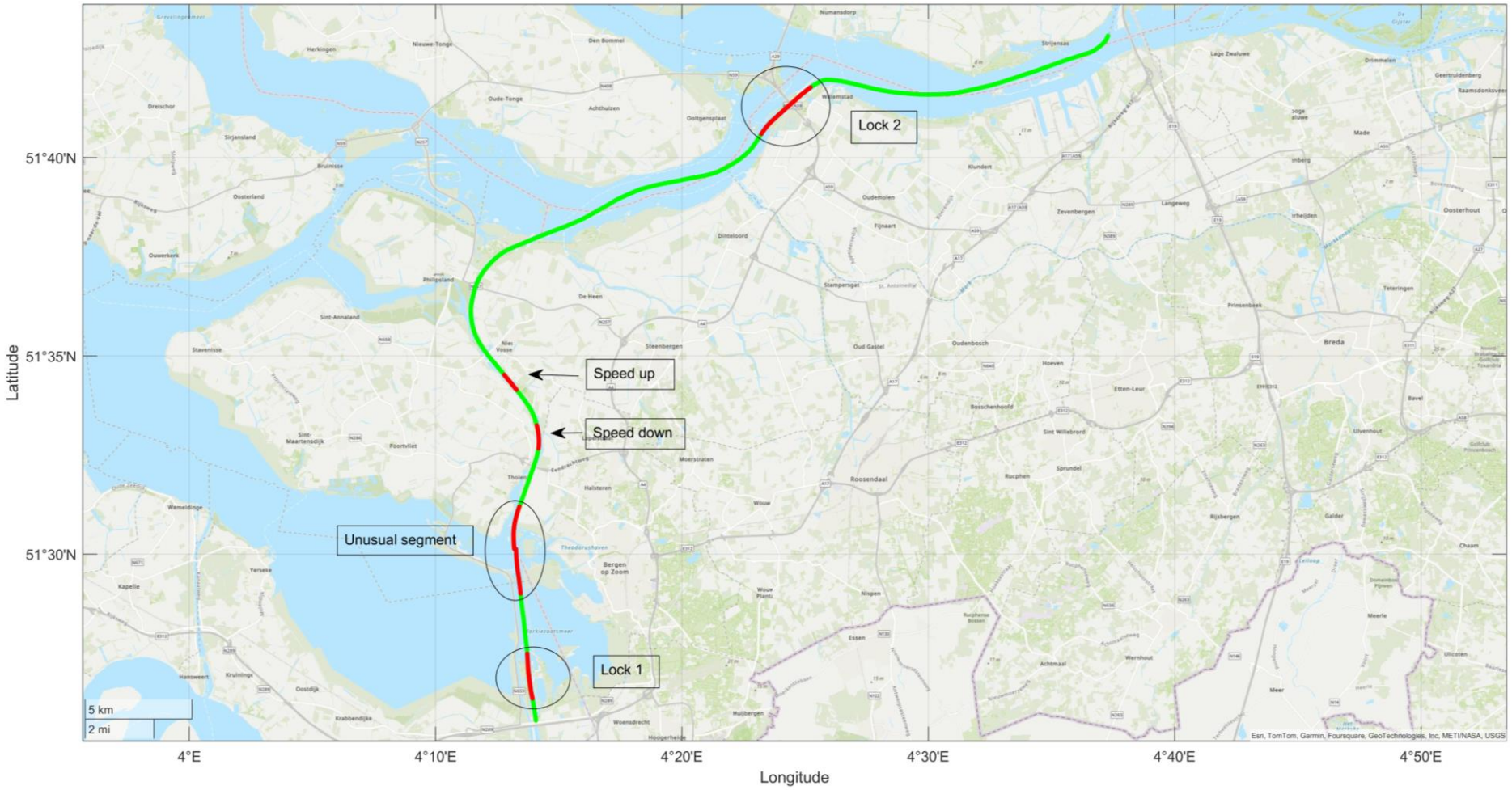

Figure 6.22 Trajectory of dataset with unusual segment

The trajectory of this continuous dataset consists of 1,288 data points, covering a duration of more than 5 hours as the vessel navigates roughly from south to north. Five red segments have been identified along this trajectory. Two of these segments correspond to the vessel passing through locks, labelled as ‘Lock 1’ and ‘Lock 2’. Additionally, two shorter segments are noted where the vessel adjusts its speed: slowing down from around 7 to 5 knots, labelled as ‘Speed down’, and subsequently speeding back up to 7 knots, as ‘Speed up’. The most notable is the ‘Unusual segment’, which is the longest red one, spanning nearly half an hour with 144 data points. The detailed trajectory of this segment is magnified and displayed in Figure 6.23, providing a closer look at this anomalous behaviour.

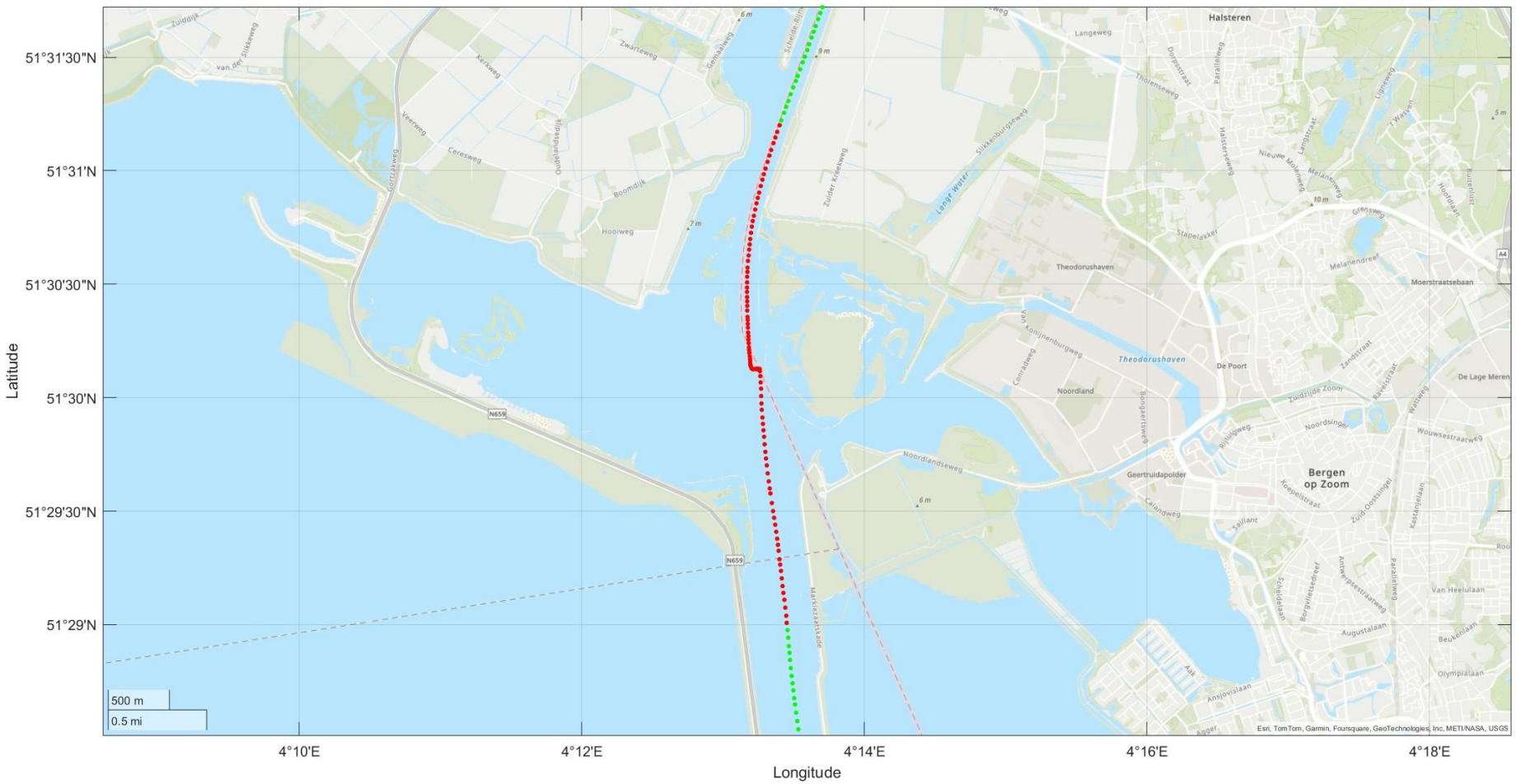

Figure 6.23 Trajectory of the unusual segment

In this ‘Unusual segment,’ a sudden course change is evident midway, accompanied by a sharp decrease in speed from around 7 knots to zero in less than one minute. Over the next 6 minutes, the vessel completes this course adjustment while maintaining a very low speed, less than 0.5 knots, before gradually accelerating back to normal conditions. This abrupt change in direction and speed is the primary reason for the ‘Manoeuvring’ detection in this segment. Such a significant deviation from the usual navigational pattern highlights the algorithm’s sensitivity to dynamic changes in vessel behaviour, accurately reflecting the operational demands during complex manoeuvres.

6.5.3 Performance of ‘Manoeuvring’ detection

To effectively evaluate the performance of the ‘Manoeuvring’ detection, the special attention is given to periods when the vessel engages in operations within harbours, which involve complex manoeuvres and are critical for assessing the algorithm’s responsiveness to dynamic operational contexts. Figure 6.24 illustrates a trajectory that records the intricate operations undertaken within the port of Antwerp, providing a detailed example of how the vessel manoeuvres in such a challenging environment.

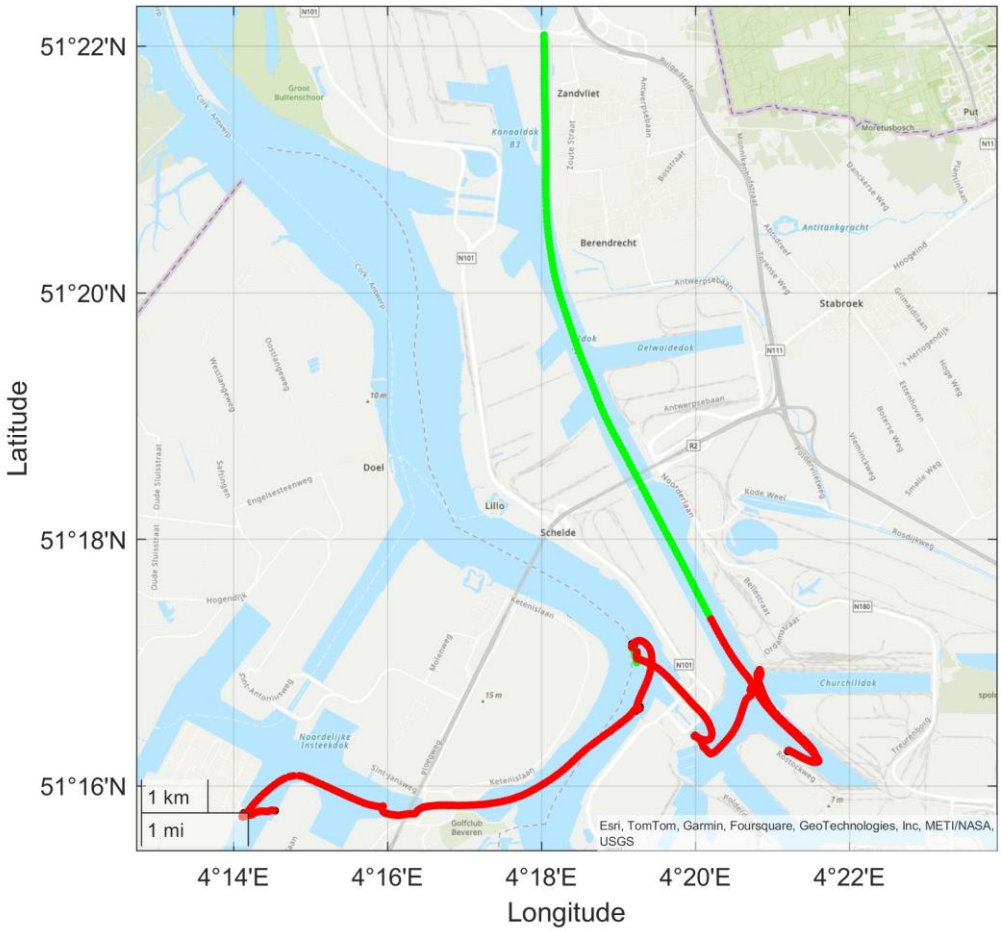

Figure 6.24 Trajectory of the vessel operating at the port of Antwerp

To comprehensively analyse a complete operation within the harbour, nine consecutive sub-datasets have been amalgamated, disregarding 10 breakpoints. This amalgamation effectively means that there are only one or two missing timestamps between each consecutive dataset, totalling less than 30 seconds of missing data. As illustrated in Figure 6.24, the trajectory originates from the left bottom corner and comprises 8,584 coordinates, covering a span of nearly 36 hours. Notably, 87.7% of these data points are detected as 'Stop', indicating that the vessel was stationary at the port for approximately 31.5 hours. After completing operations at the port, the vessel proceeds to sail in the north direction. For a more detailed analysis, Figure 6.25 provides a magnified view of the vessel's trajectory while operating within the port.

Figure 6.25 Magnified trajectory of the vessel operated at the port of Antwerp

During this port operation, 11 instances of ‘Stop’ mode have been detected, the vessel underwent transitions across six different docks and navigated through two locks within the port. Given these intricate movements, this combined dataset serves as an excellent example to evaluate the performance of the ‘Manoeuvring’ detection. Such a dataset, with its complex operational dynamics, challenges the algorithm to accurately identify and classify the distinct modes of operation.

In the trajectory illustrated in Figure 6.23, it is evident that the algorithm effectively identifies the ‘Manoeuvring’ mode, with nearly the entire trajectory marked in red to indicate active manoeuvring. The only exceptions are two short green segments located in the middle of the figure, just before the vessel approaches the second lock. These green segments represent periods where the vessel is adjusting its position and preparing to navigate through the lock. For a closer examination of these key transitional periods, the magnified trajectory of these two segments is provided in Figure 6.24.

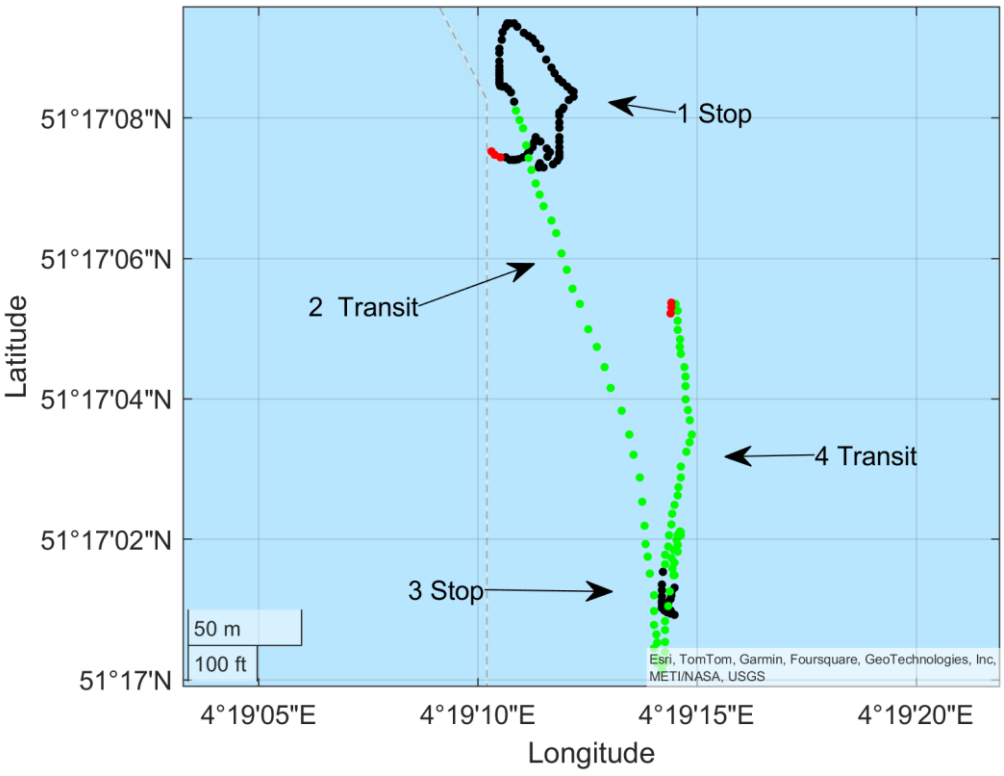

Figure 6.26 Trajectory of two green segments

In Figure 6.24, the operational modes detected during the vessel’s preparation period are sequentially labelled. Initially, a ‘Stop’ mode is detected, followed by a transition to ‘Transit’

before entering another ‘Stop’ area, then resuming ‘Transit’, and finally, the vessel manoeuvres into the second lock. This pattern reveals that the two green segments, indicating ‘Transit’, are interspersed with two short and closely positioned ‘Stop’ modes. Detailed visualisations of SpeedLL, the corresponding RIQR with DCPs, the ME running status, and the threshold settings are provided in Figure 6.27.

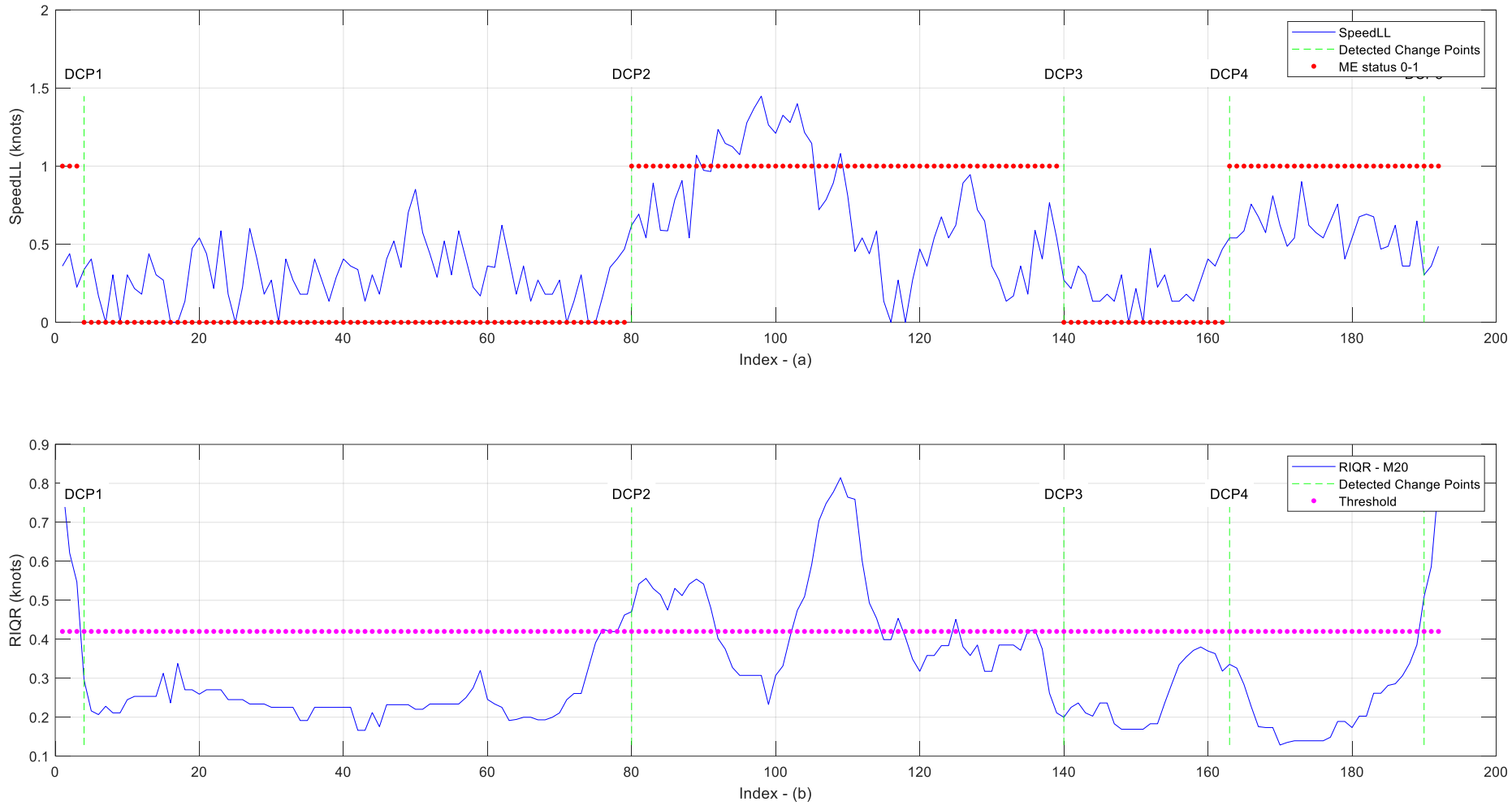

Figure 6.27 SpeedLL and related RIQR for the magnified trajectory dataset

In Figure 6.25 (a), the operational status of the ME is indicated with red dots, where '0' signifies a stop and '1' indicates running. The thresholds are marked with magenta dots in Figure 6.25 (b). During the first green segment, between DCP2 and DCP3, there is a noticeable fluctuation in SpeedLL, where speed increases from 0 to nearly 1.5 knots, then drops back to zero before bouncing up to around 1 knot. Although some of the corresponding RIQR values exceed the threshold during this period, they do not satisfy the Continuity Check, preventing them from being recognised as a change in operational mode. For the second green segment, between DCP4 and DCP5, the SpeedLL remains below 1 knot with no significant variation, indicating a more stable speed during this interval.

An overview of this dataset, specifically between DCP1 and DCP5, reveals that the SpeedLL is consistently detected as 'Steady State', indicating no significant speed variation throughout this interval. The primary reason for mode changes during this period is related to the altered running status of the ME. This can be attributed to the two 'Stop' modes being closely spaced, with only 15 minutes between them, suggesting that no extensive manoeuvring was necessary for the short-term objectives. The average SpeedLL during the two green segments is relatively low, at 0.73 and 0.60 knots respectively. Additionally, while the vessel is under adrift conditions and detected in 'Stop' modes, it exhibits minor speed variations similar to those observed in the preceding green segments. Consequently, the algorithm categorises the SpeedLL as 'Steady State' throughout this entire process, recognising the minimal speed fluctuations as consistent with a stationary or very slowly moving vessel.

However, these two green segments cannot be classified as 'Transit' due to their failure to represent the normal navigation conditions of the vessel. Furthermore, the average SpeedLL in these segments is less than 1 knot, a speed too low to qualify as 'Transit' mode. Despite the relatively low speed, the presence of 87 data points across these segments substantiates the effectiveness of the algorithm in detecting 'Manoeuvring' mode. This evidence confirms that the algorithm performs well in differentiating between operational modes.

The primary focus of this case study is to evaluate the performance of the algorithm within an inland waterway context. Given the specific characteristics of inland waterways, the operational mode detection strategy has been adapted to primarily analyse two key features - ME status and SpeedLL- instead of including curvature. This adjusted strategy has been successfully tested on the selected dataset, demonstrating its effectiveness.

Additionally, a sensitivity analysis on the selected dataset helped define the optimal rolling window combination and threshold for distinguishing binary conditions for SpeedLL. These key parameters were then applied to ten months of onboard measurements to detect ‘Stop’, ‘Transit’, and ‘Manoeuvring’ modes for the target vessel. The results confirm that the developed algorithm effectively identifies the operational modes, proving its suitability for use in inland waterway scenarios.

6.6 Summary

In this chapter, the operational modes detection algorithm was applied to an inland waterway tanker, thereby extending its validation to a complex and varied navigation area. This case study demonstrated the algorithm's adaptability and effectiveness in accurately detecting operational modes under the unique constraints of inland waterways, which are characterised by restricted navigation routes, locks, and junctions. 'Transit', 'Manoeuvring', and 'Stop' modes were defined for the inland tanker, with the detection focusing solely on the influence of SpeedLL and omitting 'Steady State' detection of Curvature due to the constraints posed by inland waterway navigation. The results from this case study affirmed the algorithm's capacity to effectively manage the dynamic and complicated conditions of inland waterways. It highlighted the versatility of the developed methodology, illustrating its applicability from open seas to inland waterways, thereby encompassing a broad range of navigational environments.

Chapter 7 Conclusion

7.1 Conclusion

In this research, a data-driven methodology for detecting operational modes in various types of vessels, based on binary categorisation, has been developed. The cornerstone of this methodology is its adaptability, as highlighted in the Literature Review chapter. To achieve this primary objective of high adaptability across different vessel types, the methodology must meet a number of requirements encompassing both external and internal factors.

For the external requirements, the algorithm must utilise a minimum of input parameters, which are already available for most vessels; these constitute the first two criteria of the methodology.

The input variables include the time series coordinates and the running status of the ME. Two key features, SpeedLL and Curvature, have been extracted from these coordinates. SpeedLL represents the operational status of the machinery, while Curvature effectively shows the patterns of the trajectory. A steady state detection algorithm has been developed to classify these features into binary conditions. Consequently, the operational status of the machinery is categorised into either a steady state or changing condition, and the trajectory patterns are identified as either steady state (approximately a straight line) or changing. Furthermore, the running status of the ME is also binary – either stopped or running. Through the binary categorisation of these three parameters, the operational modes can be detected based on the inherent characteristics of the machinery condition and trajectory patterns under different modes. In essence, the developed methodology primarily relies on the analysis of temporal and spatial information of the vessel, which does not require any additional, costly or special onboard measurements. The running status of the ME can be indicated by various parameters such as ME power, ME fuel consumption, percentage of MCR, SOG, or other available representative measurements.

The last criterion is adaptability of the developed algorithm to various types of vessels, which primarily addresses the internal requirements.

This methodology does not make assumptions regarding data distribution or the operational environment; instead, it employs visualisation techniques. By selecting exemplary sub-

datasets, the visualised change points (VCP)s has been identified, which serves as both references and objectives for conducting sensitivity analysis on the parameters. This approach is developed in detailed observations of exemplary datasets rather than on any assumptions, enhancing both reliability and robustness.

Moreover, the objective function has been developed to determine the key parameters of the algorithm. This analysis not only enhances mode detection performance, but also improves adaptability to different vessels, thereby addressing the challenge of defining key parameters for specific vessels. In table 7.1, a summary of defined key parameters are listed for various vessel types.

Table 7.1 Summary of defined key parameters for each type of vessels in three case studies

Case Study	Vessel Types	Time Interval	Window Combination	Duration of mode change
1	Ocean-going car carrier	6 minutes	E6	36 minutes
2	Tuna purse seiner	1 sec to 15 sec	M37	9.25 minutes
3	Inland waterway tanker	4 sec to 15 sec	M20	5 minutes

In Table 7.1, the differences in the defined key parameters are listed, which include the time intervals and specified rolling window combinations. According to the related time intervals, the durations of mode changes—calculated by multiplying the window size by the time intervals—are shown as 36, 9.25, and 5 minutes for the corresponding target vessels. This duration closely correlates with the manoeuvrability of different vessel types. An important aspect of the methodology, the Continuity Check, posits that a vessel cannot change its operational mode instantly; rather, a brief period is necessary to complete the transition. This brief period can, to some extent, reflect its manoeuvrability. From this table, it is evident that the defined duration of mode change aligns with domain knowledge, suggesting that it would take approximately half an hour, 10 minutes, and 5 minutes for the target ocean-going, fishing, and inland waterway vessels, particularly, to transition to their normal operational conditions. This way of considering a vessel's manoeuvrability can serve as a valuable reference for defining the key parameters of this methodology.

The crucial analysis involves steady state detection of the two extracted key features, utilising the rolling window technique to examine data point variability. One of the critical defining parameters is the construction of the rolling window, which includes the window size, the position of the target point within the window, and methods for evaluating data variability. Through sensitivity analysis, based on the developed objective function, the most effective window combination can be determined, the one that validated the VCPs and provides the maximum value for the defined objective function.

Another key parameter is the threshold for data variability used to define a steady state. Data variability, calculated based on the defined rolling window configuration, is assessed using a threshold selected on the principle of validating the VCPs.

Variability of each data point is crucial in distinguishing a steady state. To enhance detection accuracy, a data cleaning strategy has been implemented to eliminate measurement errors and outliers. After removing duplicated and missing values from the raw dataset, the 1.5 IQR technique has been applied to the discrepancies between the SOG and SpeedLL. Subsequent data aggregation and Continuity Checks, tailored to the sampling rate of the specific scenario, have transformed the raw dataset into several continuous sub-datasets that serve as the final inputs to the algorithm. This strategy, employing SOG as a reference, not only filters outliers more accurately but also enhances overall computational efficiency.

The developed methodology exhibits high computational efficiency; the key parameters of the algorithm are determined through a single analysis of the exemplary sub-dataset. Subsequent processes involve calculating the variability for each data point, using the defined rolling window, and the threshold to detect steady states.

A critical aspect of this methodology is the identification of VCPs within the exemplary sub-dataset. This leads to another significant contribution: developing an efficient method for result validation through geographic representation. Unlike traditional validation methods which are time-intensive and typically involve comparing data-driven results with expert interpretations – as seen in the comparison with the crew-pressed mode (Zaman et al., 2017b) or with one month of labelled data based on operational mode definitions (Swider et al., 2018) - geographic representation offers a more time-efficient alternative. In this approach, coordinates corresponding to each detected mode are assigned specific colours, and the trajectory of the continuous sub-dataset is segmented into coloured sections. These coloured

segments are then assessed to determine if they can be logically explained by domain knowledge, such as verifying that segments detected as 'Transit' follow a relatively straight-line pattern. This is also serves as a key criterion for defining the VCPs. Furthermore, the selection of the exemplary sub-dataset is essential for the algorithm's functionality. The detailed selection and identification of VCPs have been thoroughly discussed in three case studies, primarily based on a deep understanding of the characteristics of the data points in specific scenario. This method can be described as a hybrid approach, combining knowledge-based and statistical methods to detect operational modes.

To enhance the algorithm's adaptability, the construction of the methodology remains flexible. The selection of the three key parameters can be adjusted to accommodate different vessel types or to meet specific research objectives, such as in the third case study, which focuses solely on the analysis of SpeedLL and ME status for an inland tanker, omitting the steady-state detection of Curvature.

The methodology demonstrated high performance in mode detection across all three case studies. For the ocean-going car carrier, 4 operational modes were detected, including Transit, Manoeuvring and Stop modes, with an additional mode identified as Preparing for Proceeding to the dock. In the second case study, the 'Transit' mode was detected based on the research interest, the result provides robust evidence of the algorithm's high performance in mode detection. In the third case study, three common operational modes were detected for the inland tanker, with all the detection corroborated by domain knowledge.

Beyond the selection of exemplary sub-dataset and identification of VCPs, which have been extensively discussed in the case studies, adjustments to the methodology's structure to adapt different vessel: identification of key features for binary categorisation; addressing low precision issues, such as two decimal places in the coordinates of the first case study; and varying sampling rates were also explored. These discussions provide valuable insights and experience for applying this methodology in other specific cases.

7.2 Contribution

- Minimum input variables

The temporal and spatial information from coordinates has been leveraged to detect operational modes, thus avoiding the need for additional, costly onboard measurements.

- No assumptions and sensitivity analysis in defining key parameters

The developed methodology integrates a hybrid approach, combining knowledge-based and statistical methods. A visualisation technique informed by domain knowledge is utilised to guide the determination of key parameters for the algorithm. This approach addresses key limitations inherent in purely statistical methods while retaining the benefit of high computational efficiency.

- Efficient method for result validation

Geographic representation offers an effective method for validating detected results. By observing trajectories with colour-coded segments, it becomes straightforward to assess whether the results can be comprehensively explained domain knowledge.

- Segmented results

The detected results are presented as segments with continuous time stamps, rather than as disjointed data points. This segmentation is crucial for applying geographic representation, which employs multi-coloured segments to illustrate the trajectory. As noted by Arasteh et al. (2020), segment-based classification models have greater applicability in real-world scenarios. These detected segments lay the groundwork for developing segment-based models in further research, which could also be seen as applying temporal and spatial information within machine learning frameworks. This aspect will also form part of future work.

7.3 Future Work

- Detection of transient mode

The algorithm has already detected some of the transient modes in all three case studies, a result of implementing the Continuity Check. This check is based on the premise that vessels cannot instantly transition between operational modes; they require a brief transient period, closely linked to the vessel's manoeuvrability. Detected change points must pass the Continuity Check; those that do not align with subsequent data points within the defined window size are disregarded. Consequently, transient modes are typically identified as the end of the

proceeding operational modes. Future work will focus on refining the Continuity Check to distinguish transient modes.

A potential method for detecting transient modes involves identifying the starting and ending change points for each detected operational mode. Data points within the size of the rolling window preceding the end change points would be defined as transient mode. Since the window size represents the brief period required for the target vessel to complete the mode change, the final data points within this window are considered transient. This approach should be further explored in future work.

- Automatic parameter updating algorithm

The defining of the key parameters, such as the combination of rolling window and the thresholds to distinguish steady state is through the analysis of the exemplary sub-dataset. However, there are limitations in the developed algorithm, notably the manual selection of the exemplary sub-dataset and VCPs. Furthermore, these parameters would be time-sensitive along and will evolve with the ongoing operation of the target vessel. This future development will transform the current methodology into an online algorithm that can be applied across a broad fleet, enhancing its utility. Automatically updating these parameters in response to forthcoming measurements will significantly improve the system's adaptability and effectiveness over time.

The primary challenge of the methodology is to devise a means of detecting 'Steady State' and 'Changing' conditions mathematically. This involves using variations (RSD & RIQR), in a mathematical way, to accomplish detection, which have previously been recognised through observational techniques. Therefore, to achieve a fully automated operation, developing a mathematical method for detecting VCPs remains a key challenge. Initially, the focus should be on defining an appropriate schedule to update the VCPs and related thresholds, which can be informed by significant variations in vessel performance. Events such as the dry-docking process could trigger updates to the key parameters. However, given that the typical dry dock cycle spans five years, relying solely on this schedule is impractical. Alternative approaches for defining the updating schedule will be further explored, drawing on domain knowledge. For instance, the Planned Maintenance System (PMS) could be referenced for each target vessel to determine more frequent and relevant updates.

References

A/S, M. B. W. D. 2004. Instruction Book 'Operation' for 50-108MC/MC-C Engines.second ed., Copenhagen,DK.

ABBASI HOSEINI, A. & STEEN, S. 2017. Multivariate Time Series Data Mining in Ship Monitoring Database. *Journal of Offshore Mechanics and Arctic Engineering,* 139.

AIELLO, G., GIALLANZA, A. & MASCARELLA, G. 2020. Towards Shipping 4.0. A preliminary gap analysis. *Procedia Manufacturing,* 42**,** 24-29.

AMINIKHANGHAHI, S. & COOK, D. J. 2017. A survey of methods for time series change point detection. *Knowledge and information systems,* 51**,** 339-367.

ARASTEH, S., TAYEBI, M. A., ZOHREVAND, Z., GLäSSER, U., SHAHIR, A. Y., SAEEDI, P. & WEHN, H. Fishing vessels activity detection from longitudinal AIS data. Proceedings of the 28th International conference on advances in geographic information systems, 2020. 347-356.

ASLAM, S., MICHAELIDES, M. P. & HERODOTOU, H. 2020. Internet of ships: A survey on architectures, emerging applications, and challenges. *IEEE Internet of Things journal,* 7**,** 9714-9727.

BALDAUF, M., KITADA, M. & FROHOLDT, L. L. 2023. The role of VTS operators in new maritime safety situations: when conventional and autonomous ships meet. *Appl. Emerg. Technol,* 115**,** 413-423.

BALLOU, P. J. 2013. Ship energy efficiency management requires a total solution approach. *Marine Technology Society Journal,* 47**,** 83-95.

BARREIRO, J., ZARAGOZA, S. & DIAZ-CASAS, V. 2022. Review of ship energy efficiency. *Ocean Engineering,* 257**,** 111594.

BASURKO, O. C., GABIñA, G., LOPEZ, J., GRANADO, I., MURUA, H., FERNANDES, J. A., KRUG, I., RUIZ, J. & URIONDO, Z. 2022. Fuel consumption of free-swimming school versus FAD strategies in tropical tuna purse seine fishing. *Fisheries Research,* 245**,** 106139.

BEN-YAMI, M. 1994. Purse seining manual. Food and Agriculture Organization of the United Nations. Fishing News Books, 406pp.

BERGBAUER, S. & POLLARD, D. D. 2003. How to calculate normal curvatures of sampled geological surfaces. *Journal of structural geology,* 25**,** 277-289.

BLáZQUEZ-GARCíA, A., CONDE, A., MORI, U. & LOZANO, J. A. 2021. A review on outlier/anomaly detection in time series data. *ACM computing surveys (CSUR),* 54**,** 1-33.

BOLBOT, V., THEOTOKATOS, G., BOULOUGOURIS, E., PSARROS, G. & HAMANN, R. 2020. A novel method for safety analysis of Cyber-Physical Systems—Application to a ship exhaust gas scrubber system. *Safety,* 6**,** 26.

BOUKERCHE, A., ZHENG, L. & ALFANDI, O. 2020. Outlier detection: Methods, models, and classification. *ACM Computing Surveys (CSUR),* 53**,** 1-37.

BRYNOLF, S., LINDGREN, J. F., ANDERSSON, K., WILEWSKA-BIEN, M., BALDI, F., GRANHAG, L., JOHNSON, H., LINNé, P., SVENSSON, E. & ZETTERDAHL, M. 2016. Improving environmental performance in shipping. *Shipping and the environment: Improving environmental performance in marine transportation***,** 399-418.

BUI, V. & NGUYEN, H. 2021. A Comprehensive Review on Big Data-Based Potential Applications in Marine Shipping Management. *Int. J. Adv. Sci. Eng. Inf. Technol,* 11**,** 1067-1077.

CASTRESANA, J., GABIñA, G., QUINCOCES, I. & URIONDO, Z. 2023. Healthy marine diesel engine threshold characterisation with probability density functions and ANNs. *Reliability Engineering & System Safety,* 238**,** 109466.

CHEN, B., WANG, X., WANG, R., QIU, X., ZHU, Z. & LIANG, M. 2019. The grey-box based modeling approach research integrating fusion mechanism and data. *Journal of System Simulation,* 31**,** 2575-2583.

CHEN, S., MENG, Q., JIA, P. & KUANG, H. 2021. An operational-mode-based method for estimating ship emissions in port waters. *Transportation Research Part D: Transport and Environment,* 101**,** 103080.

CHEN, S., WANG, F., WEI, X., TAN, Z. & WANG, H. 2020. Analysis of tugboat activities using AIS data for the Tianjin port. *Transportation Research Record,* 2674**,** 498-509.

CLINSH. 2021. *CLean INland SHipping* [Online]. Available: https://www.clinsh.eu/ [Accessed 14 August 2024].

CORADDU, A., ONETO, L., BALDI, F. & ANGUITA, D. Ship efficiency forecast based on sensors data collection: Improving numerical models through data analytics. OCEANS 2015-Genova, 2015. IEEE, 1-10.

DALHEIM, Ø. Ø. & STEEN, S. 2020a. A computationally efficient method for identification of steady state in time series data from ship monitoring. *Journal of Ocean Engineering and Science,* 5**,** 333-345.

DALHEIM, Ø. Ø. & STEEN, S. 2020b. Preparation of in-service measurement data for ship operation and performance analysis. *Ocean Engineering,* 212**,** 107730.

DENIZ, C., KILIC, A. & CıVKAROGLU, G. 2010. Estimation of shipping emissions in Candarli Gulf, Turkey. *Environmental monitoring and assessment,* 171**,** 219-228.

DI VAIO, A. & VARRIALE, L. 2020. Digitalization in the sea-land supply chain: experiences from Italy in rethinking the port operations within inter-organizational relationships. *Production Planning & Control,* 31**,** 220-232.

DNV, G. 2016. Technology outlook 2025. *Høvik: DNV GLAS*.

DNVGL 2014. Big Data - the new data reality and industry impact.

DURLIK, I., MILLER, T., CEMBROWSKA-LECH, D., KRZEMIŃSKA, A., ZŁOCZOWSKA, E. & NOWAK, A. 2023. Navigating the sea of data: A comprehensive review on data analysis in maritime IoT applications. *Applied Sciences,* 13**,** 9742.

EMOVON, I., NORMAN, R. A. & MURPHY, A. J. 2018. Hybrid MCDM based methodology for selecting the optimum maintenance strategy for ship machinery systems. *Journal of intelligent manufacturing,* 29**,** 519-531.

ESMAILIAN, E. & STEEN, S. 2022. A new method for optimal ship design in real sea states using the ship power profile. *Ocean Engineering,* 259**,** 111893.

ESMAILIAN, E., STEEN, S. & KOUSHAN, K. 2022. Ship design for real sea states under uncertainty. *Ocean Engineering,* 266**,** 113127.

ESTER, M., KRIEGEL, H.-P., SANDER, J. & XU, X. A density-based algorithm for discovering clusters in large spatial databases with noise. kdd, 1996. 226-231.

EYRING, V., ISAKSEN, I. S., BERNTSEN, T., COLLINS, W. J., CORBETT, J. J., ENDRESEN, O., GRAINGER, R. G., MOLDANOVA, J., SCHLAGER, H. & STEVENSON, D. S. 2010. Transport impacts on atmosphere and climate: Shipping. *Atmospheric Environment,* 44**,** 4735-4771.

FAN, A., YANG, J., YANG, L., WU, D. & VLADIMIR, N. 2022. A review of ship fuel consumption models. *Ocean engineering,* 264**,** 112405.

FU, H., GAO, S., PENG, Y. & ZHAO, N. Prediction of fishing vessel operation mode based on Stacking model fusion. Journal of Physics: Conference Series, 2021. IOP Publishing, 012030.

GKEREKOS, C. & LAZAKIS, I. 2020. A novel, data-driven heuristic framework for vessel weather routing. *Ocean Engineering,* 197**,** 106887.

GODJEVAC, M. & DRIJVER, M. 2015. Performance evaluation of an inland pusher. *Transport of Water versus Transport over Water: Exploring the Dynamic Interplay of Transport and Water.* Springer.

GOERLANDT, F. & MONTEWKA, J. 2015. Maritime transportation risk analysis: Review and analysis in light of some foundational issues. *Reliability Engineering & System Safety,* 138**,** 115-134.

GOLDSTEIN, M. & UCHIDA, S. 2016. A comparative evaluation of unsupervised anomaly detection algorithms for multivariate data. *PloS one,* 11**,** e0152173.

GRUBBS, F. E. 1969. Procedures for detecting outlying observations in samples. *Technometrics,* 11**,** 1-21.

HANG HOU, Y., JIA LI, Y. & LIANG, X. 2019. Mixed aleatory/epistemic uncertainty analysis and optimization for minimum EEDI hull form design. *Ocean Engineering,* 172**,** 308-315.

HODGE, V. & AUSTIN, J. 2004. A survey of outlier detection methodologies. *Artificial intelligence review,* 22**,** 85-126.

HU, Z., JIN, Y., HU, Q., SEN, S., ZHOU, T. & OSMAN, M. T. 2019. Prediction of fuel consumption for enroute ship based on machine learning. *IEEE Access,* 7**,** 119497-119505.

IŞıKLı, E., AYDıN, N., BILGILI, L. & TOPRAK, A. 2020. Estimating fuel consumption in maritime transport. *Journal of Cleaner Production,* 275**,** 124142.

JAFARZADEH, S. & SCHJøLBERG, I. 2018. Operational profiles of ships in Norwegian waters: An activity-based approach to assess the benefits of hybrid and electric propulsion. *Transportation Research Part D: Transport and Environment,* 65**,** 500-523.

JAHN, C. & SAXE, S. 2017. Digitalization of seaports-visions of the future. *Fraunhofer Center for Maritime Logistics and Services (CML).*

JAMSHIDI, A., HAJIZADEH, S., SU, Z., NAEIMI, M., NúñEZ, A., DOLLEVOET, R., DE SCHUTTER, B. & LI, Z. 2018. A decision support approach for condition-based maintenance of rails based on big data analysis. *Transportation Research Part C: Emerging Technologies,* 95**,** 185-206.

KARATUĞ, Ç. & ARSLANOĞLU, Y. 2022. Development of condition-based maintenance strategy for fault diagnosis for ship engine systems. *Ocean Engineering,* 256**,** 111515.

KEE, K.-K., SIMON, B.-Y. L. & RENCO, K.-H. 2018. Artificial neural network back-propagation based decision support system for ship fuel consumption prediction.

KIM, D., HIRAYAMA, K. & OKIMOTO, T. 2017. Distributed stochastic search algorithm for multi-ship encounter situations. *The Journal of Navigation,* 70**,** 699-718.

KUNDAKçI, B., NAS, S. & GUCMA, L. 2023. Prediction of ship domain on coastal waters by using AIS data. *Ocean Engineering,* 273**,** 113921.

LI, H., WEI, X., LIU, Z., FENG, B. & ZHENG, Q. 2023. Ship design optimization with mixed uncertainty based on evidence theory. *Ocean Engineering,* 279**,** 114554.

LI, Y., LIU, R. W., LIU, J., HUANG, Y., HU, B. & WANG, K. Trajectory compression-guided visualization of spatio-temporal AIS vessel density. 2016 8th International Conference on Wireless Communications & Signal Processing (WCSP), 2016. IEEE, 1-5.

LIU, S., CHEN, H., SHANG, B. & PAPANIKOLAOU, A. 2022. Supporting predictive maintenance of a ship by analysis of onboard measurements. *Journal of Marine Science and Engineering,* 10**,** 215.

LIU, Z., ZHANG, B., ZHANG, M., WANG, H. & FU, X. 2023. A quantitative method for the analysis of ship collision risk using AIS data. *Ocean Engineering,* 272**,** 113906.

LIVINGSTON, E. H. 2004. The mean and standard deviation: what does it all mean? *Journal of Surgical Research,* 119**,** 117-123.

LU, Y., SUN, L., ZHANG, X., FENG, F., KANG, J. & FU, G. 2018. Condition based maintenance optimization for offshore wind turbine considering opportunities based on neural network approach. *Applied Ocean Research,* 74**,** 69-79.

LüTZEN, M., MIKKELSEN, L. L., JENSEN, S. & RASMUSSEN, H. B. 2017. Energy efficiency of working vessels–A framework. *Journal of Cleaner Production,* 143**,** 90-99.

MAKRIDIS, G., KYRIAZIS, D. & PLITSOS, S. Predictive maintenance leveraging machine learning for time-series forecasting in the maritime industry. 2020 IEEE 23rd international conference on intelligent transportation systems (ITSC), 2020. IEEE, 1-8.

MARAGKOGIANNI, A. & PAPAEFTHIMIOU, S. 2015. Evaluating the social cost of cruise ships air emissions in major ports of Greece. *Transportation Research Part D: Transport and Environment,* 36**,** 10-17.

MCMEEL, O. & EPARKHINA, D. 2018. Maritime Sensor Technologies for the European Market: Research, Development and Implementation. Good practice guide.

MICHAŁOWSKA, K., RIEMER-SøRENSEN, S., STERUD, C. & HJELLSET, O. M. 2021. Anomaly detection with unknown anomalies: Application to maritime machinery. *IFAC-PapersOnLine,* 54**,** 105-111.

MOHD SALLEH, N. H., SELVADURAY, M., JEEVAN, J., NGAH, A. H. & ZAILANI, S. 2021. Adaptation of industrial revolution 4.0 in a seaport system. *Sustainability,* 13**,** 10667.

MOVEIT! 2014. *Modernisation of Vessels for Inland waterway freight Transport* [Online]. Available: https://cordis.europa.eu/project/id/285405/reporting#:~:text=The%20project%20focussed%20on%20exploring,new%20building%20will%20take%20decades. [Accessed 14 August 2024].

NG, S. K., LOH, C., LIN, C., BOOTH, V., CHAN, J. W., YIP, A. C., LI, Y. & LAU, A. K. 2013. Policy change driven by an AIS-assisted marine emission inventory in Hong Kong and the Pearl River Delta. *Atmospheric environment,* 76**,** 102-112.

NIKOLOPOULOS, L. & BOULOUGOURIS, E. 2020. A novel method for the holistic, simulation driven ship design optimization under uncertainty in the big data era. *Ocean engineering,* 218**,** 107634.

NOTTEBOOM, T. E. & VERNIMMEN, B. 2009. The effect of high fuel costs on liner service configuration in container shipping. *Journal of transport geography,* 17**,** 325-337.

NWAGWU, H. C., OKEREKE, G. & NWOBODO, C. 2017. Mining and visualising contradictory data. *Journal of Big Data,* 4**,** 1-11.

OKUMUS, D., GUNBEYAZ, S. A., KURT, R. E. & TURAN, O. 2023. Towards a circular maritime industry: Identifying strategy and technology solutions. *Journal of Cleaner Production,* 382**,** 134935.

ÖLçER, A. I. 2018. Introduction to maritime energy management. *Trends and Challenges in Maritime Energy Management***,** 1-12.

OLMER, N., COMER, B., ROY, B., MAO, X. & RUTHERFORD, D. 2017. Greenhouse gas emissions from global shipping, 2013–2015 Detailed Methodology. *International Council on Clean Transportation: Washington, DC, USA***,** 1-38.

PAPANIKOLAOU, A. 2010. Holistic ship design optimization. *Computer-Aided Design,* 42**,** 1028-1044.

PAPANIKOLAOU, A., HARRIES, S., HOOIJMANS, P., MARZI, J., LE NéNA, R., TORBEN, S., YRJäNäINEN, A. & BODEN, B. 2022. A holistic approach to ship design: Tools and applications. *Journal of Ship Research,* 66**,** 25-53.

POISSON, F., SéRET, B., VERNET, A.-L., GOUJON, M. & DAGORN, L. 2014. Collaborative research: Development of a manual on elasmobranch handling and release best practices in tropical tuna purse-seine fisheries. *Marine Policy,* 44**,** 312-320.

PORTOFLONGBEACH 2010. Port of Long Beach Air Emissions Inventory - 2009. Port of Long Beach, and Starcrest Consulting Group, LLC.

PRABOWO, A. R., TUSWAN, T. & RIDWAN, R. 2021. Advanced development of sensors' roles in maritime-based industry and research: From field monitoring to high-risk phenomenon measurement. *Applied Sciences,* 11**,** 3954.

PSARAFTIS, H. N. & KONTOVAS, C. A. 2014. Ship speed optimization: Concepts, models and combined speed-routing scenarios. *Transportation Research Part C: Emerging Technologies,* 44**,** 52-69.

PYLE, D. 1999. *Data preparation for data mining*, morgan kaufmann.

RAZMJOOEI, D., ALIMOHAMMADLOU, M., RANAEI KORDSHOULI, H.-A. & ASKARIFAR, K. 2023. Industry 4.0 research in the maritime industry: a bibliometric analysis. *WMU Journal of Maritime Affairs,* 22**,** 385-416.

REILLY, G. & JORGENSEN, J. Classification considerations for cyber safety and security in the smart ship era. Proceedings of the International Smart Ships Technology Conference, 2016. 26-27.

ROBERTS, A. 2001. Curvature attributes and their application to 3 D interpreted horizons. *First break,* 19**,** 85-100.

RøDSETH, Ø. J., PERERA, L. P. & MO, B. 2016. Big data in shipping-Challenges and opportunities.

SAFEBOATING.EU. *EN Passing through bridges and locks safely and quickly* [Online]. Available: http://www.hcagrimsby.co.uk/cruising/EN%20Passing%20through%20bridges%20and%20locks.pdf [Accessed].

SIGMUND, S. & EL MOCTAR, O. 2018. Numerical and experimental investigation of added resistance of different ship types in short and long waves. *Ocean Engineering,* 147**,** 51-67.

SONG, S. 2014. Ship emissions inventory, social cost and eco-efficiency in Shanghai Yangshan port. *Atmospheric Environment,* 82**,** 288-297.

SU, Z., JAMSHIDI, A., NúñEZ, A., BALDI, S. & DE SCHUTTER, B. 2019. Integrated condition-based track maintenance planning and crew scheduling of railway networks. *Transportation Research Part C: Emerging Technologies,* 105**,** 359-384.

SULLIVAN, B. P., DESAI, S., SOLE, J., ROSSI, M., RAMUNDO, L. & TERZI, S. 2020. Maritime 4.0–opportunities in digitalization and advanced manufacturing for vessel development. *Procedia manufacturing,* 42**,** 246-253.

SUN, X., TIAN, Z., MALEKIAN, R. & LI, Z. 2018. Estimation of vessel emissions inventory in Qingdao port based on big data analysis. *Symmetry,* 10**,** 452.

SWIDER, A., WANG, Y. & PEDERSEN, E. Data-Driven Vessel Operational Profile Based on t-SNE and Hierarchical Clustering. OCEANS 2018 MTS/IEEE Charleston, 2018. IEEE, 1-7.

SZLAPCZYNSKA, J. & SZLAPCZYNSKI, R. 2019. Preference-based evolutionary multi-objective optimization in ship weather routing. *Applied Soft Computing,* 84**,** 105742.

SZLAPCZYNSKI, R. & SZLAPCZYNSKA, J. 2017. Review of ship safety domains: Models and applications. *Ocean Engineering,* 145**,** 277-289.

TAY, Z. Y., HADI, J., CHOW, F., LOH, D. J. & KONOVESSIS, D. 2021. Big data analytics and machine learning of harbour craft vessels to achieve fuel efficiency: A review. *Journal of Marine Science and Engineering,* 9**,** 1351.

THEOCHARIS, D., RODRIGUES, V. S., PETTIT, S. & HAIDER, J. 2019. Feasibility of the Northern Sea Route: The role of distance, fuel prices, ice breaking fees and ship size for the product tanker market. *Transportation Research Part E: Logistics and Transportation Review,* 129**,** 111-135.

THEOTOKATOS, G., STOUMPOS, S., BOLBOT, V. & BOULOUGOURIS, E. 2020. Simulation-based investigation of a marine dual-fuel engine. *Journal of Marine Engineering & Technology,* 19**,** 5-16.

TILLIG, F., RINGSBERG, J., MAO, W. & RAMNE, B. 2017. A generic energy systems model for efficient ship design and operation. *Proceedings of the Institution of Mechanical Engineers, Part M: Journal of Engineering for the Maritime Environment,* 231**,** 649-666.

TRODDEN, D., MURPHY, A., PAZOUKI, K. & SARGEANT, J. 2015. Fuel usage data analysis for efficient shipping operations. *Ocean Engineering,* 110**,** 75-84.

TSITSILONIS, K.-M. & THEOTOKATOS, G. 2018. A novel systematic methodology for ship propulsion engines energy management. *Journal of cleaner production,* 204**,** 212-236.

TU, H., XIA, K., ZHAO, E., MU, L. & SUN, J. 2023. Optimum trim prediction for container ships based on machine learning. *Ocean Engineering,* 277**,** 111322.

TUKEY, J. W. 1977. *Exploratory data analysis*, Springer.

TURBO, M. D. A. 2010. MAN B&W S90MC-c8-tii Project Guide. Copenhagen.

UNCTAD. Review of maritime transport 2023. United Nations conference on trade and development, Geneva, Switzerland, 2023.

UYANIK, T., KARATUĞ, Ç. & ARSLANOĞLU, Y. 2020. Machine learning approach to ship fuel consumption: A case of container vessel. *Transportation Research Part D: Transport and Environment,* 84**,** 102389.

VELASCO-GALLEGO, C. & LAZAKIS, I. 2022. A real-time data-driven framework for the identification of steady states of marine machinery. *Applied Ocean Research,* 121**,** 103052.

WEDIN, O., BOGREN, J. & GRABEC, I. 2008. Data Filtering Methods. *European Commission: Brussels, Belgium*.

WEI, N., YIN, L., LI, C., LI, C., CHAN, C. & ZENG, F. 2021. Forecasting the daily natural gas consumption with an accurate white-box model. *Energy,* 232**,** 121036.

WHITLEY, E. & BALL, J. 2001. Statistics review 1: presenting and summarising data. *Critical Care,* 6**,** 1-6.

WU, G. Fault detection method for ship equipment based on BP neural network. 2018 International Conference on Robots & Intelligent System (ICRIS), 2018. IEEE, 556-559.

WU, L., XU, Y., WANG, Q., WANG, F. & XU, Z. 2017. Mapping global shipping density from AIS data. *The Journal of Navigation,* 70**,** 67-81.

WU, Z.-X., RIND, S., YU, Y.-H. & CHO, S.-J. 2016. The development of a ship's network monitoring system using SNMP based on standard IEC 61162-460. *Journal of Advanced Marine Engineering and Technology,* 40**,** 906-915.

YAN, R., WANG, S. & PSARAFTIS, H. N. 2021. Data analytics for fuel consumption management in maritime transportation: Status and perspectives. *Transportation Research Part E: Logistics and Transportation Review,* 155**,** 102489.

YANG, D., WU, L., WANG, S., JIA, H. & LI, K. X. 2019a. How big data enriches maritime research–a critical review of Automatic Identification System (AIS) data applications. *Transport Reviews,* 39**,** 755-773.

YANG, L., CHEN, G., RYTTER, N. G. M., ZHAO, J. & YANG, D. 2019b. A genetic algorithm-based grey-box model for ship fuel consumption prediction towards sustainable shipping. *Annals of Operations Research*, 1-27.

YAU, P., LEE, S., CORBETT, J. J., WANG, C., CHENG, Y. & HO, K. 2012. Estimation of exhaust emission from ocean-going vessels in Hong Kong. *Science of the total environment,* 431, 299-306.

YEE, S., ZAINAL, N. & FANAM, P. 2020. Challenges and opportunities of digitization on container shipping industry in supply chain perspective.

ZAMAN, I., PAZOUKI, K., NORMAN, R., YOUNESSI, S. & COLEMAN, S. 2017a. Challenges and opportunities of big data analytics for upcoming regulations and future transformation of the shipping industry. *Procedia engineering,* 194, 537-544.

ZAMAN, I., PAZOUKI, K., NORMAN, R., YOUNESSI, S. & COLEMAN, S. 2017b. Development of automatic mode detection system by implementing the statistical analysis of ship data to monitor the performance. *International Journal of Maritime Engineering*.

ZHANG, M., MONTEWKA, J., MANDERBACKA, T., KUJALA, P. & HIRDARIS, S. 2021. A big data analytics method for the evaluation of ship-ship collision risk reflecting hydrometeorological conditions. *Reliability Engineering & System Safety,* 213, 107674.

ZHANG, S., ZHANG, C. & YANG, Q. 2003. Data preparation for data mining. *Applied artificial intelligence,* 17, 375-381.

ZHANG, Y., XUE, Q., GAO, D., SHI, W. & YU, W. 2022. Two-level model predictive control energy management strategy for hybrid power ships with hybrid energy storage system. *Journal of Energy Storage,* 52, 104763.

ZHOU, Y., PAZOUKI, K., MURPHY, A. J., URIONDO, Z., GRANADO, I., QUINCOCES, I. & FERNANDES-SALVADOR, J. A. 2023. Predicting ship fuel consumption using a combination of metocean and on-board data. *Ocean Engineering,* 285, 115509.

Appendices

Appendix A: Examples of Transit mode detection for target ocean-going car carrier

Appendix B: Examples of Transit mode detection for target tuna purse seiner

Appendix C: Examples of operational mode detection for target inland waterway tanker

Appendix A

Examples of Transit Mode Detection for Target Ocean-going Car Carrier

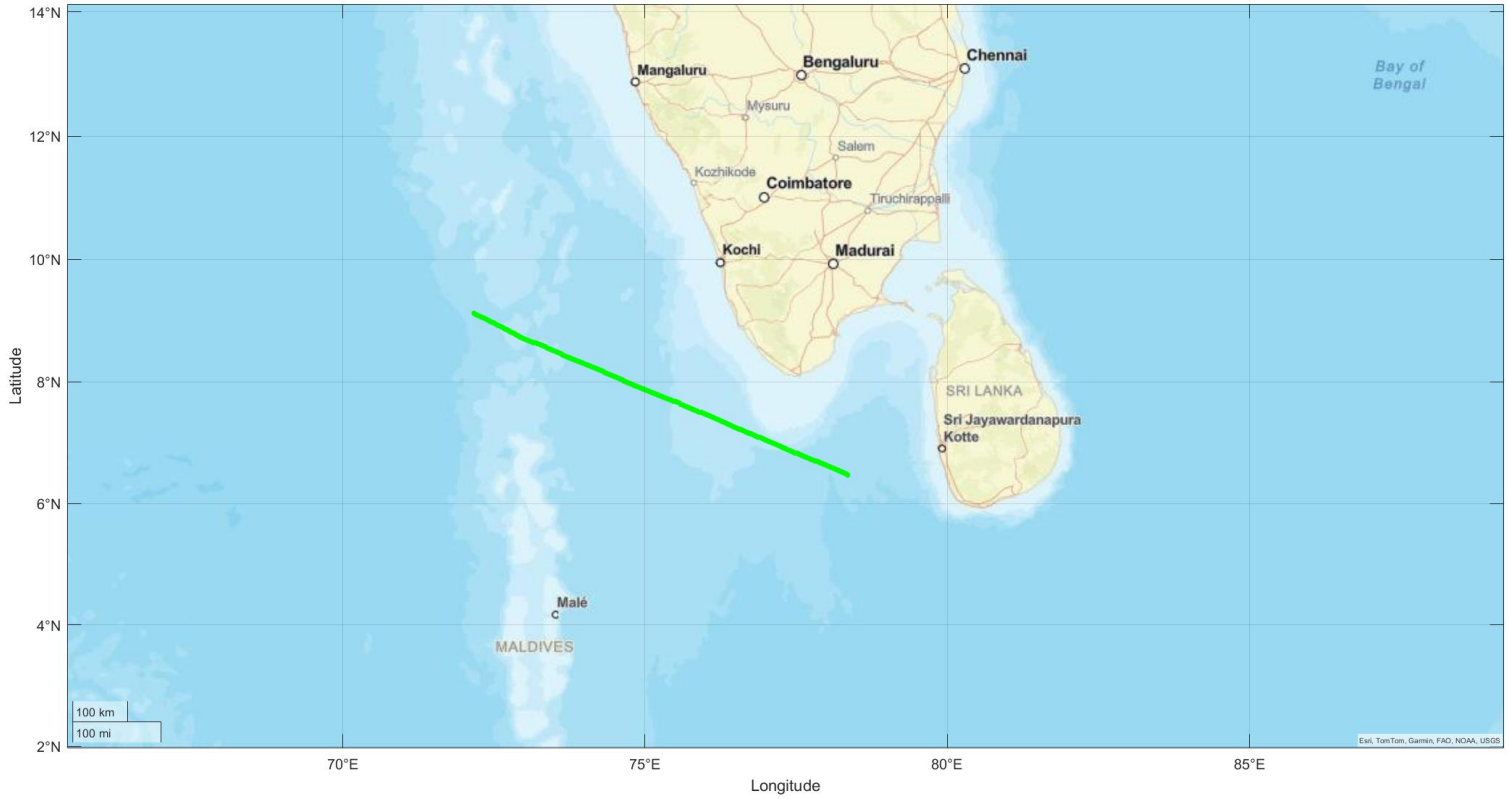

A1. Trajectory of example dataset detected as ‘Transit’ in open seas

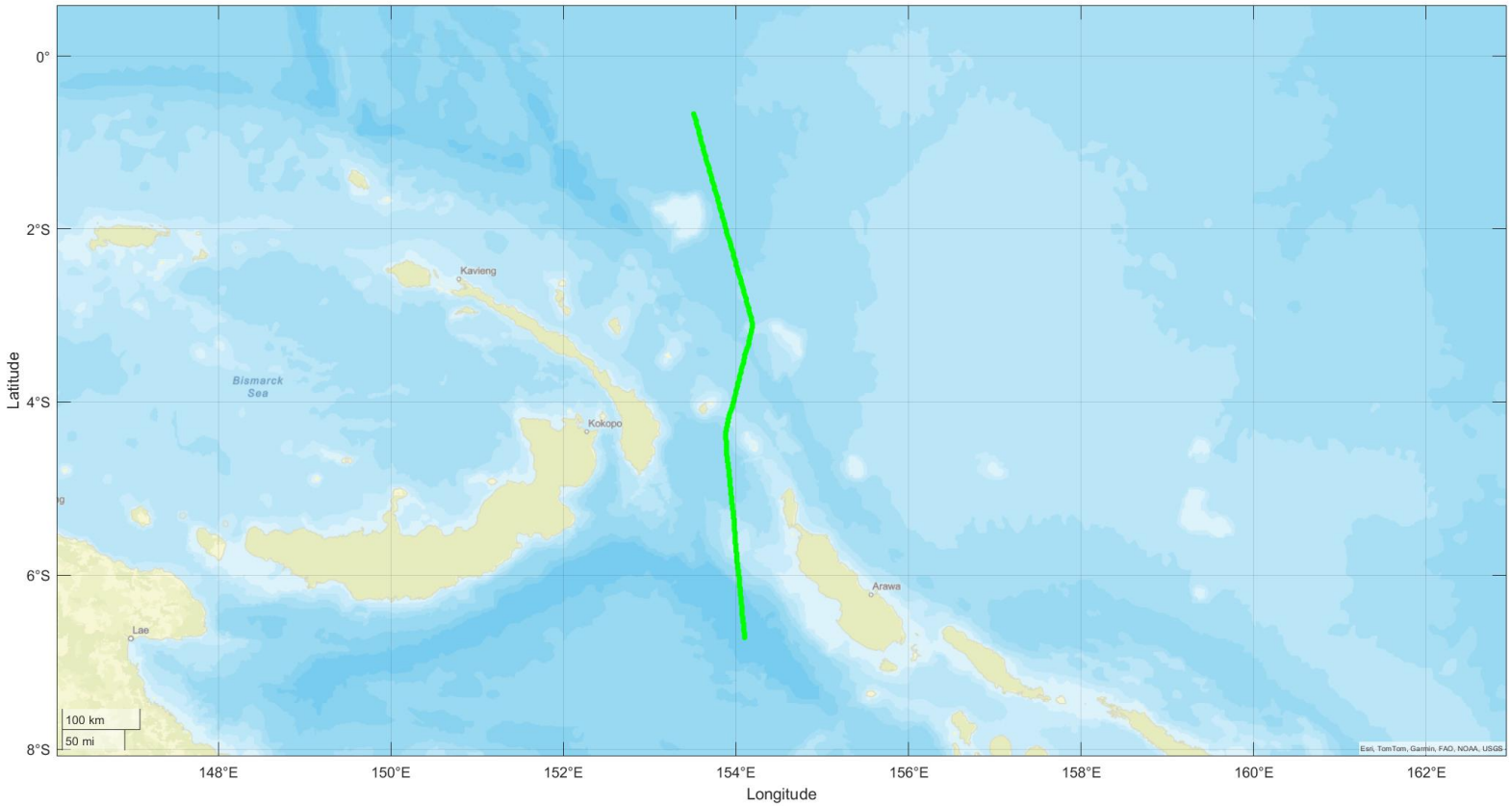

A2. Trajectory of example dataset detected as ‘Transit’ in open seas

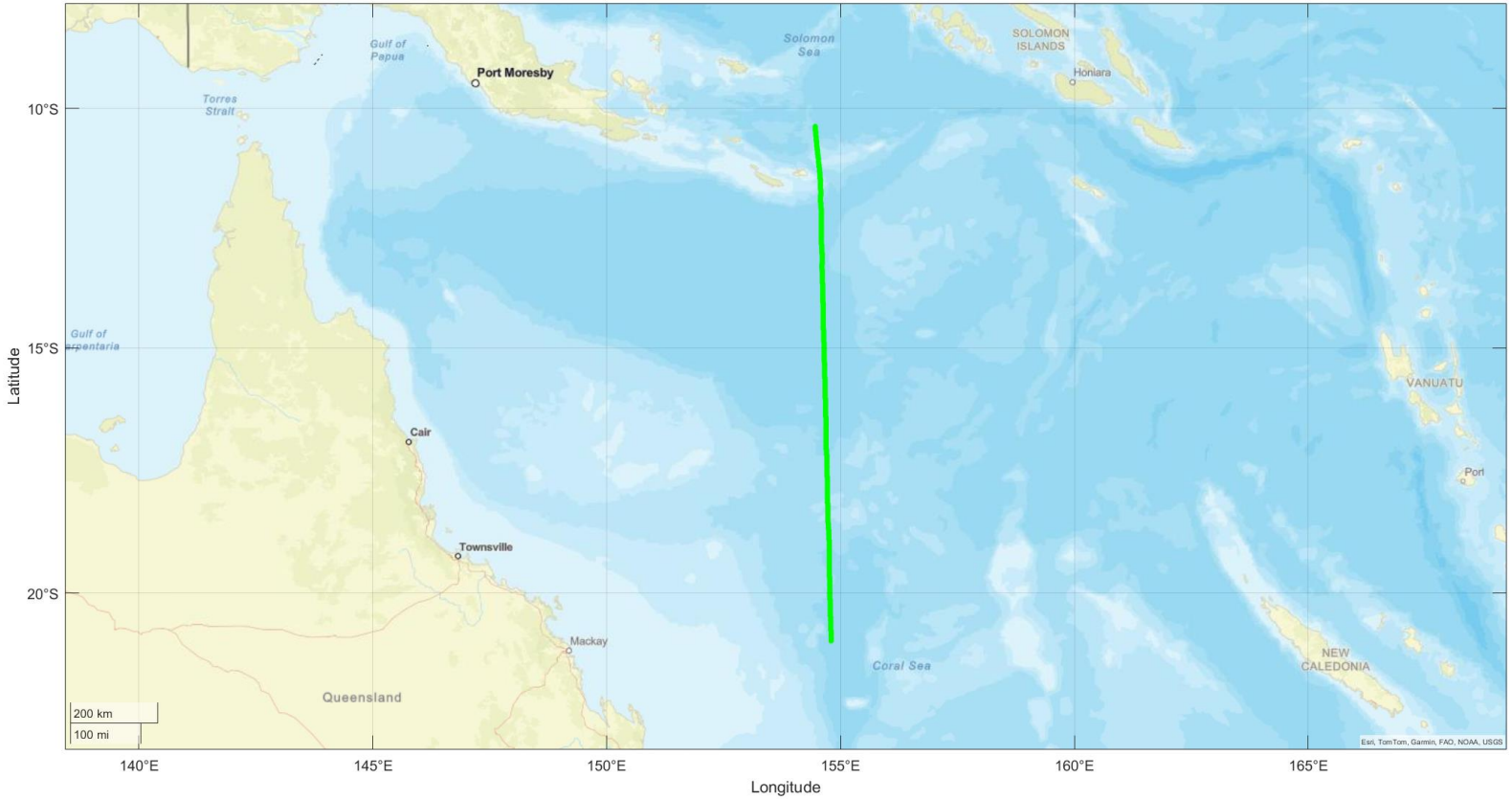

A3. Trajectory of example dataset detected as ‘Transit’ in open seas

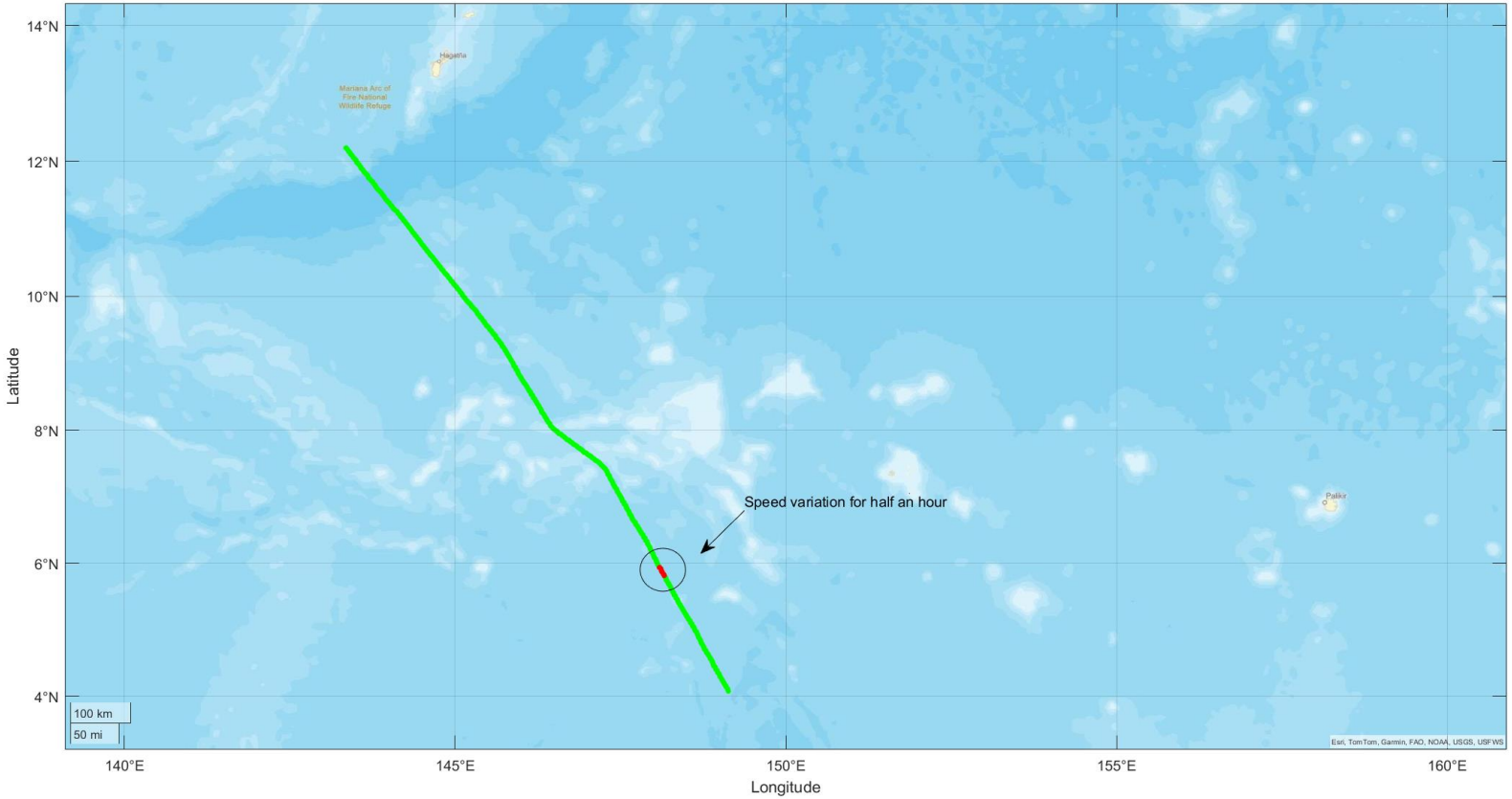

A4. Trajectory of example dataset detected as ‘Transit’ in open seas

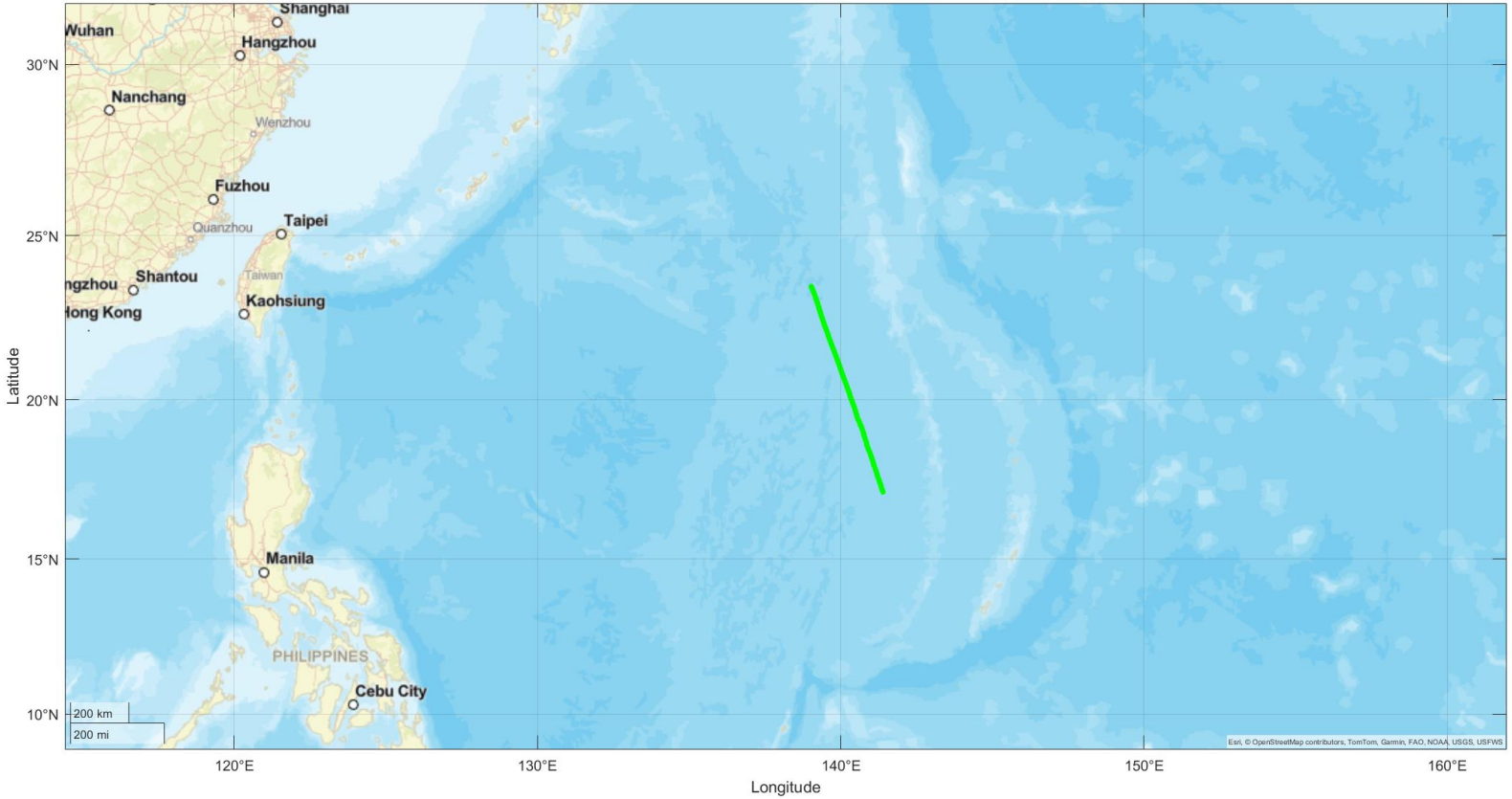

A5. Trajectory of example dataset detected as ‘Transit’ in open seas

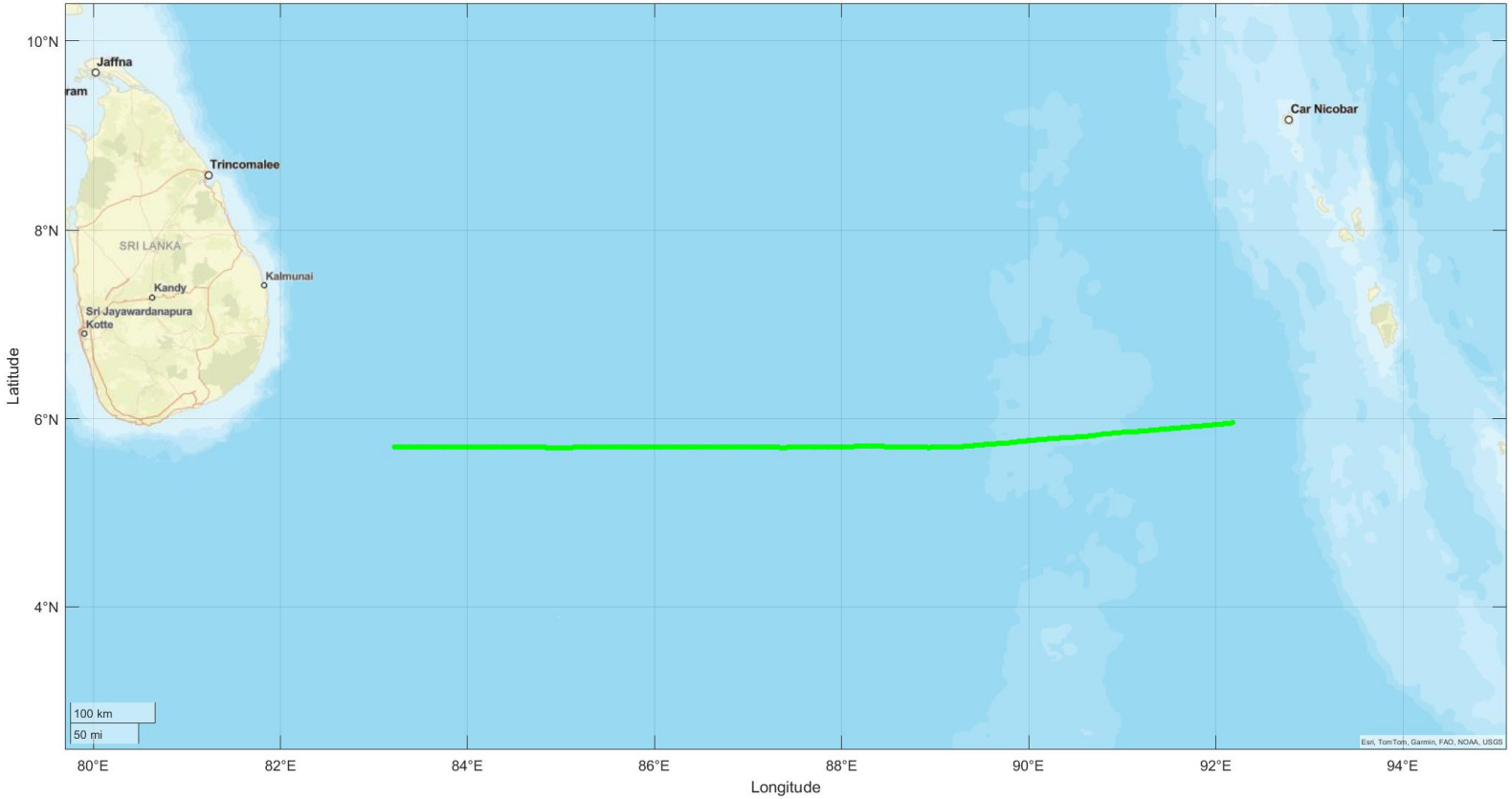

A6. Trajectory of example dataset detected as ‘Transit’ in open seas

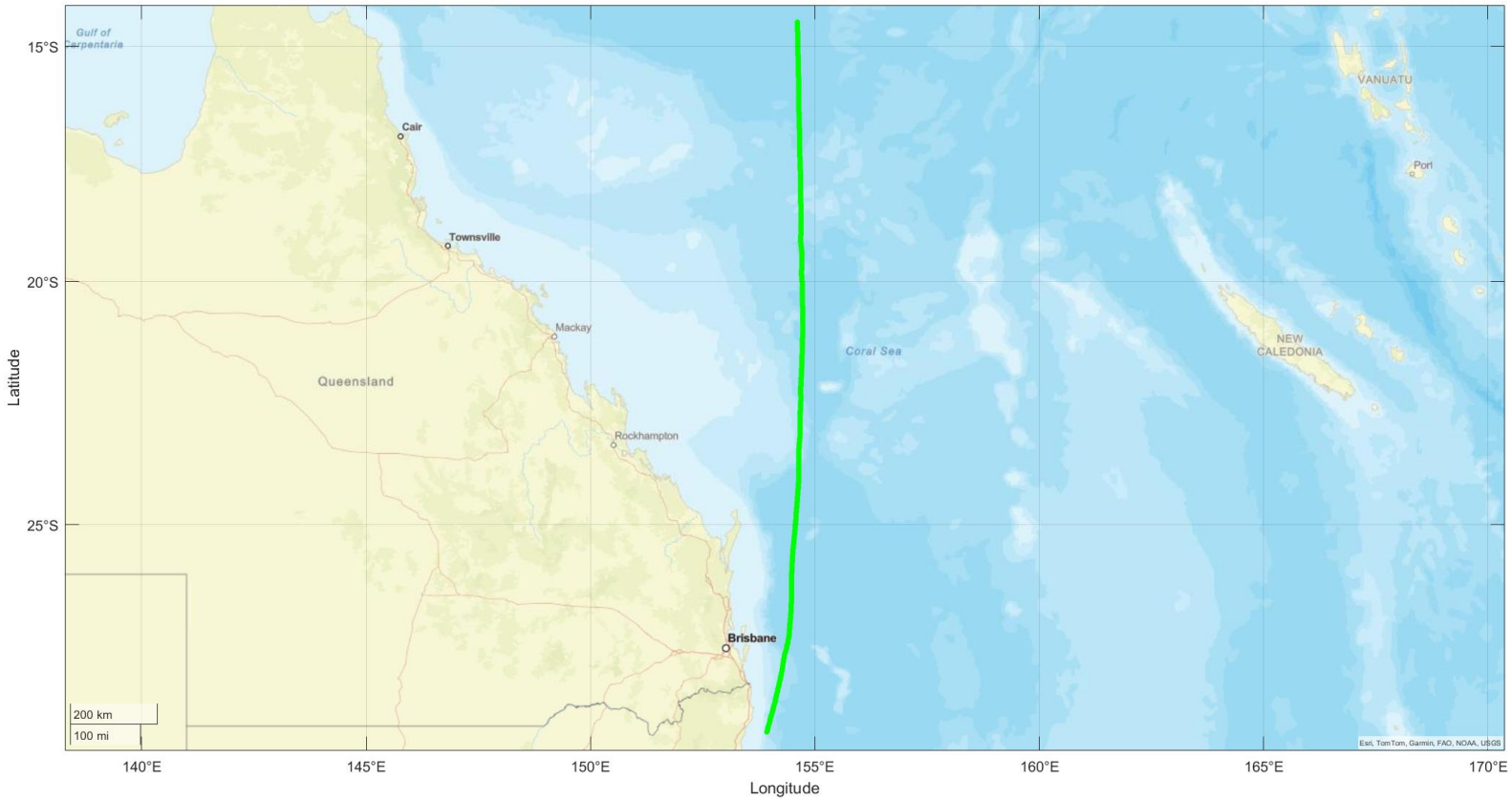

A7. Trajectory of example dataset detected as ‘Transit’ in open seas

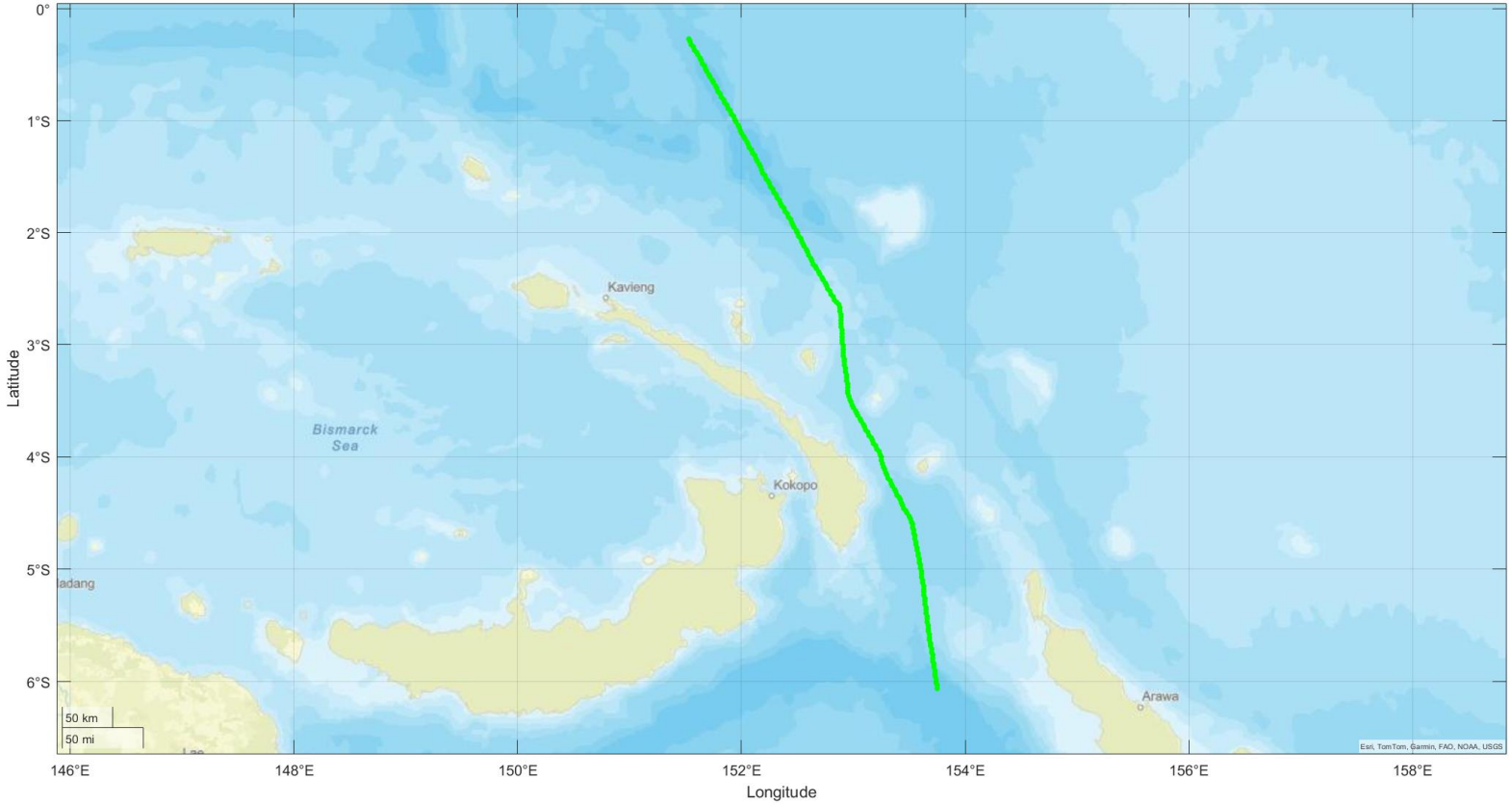

A8. Trajectory of example dataset detected as ‘Transit’ in open seas

Appendix B

Examples of Transit Mode Detection for Target Tuna Purse Seiner

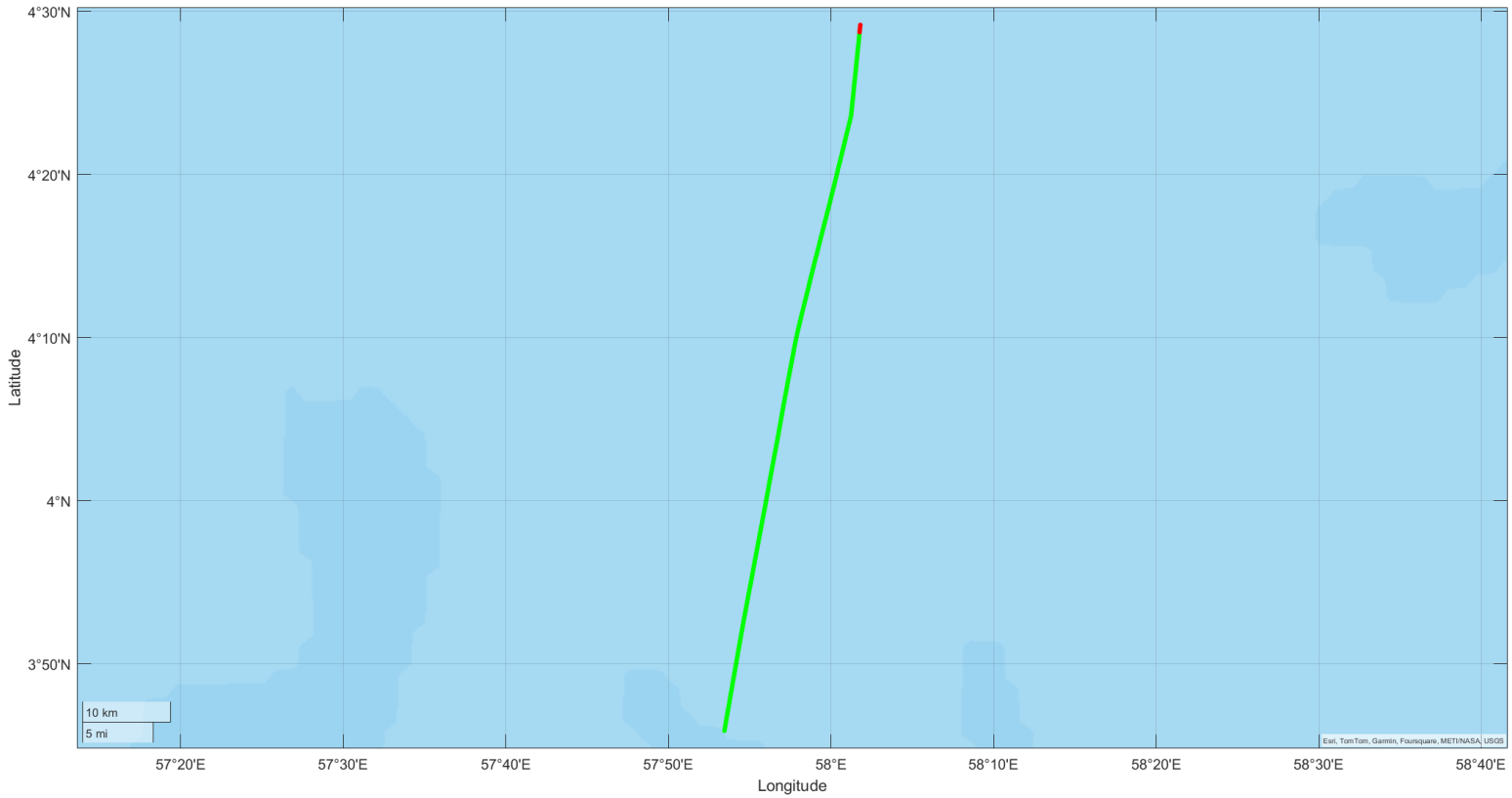

B1. Trajectory of example dataset detected as 'Transit' in open seas

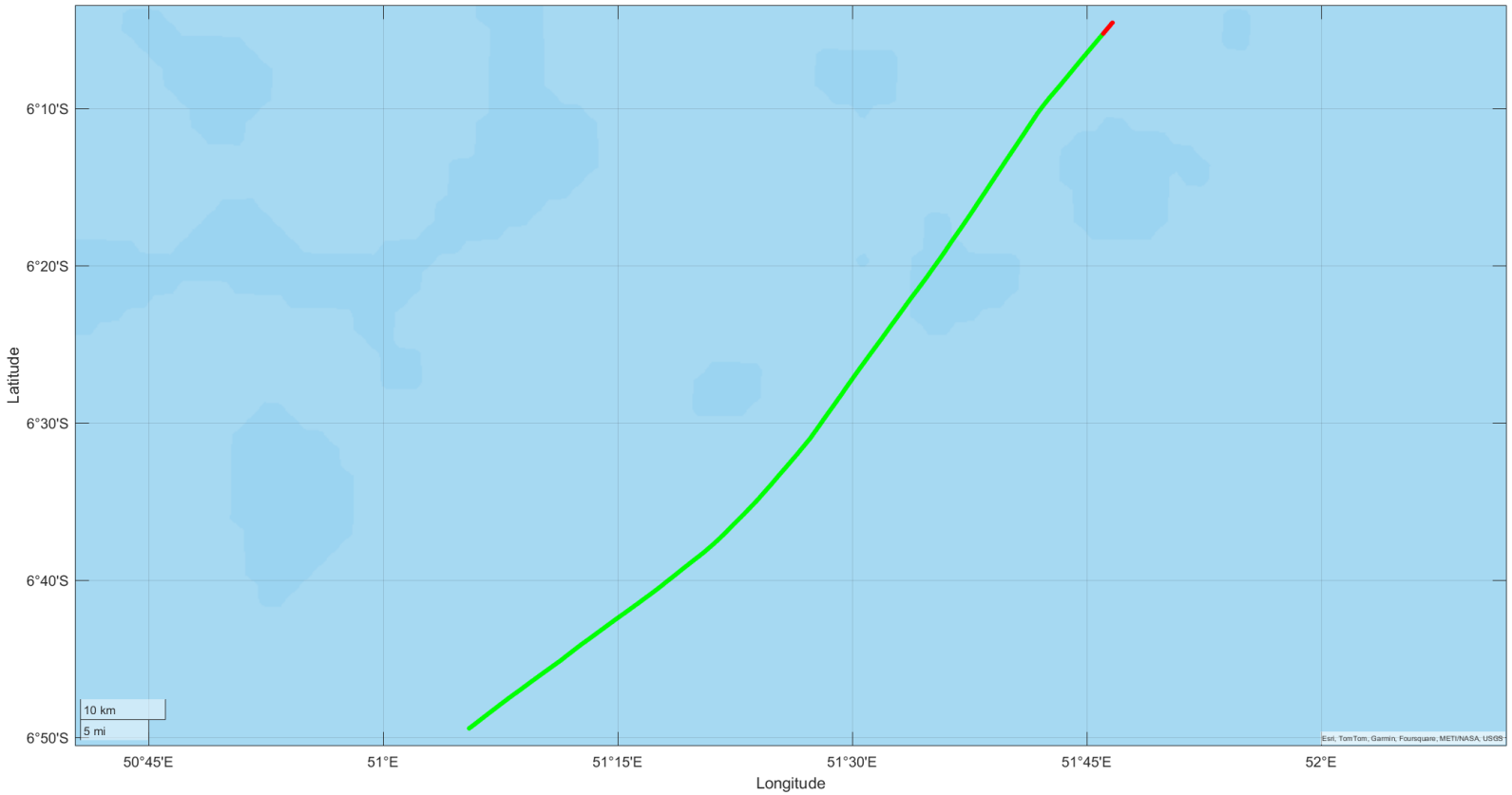

B2. Trajectory of example dataset detected as ‘Transit’ in open seas

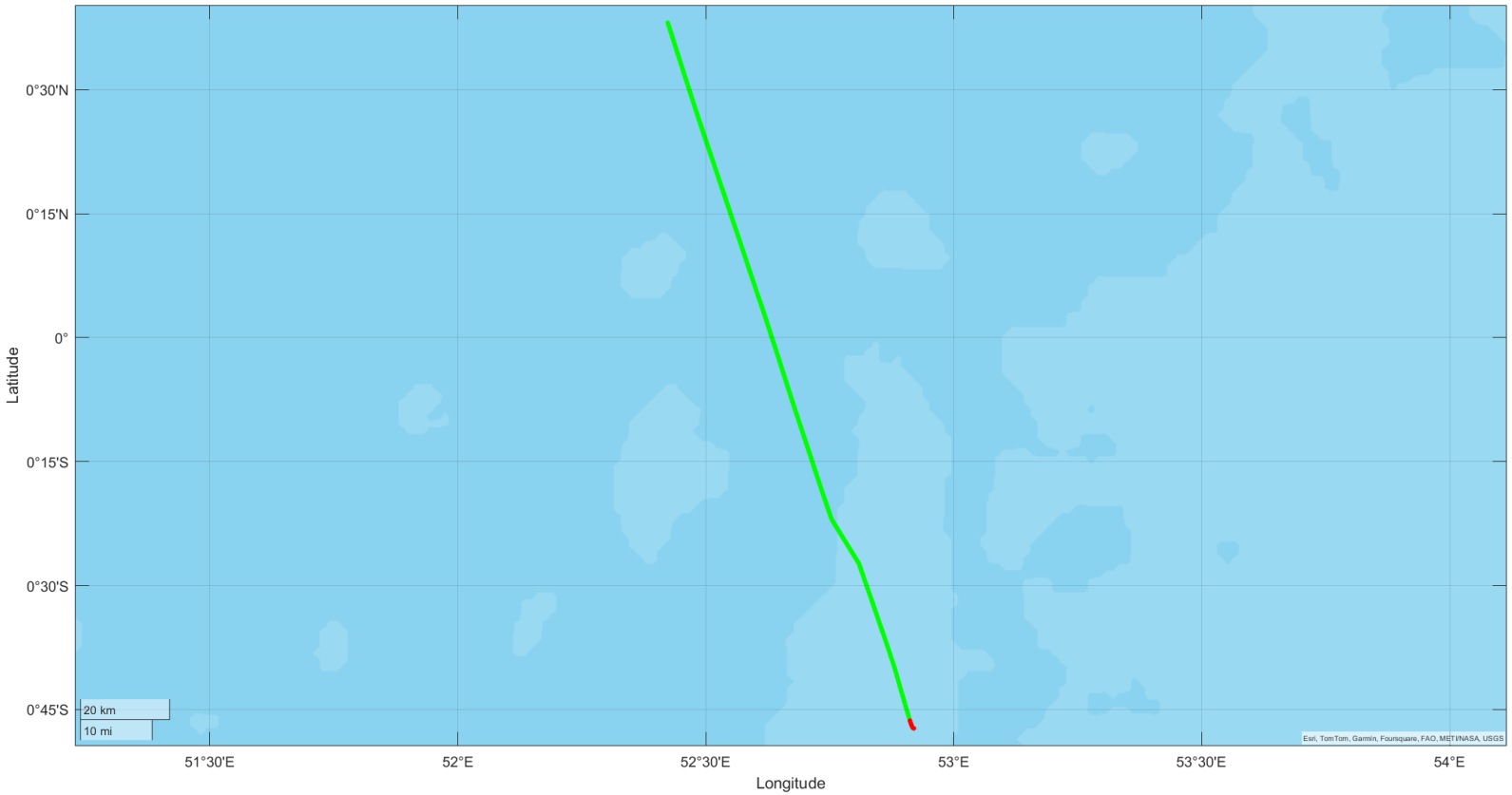

B3. Trajectory of example dataset detected as ‘Transit’ in open seas

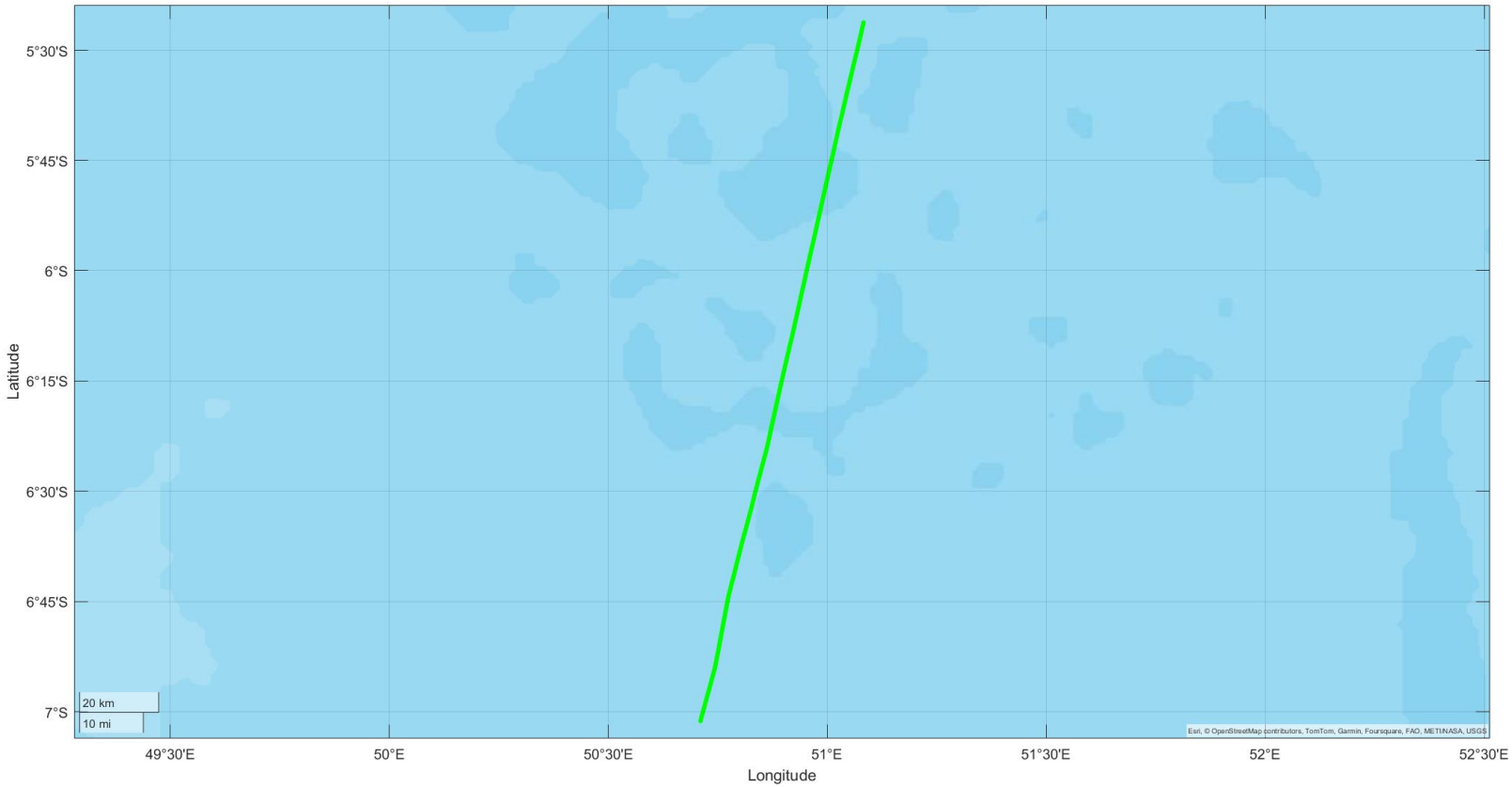

B4. Trajectory of example dataset detected as ‘Transit’ in open seas

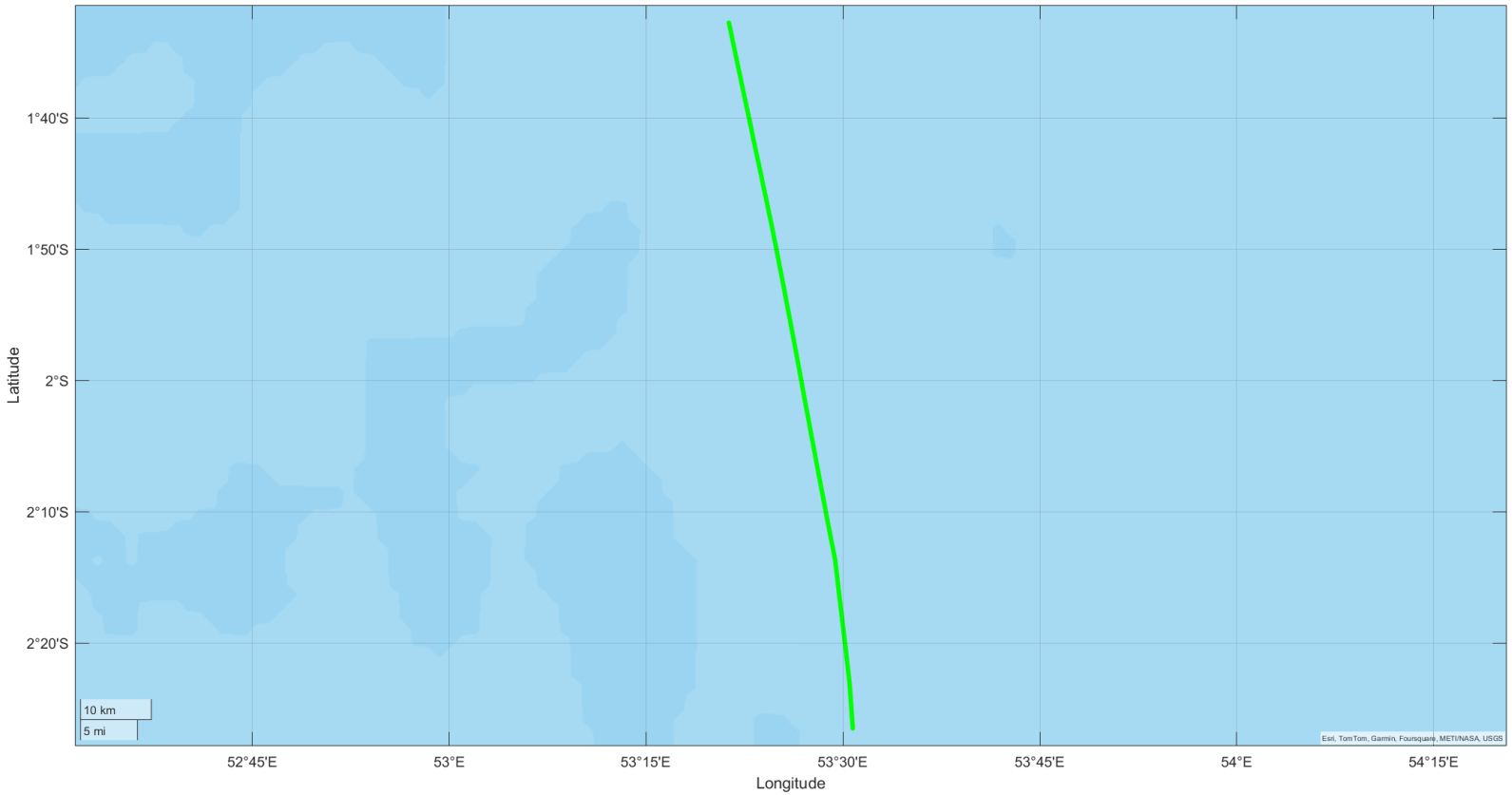

B5. Trajectory of example dataset detected as ‘Transit’ in open seas

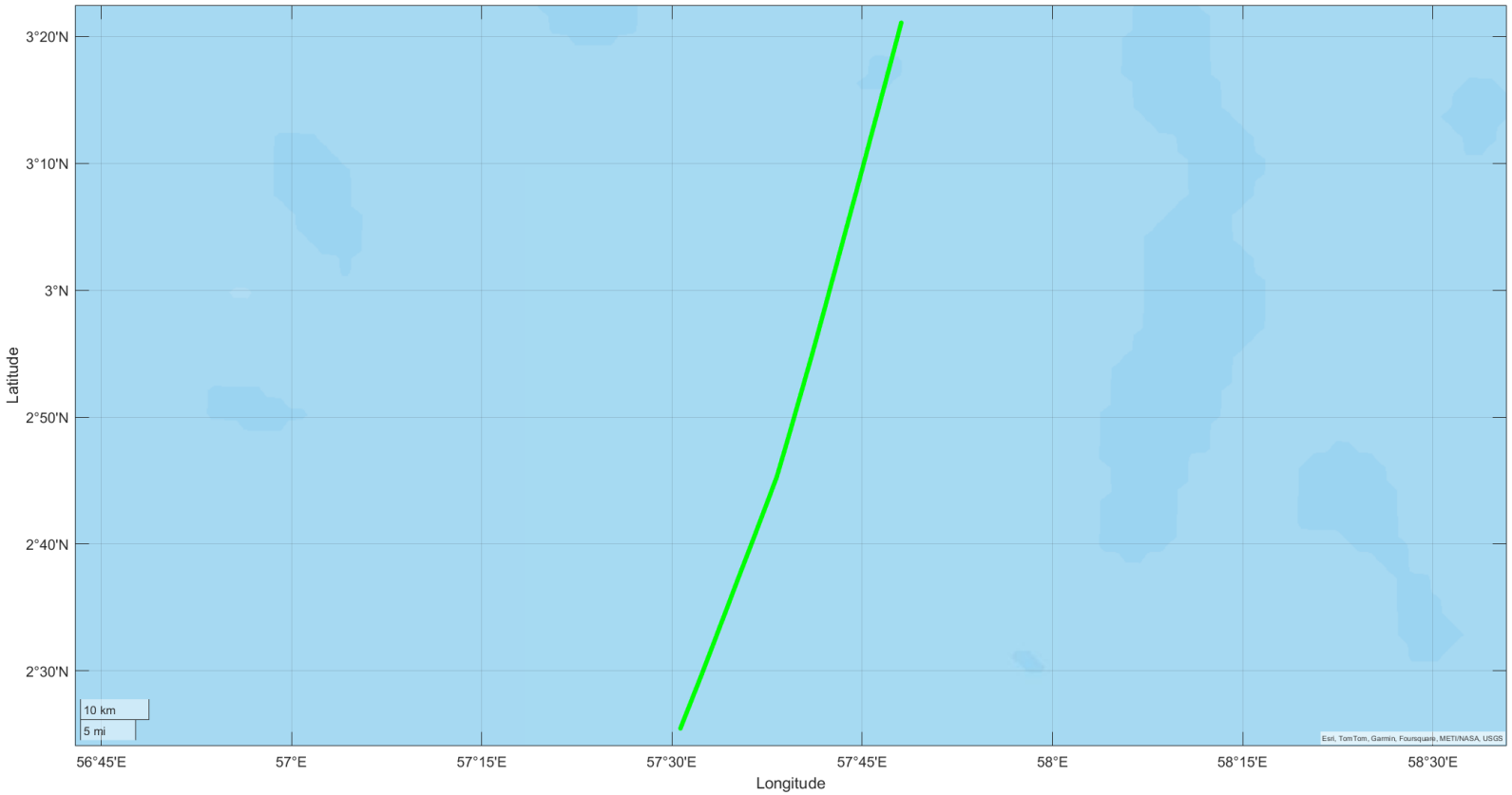

B6. Trajectory of example dataset detected as ‘Transit’ in open seas

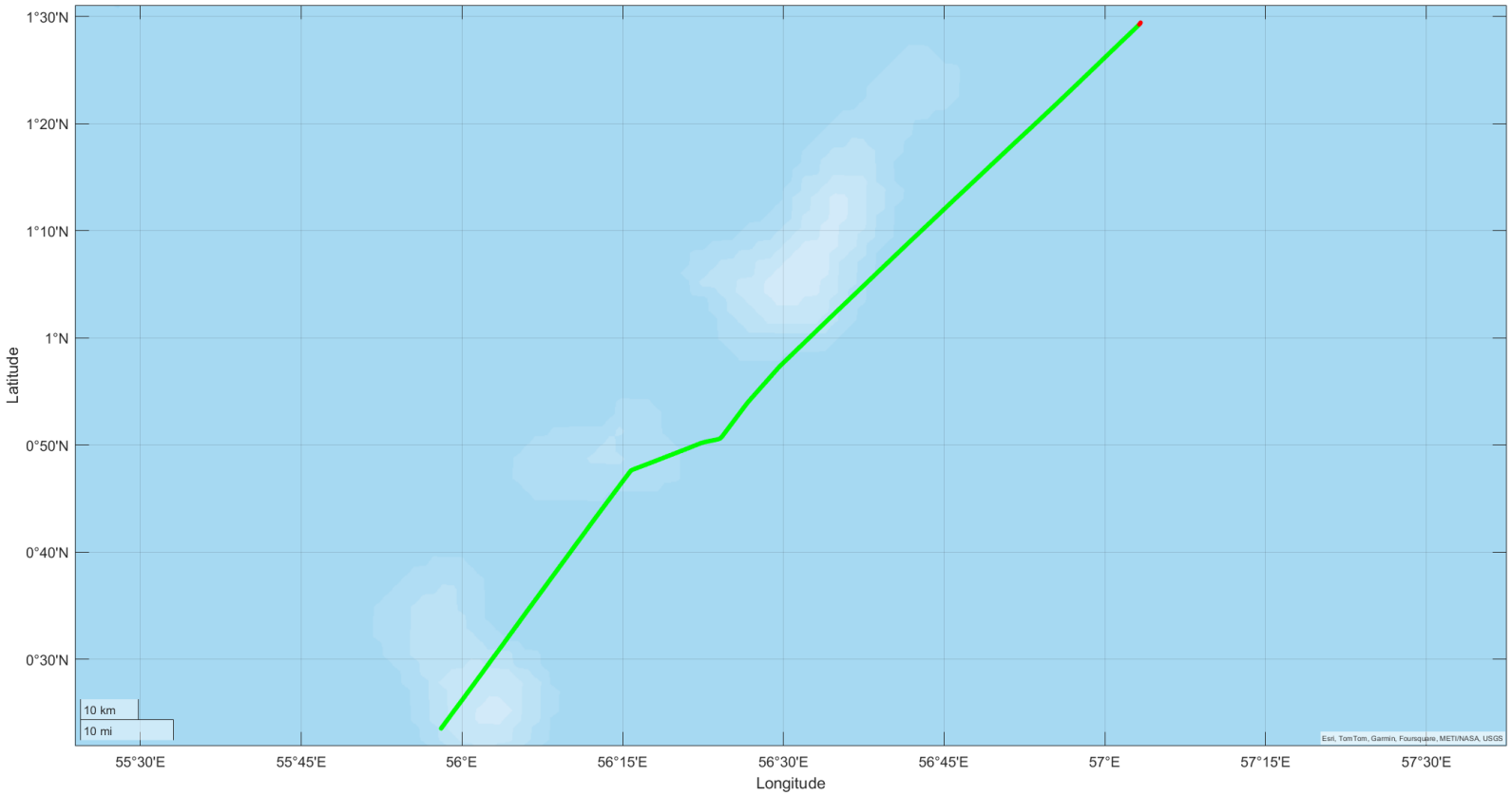

B7. Trajectory of example dataset detected as ‘Transit’ in open seas

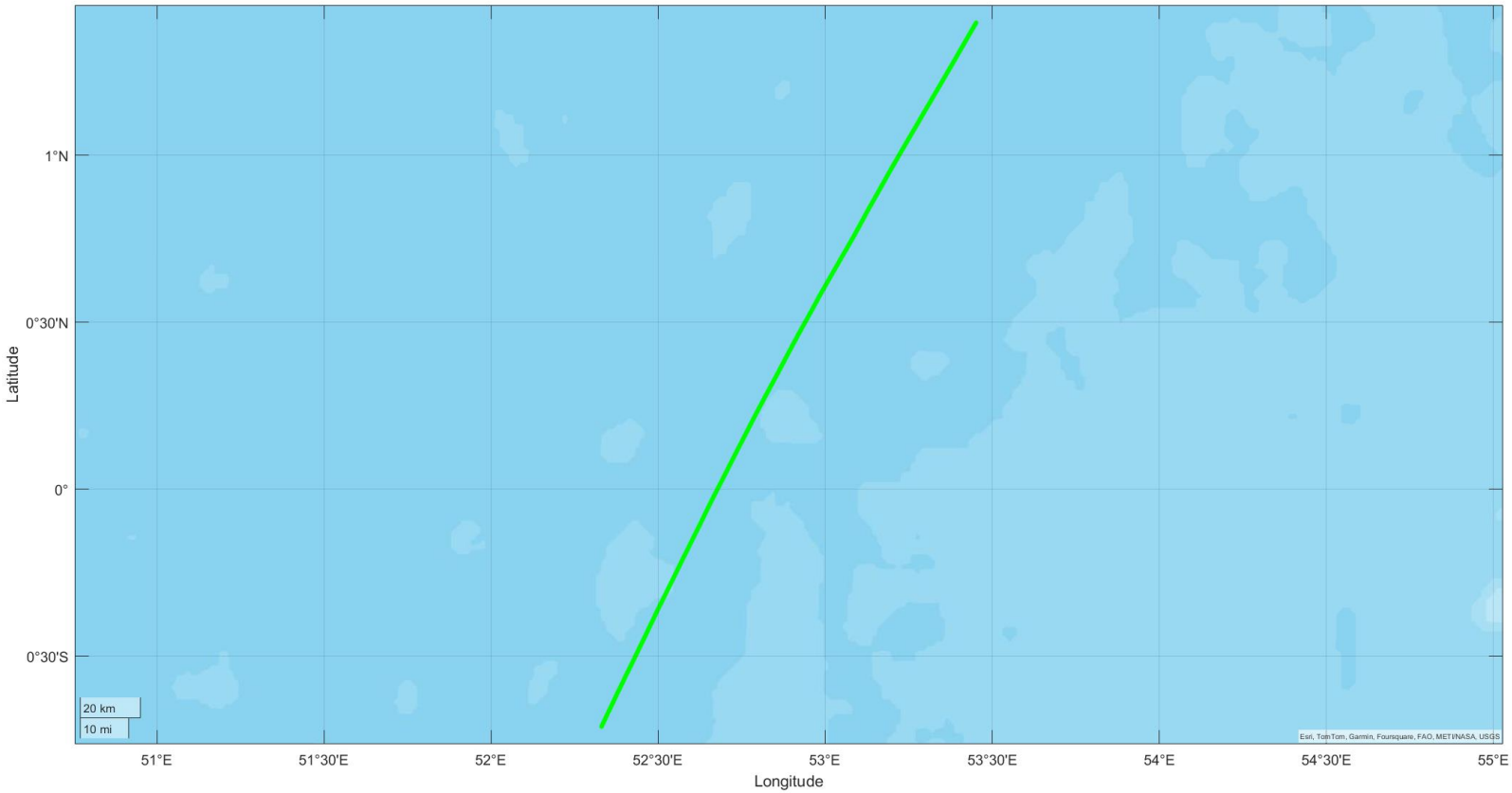

B8. Trajectory of example dataset detected as ‘Transit’ in open seas

Appendix C

Examples of Operational Mode Detection for Target Inland Waterway Tanker

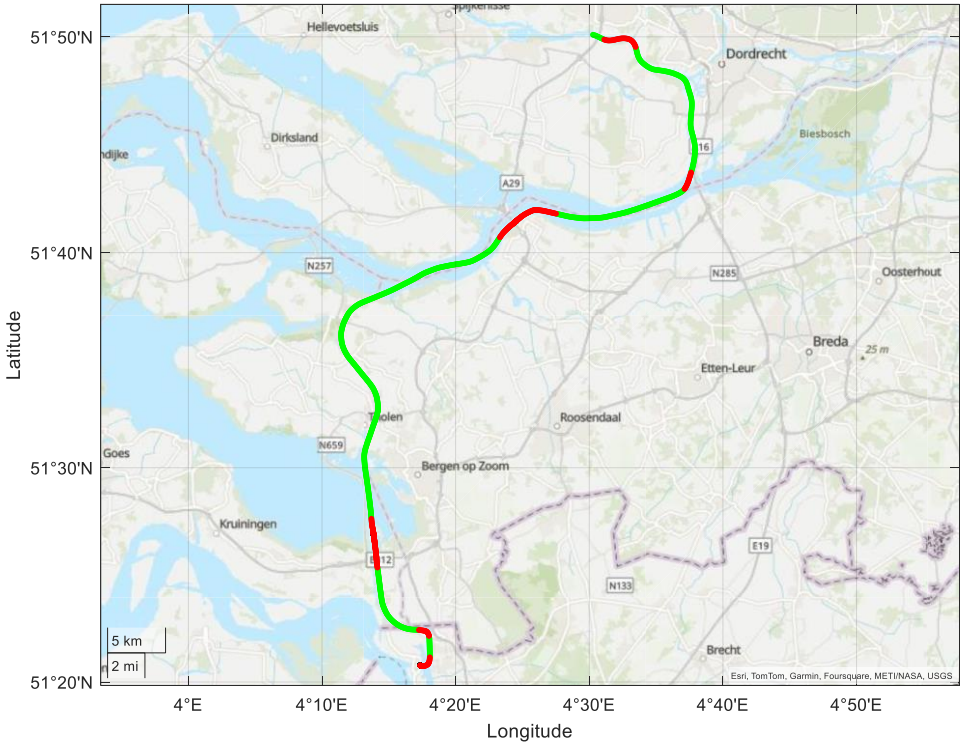

C1 Trajectory of selected dataset for checking 'Transit' detection

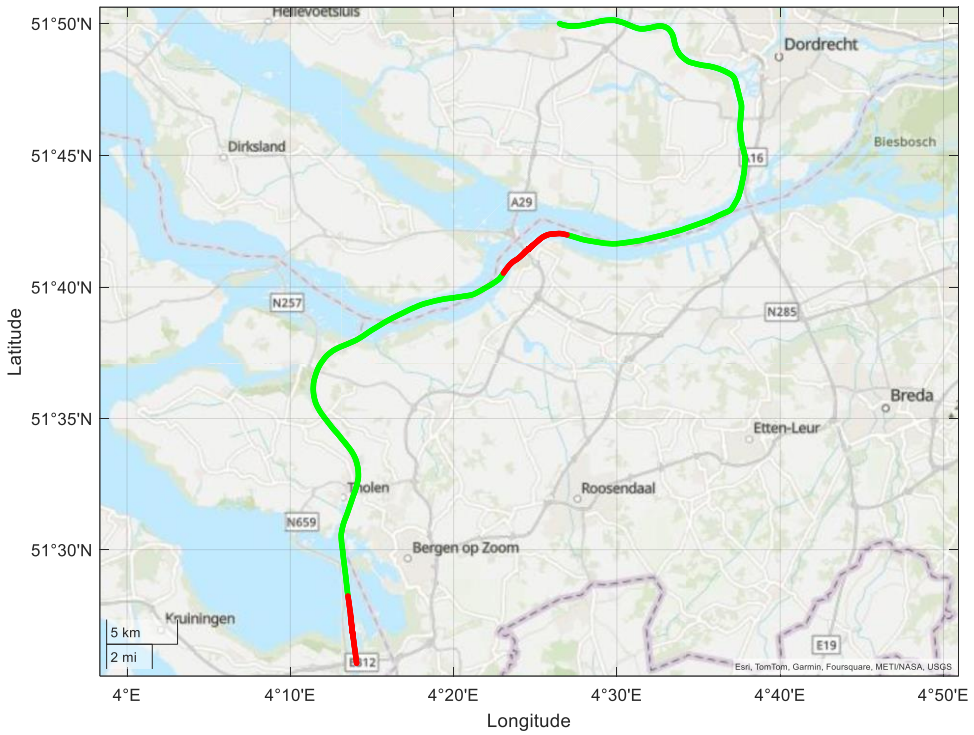

C2. Trajectory of selected dataset for checking 'Transit' detection

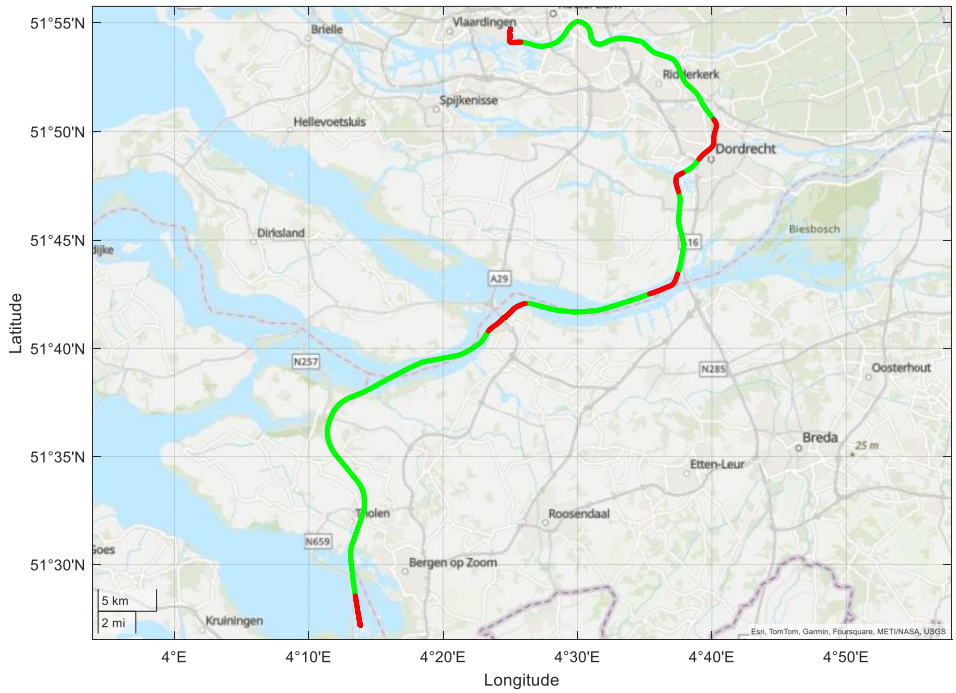

C3. Trajectory of selected dataset for checking 'Transit' detection

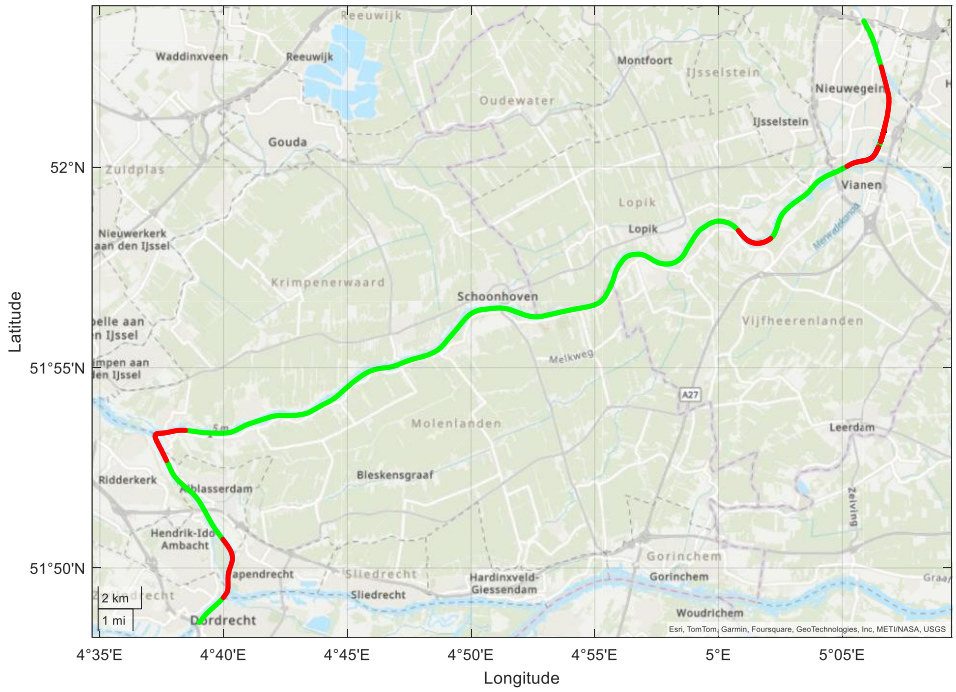

C4. Trajectory of selected dataset for checking ‘Transit’ detection

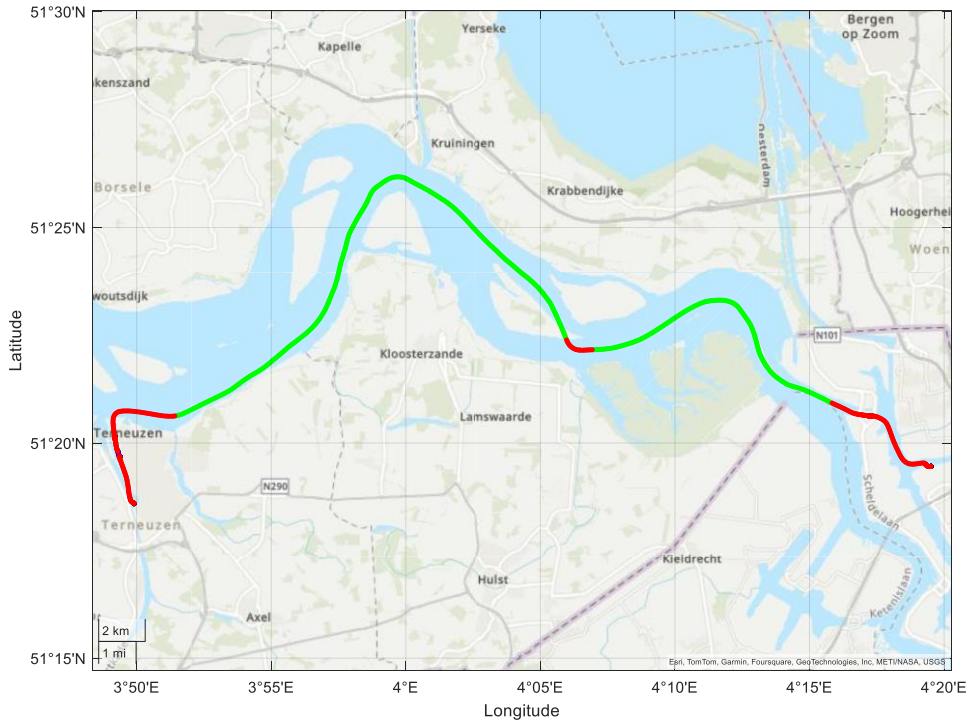

C5. Trajectory of selected dataset for checking ‘Transit’ detection

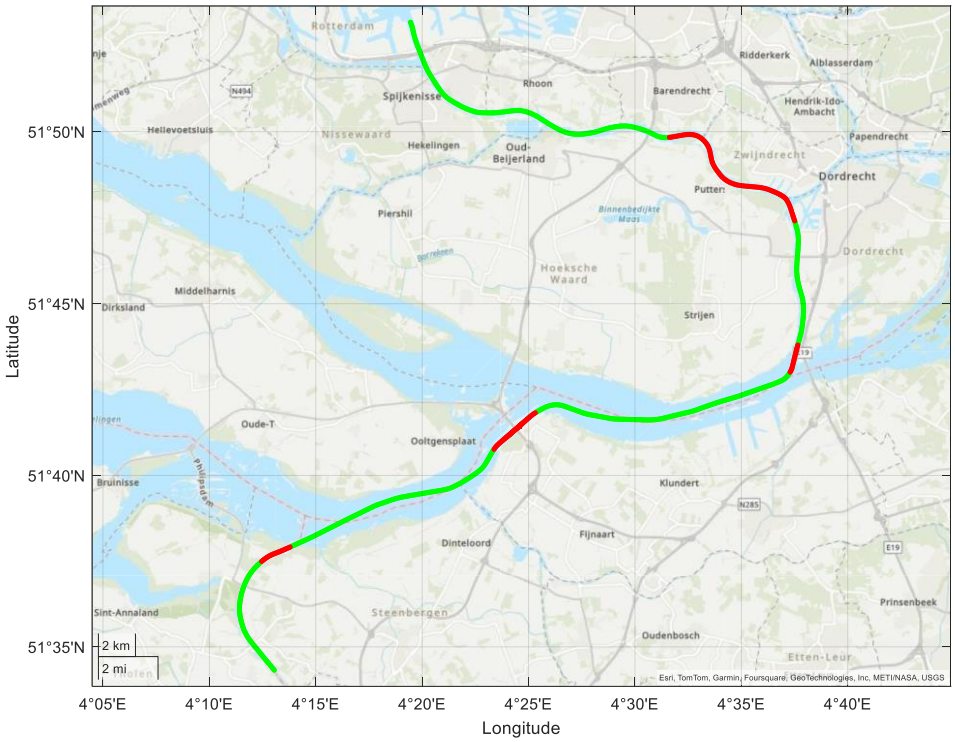

C6. Trajectory of selected dataset for checking ‘Transit’ detection

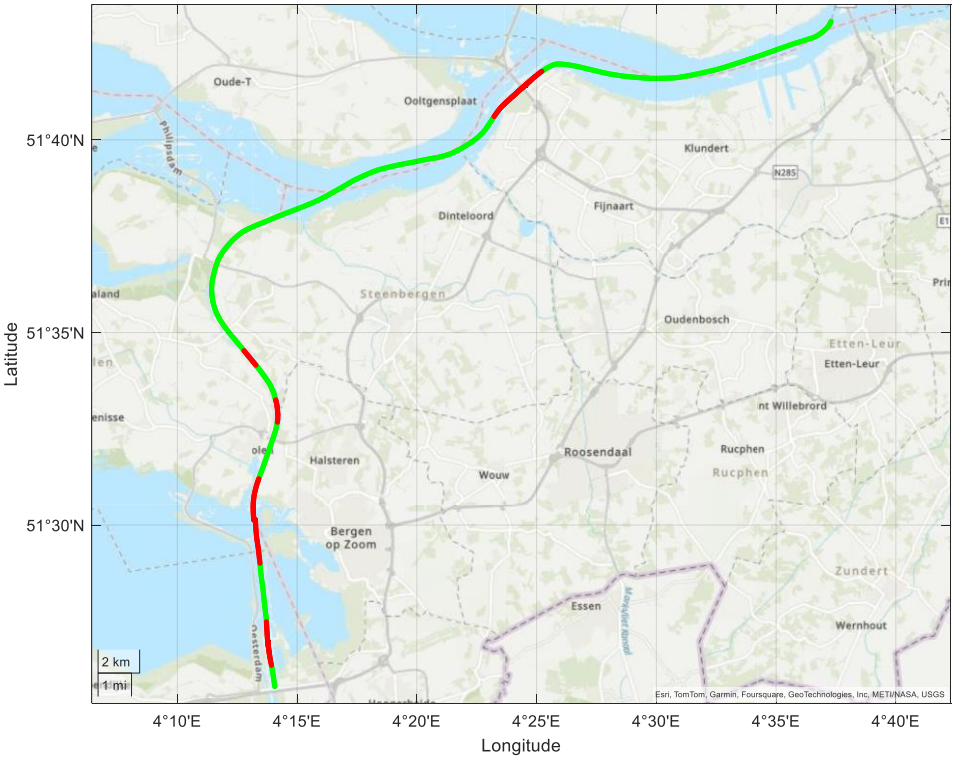

C7. Trajectory of selected dataset for checking ‘Transit’ detection

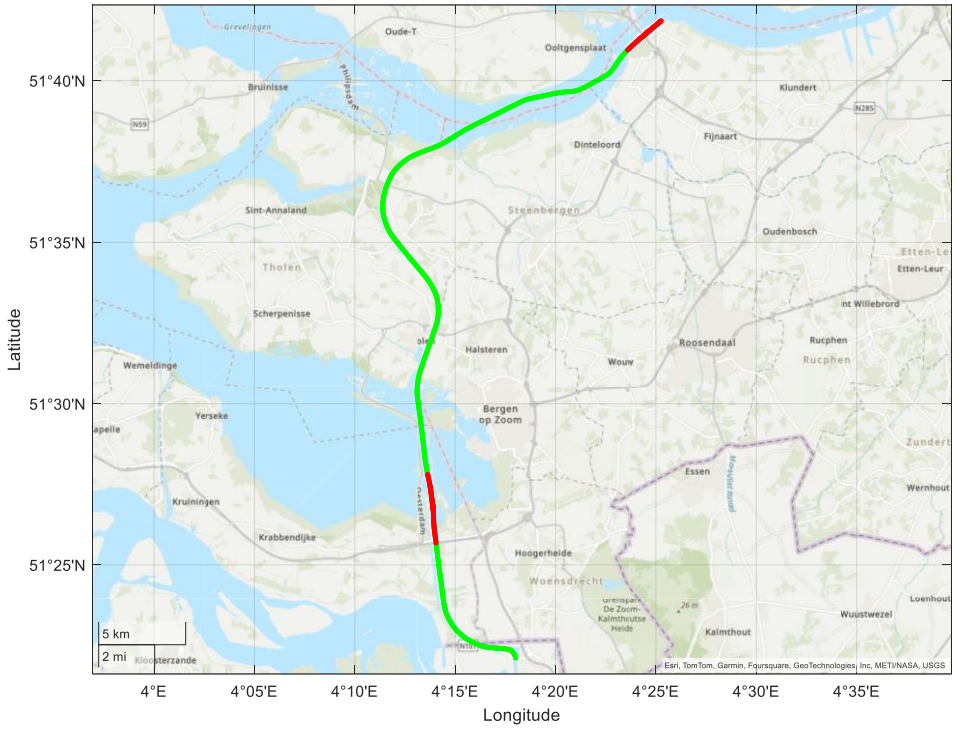

C8. Trajectory of selected dataset for checking ‘Transit’ detection